Controlled nanostructures of synthetic and biological polymers investigated by scanning force microscopy techniques

D I S S E R T A T I O N

zur Erlangung des akademischen Grades
Doctor rerum naturalium
(Dr. rer. nat.)
im Fach Chemie

eingereicht an der
Mathematisch-Naturwissenschaftlichen Fakultät I
Humboldt-Universität zu Berlin

von
Herr Wei Zhuang (M. Sc.)
geboren am 19.04.1977 in Shanghai, China

Präsident der Humboldt-Universität zu Berlin:
Prof. Dr. Dr. h. c. Christoph Markschies

Dekan der Mathematisch-Naturwissenschaftlichen Fakultät I:
Prof. Dr. Lutz-Helmut Schön

Gutacher/Gutachterin:

1. Prof. Dr. Jürgen P. Rabe

2. Prof. Dr. Klaus Rademann

3. Prof. Dr. Paolo Samorì

eingereicht am: 06.11.2009

Tag der mündlichen Prüfung : 20.11.2009

Abstract

Polymeric nanostructures from highly attractive, functional synthetic and biological macromolecules were self-assembled at interfaces and in thin films, and then explored with Scanning Force Microscopy (SFM) techniques, in order to develop a molecular level understanding, which allows to control their properties.

A widely used polymer for organic electronics, poly(3-hexylthiophene) (P3HT), was investigated in thin films in order to determine the role of molecular weight for the formation of molecular nanostructures, and the correlation with the corresponding transistor properties and charge carrier mobilities. The correlation with the electrical and optical properties indicates that the electronic properties are largely determined by the backbone conformation of the majority of the polymer chains rather than due to the previously suspected effect of the grain boundaries associated with the polycrystallinity of the material.

On the level of single macromolecules, dendronized polymers, a rather novel class of macromolecules, were investigated. For the first time, self-folding of single synthetic polymer chains into polymeric duplexes was reported. Moreover, it became possible to detect rare single polymer topologies, such as chain branching, which could not be detected by any other means so far.

The complexation of plasmid double-stranded DNA (ds-DNA) with amphiphilic small molecules allowed to control the macromolecular conformation with a “Molecular Workbench”, developed largely within this thesis. It became possible to split, stretch, overstretch, and finally break ds-DNA on molecularly modified graphite surfaces. With a newly developed “SFM blowing” technique, supercoiled ds-DNA and also synthetic block copolymers from DNA and poly(ethyleneglycol) were fully stretched on an atomically flat substrate. Quantitative experiments allowed to estimate rupture forces of ds-DNA on a time scale on the order of as much as half an hour.

In summary, this work presents new insight into highly interesting functional polymeric nanostructures as well as new methods for their investigation. The results are relevant for a development of biologically inspired functional molecular systems, which may ultimately operate close to physical limits as far as the efficiency of matter and energy is concerned.

Keyword: SFM, manipulation, polymer, DNA, nanostructure, single molecule, AFM

Zusammenfassung

Polymere Nanostrukturen aus interessanten, funktionalen synthetischen und biologischen Makromolekülen wurden an Grenzflächen und in dünnen Filmen selbstorganisiert, und dann mit Hilfe von Rasterkraftmikroskopie (SFM) - Techniken erforscht, um ein Verständnis auf molekularer Ebene zu entwickeln, das es erlaubt, ihre Eigenschaften kontrolliert einzustellen.

Eine weit verbreitetes Polymer für die organische Elektronik, Poly(3-hexylthiophen) (P3HT), wurde in dünnen Filmen untersucht, um den Einfluß des Molekulargewichts auf die Ausbildung molekularer Nanostrukturen und die Korrelation mit den entsprechenden Transistor Eigenschaften und Ladungsträger-Beweglichkeiten zu bestimmen. Die Korrelation mit den elektrischen und optischen Eigenschaften weisen darauf hin, dass die elektronischen Eigenschaften wesentlich von der Rückgratskonformation der Mehrheit der Polymerketten bestimmt werden, und weniger - wie bisher vermutet - von den Korngrenzen des polykristallinen Materials.

Auf der Ebene einzelner Makromolekülen wurden dendronisierte Polymere, eine relativ neue Klasse von Makromolekülen, untersucht. Zum ersten Mal wurde über die spontane Faltung einzelner synthetischer Polymerketten berichtet. Darüber hinaus ist es gelungen, seltene einzelne Polymertopologien wie z.B. Kettenverzweigung nachzuweisen, die nicht durch andere Methode nachweisbar sind.

Die Komplexierung von doppelsträngiger-DNA (ds-DNA) mit amphiphilen kleinen Molekülen erlaubt es, makromolekulare Konformationen durch eine "Molekulare Werkbank" zu kontrollieren, die wesentlich in der vorliegenden Arbeit entwickelt wurde. Damit wurde es möglich, ds-DNA auf molekular modifizierten Graphit-Oberflächen zu spalten, auszustrecken, zu überdehnen, und schließlich zu brechen. Mit einer neu entwickelten "SFM Blowing"-Technik wurden überdrillte („supercoiled“) ds-DNA und synthetische Block-Copolymere aus DNA und Poly(ethylenglycol) vollständig auf einem atomar flachen Substrat ausgestreckt. Auf der Basis quantitativer Experimente konnte die Reißkraft für ds-DNA auf einer Zeitskala bis zu einer halben Stunde bestimmt werden.

Insgesamt liefert die vorliegende Arbeit neue Einblicke in hoch interessante funktionale polymere Nanostrukturen sowie neue Methoden für deren Untersuchung. Die Ergebnisse

sind von großer Bedeutung für die systematische Entwicklung von biologisch inspirierten, funktionalen molekularen Systemen, die letztlich nahe an physikalischen Grenzen operieren, etwa was die effiziente Nutzung von Materie und Energie angeht.

Schlagworte: Rasterkraftmikroskopie, Manipulation, Polymere, DNA, Nanostruktur, einzelne Moleküle.

Acknowledgements

First and foremost I would like to thank Prof. Dr. Jürgen P. Rabe, who offered me the challenging projects and always generously provides me his patient education and invaluable advice, so I could learn so much not only about science but also life in general. His PMM group offers me a comfort, yet stimulating supporting network. In particular, Dr. Nikolai Severin always patiently gives me the scientific guidance and kindly shares his broad experiences and deep understanding ranging from DNA, SFM, science frictions to Karate Arts…

During my PhD studies, I have collaborated with several research groups; therefore, I want to offer my sincere appreciation to Prof. Dr. A. Dieter Schlüter and his group in ETH Zürich, especially to Dr. Edis Kasëmi, who provided me the excellent synthetic dendronized polymers involved in the thesis. I would like to thank Dr. Achmad Zen and Prof. Dieter Neher at University of Potsdam for the collaboration in P3HT thin film experiment, Dr. Fikri E. Alemdaroglu and Dr. Andreas Herrmann at the Max Planck Institute for Polymer Research in Mainz for collaboration in DNA-PEG copolymer, Prof. Igor Sokolov at Humboldt University for collaboration in working out the mechanism of blowing effect, Dr. Ken Woycechowsky and Prof. Donald Hilvert for collaboration in encapsulated engineering proteins.

I would also express my thanks to all ex- and current-members of PMM group, in particular to Hua Liang and Manuel Gensler for many exciting experiments and discussions we enjoyed together, to Jörg Barner for teaching me SFM manipulation through his powerful equipment, to PD Dr. Stefan Kirstein and Dr. Norbert Koch for their helps and the fruitful discussions, to Jörn-Oliver Vogel, Rolf Kniprath, Omar Al-Khatib and Stefan Eilers for the friendly and enjoyable time we experience together. Necessarily to keep in mind Lothar Geyer for his instantaneous help regarding all computer problems and Evi Poblenz for her technical support in labs. Sincere thanks also extend to Sabine Schönherr and Dörthe M. Eisele, who make PMM group and Sfb 448 running smoothly.

For the financial support, I gratefully acknowledge the German Science Foundation (Deutsche Forschungsgemeinschaft) under Sfb 448 Mesoskopisch strukturierte Verbundsysteme.

Last but not least, I would like to thank my family for their continuous support and inspiration. There is no way to fully express my gratefulness to my lovely wife Min and our precious son Aichen for their continuous love, support and enjoyable time.

Abbreviations

AFM	Atomic force microscopy
ALS	Aquifex aeolicus lumazine synthase
BP or bp	Base pairs
b.p.	Boiling point
C_{16}TAB	Trimethylhexadecyl- ammonium bromide
CMC	Critical micelle concentration
DA	Dodecylamine ($C_{12}H_{25}NH_2$)
Denpol	Dendronized polymer
DP	Degree of polymerization
DPN	Dip-Pen Nanolithograpy
DSC	Differential Scanning Calorimetry
FJC	Free joint chain
G4PMMA	4th generation dendronized PMMA
GPC	Gel Permission Chromatography
HOPG	Highly Oriented Pyrolytic Graphite
JC	Janus Chain
MW	Molecular Weight
MWD	Molecular weight distribution
P3HT	Poly(3-hexylthiophene)
PACs	Polyelectrolyte-Amphiphile Complexes
PCR	Polymerase chain reaction
PEG	Polyethylene glycol
PDI	Polydispersity index

PG2	Dendronized polymer generation 2
PG3	Dendronized polymer generation 3
PLO	Poly-L-ornithine
PSS	Poly(sodium 4-styrensulfonate)
PVs	Photovoltaic cells
OA	Octadecylamine ($C_{18}H_{35}NH_2$)
OFETs	Organic field effect transistors
rps	round per second
SAXS	Small-angle X-ray scattering
SFA	Surface force apparatus
SFM	Scanning force microscopy
SNOM	Scanning near-field optical microscopy
SPIP	Scanning Probe Image Processor
SPM	Scanning probe microscopy
STM	Scanning tunneling microscopy
TEM	Transmission electron microscopy
TFA	Trifluoro acetic acid
WLC	Worm–like chain
XRD	X-Ray diffraction

Constants and Variables

C_i	capacitance of the gate insulator
$\Delta\,\sigma$	Surface pressure difference
ε_0	potential energy at the minimum
E	Modulus
F_t	tangential force along the polymer
G	Gibbs free energy
H	Enthalpy
$I_{D,sat}$	drain current in the saturation regime
κ	Bending rigidity
k_BT	Thermal energy
L	Contour length
ℓ	Segment length
ℓ_p	Persistence length
L_k	Linking number
M_n	Number average molar mass
M_w	Weight average molar mass
σ	effective molecular diameter
σ_s	degree of supercoiling
R	End to end distance
r	interatomic distance
S	Entropy
T_w	Twist number
μ_{sat}	field-effect mobility in the saturation region
V_{GS}	gate voltage
W_r	Writhe number
x	Extension ratio

Table of Contents

1 Introduction

1.1 Motivation

Research on synthetic and biological polymers at surfaces and interfaces is attracting increasing interest and excitement. Prime research activities on this topic are relevant for both fundamental understanding and application perspectives, such as for nanostructured surfaces, interfaces, and thin films, polymer chain structure and phase transitions in thin films, architectures and conformations of single polymer chains, photonic and electronic applications, and also biological and bioinspired issues. It had been a great limitation that there were few laboratory methods capable of either reliably producing or characterizing lateral variations of chemical composition and topography on a surface. While significant advances in characterization instruments have always paralleled the development of new polymeric materials, instrumentation must advance as new applications are moving forward. Thus there is a strong motivation to introduce emerging nanotechnologies into polymer science, while on the same time polymer science contributes significantly to the development of nanotechnologies.

Nanotechnology is a field of applied science and technology covering a broad range of topics. The main unifying theme is the control of matter on a scale below 100 nanometers, as well as the fabrication of devices on this same length scale. The manufacturing of polymers based on precise molecular structures, or the development of computer chips or biological chips based on surface science are examples of nanotechnology in modern use. Nanotechnology cuts across many disciplines, including colloidal science, chemistry, applied physics, and biology. It could variously be seen as an extension of existing sciences to the nanoscale. In particular, the invention of scanning tunneling microscopy (STM) in the early 1980s by Gerd Binnig and Heinrich Rohrer boosted the scope of nanotechnology [1]. Following STM, the promising development of Scanning Force Microscopy (SFM) since 1986, well known also as Atomic Force Microscopy (AFM) [2], made it possible to investigate polymers and

bio-molecules, as well as their macroscopic architectures [3]. Upon scanning a sharp tip across a surface, the topography of organic or biological films deposited on a surface can be mapped. The SFM explorations can be made on length scales spanning from the hundreds of microns down to the nanometers. Through 20 years continuous development with different operative modes, SFM has been widely used in the research of synthetic macromolecules [3], biological macromolecules [4,5,6], and semiconducting polymer materials [7,8]. It can effectively characterize the length [9,10], height [11], and width [12] of macromolecules on surfaces. Moreover, by utilizing the SFM's finite tip it is now possible to manipulate molecules on surface on the nanoscale [13], in order to perform nano-lithography [14] and even to be bring about chemical reactions at well defined locations on a surface to construct novel supramolecular architectures [15].

With the advances of research on polymers at surfaces there are many new applications related to the self-assembly of multifunctional polymers, polymers integrated with organic and inorganic nanoobjects, and the interaction between synthetic polymers and the natural biological environment. To realize effective control of polymer nanostructures at surfaces has become vital in most their applications. However, the conformation and nanostructure of a polymer chain at a surface differ in general from the bulk; therefore it is hard to predict the polymer conformations directly from their bulk properties. Hence, the prime research presented in this thesis will focus on the efficient control of polymer nanostructures at surfaces, investigated by both SFM visualization and direct SFM manipulation.

1.2 Aims

The aim of this thesis is to investigate means to control nanostructures of polymers at surfaces, interfaces, and in thin films. Key methods are SFM imaging and manipulation. The following four specific questions, which initiated this thesis, are going to be answered:

1. Conductive polymers are emerging materials for electronic applications due to the tunability of their properties through variation of their chemical structure [16]. Poly(3-hexylthiophene) (P3HT) is one of the most studied polymers for organic electronic applications, which is mainly due to the fact that P3HT exhibits excellent electrical properties while the presence of the hexyl substituents greatly improves the solubility and processability of P3HT. However, the charge carrier mobility in P3HT in thin films is strongly depending upon the morphology. For example, the McGehee group has shown that different self-assembled thin film morphologies of P3HT obtained from different thin film preparations can cause very different charge carrier mobilities (Figure 1.1) [17]. There are many parameters affecting the morphology of P3HT thin films. The question is: how to effectively control the thin film morphology of a polymer like P3HT through self-assembly and thereby eventually influence its charge carrier mobilities, and what are the reasons behind the phenomenon?

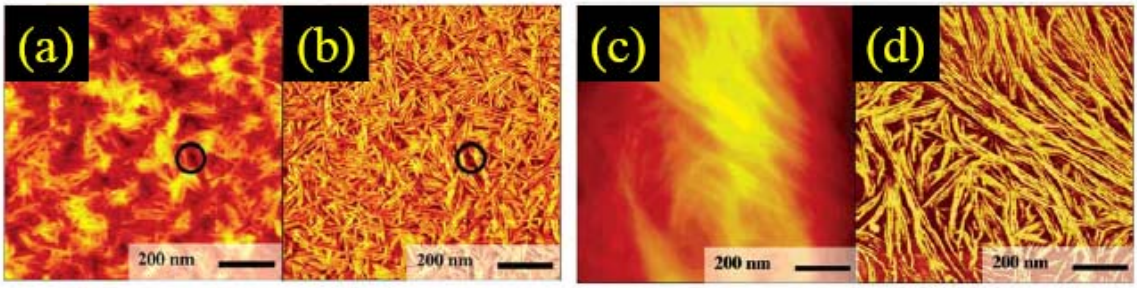

Figure 1.1: SFM images comparing low-Mw P3HT dissolved in chloroform and deposited using spin-casting ((a) topography and (b) phase image) and drop-cast methods ((c) topography and (d) phase image) [17].

2. Folding and aggregation of biopolymers, such as proteins, driven by non-covalent interactions leads to highly ordered hierarchical structures, which exhibit important functionality and materials properties. Although the performances of synthetic polymers are quite different from biopolymers, several synthetic polymers have been reported to fold into hierarchical superstructures driven by hydrogen bonding or steric restrictions. Dendronized polymers consist of a backbone to which dendrons of various generations and functional peripheries exhibit interesting application options [18]. Cyro-Transmission Electron Microscopy investigations have shown that positively

charged representatives self-assemble into highly ordered molecular aggregates (Figure 1.2) [19], which have a potential for the construction of hierarchically structured molecular objects of unprecedented dimensions. Thus organic chemists develop dendronized polymers with such peripheral functional groups that they can be turned into negatively charged ones (like the charge of DNA). The question is: through controlled dendronization, can these highly negatively charged dendronized polymers self-assemble at the single molecular level as many biopolymers do?

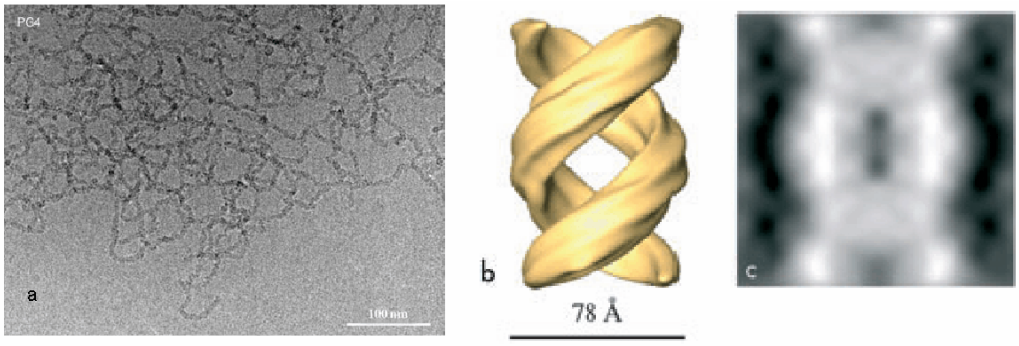

Figure 1.2: (a) Representative cryo-TEM image of a cationic dendronized polymer fiber network embedded in a vitrified layer of water; (b) Reconstruction of a piece of zoomed individual fiber from (a) in three-dimensional volume; (c) The reprojection of (b) into the two-dimensional image [19].

3. The 21st century is a nanotechnology era and a genomic science century, therefore applying cutting-edge nanotechnologies into genomic sequencing would be a most fascinating contribution to modern science. Besides ensemble (multicopy) sequencing, sequencing DNA in a single molecule approach is practically needed within the next decade. Thus, to design and fabricate a DNA chip that can be used in arrays for gene expression studies, for identifying diseased cells and moreover for genomic analyses is a crucial and hence central step. Since it has been well known that long alkyl chain strongly adsorb in highly ordered monolayers to the hydrophobic basal plane of highly oriented pyrolytic graphite (HOPG) [20,21], an approach has been developed to apply single ds-DNA molecules onto alkyl amine amphiphiles (e.g. $C_{12}H_{25}NH_2$) coated HOPG surfaces, which allows DNA chains to be fully stretched by an SFM tip on the surface (Figure 1.3) [22]. However, this approach is requiring an SFM tip, which requires space

and limits speeds. The question is: Is it possible to design a DNA chip based on the "alkyl amine amphiphiles" approach, and spontaneously control the DNA conformation on the surface without the help of SFM tip manipulation?

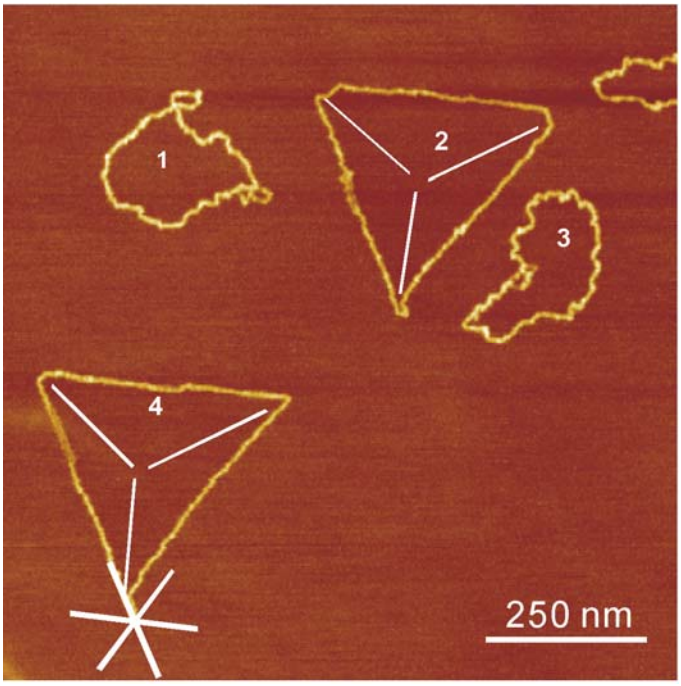

Figure 1.3 Tapping mode SFM image of plasmid ds-DNA on $C_{12}H_{25}NH_2$ monolayer coated HOPG; molecules 2 and 4 have been stretched by an SFM tip in contact mode [22].

4. The elasticity of a ds-DNA chain has been investigated by different single molecule manipulation methods. The most often used tools to stretch and overstretch ds-DNA molecules in buffer solutions are: SFM cantilevers [23,24], flow field [25,26], optical tweezers [27,28], microneedles [29] and magnetic beads as shown in Fig. 1.4 (a) [30]. It has been shown that ds-DNA can be overstretched up to 2.0 times of its original B-form length [25,26]. A structural transition from the B-form to other forms such as S-form DNA occurs during DNA overstretching as shown in Fig. 1.4 (b) [29]. But due to the fact that the attachments between DNA molecule and force sensor are typically weaker than the DNA molecule itself, they break prior to the DNA molecule rupture; therefore it is still difficult to directly measure the rupture force of ds-DNA in solution. On the other hand, currently many groups are actively trying to combine single molecule manipulation with single molecule visualization, i.e. to visualize the displacement and

activity of a single molecule under stress. SFM tip manipulation results have demonstrated that single ds-DNA can be overstretched on a surface and be visualized afterwards [22]. However, this method cannot be applied to systematically study the mechanical properties of ds-DNA, since SFM tip manipulation can only exert a point force on a polymer chain at once. This causes a challenge: Is it possible to develop a new manipulation method in a pure physical level, which exerts a continuous and homogeneous force on polymer loops, e.g. plasmid ds-DNA, such that the mechanical properties of ds-DNA up to its rupture can be investigated on the surface and the manipulation process can be visualized *in situ*?

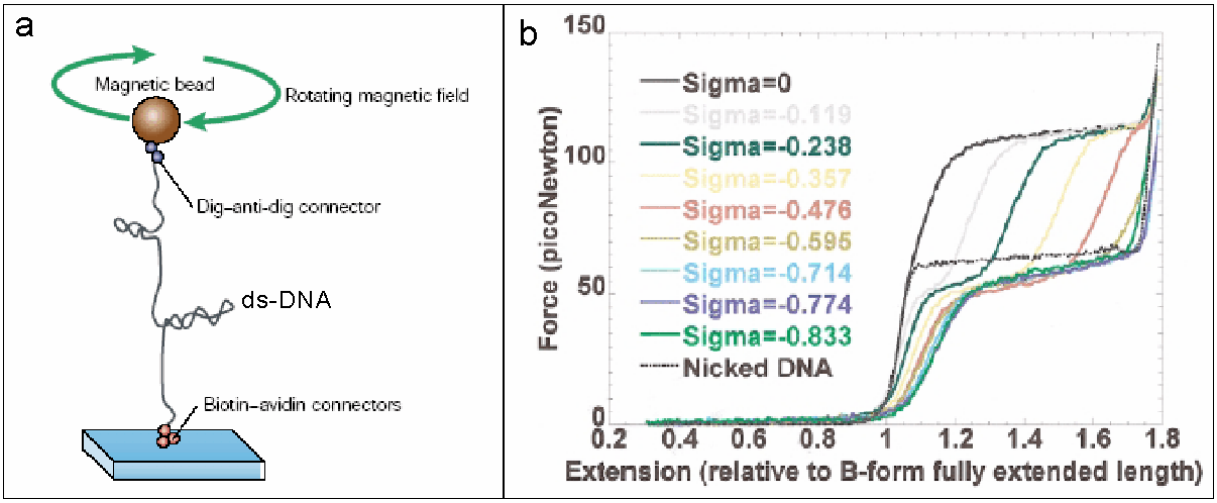

Figure 1.4: (a) A rotating magnetic field is used to under- or overwind double-stranded DNA tethered between the glass slide and a magnetic bead [30]. The resulting supercoils (plectonemes) can be studied by measuring the displacement of the bead perpendicular to the glass slide as a function of the magnetic force. (b) Typical force versus extension diagram for underwound ds-DNA at transition from B-form to S-form (σ from 0 to -0.833 according to the color code given in inset), in comparison with force extension diagram of a nicked molecule (dotted black line) [29].

1.3 Outline of the thesis

After this introduction, Chapter 2 introduces first the scientific background for the polymers used in the thesis, including previous work on the self-assembly of the polymers. Then the principles of single molecule manipulation techniques and the highlights of their applications are presented.

Chapter 3 on Materials and Experimental Methods will describe the methods to prepare the polymers and substrates used in this work for SFM measurements. The sample analysis of height, length and width based on SFM data and SFM tip calibration will be presented, and the procedure of SFM tip manipulation will be introduced.

Chapter 4 on Results and Discussion will include four sub-chapters, where controlled nanostructures of P3HT, superstructure dendronized polymers, spontaneous control plasmid DNA conformation and SFM manipulation of ds-DNA will be introduced, respectively. In sub-chapter 4.1 the results of the SFM investigation of thin films of P3HT from different molecular weights will be presented. The relationship between the self-assembly of P3HT and its molecular weights is discussed. In sub-chapter 4.2 the results of SFM investigations on dendronized polymers are presented, including the formation of self-folding duplex supramolecular structures for electrically charged species. The mechanism of the formation of the superstructure and attempts for decomplexation are presented. In sub-chapter 4.3 the focus is shifted from synthetic polymers to DNA. Results are presented on how the variation of the surface coverage of amphiphiles can control the conformation and the topology of ds-DNA on the surface. A DNA chip is developed, which allows to control the DNA conformation. The mechanism of such a control is discussed. At the end, in sub-chapter 4.4 beyond conformation control in a physical-chemical manner a new SFM manipulation method based on a so called “blowing effect” is presented. Its advantages over the SFM tip manipulation and other single molecule manipulation methods in solution are discussed. The mechanism of the “blowing effect” is also discussed. Finally the mechanical properties of ds-DNA investigated by this new manipulation method are presented.

The thesis ends with a summary of the presented results and a perspective for further experiments in Chapter 5.

2 Theory and Scientific Background

2.1 Biological polymers

A POLYMER is a chemical substance, consisting of large molecules with many molecular repeat units. Typically covalent bonds provide the intramolecular forces which keep the polymer molecule intact. In addition, other intermolecular forces, such as hydrogen bonds, dipole-dipole interactions, and electrostatic forces hold assemblies of these molecules together. In nature, a wide variety of biological polymers are synthesized by living organisms. Among the biological polymers the proteins and the nucleic acids are particularly important categories. Proteins perform many different functions, such as acting as catalysts or regulators, and the nucleic acids carry genetic. Since Deoxyribonucleic acid (DNA) is a biological polymer, which has been intensely studied within this thesis, it will be introduced in some detail in the following.

2.1.1 DNA

DNA plays an essential role in storage and transmission of hereditary information from the mother to the daughter organism. Due to the importance of nucleic acids in biological research, they became a focus of interest in modern science. On the other hand, DNA is an extensible linear polymer with unique mechanical properties. Thus it is the most intensely investigated molecule for the emerging nanotechnology.

2.1.1.1 Structure of ds-DNA

DNA is a polymer, i.e. a linear chain made of repeating structural units. These consist of a ribose-phosphate to which four different groups can be linked: adenine (A) guanine (G), cytosine (C) or thymine (T) as shown in Fig. 2.1 (a). The central role of DNA in biological processes was first demonstrated by Avery, who showed that DNA is the molecule that carries genetic information [31]. However, how DNA stores and encodes the genetic information was not understood until the secondary structure of DNA was discovered. In April 1953 Watson and Crick published their famous article in *Nature* [32], which reported on the structure of the nucleic acid double helix resolved by X-ray crystallography. They investigated DNA in its crystalline state and reported dimensions for the double helix that correspond to B-form DNA (Fig. 2.1 c). In their model, two stands of a DNA molecule are

intertwined with each other, forming the so called 'double helix'. Although crystal structures of DNA were not available until 1979, considerable indirect evidence quickly suggested that the Watson-Crick model was essentially correct. The X-ray diffraction pattern indicates that the staked bases are regularly spaced 0.34 nm apart along the helix axis. The helix makes a complete turn every 3.4 nm, thus there are 10.4 base pairs per turn. The width of the double helix is about 2.4 nm. The double-helix is not perfectly symmetrical, but is instead characterized by a major groove 12 Å wide and a minor groove 6 Å wide. The various interactions that stabilize the B-form of DNA determine its rigidity. The base pairs are stacked in between the strands. They are held together by hydrogen bonds to the complementary base pairs on the antiparallel strands (Fig. 2.1 b). The complementarity of A with T and C with G imposes rules to the self-assembly of a DNA molecule.

Besides the hydrogen bonds between complementary base-pairs and the topological constraint generated by the wrapping of the two strands about one another, two other types of interactions play an important role for the rigidity and stability of the double helix. First, due to their hydrophobicity and planar nature, the bases in DNA tend to stack at the centre of the molecule one upon the other, much like a pile of plates. This stacking interaction is responsible for the unusually large bending rigidity of ds-DNA ($\kappa = 2.7*10^{-28}$ Nm^2, about 50 times larger than synthetic polymers, such as polyethylene, polystyrene, PVC, etc [28]). Second, the stability of DNA, i.e. the cohesion of its two strands (their melting temperature T_m), is largely controlled by the screening of the negative charges carried by the phosphate groups on their backbones. A factor of two decrease in the monovalent ionic concentration decreases T_m by about 5˚C [33]. There fore due to its unique structure, the ds-DNA molecule is not flexible, but semi-flexible in the language of polymer physics.

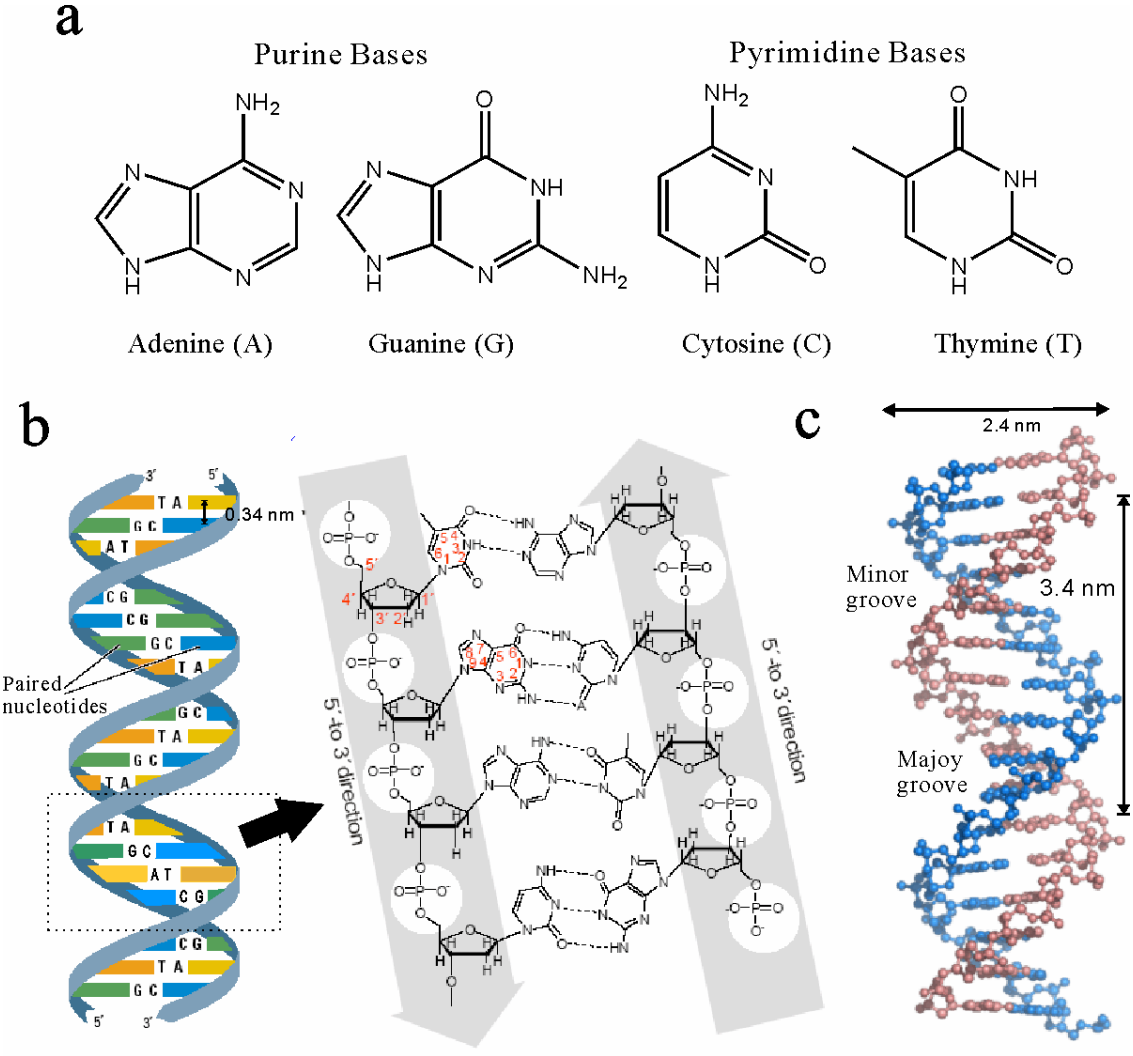

Figure 2.1: (a) Chemical structure of the purine and pyrimidine bases. (b) Schematic structure of a double helix DNA. The DNA fragment containing four common bases, together with the numbering schemes used for the bases as well as for the ribose residue. The sugar component of a nucleotide is linked between the base and the phosphate group. The nucleotides are linked together by covalent phosphordiester bonds that join the 5´ carbon of one group to the 3´carbon of the deoxyribose via a phosphate residue. This directionality has given rise to the convention that polynucleotide sequences are written and read in the 5´-3´ direction. The purines A and G pair with the pyrimidines T and C via hydrogen bonds, which are indicated with dashed lines. (c) The model of B-form double helix DNA. The intertwined strands make two grooves of different widths, referred to as the major groove and the minor groove, which may facilitate binding with specific proteins (after [34]).

2.1.1.2 Model of DNA elasticity

Just like any polymer in solution, free DNA adopts a random coil conformation which maximizes its entropy [35]. Pulling on the molecule reduces this entropy and costs energy. The associated entropic forces result from a reduction of the number of possible configurations of the system consisting of the molecule (be it a synthetic polymer, DNA or a protein) and its solvent (water, ions), so that at full extension there is but one configuration left: a straight polymer linking both ends. To reach that configuration work has to be done

against entropy, i.e. a force has to be applied. The entropic forces are rather weak, typically < 10 pN. Beyond this regime and up to about 70 pN DNA stretches like any spring, i.e. it is in an enthalpy dominated regime.

In polymer physics, the model of an ideal macromolecule can be represented by a chain of immaterial links, each jointed with two nearest neighbors having no interaction either with solvent molecules or with other links of the same or another macromolecule. The simplest model is that of a freely jointed chain leading to a random coil. It describes a hypothetical chain, which, however, is very difficult to realize in practice [35].

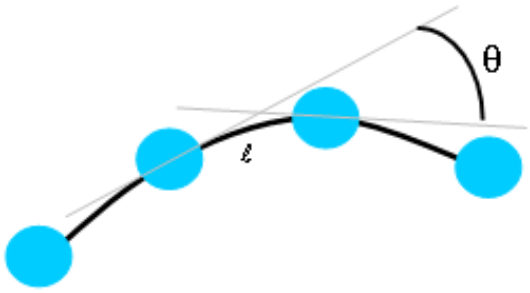

Figure 2.2: Illustration of the definition of θ and *l*.

Many rigid-chain polymers or helical macromolecules are characterized by a more sophisticated model, the so called worm-like chain model. In this model, the rigidity of molecules can be described by means of the persistence length. The persistence length can be defined as the length scale over which the memory of the initial direction of the chain is lost.

Rigid chains are semi-flexible, namely they have angles between two adjacent repeat units (r.u.) ~180°. The r.u. following the first r.u. thus cannot occupy any arbitrary position in space. The chain direction has a persistence that causes a resistance against coiling. The persistence length l_p is here defined as $l_p = \left\langle \frac{l}{1-\cos(\theta)} \right\rangle$, with θ the angle between the tangents at two points separated by a distance l along the contour of the chain (see figure 2.2).

The average cosine of the angle θ can be calculated [36]:

$$\langle \cos(\theta) \rangle = \int_{-\infty}^{\infty} \mathrm{P}(\theta(l)) \cos(\theta) d\theta = e^{-\frac{l}{2l_P}} \qquad \text{Eq. 2.1}$$

It shows that the average cosine of the angle between two r.u. in the polymer decreases exponentially with the separation *l*. The persistence length, l_p, is the decay length over which the memory of the initial orientation of the molecule persists. Using equation 2.1, if the molecule is in two dimensions, the mean square end-to-end distance of the polymer can used to approximate its persistence length [36]:

$$\left\langle R^2 \right\rangle_{2D} = 4Ll_p(1 - \tfrac{2l_p}{L}(1 - e^{-\frac{L}{l_p}})) \qquad \text{Eq. 2.2}$$

where *L* is the contour length of polymer. If $L \rightarrow \infty$, $\left\langle R^2 \right\rangle_{2D} = 4Ll_p$

In three dimensions the molecule can also bend in a direction perpendicular to the plane and the mean-square end-to-end distance is given by [36]:

$$\left\langle R^2 \right\rangle_{3D} = 2Ll_p(1 - \tfrac{2l_p}{L}(1 - e^{-\frac{L}{l_p}})) \qquad \text{Eq. 2.3}$$

If $L \rightarrow \infty$, $\left\langle R^2 \right\rangle_{3D} = 2Ll_p$

Different studies have used the worm–like chain (WLC) model to determine the persistence length of ds-DNA on surfaces. For example SFM provides the possibility to image the contour of DNA on surface, and thereby to determine its apparent contour length and its 2D end-to-end distance. The persistence length of the DNA molecule can be determined according to eq. 2.2. Using SFM, the equilibration of DNA molecules on surfaces has been the subject of a systematic study of Rivetti *et al.* [36]. In their experiments they obtained a persistence length of 52.3 ± 0.3 nm in physiological conditions (10 mM phosphate buffer (pH=7.5), 10 mM NaCl) that is in agreement with the 45 ± 15 nm obtained by the ligase-catalyzed DNA cyclization method [37] and the 53.4 ± 2.3 nm calculated by force

spectroscopy [4]. It demonstrates that the ds-DNA conformation can be well described by the worm-like chain model.

The WLC model also provides an excellent description of molecular elasticity at low and intermediate forces. The exact force (F) required to induce an end-to-end distance extension $x = l / l_0$ can be approximated by [38]:

$$\frac{F \cdot l_p}{k_B T} = \frac{1}{4(1-x)^2} + x - \frac{1}{4} \qquad \text{Eq. 2.4}$$

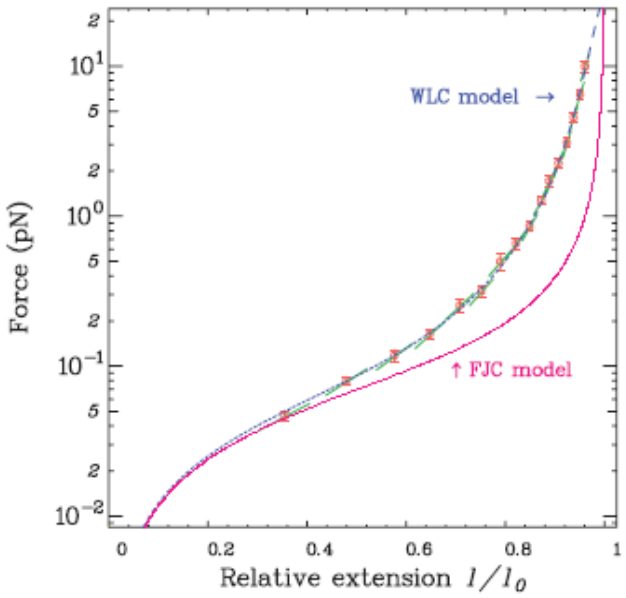

Figure 2.3: Force *vs* relative extension for (a) a λ-DNA (L=15.6 μm) in 10 mM phosphate buffer (red points); (b) FJC model (pink curve); (c) WLC model (green curve) [39].

A comparison of FJC and WLC models is plotted by Strick *et al.* together with experimental data for DNA stretching as shown in Fig. 2.3 [39]. The dots correspond to several experiments performed over a wide range of forces. The force was measured using the Brownian fluctuation technique [30]. The green curve is a fit to the WLC model for forces smaller than 5 pN. The pink curve is the result of the FJC model with the same persistence length. It is clear that the WLC model gives a better description of the behavior of DNA under stress than the FJC model. With increasing forces, the molecule elongates slightly, as would any material in its elastic regime. Above 70 pN (Fig. 2.4), the length abruptly increases, corresponding to the appearance of a new structure called S-form DNA.

2.1.1.3 Structural transitions induced by stretching DNA

The experiments on torsionally unstressed DNA previously described were done in the entropic regime (at $F < 10$ pN) where the molecule behaves as an ideal (WLC) polymer of persistence length $l_p \sim 50$ nm. Beyond the entropic regime, i.e. from 10 pN to about 70 pN, (Fig. 2.4) DNA behaves like an elastic rod with an elastic modules times cross-section $F=E^*A$ = 1087 pN [28] (where E is the Young modulus of DNA and A its effective cross-sectional area [40]). Neglecting entropic contributions, the force vs. extension curve follows a simple Hookean law: $F = E\,A\,(x-1)$ *(with* $x = l / l_0 > 1$*)*.

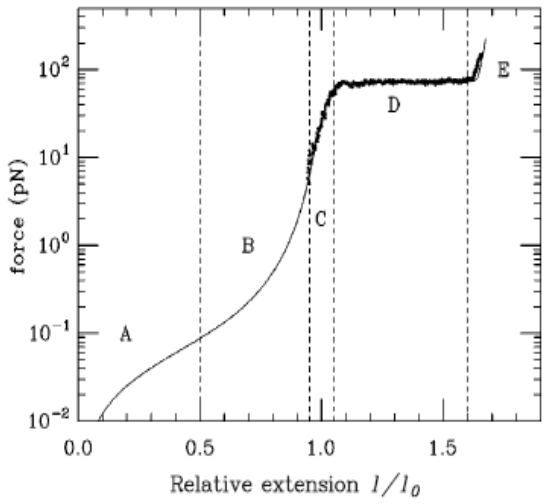

Figure 2.4: Force *vs* relative extension a λ-DNA (L=15.1 µm) in 100 mM phosphate buffer. (A) random-walk fluctuation region, (B) curvature fluctuation region, (C) linear elasticity region, (D) Plateau region, (E) overstretched region [41].

However, at about 65 pN a surprising transition was discovered, where DNA stretches to about 1.7 times its crystallographic B-form length [28,42]. That transition is highly cooperative: a small change in force results in a large change in extension as shown in Fig. 2.4. In order to address the possible structural modification in the molecule resulting from pulling on it, a numerical energy minimization of DNA under stress was performed by Lavery *et al.* [43]. They proposed the existence of a conformational transition to a new form called S-from DNA, which indeed is 70% longer than B-form DNA, whose exact structure depends on which extremities of the DNA are being pulled (3′ − 3′ or 5′ − 5′). If both 3′ extremities are being pulled, the double helix unwinds upon stretching. The final structure resembles a ladder as shown in Fig. 2.5. If both 5′ ends are pulled, a helical structure is preserved. It is characterized by a strong base pair inclination, a narrower minor groove and a diameter roughly 30% less than that of B-form DNA (Fig. 2.5). In both cases the rupture of

the molecule is predicted to occur as observed in other experiments when its extension is more than twice that of B-form DNA [25,26].

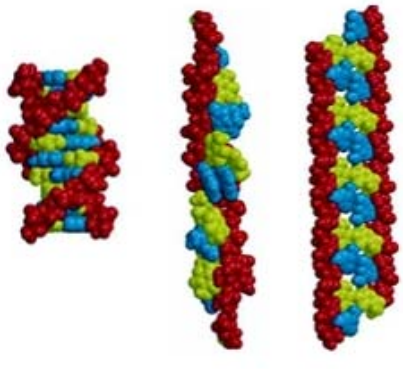

Figure 2.5: The new structures of DNA obtained in numerical simulations when pulling on the molecule [43]. Left: usual B-DNA structure. Middle: if the molecule is pulled by its 5′ ends, it keeps a double-helical structure with tilted bases. Right: if the DNA is pulled by its 3′ extremities the final structure resembles a ladder.

It is important to note that the B → S transition is observed at 65 pN (in ~150 mM monovalent ions) only when the DNA molecule presents a break (or 'nick') along one of its two constituent strands. In this case, significant hysteresis is observed in the stretch-relax cycle, which is not the case when the B → S transition occurs on unnicked DNA (at a higher force F = 110 pN) [29]. This is because a nicked DNA can relax the torsion generated upon denaturation when the molecule unwinds. That pathway from S-form DNA to the energetically more favorable ds-DNA does not exist on a torsionally constrained molecule. On a nicked DNA, as the force is decreased the two strands may rehybridize (if they have not been completely unwound and separated), albeit with a slow kinetic due to the possible formation of secondary structures in the displaced strand.

Besides the B → S transition induced by stretching, DNA can undergo other structural transitions through the changing of the environment or the application of a strong torque. For instance, DNA crystallized in various conditions of humidity or salinity show that the double helix is structurally polymorphic. If the molecule undergoes crystallization in low humidity and in the presence of low amounts of cations, one observes a structure of DNA more compact than the B-form (the spacing between bases in this A-form is 2.6 Å [34], but with the same handedness. There also exists a left-handed double helix with a pitch of 12 bps per turn [34] known as Z-form DNA. This DNA structure is stable given a sequence of alternating purines and pyrimidines in strong ionic conditions. When a torque force is

applied to overwinding DNA with a force F > 3 pN or to underwinding DNA with a force F > 0.5 pN, DNA adopts an inside-out helical structure with a very short pitch, the so called P-form DNA. The P-form is 75% longer than the B-form with 2.4 base pairs per turn [44].

2.1.1.4 Tertiary structure of DNA

DNA is one of the longest molecules in nature. A human chromosome for example is a few centimeters long. In order to squeeze such a long molecule into a micron-size nucleus DNA it is strongly bent and wrapped around proteins, forming the bead-on-a-string structure of chromatin, which itself is further compactified by extensive coiling. The compactification is called supercoiling, which generates the tertiary structure of DNA.

There are two types of tertiary structures generated by supercoiling. (A) The DNA chain wraps around small, positively charged globular proteins called histones, as in eukaryotic nucleosomes, forming a left-handed solenoidal structure as shown in Fig. 2.6 (a) [45]. (B) The torsional constraint imposed upon underwound or overwound closed circular DNAs free in solution, forming right handed plectonemical structures as shown in Fig. 2.6 (b) [46]. Both sources of supercoiling are important *in vivo*. Since the control over the conformation of circular DNA is of main interest within this thesis, the plectonemic supercoiling structure will be introduced in the following.

Figure 2.6: Two supercoiling structures are illustrated (a) the solenoidal structure results from the binding of DNA to proteins, (b) circular DNA plectonemic structures results from torsional constraint.

Circular DNA, also known as vector DNA or plasmid DNA forms a closed circular loop by covalent bonds. The distinctive feature of a closed circular molecule is that its topological states cannot be changed by any conformational rearrangement without breaking the strands. In order to describe DNA under torsional constraint it is first necessary to introduce some topological concepts. The first is the twist (T_w), the number of helical turns along the molecule. For a torsionally unconstrained B-form DNA, $T_w = T_{w0} = N/h$ where N is the

number of base-pairs and $h = 10.4$ is the number of base-pairs per turn of the helix. The second topological quantity of interest is the writhe (W_r) of the molecule. W_r is a measure of the coiling of the DNA axis about itself. If the DNA molecule is torsionally constrained, then the total number of times the two strands of the helix cross each other (either by twist or writhe) is a topological invariant of the system called the linking number $L_k = T_w + W_r$ [47]. For relaxed linear DNA molecules, assuming the absence of any spontaneous local curvature, $L_k = L_{k0} = T_{w0}$. The relative difference in linking number between the supercoiled and relaxed forms of DNA is called the degree of supercoiling, $\sigma_s = (L_k - L_{k0}) / L_{k0} = \Delta L_k / L_{k0}$.

The value of σ_s for most circular molecules isolated from cells or virus is roughly −0.06, i.e. DNA is negatively supercoiled, the helices wind about each other in a right handed path in space. The DNA undewinding, or negative supercoiling was first discovered by Vinograd's group in 1963, when they found that the circular DNA chromosomes isolated from small viruses like SV40 or polyoma were in highly compact or folded conformation [48]. They concluded that the compact form corresponds to circular ds-DNA possessing superhelical turns. The introduction of a break, or 'nick', along one of the two strands of the double helix transformed this species into 'relaxed' circular DNA, while a double strand break transformed it into linear DNA.

In cells, topoisomerases are cell's tools for regulating DNA coiling: they unwind DNA and relax any torsional constraint on a DNA molecule and also untangle or unknot DNA. They are ultimately responsible for disentangling replicated chromosomes. But even if there is no topoisomerases existing outside the cell, the environmental conditions can also change the DNA supercoiling, since the number of T_w changes and W_r has to vary to keep L_k constant. This is the driving force for the formation of highly supercoiled DNA; for example, Fig. 2.7 shows different degrees of DNA supercoiling under higher and higher torsional stress.

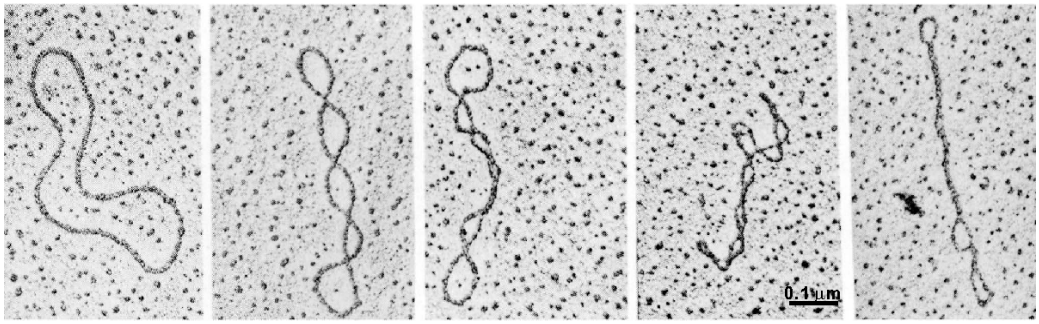

Figure 2.7: Electron microscopy images of supercoiled plasmids (5k bp). The degree of supercoiling increases from left to right [49].

2.2 Synthetic polymers

In contrast to natural polymers, synthetic polymers are by definition materials that can be prepared in the laboratory. They can be synthesized from monomers, for example, units of the monomer styrene may be linked to form polystyrene:

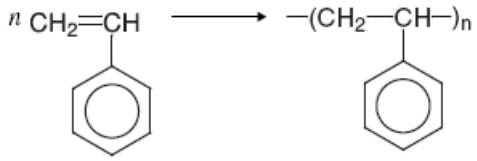

Figure 2.8: Chemical reaction of styrene polymerization

2.2.1 Homopolymer

A homopolymer is prepared by the addition polymerization of a single monomer or by the condensation polymerization from two monomers. They are also termed as chain growth and step growth polymerization, respectively. One important difference between the two mechanisms is the polymer molecular weight versus monomer consumption.

In chain growth polymerizations, an active center, e.g. a radical, an anion, a cation etc. is generated in the initiation step. This active center adds monomer and grows into a polymer chain with an active chain end. This process is called chain propagation. At any stage of chain propagation, the reacting system in effect consists of two species: monomers and very large molecular weight polymers. With the exception of so-called 'living' chain polymerizations, there is always the possibility that the active center is quenched. Depending on whether during this process a new chain is started or not, the result is chain termination or chain transfer. The average molecular weight depends on the relative rates of chain propagation, chain transfer, and chain termination. Both termination and transfer are statistical processes. For this reason, the obtained polymers have a broad molecular weight distribution (MWD), typically with a polydispersity index PDI > 2.

In step growth polymerization, for example in the reaction of diol and diisocyanate to form polyurethane as shown below, the growing molecules remain reactive and continue to grow by condensation throughout the reaction period, which may be several hours. Although the "monomers" remain, their proportion on a weight basis rapidly becomes negligible.

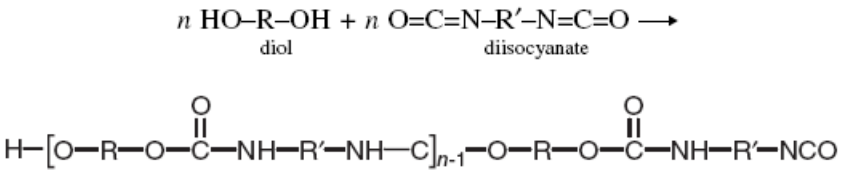

Figure 2.9: Chemical reaction of urethane polymerization

Except "traditional" addition and condensation polymerizations, recently controlled polymerization has been more and more used to synthesize homopolymers. Recently synthetic methodologies for controlled polymerization have been expanded with recent developments in stable free-radical polymerization (SFRP), atom transfer radical polymerization (ATRP), and the reversible addition and fragmentation technique (RAFT) as examples shown in Fig. 2.10. During the transferless polymerization, the number of polymer molecules remains constant. There is no termination, so the chain ends remain active when all of the monomer has been polymerized, and when fresh monomer is added, polymerization resumes. Because the chains are all growing at the same rate, they are more uniform than those prepared by other methods. Controlled polymerization routes permit the synthesis of well-defined macromolecules with controlled chemical composition, predictable molecular weight, and narrow molecular weight distribution. The ability to control the polymer architecture is essential in advanced applications where well-defined macromolecular architectures are required. This makes controlled living polymerizations an invaluable method for preparing copolymers and narrow MWD polymers.

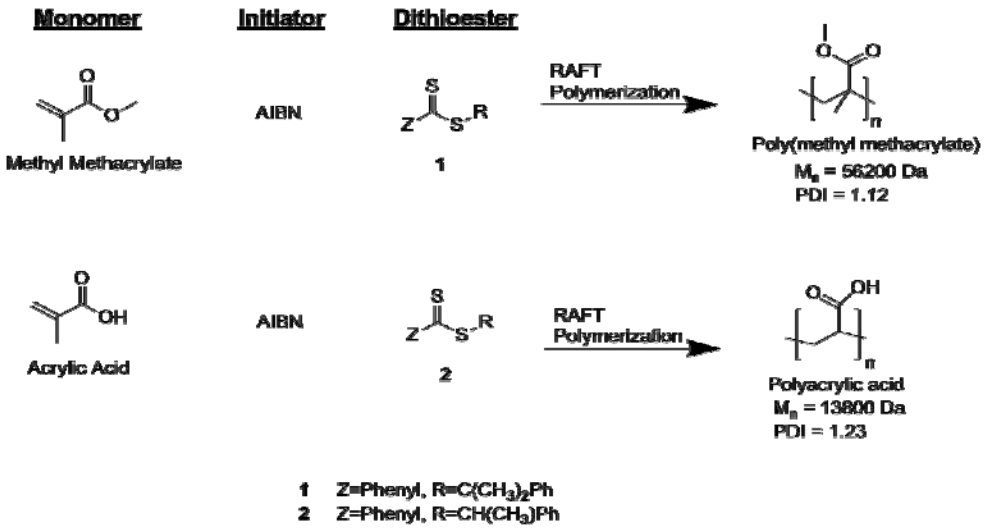

Figure 2.10: Examples of RAFT polymerization

2.2.2 Copolymers

Copolymers are composed of two or more monomer units and can occur in random, alternating, block or graft structures as shown in Fig. 2.11.

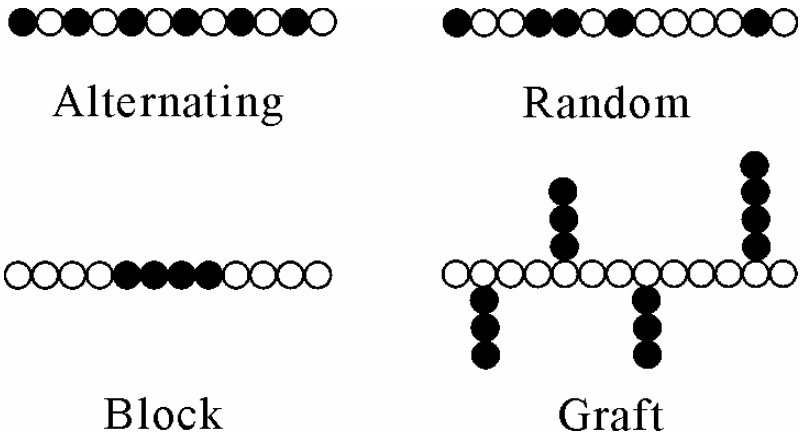

Figure 2.11: Schematic representation of various types of copolymer structures. White circle and black circle represent monomers A and B, respectively.

Starting from monomers A and B, an alternating copolymer has a regular pattern of alternating repeat units in poly(A-alt-B); a random (or statistical) copolymer is one in which the A—B sequence is governed strictly by chance, subject only to the relative abundances of repeat units; block copolymer exhibit long, uninterrupted sequences of each monomer; the structure in Fig. 2.11 has three blocks, and is called poly(A-block-B-block-A), or an ABA triblock copolymer; if a copolymer is branched with different repeat units occurring in the branches and the backbone, it is called graft copolymer [50]. This segregation is often accomplished by first homopolymerization of the backbone, which is then dissolved in the second monomer, with sites along the original chain becoming the origin of the comonomer side-chain growth. It is clear that the alternating, random and block copolymers are linear polymers, while graft polymers are branched. Furthermore, if a series of uniform branches emanate from along the length of a common backbone, it is called comb polymer [50].

2.2.3 Dendronized polymers

A dendronized polymer (C in Fig. 2.12) is a merger of a comb polymer (A) and a dendrimer (B).

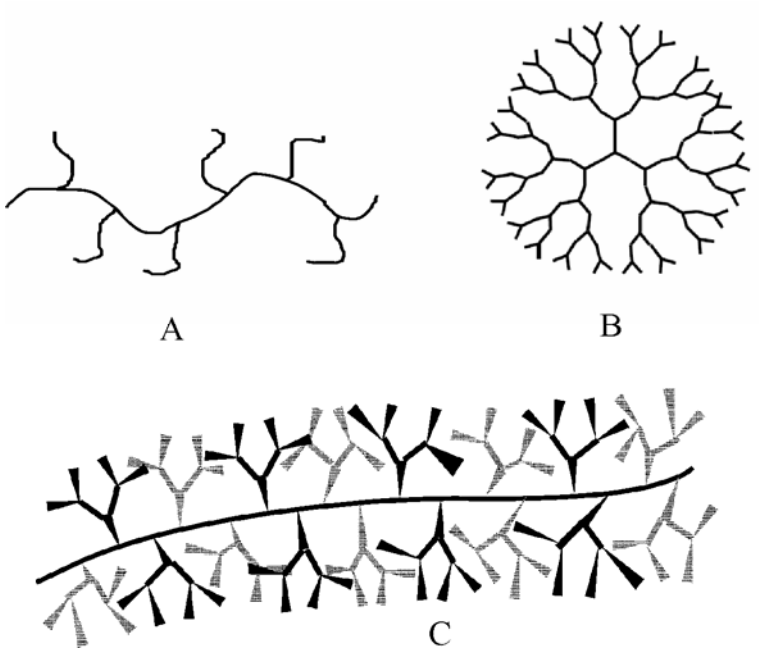

Figure 2.12: Schematic illustration of comb polymer (A), dendrimer (B) and dendronized polymer (C)

Dendrimers are among the most exciting molecular architectures that have been developed in recent years. They comprise a monodisperse, low molecular weight, multifunctional core unit to which a defined number of dendrons are attached, i.e. monodisperse, branched, oligomeric segments consisting of repeating units with an AB_m type functional group pattern and a degree of branching of 100%. The number of repeating units between the core and a terminal unit is referred to as the dendron generation (Gx) [51]. Different to another kind of highly dendritic polymers - hyperbranched polymers, ideal dendrimers are structurally perfect, monodisperse molecular species with well-defined dimensions, surface and interior. These characteristics make them interesting targets for various applications [52]. However, the feature size accessible with classical dendrimers is limited to a few nanometers due to the inherent problem of packing the increasing number of branches.

Hence, due to the quest for larger size, well-defined molecular objects with various conceptual extensions of the dendrimer concept, the idea of incorporating dendrimers into uniform branches of a comb polymer has been realized by a completely new polymer architecture referred to as “dendronized polymer”, or abbreviated “denpol” [53].

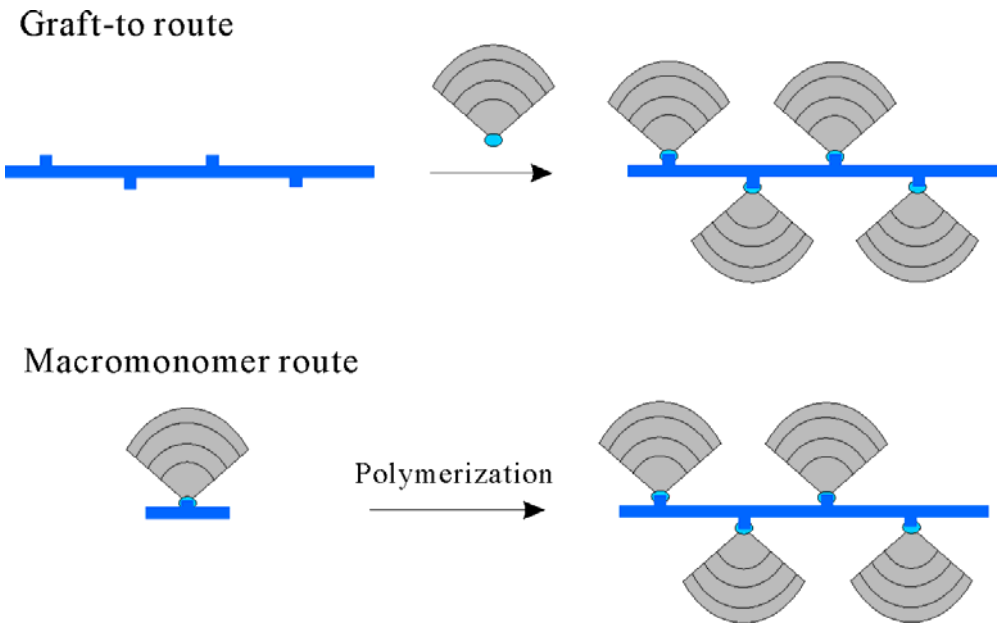

Figure 2.13: Schematic illustration of the two different general synthetic strategies toward dendronized polymers: the graft-to route and the macromonomer route.

2.2.3.1 Synthesis of dendronized polymers

There are two major strategies to synthesize denpols as shown in Fig. 2.13. One is the graft-to strategy, in which dendrons of the desired generation are coupled to the preformed polymer. The other is the macromonomer strategy in which dendrons of the desired generation are equipped with a polymerizable group at their focal point and polymerized.

In the graft-to strategy the synthesis starts from a preformed polymer chain with reactive functional groups along the backbone, ideally one at every repeating unit, to which the likewise preformed dendrons of the desired generation are then connected with their focal points in a single step. From the standpoint of polymer chemistry, the result is actually a graft copolymer rather than a structure perfect comb copolymer, with the preformed dendritic side chains being grafted to the polymer backbone. An obviously critical issue associated with this strategy is achieving complete coverage of the backbone anchor groups with dendrons. Even if a very efficient coupling chemistry is available, a large excess of dendron may be required to drive the reaction to completion. This excess may, in turn, make it difficult to purify the product. If large dendrons are to be attached, steric hindrance also comes into play due to the shielding of unchanged anchor groups on the backbone and the conformation of

the dendron, which may lead to a self-shielding of the functional group at the focal point through which the attachment should take place.

In the macromonomer strategy, the dendronized polymers are obtained via the attachment of a polymerizable group to the focal points of a preformed dendron and subsequent polymerization of the obtained 'macromonomers'. The term 'macromonomer' takes into account the oligomeric (dendritic) nature of the monomers, i.e. their already considerable molecular weight. The obvious advantage of this strategy lies in the fact that it does not involve a post-polymerization reaction. As a result, if a polymerization is feasible at all, the resulting polymers must, by definition, exhibit a quantitative degree of dendron attachment. Hence, they are 'structurally perfect' comb polymers. Of course, they are still not monodisperse due to the inherent polydispersity in molecular weight inevitably associated with any type of polymerization reaction. The macromonomer approach, however, has the decisive disadvantage that the steric demand of the dendrons will have a large effect on the kinetics of the polymerization reaction. Steric hindrance may inhibit a polymerization completely or lead to unexpected results, e.g. oligomeric products or very broad MWD. Nevertheless, recently more and more reports in the literature have shown that the macromonomer route is a more successful route; especially with the emerging advanced controlled polymerization it is possible to synthesize high generation denpols with several million g/mol molecular weight and PDI < 1.2 [54,55]. An example is the 4th generation PMMA shown in Fig. 2.14

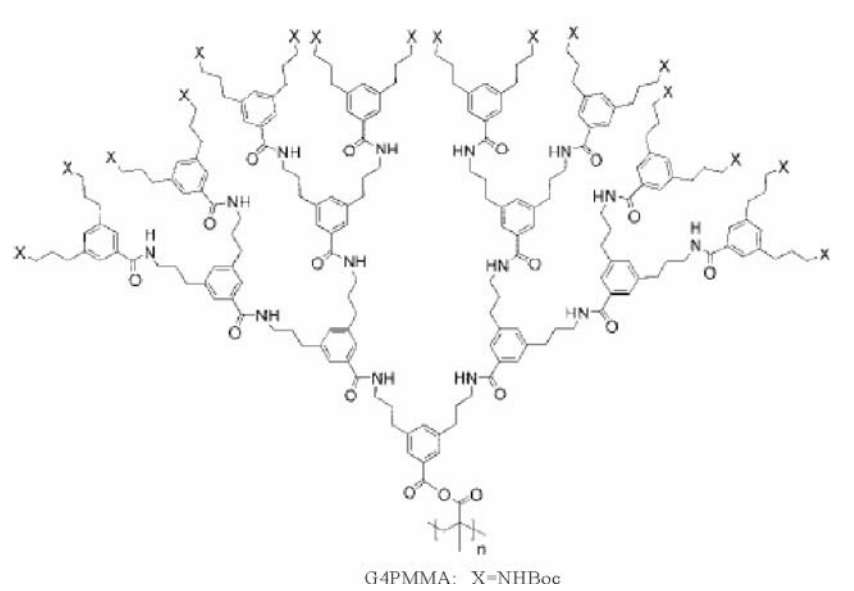

Figure 2.14: Structure of 4th generation dendronized PMMA [55]

2.2.3.2 Application of dendronized polymers

Dendronized polymers have a set of features which make them unique macromolecules and interesting candidates for a variety of applications. They are not only huge molecular objects with a cylindrical or near-cylindrical shape but their surface and backbone's chemical nature are engineerable as well. One of the most remarkable features is that high molecular weight, high generation dendronized polymers have been proven to be shape persistent, rigid, cylindrical molecular objects with a length close to the contour length of the polymer backbone, an almost monodisperse diameter defined by the length of the extended dendritic branches, and a densely packed surface. These objects are large enough to be readily visualized as individual molecules, sometimes exhibiting lengths of several hundred nanometers. Hence, denpols become very valuable as nanoscopic building blocks for self-assembled polymer systems.

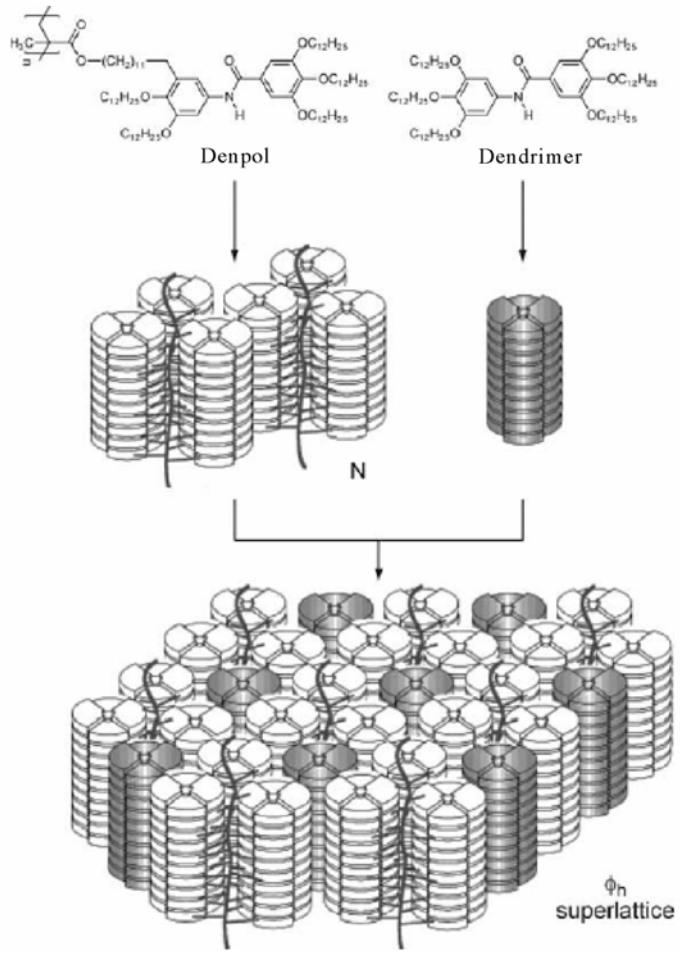

Figure 2.15: Co-assembly of dendronized polymers and dendrimers to form superlattice [56]

Dendronized polymers as amphiphiles with different hydrophobicity on core and shell are among the most interesting target structures. The exciting concept of amphiphilic nanoscopic cylinders with the propensity to segregate lengthwise was reported by Schlüter *et al.* [57]. Such polymers may be able to construct bundles and objects resembling ion channel in lipid membranes. One example as shown in Fig. 2.15 was reported by Percec *et al.* who synthesized dendrimers that were capable of self-assembling into cylindrical superstructures by a combination of hydrogen bonding along the cylinders' cores and π–π stacking of the dendrons. The dendrimers carried a polymerizable methacrylate unit on one of their peripheral branches and were subjected to radical polymerization. Samples of the pure dendronized polymers only exhibited a nematic LC phase but binary mixtures with low molecular weight dendrimers formed hexagonal columnar phases. The exact analysis of the XRD reflections led the authors to conclude that the polymers self-assembled into three-cylinder bundles. The fourth column constituting the unit cell of the hexagonal columnar phase was formed by low molecular weight dendrimers [56].

Another of the most remarkable features of denpols and an important difference to classical dendrimers, is their extremely high aspect ratio. They are not only molecular objects but also anisotropic nanoscopic objects, constituting a new link between the molecular and the nanoscopic scale. Hence such nanoscopic objects with highly dense chemical functionality on the backbone and periphery may be applied as functional materials. One obvious application of functionalized dendronized polymers is their use in catalysis. van Koten *et al.* have reported catalysis on the dendronized polymers' surface [58]. They made use of the amine functionalized G1–G3 dendronized polymers and decorated them with "NCN-palladium and platinum pincers" which previously had been successfully introduced into classical dendrimers [59]. Depending on the number of repeating units of the polymer and the dendron generation, thousands of catalytically active sites were created on the surface. Interestingly, the catalytic activity per metal center in a condensation of benzaldehyde and methyl isocyanoacetate was a little bit lower as compared to a low molecular weight catalyst, but it did not depend on the dendron generation. This was interpreted as evidence that, in fact, all metal centers were well accessible on the 'dense' surface and not buried in the polymer. There are many other sophisticated applications of denpols such as in optoelectronics, bioscience, single molecule reaction and surface patterning, which can be found in several reviews [18,54,55]. We will also introduce some examples in Chapters 2.3.2 and 2.4.3.

2.3 Self-assembly of polymers

As introduced in the last sub-chapter, self-assembly of dendronized polymers may be used to construct functional superstructures on mesoscopic scales. Therefore the question arises, what is self-assembly really meaning?

The terms “supramolecular chemistry” and “self-assembly” were introduced by Prof. Jean M. Lehn [60]. For millions of years, nature has capitalized on self-processing strategies based on non-covalent interactions, such as hydrogen bonds, salt bridges, hydrophobic interactions and even metal coordination, to organize biological systems. It is well known that the protein function largely depends on the global conformation of the protein, and the folding process is governed by a multitude of reversible non-covalent interactions [61]. The folding is guided by several elements of control, such as recognition and self-sorting, which lead the way to the desired shape. By learning these lessons from biology, chemists are starting to compose highly complex chemical systems from components that interact via non-covalent intermolecular forces.

Supramolecular chemistry has relied on more or less rigidly organized, synthetically built-up molecular receptors for effecting molecular recognition, catalysis, and transport processes and for setting up molecular devices [62]. The controlled build-up requires a system capable of spontaneously generating a well defined supramolecular architecture from its components under given conditions through self-processes. Thus, the spontaneous generation of self-processes led to implement the concepts of self-assembly [60,63].

For many years self-assembly techniques have been proven as technologically and commercially viable solutions for constructing hierarchical superstructures in which the advantages of conventional microelectronic technologies such as lithography and new nontraditional approaches can be merged effectively. A supramolecular polymer is a typical product based on self-assembly techniques. Supramolecular polymers are molecular assemblies, where large numbers of components assemble spontaneously into a polymeric structure that has reasonably well defined microscopic organization and displays characteristics typical of macromolecules, e.g., as far as rheology, fibre formation, glass and melting transitions, chain entanglement and high functionality/weight ratios are concerned. Since they exhibit these typical properties these extended-chain molecular assemblies are frequently referred to as “supramolecular polymers”. Examples are inorganic and

hydrogen-bonded multicomponent entities [Lehn90; Whitesides00] and interlocked mechanically linked compounds [Philp96] that would otherwise have been too difficult to construct. However, since self-assembly of supramolecular polymer is a so broad topic, based on the research presented in this thesis, the following will focus on introducing the self-assembly based on polymeric materials.

2.3.1 Self-assembly of polymeric supramolecules

The field in which supramolecular chemistry and polymer science meet has developed into a vast area of research, ranging from the study of interacting biomacromolecules, such as DNA and proteins, to the self-assembly of large synthetic macromolecules into well-defined architectures. Examples include the formation of PMMA stereocomplexes [64], and highly organized block copolymer architectures [65]. It should be noted that here the driving forces to fold macromolecules into well-defined conformations are non-specific intra- or intermolecular interactions, i.e. noncovalent interactions such as hydrogen bonding, π–π interaction, the hydrophobic effect and so on, which are used to functionalize covalently bonded polymers in a highly controlled fashion.

Block copolymers provide one the most well-known example for polymeric self-assembly due their ability to form ordered superstructures in a bulk state caused by the microphase separation of incompatible blocks. For instance, one of the blocks in a diblock copolymer being a stiff, rigid segment results in a rod-coil block copolymer. On the other hand π-π interchain interactions can also be employed as the major driving force to self-assemble conjugated macromolecules into specific structures, for instance 1D nanoribbon structures formed by hexyl-substituted poly(para-phenylene ethynylene) (PPE) [12]. Similarly to what has been observed for conjugated homopolymers, it has also been found that these rod-coil block copolymers self-assemble into nanoribbons. The nanoribbons form with block copolymers based on conjugated PPE, poly (para-phenylene) (PPP), or poly(fluorene) (PF) segments covalently linked to flexible chains, such as poly(ethylene oxide) (PEO) [66]. In these copolymers, the nanoscopic morphology can be tuned by varying the relative block volume ratio: with PF–PEO copolymers for instance, the fibrillar morphology survives up to a relative volume ratio of 0.3 in PEO, beyond which nm-thick platelets or mm-sized untextured polymer aggregates form, due to the assembly of PEO chains, which prevents π–π interactions from taking place [67].

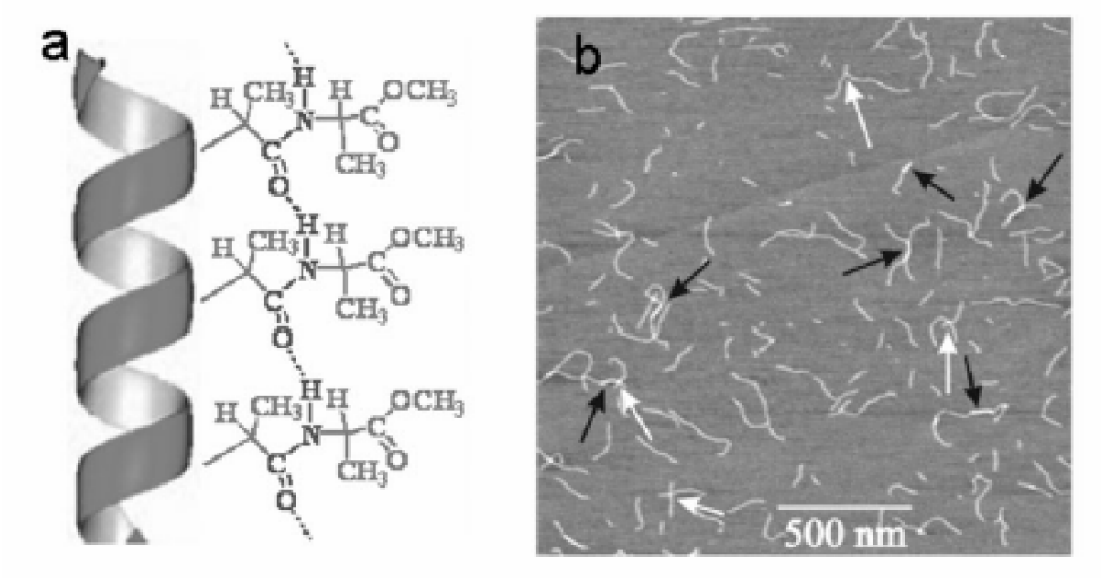

Figure 2.16: (a) Structure of poly(isocyano-L-alanine-D-alanine methyl ester) (PIC) showing the hydrogen-bonded array within the side chains of the polymer. (b) SFM image of a PIC sample. Film prepared from a chloroform solution containing 0.01 g/L of PIC–Ni. White arrows indicate intersections of separate chains and black ones mark segments consisting of intercoiled chains [10].

Another kind of polymeric self-assembly results from self-organization of single polymers. The helical conformation of polymer chains results from hydrogen bonding on side chains or some steric restrictions due to the presence of bulky substituents in the side chain, and/or a hindered rotation around single bonds in the backbone. Most polymers were made from optically active monomers, often employing chiral initiators or catalysts (asymmetric polymerization) to produce an excess of helices with one screw sense. Considerable work has been devoted to polymethacrylates, polyaldehydes, polysilanes, and polyisocyanides, [64,68]. For example, isolated polymeric chains of poly(isocyanodipeptides) (PICs), as shown in Fig. 2.16 are equilibrated in quasi 2D on cleaved mica surfaces. It was revealed that the chains exhibit a persistence length l_p of 76 nm, which indicates that these single polymer molecules are very rigid, even more than double-stranded DNA. Rigidity was attributed to the helical structure of the polymer backbone and, in particular, to the hydrogen-bonded network present between the alanine moieties in the side chains [10].

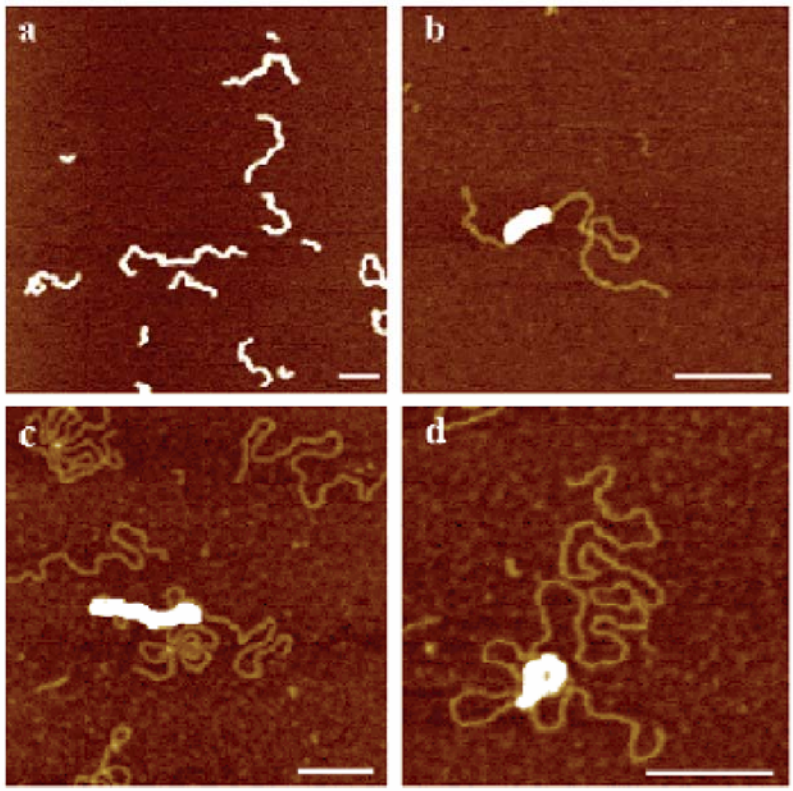

Figure 2.17: SFM images of (a) fourth-generation dendronized polymer (PG4) deposited onto freshly cleaved mica. (b–d) DNA–PG4 complexes of charge ratio 1:0.7 precipitated onto poly-L-ornithine-coated mica [69].

While helical architectures based on single polymers are already a great challenge, the formation of helical motifs from two polymers is even more difficult. The Rabe group has shown that the control over the electrostatic interactions between macromolecules allows to form helical supramolecular architectures by mixing synthetic and biological polymers. This was demonstrated on positively charged G4 dendronized polymers, which were found to be able to complex with DNA, forming cylindrically shaped nano-objects as shown in Fig. 2.17. For the different dendron generations, it was proposed that the interplay between the electrostatic energy and elastic energy defines both the overall charge of the complex and the different pitch sizes for the wrapped DNA [69]. The dendronized polymers together with DNA are a useful model system to test theories on the interaction of oppositely-charged polyelectrolytes. Moreover, this novel complex might be used for nonviral gene delivery systems and help to optimize the transfection efficiency based on the structure of the vector system.

Presented above are just a few highlights among many self-assembled polymeric supramolecules. Self-assembly of polymeric supramolecules became a powerful tool for

producing functional materials that combine several properties and may respond to external conditions. Hierarchically structured materials obtained by applying different self-organization and recognition principles can eventually form a basis for tunable nanoporous materials, smart membranes, preparation of nano-objects, and nanoelectronics [70,71].

2.3.2 Polyeletrolyte Amphiphile Complexes (PACs) through ionic self-assembly

As described above, in classical supramolecular chemistry the interactions are usually hydrogen bonds, metal coordination binding, or hydrophobic association. However, these short range interactions are either relatively weak (< 50 kJ/mol) or very selective. The employment of Coulombic interactions for self-assembly of building blocks – so called ionic self-assembly has been for a long time underestimated in supramolecular chemistry [72]. Different to simple salt association, ionic self-assembly not only results from the non-selective and long range character of the Coulombic interaction, it also has to make use of distinct geometric shapes, functionality patterns, and distributions of cohesion energy along the charged objects, in which the secondary structural elements support the alignment, driven by the charge-charge coupling [72].

Among many examples of ionic self-assembly, the self-assembly of amphiphiles with polyeletrolytes towards complexes with a well-defined nanostructure is presumably the most well-known and best examined case [73]. Polyelectrolytes are polymers containing electrostatic charges along their chain. Typical synthetic polyanions include (with the corresponding counter ions) poly(stytrene sulfonate), polymethacrylate and polyacrylate, and as natural examples DNA and polyglutamate; typical synthetic polycations include polyethyleneimine, poly(N-alkyl vinyl pyridine), polyaniline, and polypyrrole, and as natural examples polylysine and poly-L-Ornithine. The oppositely charged amphiphiles in the complexes are amphiphilic molecules consisting by definition of a hydrophilic ‘head group’ and a hydrophobic ‘tail’, which are usually alkyl chains. They are typically referred to as chemical surfactants [74]; examples are alkylated sulfate, phosphonate, phosphate, and carboxylic acids as anionic surfactants or alkylated quaternary ammonium salt, alkylated primary amine as cationic surfactants, or biological lipids [75].

2.3.2.1 Formation of Polyelectrolyte Amphiphile Complexes

The relatively facile formation of complexes of amphiphiles with oppositely charged polyelectrolytes occurs spontaneously in a variety of technological processes and formulations including the production of photographic film, cosmetics, paper manufacture, and food science, among many other well-known technologies. Their structure depends greatly on the competition between the rate of complex formation and the rate by which a thermodynamically equilibrated complex phase is eventually formed [76]. Basically, when a polyelectrolyte solution is added to an oppositely charged amphiphile solution or vice versa, Polyelectrolyte - Amphiphile Complexes (PACs), as driven by both electrostatic and hydrophobic interactions, will be formed spontaneously. The complexation occurs at concentrations much below the critical micelle concentration (CMC) of the amphiphiles in the external phase. The binding process of amphiphiles to polyelectrolyte chains is highly cooperative. The resulting complexes, produced during the combined use of polyelectrolytes and amphiphiles in the same process, may be either soluble or insoluble depending on the precise stoichiometry of the reactants. The non-stoichiometric complexes containing excess surfactant molecules or charge sites of polyelectrolyte chains are generally soluble in water [77]. Near the stoichiometric charge ratio, the complexes are insoluble in water. The precipitated complexes can be easily isolated, purified, and dried to form solid materials.

As described above, the addition of a surfactant to a polyelectrolyte is in principle quite simple, but there exist several routes to complex formation. Most researchers add aqueous solutions of polyelectrolyte to amphiphiles to form the complex using metathesis (or ion exchange). For example, if the salt of poly(acry1ic acid) and a quaternary ammonium salt are mixed, a gel will form when the polyelectrolyte and amphiphile are added in stoichiometric quantities. The gel is then extracted until no more soluble amphiphile can be removed. The resulting purified gel is dried to form a solid with properties varying from elastomeric to brittle and from crystalline to non-crystalline depending on the components of the complex. This simple process is subject to many variations depending on the nature of the polyelectrolyte, the surfactant and the counterions. Examples of synthetic complexes are dominated by polyanions based on poly(acry1ic acid) derivatives and salts of poly(styrene sulfonic acid). The use of multivalent counterions complicates the complex-forming process. Polycations have also been used as the polyelectrolyte in complex formation and are also described above along with possible counterions. There are generally more examples of complexes based on polycations described in the literature. Of particular

interest are conjugated polycations which can be simultaneously doped during complex formation. Such complexes have been used to produce processable conducting polymers and blends; for example, the complexes, prepared by Wegner and coworkers, could be prepared as self-supporting films by electrochemical polymerization of pyrrole in water in the presence of an anionic surfactant, for example, Sodium Dodecyl Sulfate. The resulting polypyrrole was a stable, conducting polymer with tailorable conductivity [78].

In addition to metathesis, several other processes are conceivable. This includes neutralization, chemical change, redox chemistry, and quaternization reactions [76]. Several of these processes are not necessarily solution reactions, and may be carried out in the polymer melt or at the interface of two immiscible solutions. This can be an advantage when processing new materials. Several factors in complex formation should be commented on at this point. In the studies of PACs of conducting polymers described above it has been observed that conductivity suddenly jumps when the mixture is heated above a certain temperature [78]. After cooling, the enhanced conductivity remains as an indication of an organizational change in the complex. This effect is associated with a kinetically-controlled change in complex structure and a competition between kinetic and equilibrium effect is therefore present in these and other types of complexes. It is therefore important that care is taken in the analysis and assessment of complex structures in polyelectrolyte - amphiphile mixtures as they may not be in equilibrium. Despite the many possible synthetic strategies, the majority of complexes are still produced using the ion exchange or metathesis reaction.

2.3.2.2 Application of Polyelectrolyte Amphiphile Complexes

Among the mostly investigated PACs are systems containing biological or naturally occurring polyelectrolytes for their ability to serve as drug delivery systems. For example Safinya and co-workers complexed positively charged lipids with DNA and found interesting, highly organized packing motives [79]. These structures are currently being discussed as vehicles for gene delivery. Synchrotron Small-Angle X-ray scattering (SAXS) has been used to study the self-assembled structures of globular particles of DNA - cationic liposome complexes with sizes of a few hundred nanometers in 1 wt.-% aqueous solutions [79,80]. A multi-lamellar structure (L_α) with alternating lipid bilayer and DNA monolayers was revealed. Later, a 2D hexagonal columnar structure (H_{II}) - consisting of DNA coated by cationic lipid monolayers and arranged on a hexagonal lattice - was derived from synchrotron SAXS. The structural transition from the lamellar to the columnar inverted

hexagonal could be induced by two pathways: i) driving the natural curvature of the cationic lipid DOTAP (dioleoyl trimethylammonium propane) monolayer to negative charged polymer by the addition of the neutral helper-lipid DOPE (dioleoyl phosphatidylethanolamine), and ii) reducing the membrane-bending rigidity by the addition of neutral helper-lipids DOPE and the cosurfactant of hexanol. Fig. 2.18 shows two distinct pathways to induce the structural transition from L_α to H_{II} for the DNA - cationic liposome complexes.

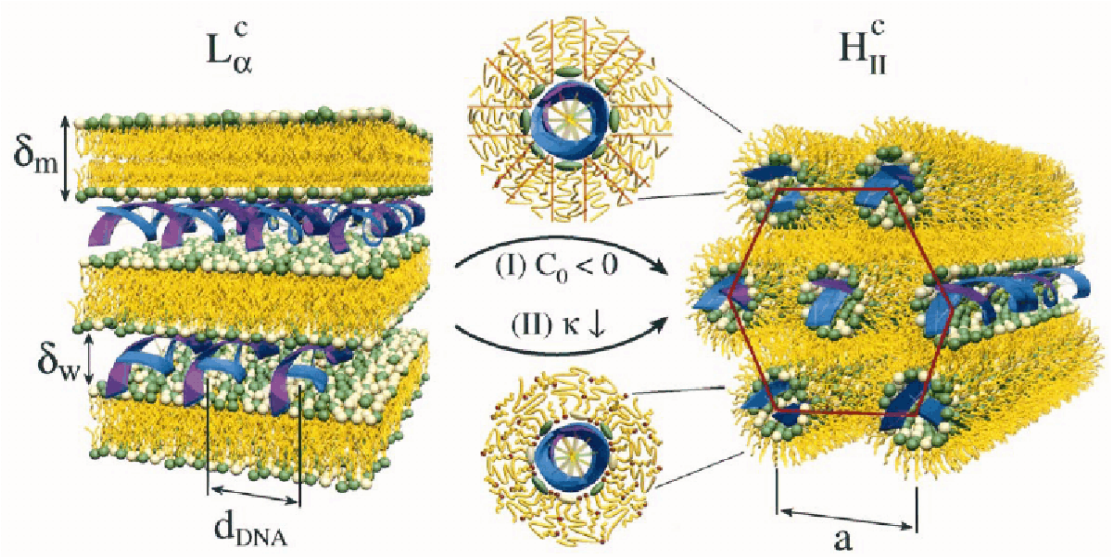

Figure 2.18: Schematic diagrams of two distinct pathways to induce the structural transition from the lamellar L_α to inverted 2D hexagonal H_{II} for the DNA-cationic liposome complexes [80].

Recently Severin *et al.* have found that the nanostructure of PACs can also be influenced by application of a substrate. The PAC used here consists of a poly(styrene sulfonate) (PSS) backbone complexed with cationic amphiphiles trimethylhexadecyl-ammonium bromide (C_{16}TAB), which are attached to the polymer backbone through electrostatic interactions of ammonium head groups and the oppositely charged sulfonate groups. PACs assemble into raftlike structures of highly oriented and fully extended PACs on a graphite surface, when spin-coated from chloroform solution [81]. The stretching of PACs is attributed to the interaction of the alkyl tails of the amphiphiles with the substrate. The formation of the raftlike structures is related to the initial mobility of PACs on the surface. As shown in Fig. 2.19, the self-assembly of rafts is accompanied by length segregation of PACs, such that PACs of similar length tend to be neighbors in the structure. The spacing of amphiphile molecules in a crystalline monolayer on graphite is close to the projected length of two PSS repeat units in the preferred anti conformation. Assembly of the amphiphiles along the

lattice axis in two parallel, head-to-head oriented, staggered rows, therefore, causes efficient stretching of the PSS backbone. In fact, the PAC on the surface may be regarded as an overstretched helix. The straightening leads to the organization of PACs into rafts because it eliminates the conformational entropy cost that works against ordering. Therefore the raft formation corresponds to a self-sorting process. Self-assembly of PACs on surfaces will provide an interesting opportunity to control the size of the aggregates, for instance, for the fabrication of well-defined nanoarchitectures by self-assembly and further molecule manipulation on the surface.

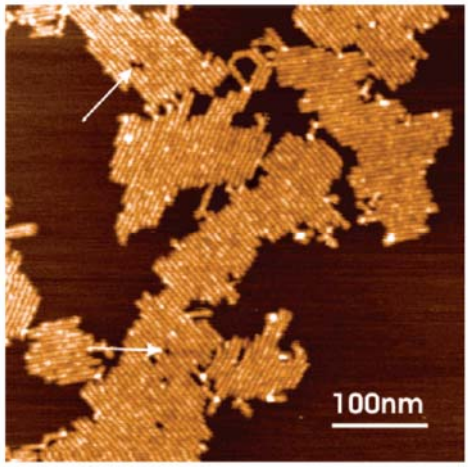

Figure 2.19: Raftlike PAC structures on graphite. The rods are considered to be single PACs. Most PACs neighbor exactly one PAC on each side: only in a few cases, a longer PAC neighbors several shorter PACs as indicated by the arrows. PACs follow the hexagonal symmetry (60° rotational symmetry) of the graphite substrate [82].

A tremendous amount of research papers on PACs has been published in the last 20 years. The building of various highly ordered structures in complexes with special mechanical, electrostatic, interfacial, optical, and biological properties remains an exciting field. The modification of molecular architecture of polyelectrolyte chains and amphiphiles may be of future interest for exploring more assembly structures and functions of the PACs in nanoscience. On the other hand, the DNA – cationic lipid complexes used in gene therapy are a special type of PACs. The structural study of DNA - lipid complexes at the molecular assembly level is very important for understanding structure-activity relationships and future applications.

2.4 Single molecule manipulation

Many structures or devices used in modern industry are becoming progressively smaller and have reached the scale of nanometers. One approach for the creation of such nanostructures is the assembly from atomic- or molecular sized components, known as the bottom-up approach. The development of self-assembly of molecules has provided such an opportunity to build and control molecular nanostructure with high complexity. At the same time, since the invention of Scanning Tunneling Microscope (STM) in the early 1980s, the emerging development of a Scanning Probe Microscope (SPM) based technology provides another great opportunity to control molecular nanostructure in a more direct route. A promising strategy is using SPM as a manipulation tool to move and position single atoms or molecules for patterning nanoscale structures. The SPM-patterned nanostructures can be asymmetric with different functionalities and are less restrictive than those built by self assembly, which are normally regular and symmetric [83].

The manipulation method based on SPM originated from STM lithography with atomic resolution. However, STM manipulation is severely restricted by the environmental conditions and the requirement of conductive substrates. With its inception in the middle of the 1980s, Scanning Force Microscopy (SFM) makes the manipulation of single molecules and even single macromolecules possible. The SFM based techniques are less restrictive than those based on STM because SFM can be conducted in a normal room environment and is not limited by the conductivity of the employed materials. Therefore in the following the focus will be on the manipulation based on SFM, with at first the Scanning Force Microscopy technique being introduced.

2.4.1 Scanning Force Microscopy

Microscopy is undergoing a remarkably innovative period, deriving in large part from the invention by G. Binnig and H. Rohrer (Nobel Prize in Physics in 1986) of the Scanning Tunneling Microscope (STM) in 1982 [1] and the creation of the Scanning Force Microscope (SFM) [2] in 1986 by Binnig, Quate and Gerber. The Scanning Force Microscope, also well known as Atomic Force Microscope (AFM), has provided new opportunities for studying surfaces with sub-nanometer resolution by scanning over them very gently with a tip. In fact the physical properties that are measured with this apparatus, namely the interaction forces between a sharp conical tip and the sample surface, allow

investigations to be performed on ionic crystals, on organic molecules and also on biological materials.

A schematic representation of an SFM is shown in Figure 2.20. SFM probes the surface of a sample with a sharp tip with a terminal radius on the order of 10 nm. The tip is located at the free end of a ~ 100 µm long cantilever that exhibits an elastic modulus that can reach tens of N/m. A piezo element is used to move the tip or substrate very accurately line by line with sub-Ångström precision. The scanning range may span from a few tens of nm to a few tens of micrometers. While scanning, forces of a few pico-Newton between the tip and the sample surface cause the deflection of the cantilever on the Ångström spatial scale. A laser beam bounces off the back of the cantilever onto a position-sensitive photo diode detector. As the cantilever bends, the position of the laser beam on the detector shifts (see Fig. 2.20). The photodetector itself can measure displacements of light beams as small as 1 nm. The ratio of the path length between the cantilever and the detector to the length of the cantilever itself produces a mechanical amplification. As a result, the system can detect sub-Ångström vertical movements of the cantilever tip. The measured cantilever deflections enable the computer to generate a map of the surface topography.

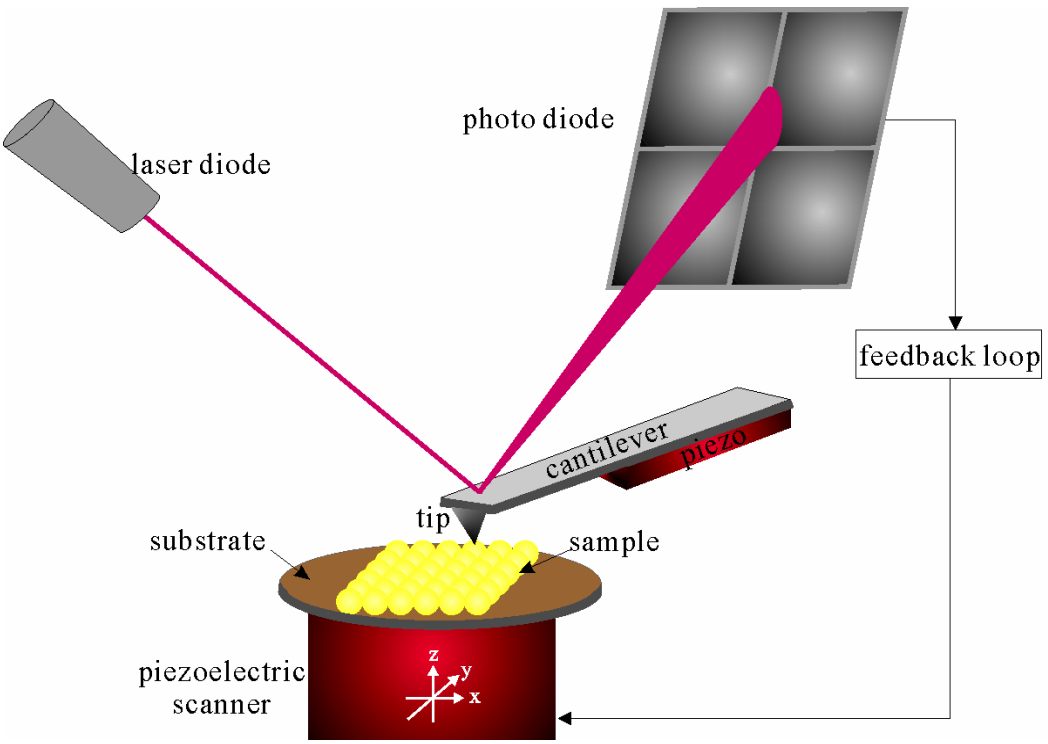

Figure 2.20: Schematic setup of SFM

2.4.1.1 Interaction forces

Many different forces play a role in the interaction between tip and sample. It is important to distinguish the type of forces in order to separate the contributions and correctly interpret the experimental results [84]. Principally they can be divided in long range forces (including van der Waals force, electrostatic force, capillary force, etc.) and short-range forces (hard core repulsive force, covalent bond, metallic adhesion, friction force, etc.).

Among long-range forces, the van der Waals force plays the most important role, since van der Waals forces exist between every type of atoms or molecules. They are proportional to $1/r^6$ where r is the distance between them, and important in the range from fractions of one to tens of nanometers. On the other hand, among the short-range forces, repulsive forces play the most prominent role on the short range. They are roughly proportional to $1/r^n$ with $n > 8$. The interatomic repulsion forces have two origins: a) Repulsion between nuclei: the overlap of two electronic clouds gives rise to an incomplete screening of the nuclear charges; this generates columbic repulsions; b) Pauli repulsion: according to the exclusion principle of Pauli, two electrons with the same spin cannot occupy the same orbital. Thus the electrons can only overlap when the energy of one electron is increased, which causes a repulsive interaction.

The main forces contributing to the deflection of an SFM cantilever are therefore often the van der Waals and the repulsive forces, which define the Lennard - Jones potential:

$$\varepsilon(r) = -4\varepsilon_0\left[\left(\frac{\sigma}{r}\right)^6 - \left(\frac{\sigma}{r}\right)^{12}\right] \qquad \text{(Eq. 2.5)}$$

with: ε_0 = potential energy at the minimum;

σ = effective molecular diameter;

r = interatomic distance.

The force, which is the negative gradient of the energy, is plotted in Fig. 2.21. Two distance regimes are highlighted: 1) the contact regime, and 2) the non-contact regime. In the contact regime, the cantilever is held less than a few Ångström from the sample surface, and the interatomic force between the cantilever and the sample is repulsive. In the non-contact

regime, the cantilever is held on the order of a few to a few 10 nanometers from the sample surface, and the interatomic force between the cantilever and sample is attractive. In between these two regimes there is the intermittent contact regime, in which the so called Tapping Mode™ is operating.

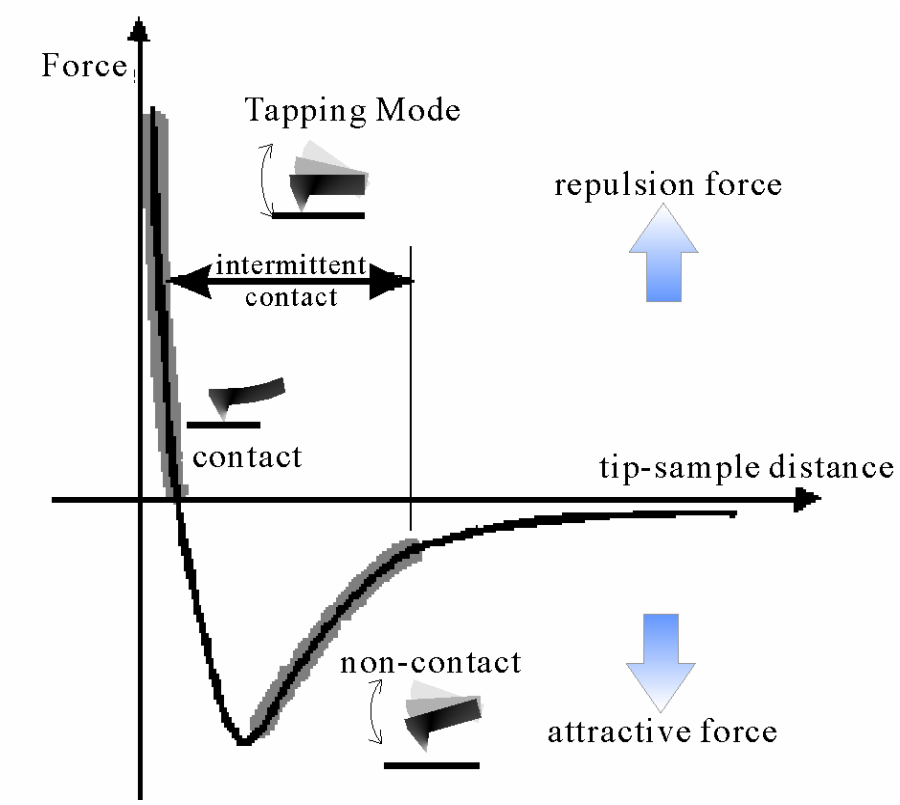

Figure 2.21: Dependence of interatomic force on distance and the regimes of SFM operation.

2.4.1.2 SFM operation modes

Depending on the samples and the sample properties that should be measured, different SFM operation modes can be used. There are three main modes: contact mode, non-contact mode and tapping mode as illustrated in Fig. 2.21.

1. Contact mode

In the contact mode the SFM tip makes soft "physical contact" with the sample. The tip is attached to the end of a cantilever with a spring constant lower than the effective spring constant holding the atoms of the sample together. As the scanner moves the tip across the sample (or the sample moves under the tip), the interaction forces cause the cantilever to

bend, in order to follow the topographic profile. Thus in *constant height mode*, the cantilever deflection reflects the topography of the sample surface. In this mode the tip scans at a constant height from the surface. In *constant force mode*, the deflection of the cantilever is used as input to a feedback loop, which acts on the piezo translator. The piezo translator moves up and down in z-direction, responding to the topography, in order to keep the cantilever deflection constant. In this case, the image is generated from the scanner's motion in the vertical direction. With the cantilever deflection held constant, the total force applied to the sample is constant. The major shortcoming with contact mode is that the movement of the tip can introduce large frictional (shearing) forces on the sample, and that the sample can suffer from the effect of capillary forces, pulling the tip down to the surface.

2. Non-contact mode

In order to measure the local electric or magnetic properties of a sample surface, the non-contact mode is used. In non-contact mode, the tip is set close to the surface, but not in contact with the sample, and either the coulombic or the magnetic interaction between tip and sample is measured (known as Electric Force Microscopy and Magnetic Force Microscopy, respectively). In non-contact mode, the tip samples the surface in the attractive region of the Lennard-Jones potential. Thus the effect of friction and the capillary forces are minimized while the effect of the electric force or the magnetic force is emphasized. Since the tip does not contact the sample, the sample surface is not damaged during the experiment.

3. Tapping mode

In recent years tapping mode has attracted increasing attention. Tapping Mode SFM has been invented [85] in order to overcome the problems of frictional forces in contact mode. In tapping mode, the cantilever is forced to vibrate in the intermittent-contact operating region as is indicated in the force-distance curve. A rather stiff cantilever has to be used because soft cantilevers may be pulled into contact with the sample surface. The cantilever is forced to oscillate near its resonant frequency with an amplitude of a few ten nanometers. The piezo material attached to the SFM cantilever controls the oscillation of the cantilever as shown in Fig. 2.20. While the tip scans over the sample the system detects the shift in the phase and the amplitude of the swing of the cantilever and keeps it constant with the help of a feedback system that moves the scanner up and down (see Fig. 2.20). By keeping the amplitude

constant, the system keeps the average tip-to-sample distance constant. The sensitivity of this detection scheme provides sub-Angstrom vertical resolution in the image, as in contact mode SFM. Since the oscillation frequency of the tip is very high compared to the scan speed (1-2 lines/s), the frictional forces can be negligible. Because of the overall reduced interaction forces between tip and surface, tapping mode is particularly useful for studying soft materials such as biological and organic molecules. Also as a consequence of the reduction of the overall interaction, this mode suffers less from tip or sample degradation effects that are sometimes observed after taking numerous scans with contact SFM.

2.4.2 Adsorption

The prerequisite for a successful SFM investigation of molecules is the proper adsorption of the molecules on a substrate. Depending on the nature of attractive forces existing between the adsorbate and adsorbent, adsorption may be classified in two limiting cases.

i) Physical adsorption (Physisorption)

In physical adsorption, the forces of attraction between the molecules of the adsorbate and the adsorbent are long range, such as van der Waals attraction, which is typically realatively weak. Normally physisorption does not need to overcome an activation barrier. Since the forces of attraction are long range and weak, the process of physisorption allows multilayer formation and can be easily reversed by heating or delution of a supernatant solution. Adsorption is generally accompanied by the release of free energy, i.e. most adsorption processes are exothermic in nature. However, the entropy change associated with adsorption is generally negative because the adsorbate molecules lose their translation freedom when they get attached to the surface of the adsorbent. Therefore, in order to keep ΔG to be negative, the enthalpy change (ΔH) must be sufficiently negative, i.e. $\Delta G = \Delta H - T\Delta S < 0$. This explanation accounts for the exothermic adsorption processes. The enthalpy of adsorption, which is the enthalpy change for the adsorption of one mole of an adsorbate on an adsorbent surface, is usually in the range of 20 kJ/mol to 40 kJ/mol for physisorption [86]. The adsorption of ordered alkane chains on graphite is a typical example of physisorption ([21] and refs therein).

ii) Chemical adsorption (Chemisorption)

In chemisorption, the forces of attraction between the adsorbate and the adsorbate are short range and relatively strong; the molecules of the adsorbate form chemical bonds such as covalent, ionic or metallic bonds with the molecules of the adsorbate present on the surface. The reaction with the surface is dependent on the chemical species involved. The enthalpy change for the chemisorption is usually in the range of 200 kJ/mol to 400 kJ/mol [86]. Chemisorption is often irreversible and monolayer limited.

In case of a particle adsorbing from its solution onto a solid surface, the first stage is to come into contact with the surface. The particle needs to be trapped onto the surface by not possessing enough energy to leave the surface potential well. If it elastically collides with the surface, then it would return to the bulk liquid. If it loses enough momentum through an inelastic collision, then it "sticks" to the surface, forming a precursor state bonded to the surface by weak forces, similar to physisorption. The particle diffuses on the surface until it finds a deep chemisorption potential well. Then it reacts with the surface or simply desorbs after some time into the liquid. Self-assembly of alkanethiols at Au (111) surfaces shows a typical picture of the adsorption process including physisorption, chemisorption and a polar interaction (Fig. 2.22).

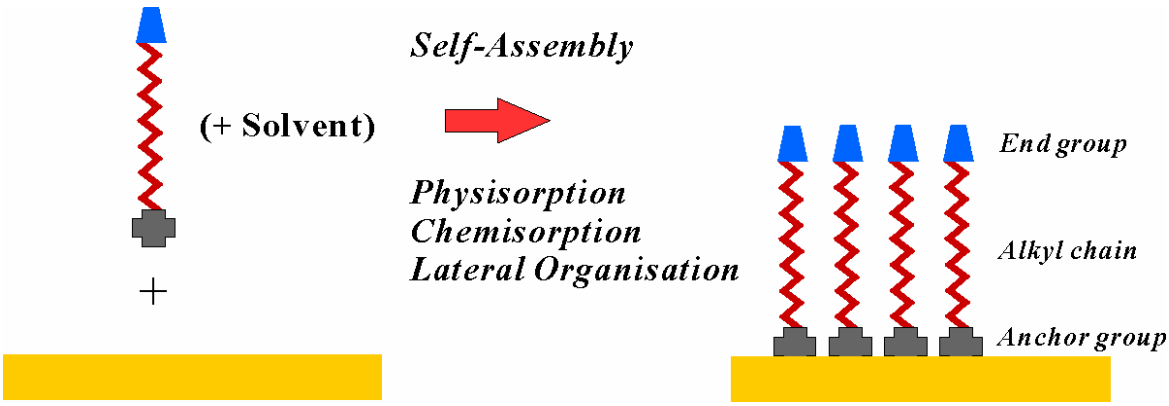

Figure 2.22: Schematic illustration of self-assembly of alkanethiols on Au (111) surface.

2.4.3 Manipulation of single molecules on surfaces

Compared to higher resolution STM manipulation, SFM manipulation can have higher scan speeds on any kind of surfaces in ambient conditions, thus it fits well for the application to single molecule manipulation.

In most SFM manipulation experiments, elaborate chemistry is required to treat the surface and tools. With the aid of chemically induced forces, the manipulation of single or multiple molecules become manageable. One of the most popular methods of SFM manipulation on surfaces is the Dip-Pen Nanolithograpy (DPN). This SFM-based lithography technique was discovered by the Mirkin group [14]. DPN is a scanning probe nanopatterning technique in which an SFM tip is used to deliver molecules to a surface via a solvent meniscus, which naturally forms in ambient atmosphere. This direct-write technique offers high-resolution patterning capabilities for a number of molecular and biomolecular 'inks' on a variety of substrate types such as metals, semiconductors, and monolayer functionalized surfaces.

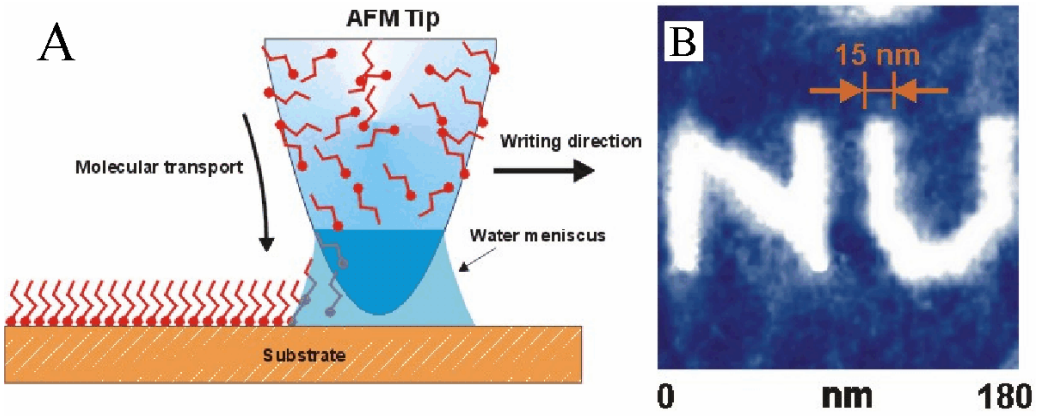

Figure 2.23: (A) Schematic illustration of DPN; (B) Ultra-high resolution pattern of mercaptohexadecanoic acid on atomically-flat gold surface [14].

As illustrated in Fig. 2.23 (A), the water meniscus acts as a bridge over which the ink molecules migrate from the tip to the substrate surface where they are self-assembled or anchored; an example is l-octadecanethiol as ink on a gold surface. The tiny meniscus is critical in defining the limit of the resolution of DPN. Using a conventional SFM it is possible to achieve ultra-high resolution features – as small as 15 nm line widths and 5 nm spatial resolution are shown in Fig. 2.23 (B). The capillary transport from the probe towards the tip apex provides a resupply of new molecules for a continuous writing. The molecules and substrates are chosen in order to have chemical affinity and favorable adhesion of the

deposited film. Rigorously speaking, in DPN, the ultimate patterning ability is dependent not only on the tip-adparticle manipulation but also on the self-assembly ability of the admolecules (coated ink molecules) with the substrate. Since atomic or molecular manipulation is a time consuming process, using DPN with its self-assembly ability can shorten the patterning process to have a higher fabrication throughput. Consequently, the increase of the patterning speed in DPN can be considered as the self-assembly effect on patterning.

Besides using the meniscus between an SFM tip and a substrate, one may also use a strong interaction between the tip and the molecule for irreversible modification of the molecule surface or conformation. Thereby one is able to structure matter with the SFM tip-induced manipulation. SFM tip-induced manipulation on a surface is a non-destructive manipulation of molecular conformations in spite of strong tip sample interaction. To achieve this purpose an intermediate interaction between sample and surface should carefully designed. Recently our group has developed such a system based on the mild interaction between long alkyl chains and the atomically flat basal plane of HOPG. Single macromolecules grafted with long hydrocarbon chains such as dendronized polymers can be physically adsorbed to the HOPG surface. However, the immobilization is weak with respect to the strong lateral tip-sample interaction, which can be turned on with the SFM. Thus, by applying SFM in contact mode with a strong lateral force, the polymer chain can be moved to desired positions or conformations; then by switching the SFM to the tapping mode (intermittent contact mode), which only exerts a weak lateral force to the polymer chain, it can be used to immediately visualize the surface [13].

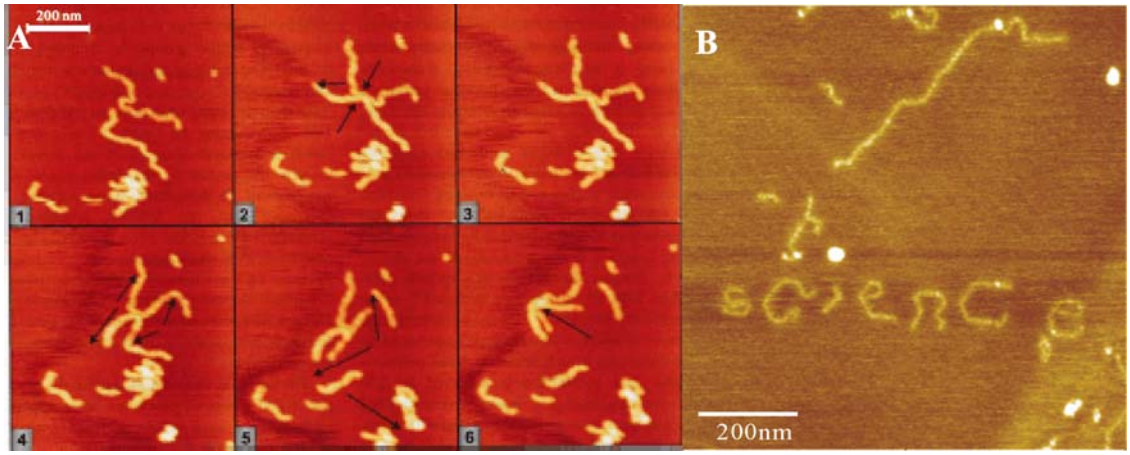

Figure 2.24: (A) A sequence of tapping mode SFM images of dendronized polymers on HOPG in a "move-connect-prove" circle, black arrows indicate the moving traces of SFM tip in contact mode [15]; (B) Tapping mode SFM image of ds-DNA on dodecylamine coated HOPG surface after SFM tip manipulation [22].

Fig. 2.24 shows two examples of this manipulation. In Fig. 2.24 (A) Barner *et al.* had moved individual dendronized polymer molecules across an HOPG surface in a predetermined way, and then this movement of a molecule was combined with a chemical reaction within the SFM [15]. The experiment proceeded in a 'move-connect-prove' sequence. Two strands of alkylated dendronized polymers, decorated with photosensitive azide groups in some of their peripheries, were brought into tight contact using the SFM tip, and then exposed to UV irradiation (Fig. 2.24 (A) 1-3). Thus, the azides were converted to highly reactive nitrenes that exhibit a very high, non-selective reactivity toward almost any other functional group in close proximity. While reactions take place intramolecularly in both polymer strands, also an intermolecular reaction will occur at the site where the two strands are in intimate contact. In order to prove that the covalent linkage of the two strands had been successful, the resulting four segments were moved with the SFM tip again. Even extreme mechanical stress did not lead to a rupture of the two strands (Fig. 2.24 (A) 4-6). By contrast, in a control experiment without UV irradiation, the two strands were easily separated again. Fig. 2.24 (B) shows another strategy to achieve SFM tip manipulation on a surface [22]. Instead of chemically grafting hydrocarbon chains on a polymer Severin *et al.* have deposited ds-DNA on $C_{12}H_{25}NH_2$ (dodecylamine) precoated HOPG. Under ambient conditions ds-DNA chains and protonated dodecylamine chains form polyelectrolyte amphiphile complexes (PACs) on the surface as described in *Chapter 2.32*. The formed PAC chains can be easily manipulated by the SFM tip in contact mode and stably imaged SFM in tapping mode; furthermore by tuning the SFM tip moving velocity and the tip deflection, the polymer chains can even be cut by

the SFM tip. Thus a long ds-DNA chain was cut into pieces and moved to designed topology, with the result shown in Fig.2.24 (B).

To summarize, it was demonstrated that SFM might find an application that goes far beyond the mere analysis of molecular structure and toward its manipulation. This represents a step towards the construction of even more sophisticated nanoscopic objects in a true bottom-up approach. Manipulations performed on single polymeric chains may allow to probe the mechanical properties of supramolecular architectures and to construct more and more complex species via reactions on and at surfaces, which could combine the formation of covalent and noncovalent bonds in a hierarchical fashion.

2.4.4 Manipulation of single molecules in solutions

After introducing the manipulation of single molecules on surfaces, which provides a bottom-up approach to construct complex nanostructures, also another aspect of single molecule manipulation should be introduced – manipulation of single molecules in solutions. The manipulation is performed in solution because the main purpose of this manipulation is to carry out force spectroscopy of single molecules, especially bio-molecules in their native environment. Today, a number of techniques differing in force and dynamical ranges are available, the most prominent of which are magnetic beads [30,87], optical tweezers [28,88], glass microneedles [89], and SFM cantilevers [90,91], as shown in Fig. 2.25. The single molecule manipulation techniques require two basic elements: a probe, which is usually of microscopic scale, which can generate or detect forces and displacements, and a way to spatially locate the molecules [23]. Usually the molecule is fixed to the surface by one end, and the other end is fixed with a force transducer. Force transducers apply or sense forces through the displacement of a bendable beam. The most common examples are SFM cantilevers and microneedles. The spatial control of transducers can be accomplished efficiently by piezo electrical positioner.

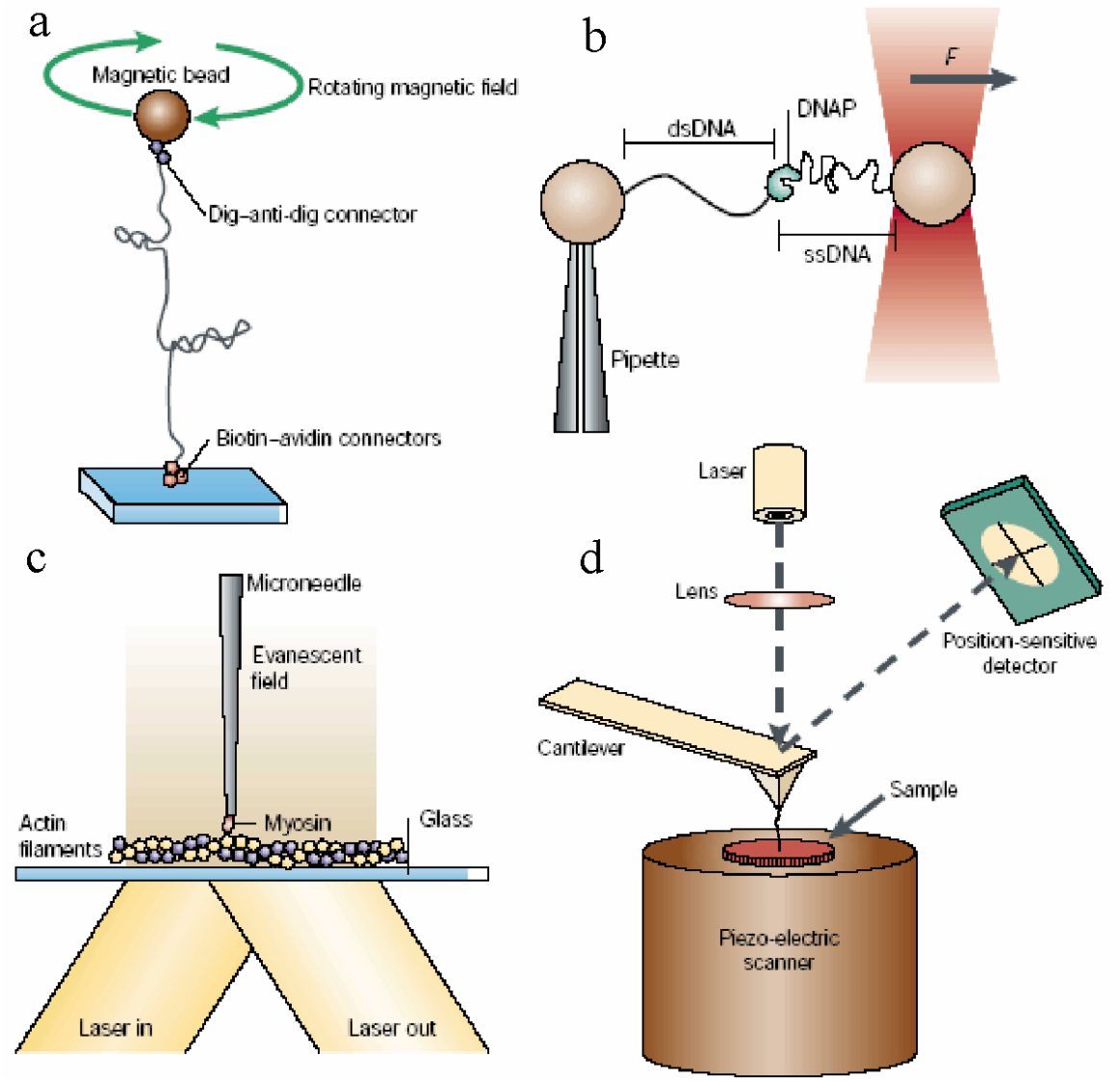

Figure 2.25: Illustration of typical single molecule manipulation methods (after [23]): (a) A magnetic bead experiment in which a rotating magnetic field is used to under- or overwind ds-DNA attached between the glass slide and a magnetic bead [30,87], the resulting supercoils (plectonemes) can be studied by measuring the displacement of the bead perpendicular to the glass slide as a function of the magnetic force; (b) An optical tweezers experiment in which a single stranded DNA molecule, bound with a primer, connects a polystyrene bead fixed at the end of a micropipette and a polystyrene bead held in the optical trap. A feedback circuit is used to keep the DNA molecule at a fixed tension, F. As the DNA polymerase molecule (DNAP) converts single stranded DNA into double stranded DNA, keeping the tension constant requires the pipette to adjust its position relative to the optical trap by an amount proportional to the movement of the enzyme over the template [92]; (c) A microneedle experiment in which a single myosin head attached to a microneedle moves along an actin filament. The motion of the myosin is observed with a laser by total internal reflection fluorescence microscopy, while the forces are detected by observing the displacement of the microneedle [93]; (d) A typical SFM cantilever experiment in which Laser light is focused onto the back of a cantilever that ends with a nanometer scale tip. The reflection and corresponding position of the tip is detected by a position-sensitive photodiode. A piezo-electric scanner moves the sample in all directions, enabling the tip to scan topography or to extend molecules attached to the surface.

Different force ranges and measurement time scales are afforded by these techniques. Table 2.1 shows the typical applications of each method according to their force ranges and time scales. With the accessible force window, the whole range from entropic forces at several femtonewtons (fN) to the rupture of covalent bonds at a few nanonewtons (nN) can now be investigated by a suitable technique.

Table 2.1: Comparison of different single molecule manipulation methods (after [24])

Method	Force range (pN)	Dynamical range	Typical applications
SFM Cantilever	>1	≥10 μs	DNA, proteins, receptor-ligand pairs
Microneedles	>0.1	≥100 ms	Actin, stretching, unzipping and twisting DNA
Optical tweezers	0.1 - 150	≥10 ms	Actin, DNA, proteins, molecular motors
Magnetic beads	0.01 - 100	≥1 s	Stretching and twisting DNA

For many bio-molecules, the external force is one of the most important functional and structural parameter. With the help of single molecule manipulation techniques, single-molecule force spectroscopy has been realized, which becomes a versatile analytical tool for the structural and functional investigation of single bio-molecules in their native environments. Within the past years, detailed insights into binding potentials of receptor ligand pairs, protein folding and unfolding mechanisms, DNA mechanics as well as the function of molecular motors have been obtained. Among them DNA mechanics is probably the most intensely investigated topic.

DNA was one of the first molecules investigated with single molecule force manipulation [94]. As more details about its mechanical properties are revealed, a complete picture emerges that explains the coupling of stretch and twist, overstretching mechanics, and base pairing forces, in a consistent way: after the discovery of S-DNA by Bustamante *et al.,* which is highly overstretched and underwound [28], and of P-DNA [95,96], an overstretched and overtwisted DNA structure which was proposed by Pauling in 1953 [97], Leger *et al.* have investigated the coupling of stretching and twisting DNA up to forces of 150 pN [29]. By using a glass microneedle setup, which permitted them to rotate the molecule around its axis before stretching it, they were able to determine the helicity of S-DNA for the first time.

They have also proposed a model that uses several different structures to explain the entire force spectrum obtained by stretching and twisting DNA: the relaxed B-DNA and Z-DNA structures, the overstretched S-DNA and P-DNA, as well as supercoiled P-DNA. Using SFM-based single-molecule force spectroscopy, a new force induced melting transition, during which double-helical DNA is split into two single strands, has been reported [98]. It could be shown that the mechanical energy deposited in the DNA double helix before melting varies with counter ion concentration, temperature, and sequence, and agrees well with the base pairing free enthalpy of DNA under the given experimental conditions [99]. By unzipping synthetic DNA sequences, Rief *et al.* could directly determine the sequence-specific base-pairing forces of DNA as 9 pN for AT and 20 pN for GC base pairs [98]. These values are consistent with earlier results by Essevaz-Roulet *et al.* [100], who unzipped lambda phage DNA using glass microneedles. Again, the mechanical energy needed to separate the two strands agrees well with the base pairing free enthalpies of AT and GC sequences. Strunz *et al.* have measured the unbinding force of complementary DNA strands using dynamic force spectroscopy [101]. The unbinding force has been determined as a function of the force loading rate as well as the number of base pairs. Interestingly, although obtained for short oligonucleotides, the extrapolation of their data to long sequences suggests that the complementary strands should separate at around 70 pN, which has indeed been observed [99].

Following the investigation of DNA mechanics itself, dynamic studies of DNA and its interactions with proteins have recently come into the focus of biophysical research. For example as shown in Fig. 2.25 (b) Wuite *et al.* have examined the activity of T7 DNA polymerase as a function of the mechanical tension applied to the DNA template [92]. It could be shown that the force needs to be generated by the enzyme during its rate limiting step in order to mechanically adjust for the different lengths of single- and double-stranded DNA. Therefore, enzyme activity increased twofold when the single-stranded DNA was prestretched to the length of double-stranded DNA. Upon further stretching, the enzymatic DNA polymerization process slowed down until at high extensions of single-stranded DNA, the enzyme switched to its exonucleolysis mode of activity.

Today the emerging single molecule manipulation techniques provide more and more details in DNA mechanics. Nonetheless, at the end one has to point out an unsolved problem by current single molecule manipulation techniques, i.e. to measure the rupture force of single

ds-DNA backbone. In all DNA (over)stretching experiments four terminals of a ds-DNA should be attached to a substrate or a micro probe. However, results always indicate that the attachments are weaker and break prior to the DNA backbone itself; therefore the mechanical properties of ds-DNA over the full range of extension are incomplete. New single molecule manipulation concerning the rupture of ds-DNA should be developed.

3 Materials and Experimental Methods

In this Chapter sub-chapter 3.1 will start with the introduction of the substrates for the SFM experiments and then continue with describing the molecules investigated in this thesis. Sub-chapter 3.2 will describe experimental procedures of the SFM experiments. The analysis of the data obtained by SFM, including height, length, width and volume of molecules, will be introduced in sub-chapter 3.3. Finally, the method of manipulation with the SFM tip will be briefly described in sub-chapter 3.4.

3.1 Materials

3.1.1 Substrates

Mica and graphite were the most often used substrates in this thesis. Due to their different properties, they are prepared and used for different purposes.

Mica

Mica is characterized by its layered crystal structure. The mica structure is built from so called T-O-T (Tetrahedral $(Si, Al)_2O_5$ - Octahedral $Al_2(OH)_6$ - Tetrahedral) layers. The silica tetrahedra and alumina octahedra covalently bond together into sheets of 1 nm thickness that are weakly ionically bonded together through potassium ions (K^+) (see Fig. 3.1). This gives rise to its good basal plane cleavage, revealing a surface terminated with oxygen atoms. Potassium ions sit in a regular array of binding sites at the surface. When immersed in aqueous solution the K^+ ions diffuse away from the surface to be replaced by a counterion cloud. This renders the mica surface negatively charged with a diffuse double layer of cations above it. Hence, the average cleaved surface of mica is negatively charged [102]. Also it has excellent dielectric strength and thermal stability and is completely inert to the reaction of acids or alkanes. Because of these properties, mica has become a commonly used substrate for SFM.

In this thesis, freshly cleaved muscovite mica (PLANO W. Plannet GmbH, Wetzlar, Germany) or poly-L-ornithine coated mica were used. For the coating, a freshly cleaved

mica surface was placed onto a droplet of 10 µl of a 0.1 mg/ml poly-L-ornithine (molar mass 30.000-70.000 g/mol, Sigma, St. Louis, MO) solution for 10 seconds and then spun off on a spin-coater. The substrate was dried under a stream of N_2 gas before use. While freshly cleaved mica serves as a negatively charged surface, the poly-L-ornithine coated surface is positively charged. Thus, through strong electrostatic interaction a mica surface is often used to adsorb positively charged molecules, while a poly-L-ornithine coated mica surface adsorbs negatively charged molecules.

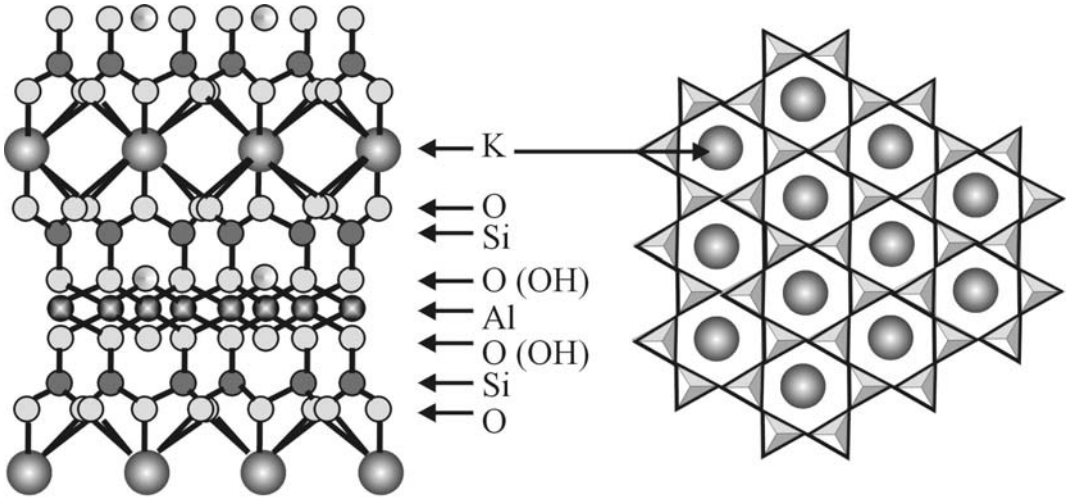

Figure 3.1: Layered structure of mica from side-view (A) and top-view (B) (after [Zhong2003]).

Highly Oriented Pyrolytic Graphite (HOPG)

The lowest-energy state of elemental carbon at ambient pressure and temperature is graphite. Graphite consists of individual graphene layers, each composed of interlinked hexagonal carbon rings tightly bonded to each other, stacked relatively loosely into a three dimensional material. Within a single graphene layer (Figure 3.2), oriented in the x-y plane, each carbon atom is tightly bonded to three neighbors within a plane. The in-plane sp^2 bonding is best understood by first considering graphene, a single layer of graphite. In the plane, the distance between two neighboring C atoms is 0.142 nm [103]. Perpendicular to the plane, the graphene sheet is quite thin (about 0.335 nanometers). The neighboring two graphene layers are very weakly bonded, thus shift relatively to each other. The electrons from these two layers overlap after shifting, therefore induce a new lattice in the plane with the lattice

spacing α is 0.246 nm, which is a characteristic feature in STM image of the basal plane HOPG.

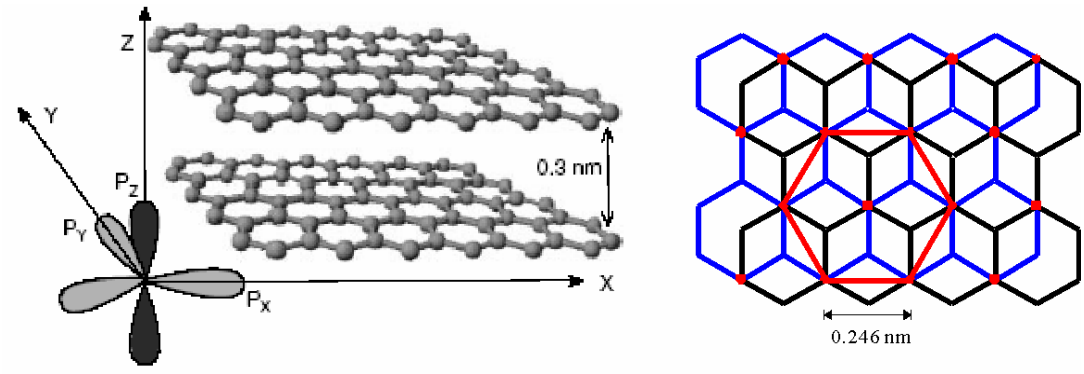

Figure 3.2: Layered structure of HOPG from side view and top view. The blue lattice in top view denotes the bottom layer and the black one denotes the upper layer. The red dots mark the overlap of the electrons from these two layers (after [103]).

In this thesis, highly oriented pyrolytic graphite (HOPG) was bought from Advanced Ceramics Corporation, Ohio, USA. Products of two different qualities were used: grades ZYH and ZYB. According to the supplier's information, the lateral grain size is between 30 to 40 nm for ZYH and "up to 1μm" for the ZYB.

HOPG may be used to adsorb conjugated molecules with aromatic rings due to strong π–π interaction. It is also well-known that alkanes and alkylated molecules tend to physisorb in two-dimensional lattices on the HOPG surface. In this thesis alkylamines or fatty acids were used to coat the HOPG surface in order to allow polyelectrolyte molecules to subsequently adsorb onto such modified HOPG surfaces. Monolayers or submonolayers of long chain alkylamines were prepared by spin coating with a drop of pre-heated (40°C) alkylamine solution, e.g. an octadecylamine chloroform solution (concentration: 1 ~ 100 mg/L) onto the basal plane of HOPG at 40 rounds per second. The samples were dried afterwards for 45 minutes in ambient air.

3.1.2 Polymer molecules

Three kinds of polymer molecules were investigated in this thesis. These are conjugated polymers (poly(3-hexylthiophene) P3HT and copolymers thereof); dendronized polymers

(with different generations and peripheries), and biological polymers (ds-DNA with different lengths).

P3HT: P3HT is usually synthesized via polycondensation of the Grignard reagent. Details of the synthetic procedures can be found in the literature ([104] and references therein). P3HT can have different configurations and regioregularities. These differences have a huge effect on the ordering, the crystallinity and the electrical properties. For this reason in the present thesis highly regioregular P3HT (>99% HT-HT couplings) was investigated (Fig. 3.3 (a)), which was fractionated into several fractions. The synthesis of regioregular P3HT and the fractionation were performed by the group of Prof. Ullrich Scherf at the University of Wuppertal, Germany. The fractionation of P3HT can be briefly described as follows. P3HT obtained via polycondensation was first precipitated with methanol, filtered, and washed with a mixture of water and methanol. This crude polymer was then dried until a constant mass was reached. The crude polymer was first extracted with ethyl acetate in a Soxhlet apparatus until the filtrate was colorless. The remaining insoluble part was then extracted consecutively with hexane, dichloromethane and chloroform in the same manner as in the case of ethyl acetate [105]. NMR studies on different molecular weight fractions revealed that the relative concentration of structural defects due to irregular head-to-head or tail-to-tail linkages only very slightly increases with decreasing molecular weight. Poly(3-octylthiophene) P3OT was originally synthesized in order to obtain a high solubility in common organic solvents. Compared to P3HT, P3OT is more soluble in organic solvents but exhibits lower charge mobility due to an increase of the insulating property (longer alkyl side-chain) of the material. In order to combine the best solubility and charge carrier mobility, the group of Prof. Ullrich Scherf synthesized a copolymer, which is based on 3-hexylthiophene (3HT) and 3-octylthiophene (3OT) as the repeating units. It was also investigated and described in sub-chapter 4.1. Poly[(3-hexylthiophene)-co(3-octylthiophene)] (P3HTOT) as shown in Fig. 3.3 (b) is a statistical copolymer with a one to one ratio of 3HT and 3OT repeating units that form the copolymer backbone (M_n = 36,000 g/mol, PDI = 1.27).

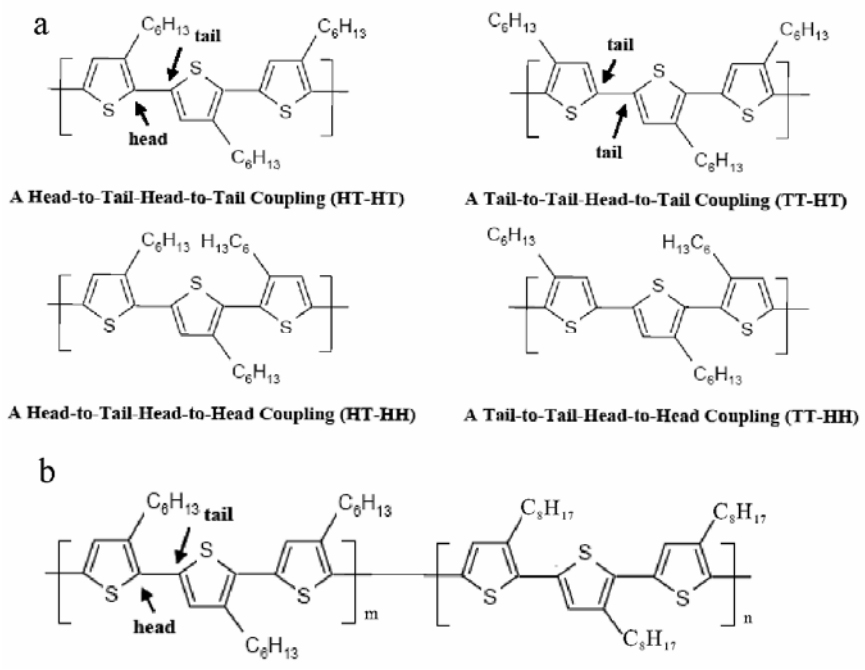

Figure 3.3: (a) Chemical structure of P3HT and its possible regiochemical couplings; (b) chemical structure of P3HTOT.

Dendronized polymers: The synthesis of dendronized polymers was performed by the group of Prof. A. Dieter Schlüter of ETH Zurich, Switzerland. The Macromonomer route is applied in this synthesis. The synthetic steps of Macromonomer ***6*** are briefly presented in Schemes 3.1 and 3.2. For the details of the synthetic procedures refer to reference [106]. The polymerizations were performed under nitrogen in highly concentrated DMF solution [2 : 1 (w/w) = ***6*** : DMF] at 65 °C using 0.5-1.0 mol% of recrystallized AIBN. The initially clear and homogenous solutions after 2-3 h exhibited a viscosity increase and polymerization was continued for further 8-10 h when the mixture had completely solidified. After three dissolution/precipitation cycles, polymer ***7a*** was obtained as a colorless, amorphous solid in 75-90 % yield. The deprotection of dendronized polymer ***7a*** to give ***7b*** was achieved with trifluoro acetic acid (TFA). A large excess of the acid per protecting group was applied at room temperature to the polymer in dichloromethane. If the deprotection was first done in neat TFA followed by a second treatment in solution even a highly amplified NMR spectrum did not show any indication of a tert-butyl signal anymore. It can be concluded that the deprotection is virtually quantitative. Given the molar mass of the sample of approximately M_w = 7 x 10^6 approximately 20,000 esters per macromolecule were hydrolyzed. The deprotection procedure was not further optimized. The deprotonation of ***7b***'s carboxylic acid functions to give the negatively charged polyelectrolyte ***7c*** was easily done with potassium hydroxide. Polymer ***7c*** was fully soluble in deionized water with pH = 8.5.

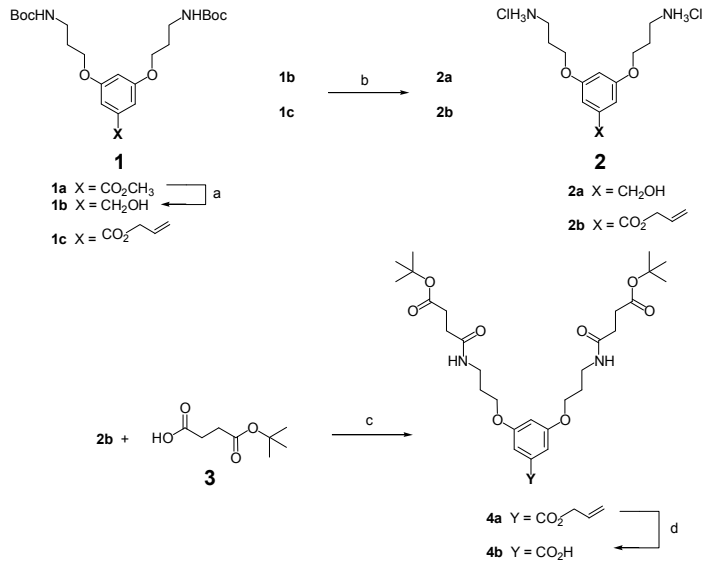

Scheme 3.1: Reagents and conditions: a) 1a, LAH, THF, 0^{o}C, 16 h (86%); b) 1b ,1c , HCl/THF , RT, 6h (95%); c) HOBt, EDC, DCM, -20^{o}C, 16h (76%) ; d) 4a, $Pd(PPh_3)_4$, $C_7H_7NaO_2S.H_2O$, DCM/MeOH , RT, 4h (80%)

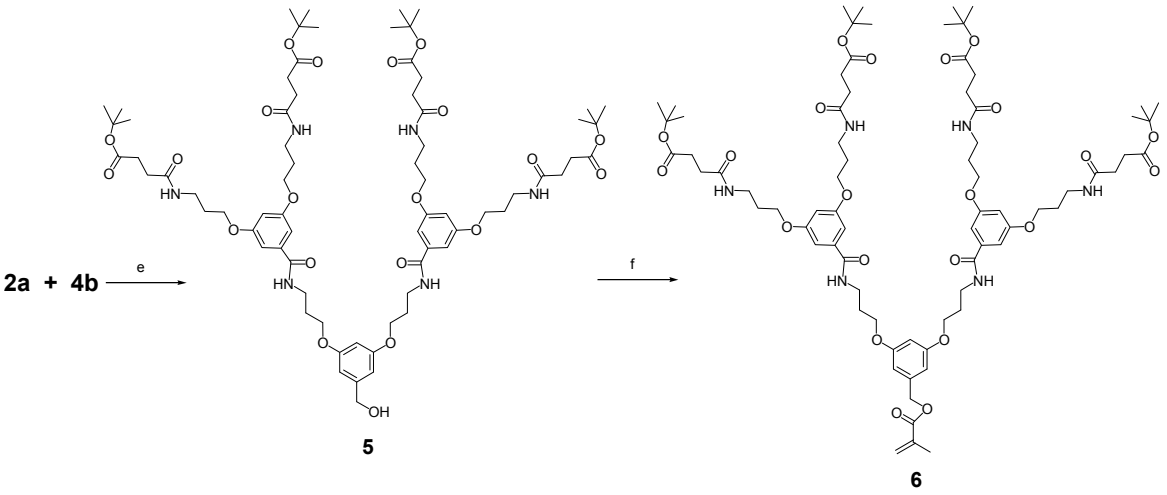

Scheme 3.2: Reagents and conditions: e) HOBt, EDC, DCM, -20^{o}C, 16h (60%) ; f) MAC, DMAP, THF, RT, 16h (85%)

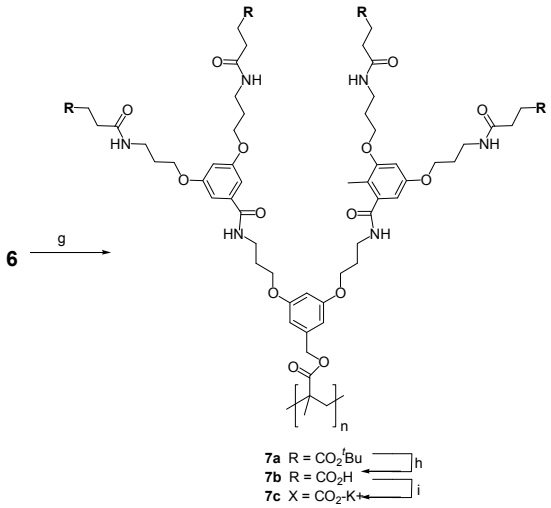

Scheme 3.3: Reagents and conditions: g) AIBN, DMF, 65^{o}C, 12h (90%) ; h) TFA, RT, 24h (95%); i) KOH, MeOH, RT, 3h

DNA: Circular pUC19 (2686 bp), pBR322 (4361 bp) and pBR325 (5994 bp) plasmid DNA were purchased from MoBiTec GmbH, Göttingen, Germany. These DNA samples could be used for SFM measurements without additional purification. All DNA samples were stored in a TE buffer solution (10 mM Tris and HCl, pH 8.0, 1mM EDTA) with a concentration of 1000 mg/L. DNA samples were diluted by milli-Q water to a concentration of 10 mg/L and stored in the refrigerator (4 °C) for higher concentrations in the freezer (−20 °C). Note that original DNA samples are over 80% supercoiled; during storage in dilute solution plasmid DNA will slowly convert from supercoiled to relaxed circles. If there is not any topoisomerase enzyme present in solution, the relaxed plasmid pUC19 is in B-form and thus $L_k = T_w = 2686/10.4 = 258$.

3.2 Experimental procedures

SFM images were recorded using a MultiMode Scanning Probe Microscope (Veeco Instruments, Santa Barbara, CA, USA) with a NanoScope IIIa or IV controller operated in tapping mode. The sample is placed on a piezoelectric E scanner, allowing a maximum X-Y scanning size of 12μm*12μm and a z-extension of 2.5 μm. The scanner was calibrated by imaging a rectangular platinum grid of 1 μm x 1 μm mesh size. Height and phase images were recorded with scan rate of 2 - 4 lines/s and a resolution of 512 x 512 pixels. Two kinds of tapping mode Olympus etched silicon cantilevers were used, with a typical resonance frequency in the range of 200-400 kHz and a spring constant around 42 N/m or with a typical resonance frequency in the range of 60 - 80 kHz and a spring constant around 2 N/m. The etched silicon tip is mounted on a 160 μm long and 50μm wide cantilever as shown in Fig. 3.4. The new tip terminal radius is typically smaller than 15 nm. All samples were investigated at room temperature in air environment.

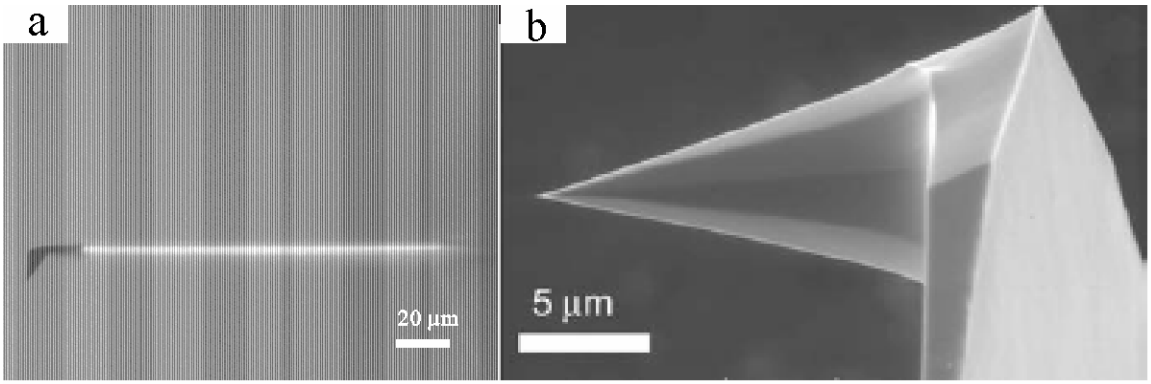

Figure 3.4: (a) Optical microscope image of side view of Olympus etched silicon cantilever and tip; (b) Scanning electron microscope image of etched silicon tip.

The films of P3HT and its copolymer were prepared by using the spin coating technique to provide organic thin films with an average thickness of 20-40 nm. The fractionated organic conductive molecules were dissolved in corresponding organic solvents used in fractionation (Chloroform, Dichloromethane, Hexane and Ethyl acetate, respectively) and spun onto Si/SiO_2 substrates. The Si/SiO_2 substrates are highly-doped silicon with a thermally grown 300 nm thick silicon dioxide top layer (capacitance per unit area is 11 nF/cm^2, purchased from Silchem Co. Freiberg, Germany).

In order to prepare isolated non-charged dendronized polymers (denpols) on mica, a drop (10 μl) of a denpol chloroform solution (2-5 mg/L) was spin-coated (ca. 40 rps) onto freshly cleaved mica. To prepare negatively charged denpols on mica, poly-L-ornithine (molar mass 30.000-70.000 g/mol, Sigma, St. Louis, MO) was spin-coated onto mica, and then a drop (10 μl) of denpol aqueous solution (5-10 mg/L) was deposited onto poly-L-ornithine coated mica for 10 seconds; finally the remaining extra liquid was spun away. To prepare negatively charged denpols on HOPG, first an octadecylamine chloroform solution (100 mg/mL) was spin-coated (50 rps) onto freshly cleaved HOPG to form a monolayer; the precoated HOPG surface was then dried in ambient condition for at least half hour; finally a drop (10 μl) of denpol aqueous solution (5-10 mg/L) was deposited onto poly-L-ornithine coated mica for 10 seconds; afterwards the remaining extra liquid was spun off.

In order to prepare immobilized individual ds-DNA on mica, plasmid or linear ds-DNA was first diluted to 1 mg/L by distilled water. A drop (20 μl) of DNA aqueous solution (1 mg/L) was deposited onto poly-L-ornithine coated mica for 10 seconds; afterwards the remaining extra liquid was spun off. To prepare individual ds-DNA on HOPG, a drop (~10 μL) of a

100-1000 mg/L dodecylamine ($C_{12}H_{25}NH_2$) or a 30-100 mg/L octadecylamine ($C_{18}H_{37}NH_2$) chloroform solution wase spin coated onto freshly cleaved HOPG surfaces. Different surface coverage can be obtained by varying the alkyl-amine concentrations. Note that before applying onto the surface, $C_{12}H_{25}NH_2$ or $C_{18}H_{37}NH_2$ chloroform solution should be heated up to 40°C. The precoated HOPG surface was then dried in ambient condition for at least half hour. Finally a drop (20 μl) of DNA aqueous solution (1 mg/L) was deposited onto alkyl-amine coated HOPG for 10 seconds; afterwards the remaining extra liquid was spun off. The detailed procedure to prepare circular ds-DNA on HOPG for the so-called blowing effect will be described in *sub-chapter 4.42*.

3.3 SFM data analysis

3.3.1 Height

The SFM data were first processed by using NanoScope® software (Veeco Instruments). The raw data were modified using the filter for flattening the images. This filter removes the vertical offset between scan lines, i.e. z-drift of the piezo scanner, and the tilted sample orientation relative to the scan plane. The height of particles or polymers was measured by cross section profiles with the software. However, since the vertical offset between scan lines is removed, the information in y-direction of the image is not conserved. Thus, in order to make accurate cross sectional height measurements, the cross-sectional lines are only drawn along the fast scan direction (x-direction). The vertical profile along this line assures the accurate height measurement of the molecules. On the other hand an SFM image process software called SPIP (The Scanning Probe Image Processor, Image Metrology, Hørsholm, Denmark) can also analyse height data with the same manner. A height anomaly due to environment has been discussed before [11] and will be not considered in this thesis.

3.3.2 Width

In principle width measurement can be also performed in cross section profiles. The apparent bottom widths of objects in SFM images were measured by drawing cross sections along the X axis and perpendicularly over objects. For example, as shown in Fig. 3.5, several particles on mica were measured by SFM in tapping mode. They were icosahedral protein

capsids formed by Aquifex aeolicus lumazine synthase (ALS), which may be regarded as spherical particles (for details of the experiments refer to [107]). From the height profiles on the right side the bottom widths of particles 1, 2, and 3 have been measured. However, the measured width should be always calibrated by taking into account the broadening effect caused by a finite SFM tip [108].

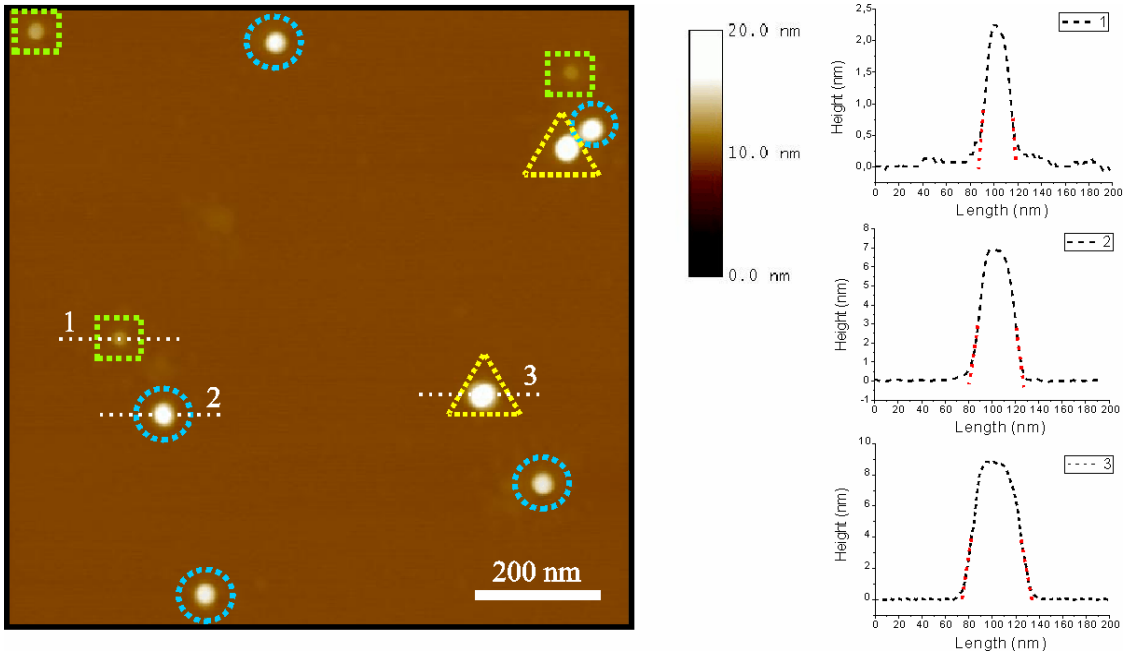

Figure 3.5: SFM tapping mode height images of wild type ALS. Particles in each sample within 3 size categories are presented in rectangles (small particle), circles (middle particle) and triangles (large particle), respectively. Right part shows cross section along white slash lines in left image through 3 typical particles belonging to different size categories. The apparent bottom widths (width of extended peak sides) of 3 particles reach 35 nm, 45 nm and 71 nm, the apparent peak heights are 2.3 nm, 7.0 nm and 8.9 nm, respectively [107].

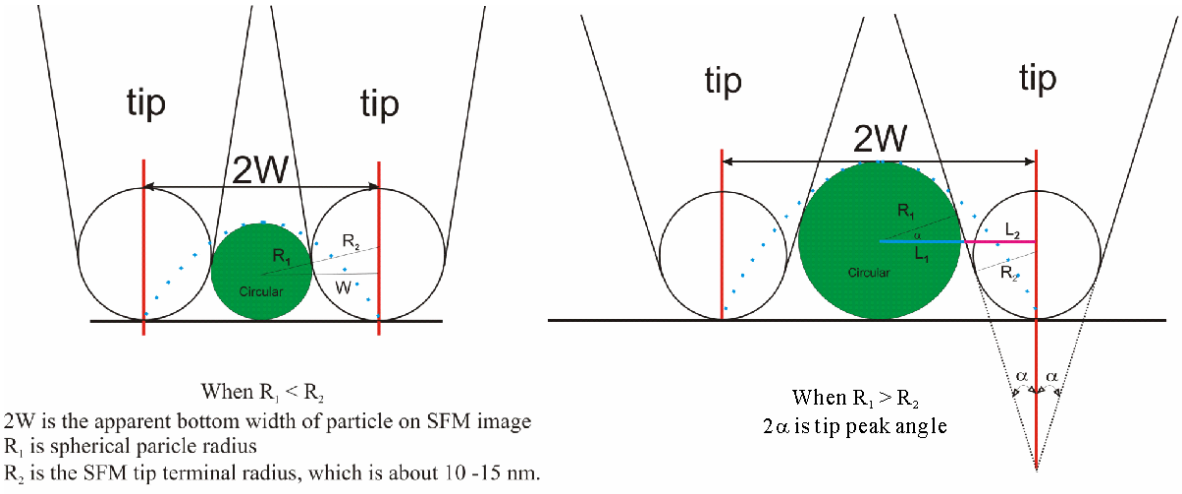

Figure 3.6: Schematic drawing of two scenarios of SFM tip broadening effect on spherical particles.

In a traditional calibration process, a sharp commercial silicon tip is assumed with a terminal radius $R_2 = (15 \pm 5)$ nm to measure a spherical particle with radius R_1 as sketched in Fig. 3.6. The apparent measured particle width is 2W, the corrected particle diameter D can be calculated by:

$$D = 2R_1 = \frac{W^2}{2R_2} \quad \text{(Eq. 3.1)} \quad \text{when } R_2 > R_1;$$

or $D(\frac{1+Sin\alpha}{Cos\alpha}) = 2W - 2R_2(\frac{1-Sin\alpha}{Cos\alpha})$ (Eq. 3.2) when $R_2 < R_1$ and 2α is tip peak angle which is typically about 35^o.

This calculation also fits to measure the width of a cylindrical object, whose cross section is round. If in case the cross section of the object is assumed to be rectangle, the corrected width is $D = 2W - 2\sqrt{h^2 + 2hR}_2$ (Eq. 3.3), where ***h*** is the height of the rectangle [12].

However, since the traditional calibration requires an estimated tip terminal size, large errors may be induced into the corrected width. Therefore an advanced process of SFM width measurement was also applied. At first, spherical gold colloid particles with an average diameter 15 nm were applied onto a PLO coated mica surface as a standard calibration sample, and then gold particles were scanned by an SFM tip in tapping mode as shown in Fig. 3.7 (a). The maximum height of each particle is measured in order to reconstruct the tip; it is listed besides each particle. Since these gold particles are uncompressible, the height values represent the particles' real diameters. Thus the real shape of isolated gold particle can be reconstructed as shown in Fig. 3.7 (a) (red circles). With the reconstructed gold particle shape, a 3D shape of the SFM tip terminal can be sufficiently reconstructed as shown in Fig. 3.7 (b). If only its cross section in the fast scanning direction (x axis) is taken, as illustrated in Fig. 3.7 (c), one can perform a more precise reconstruction of the object's real cross section (grey shadow) based on the apparent result (black curve).

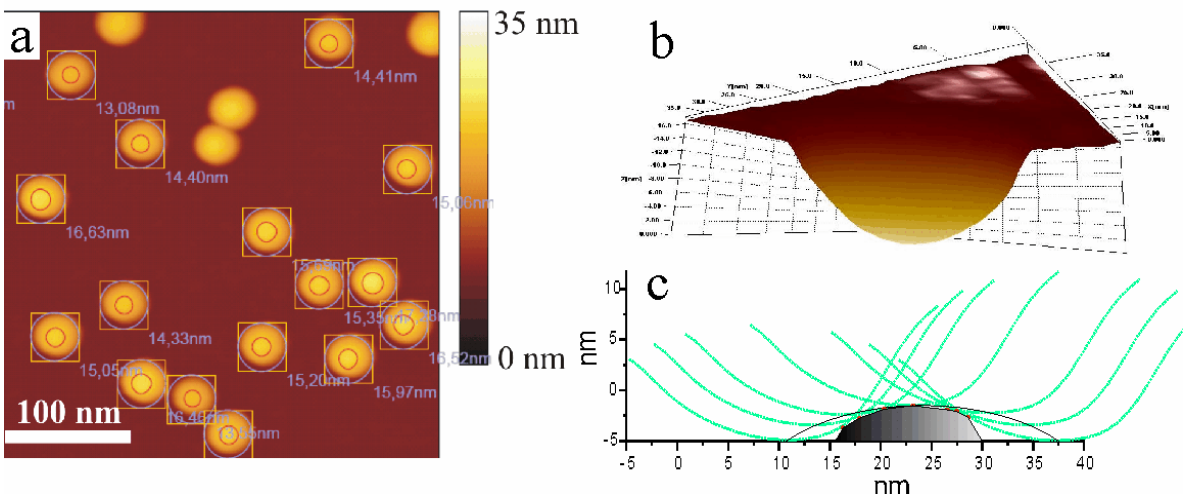

Figure 3.7: (a) A processed image of gold particles to calibrate an SFM tip by showing the height of each particle and the corresponding "real" sphere as red circle; (b) 3D image of reconstructed SFM tip with terminal radius around 15 nm (c) Cross section view along x axis (fast scanning direction) of the reconstructed tip to deconvolute an apparent semi-spherical object.

With a reconstructed 3D SFM tip, SPIP provides an advanced feature for "deconvolution" of an SFM image. This means all the tip induced broadening parts on the measured objects can be removed by the deconvolution process. Thus it is possible to measure the "real" volume of deconvoluted objects based on an SFM image, which was not able to be measured due to the convolution with the tip. The details of volume measurements based on SFM images can be found in [109].

3.3.3 Length

For the quantitative determination of the contour lengths of single molecules SFM images were recorded with a resolution of 512×512 pixels for 1x1 μm^2. Using the drawing program sketch (www.sketch.sourceforge.org), one can draw a free hand line roughly along a single molecule following its contour on the image. Then a home-developed program [110] is able to align this line precisely along the molecule contour and vectorize it into many small segments; the final vectorization leads to the segment between 2 neighboring points, which is shorter than 2 pixels. The image with the vectorized lines along the chain contour is saved as *.sk* file. For further length data processing, this file will be loaded and the vectorized segments will be calculated to determine the persistence length. Note that the standard

deviation with equation $\sigma = \sqrt{\sum (\bar{x} - x_i)^2 / (N-1)}$ will be taken as the error in the average contour length evaluation.

3.4 SFM tip manipulation

For single molecule manipulation on surfaces with an SFM tip a script called "Litho" for the NanoScope IIIa Controller is applied. In this case a high resolution image (typically < 500 nm x 500 nm) with single molecules is recorded in the tapping mode, then the SFM is switched from tapping mode to contact mode. The tip moves with about 100-500 nm/s while applying a force of about 1.6 μN across the substrate and scratches the surface [111]. The movement of the tip along the x and y directions and the velocity of the tip movement can be setup in advance in the script. The force applied to the SFM tip depends on the deflection depth the SFM tip moves down from the tapping mode position to the contact mode position. After manipulation it switches back to the tapping mode and records another image to check the result. Generally the silicon tip used in tapping mode with a spring constant around 2 N/m fits well to this application.

4 Results and Discussion

4.1 Morphology of poly(3-hexylthiophene) films – the molecular weight effect

Conjugated polymers are emerging materials for electronic applications due to the tunability of their properties through variation of their chemical structure [16]. They have been developed into very useful materials for a variety of applications, including light-emitting diodes [112], photovoltaic cells (PVs) [113], and organic field effect transistors (OFETs) [114]. Two critical parameters that determine the function of conjugated polymer-based devices are the chemical structure and the nanostructure of a conjugated polymer in the solid state [115]. While the physical properties of isolated polymers are primarily controlled by their chemical structure, these properties are drastically altered in the solid state due to electronic coupling between polymer chains as determined by their conformation and the interchain packing. However, the development of effective and precise methods for controlling the nanostructure of polymers in the solid state has been limited because polymers often fail to assemble into organized structures, partly due to their large molecular weight. It is difficult to use conjugated polymers for hierarchical self-assembly, as their solubility is drastically smaller than that of flexible polymers due to their totally rigid or semi-rigid nature. Therefore it is well known that side chains improve solubility and cause self-assembly, e.g. in poly(3-alkylthiophenes) [116], leading to improved electro- and photoactive properties.

The operation of polymer PVs and OFETs is limited by the charge carrier mobility of a thin polymer film on a solid substrate. Therefore, understanding the determining factors of the mobility is key to improving the performance of polymer PVs and OFETs [117]. High-mobility polymer OFETs (mobility of 0.01-0.1 cm^2/Vs) have been made with regioregular poly(3-hexylthiophene) (RR P3HT) as shown in Figure 4.1 (a). The charge carrier mobility of P3HT has been strongly related to the regioregularity [116]. It is known that processing and organization of polymers in bulk phases, thin films or individual nanostructures depend generally on molecular weights and their distribution [118]. However, while highly regioregular P3HT can be effectively prepared [104], the effect of the molecular weight of P3HT has not been thoroughly investigated. Thus, in chapter 4.1 we will present an SFM investigation on the morphology of RR P3HT thin films of different

molecular weights, combined with structural and electrical characterizations, which reveals a very pronounced dependence of molecular weight on the OFET mobility.

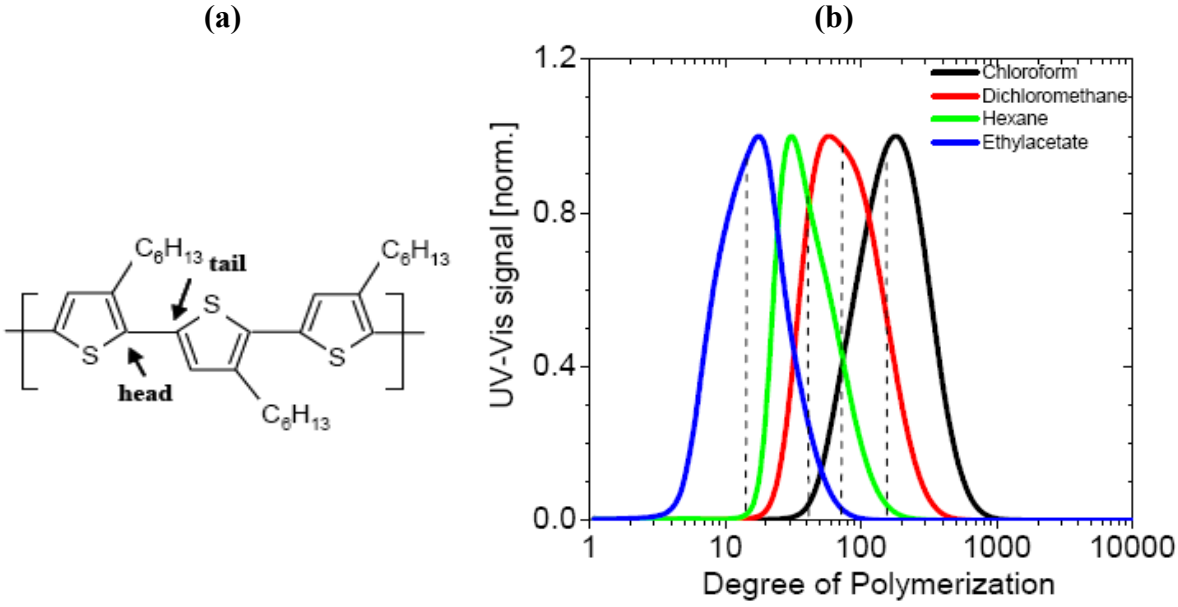

Figure 4.1: (a) Chemical structure of regioregular poly(3-hexylthiophene) with head-tail-head-tail coupling; (b) GPC diagrams of the four fractions obtained by selective extraction of regioregular P3HT [8].

4.1.1 Morphology studies of thin films by SFM

In a recent paper, Trznadel and coworkers have presented an approach to prepare fractions of RR P3HT with the number average molecular weight (M_n) ranging between M_n = 3,100 and 26,000 g/mol, utilizing solvent extraction [105]. Following this approach, RR P3HT samples (>99% HT-HT couplings) were fractionated using different solvents. As a result, polymers with similar chemical structure but differing significantly in their molecular weight were obtained. The average molecular weights and M_n distribution are summarized in Table 4.1. GPC (Figure 4.1 (b)) was performed with THF, and calibrated with narrowly distributed polystyrene standards. The number of alkylthiophene units (degree of polymerization, *DP*) of these fractions as calculated from M_n are between 13 (ethyl acetate fraction) and 114 (chloroform fraction). Differential Scanning Calorimetry (DSC) analysis shows that the lowest molecular weight fraction (ethyl acetate) melts at approx. 205°C, and the highest molecular weight fraction (chloroform) at approx. 238°C.

Thin films with about 20-40 nm thicknesses were prepared by spin-coating the different polymer fractions onto silicon oxide/silicon substrates. The morphologies of the P3HT

fractions with different molecular weights (MW, referring to number average molecular weight M_n) have been studied as prepared, and after annealing at 150 ^oC for 5 minutes, using Tapping Mode SFM at room temperature in air with a relative humidity of 30-40%.

Table 4.1: Molecular weight of all P3HT fractions obtained using GPC; M_n, number average molecular weight; M_w, weight average molecular weight; *PDI*, polydispersity index; *DP*, degree of polymerization calculated from M_n.

Poly(3-hexylthiophene) fractions	M_n [g/mol]	M_w [g/mol]	PDI	DP
Fractionated with Chloroform	19,000	25,650	1.35	114
Fractionated with Dichloromethane	13,800	20,424	1.48	83
Fractionated with Hexane	5,600	6,608	1.18	33
Fractionated with Ethyl acetate	2,200	3,146	1.43	13

The SFM images shown in Figure 4.2 (a)-(b) reveal that as-prepared layers of the ethyl acetate fraction contain "ribbon-like" crystallites. A height image of the material with the lowest molecular weight (Fig. 4.2 a) reveals ribbons with a height of 2.0 ± 0.5 nm, while a phase image (Fig. 4.2 b) allows to determine their width. The average width of the ribbon is measured as 25 ± 4 nm from 127 different ribbon profiles. According to the method described in ref. [119], a corrected rod width of ~11 nm can be estimated by taking into account a terminal tip radius of 13 ± 7 nm and the rod heights determined above (See details of ribbon width correction in *Chapter 3.3.2*). This value is confirmed by high resolution TEM measurements, where the ribbon width was determined as 11 ± 2 nm. The step height was an average of measurements from bottom to top at 30 different positions. The standard deviation is used as an error bar, which is quite large, since probably the layer at the bottom is quite high and/or they might not be a single layer. After annealing, this "ribbon-like" structure is converted into a "terrace-like" structure with a step height of 3.01 ± 1.38 nm (Figure 4.2 c-d).

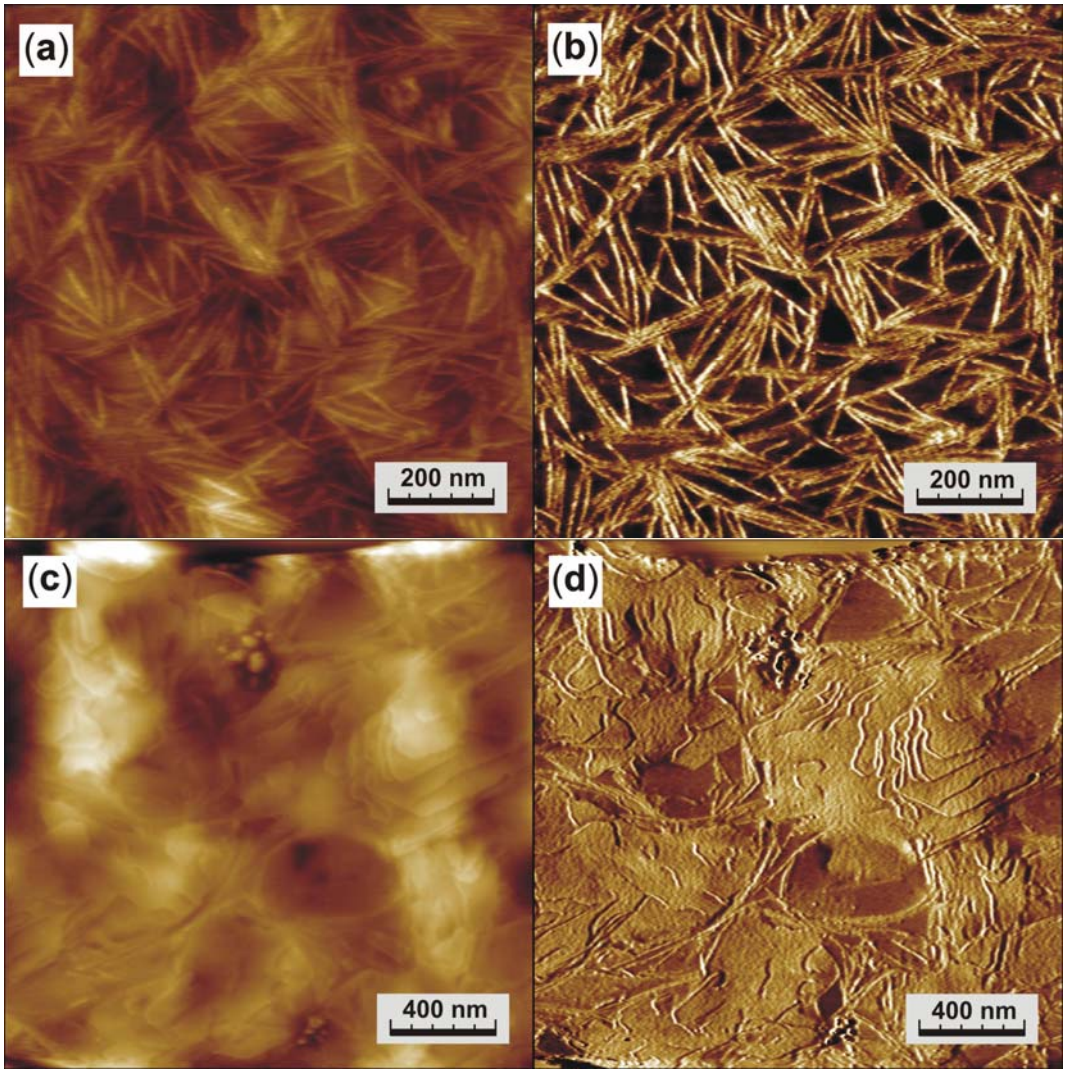

Figure 4.2: SFM images of films of the ethyl acetate fraction, spin-coated on SiO_2/Si substrate: (a) height and (b) phase images of the as-prepared sample. (c) height and (d) phase images of the sample after annealing at 150^{0}C for 5 minutes and cooling back to room temperature [7].

For a spin-coated film from the hexane fraction, no well ordered ribbon-like structure is observed and the sample shows a granular morphology (Fig. 4.3 a-b). After annealing, a smoother, lamellar morphology is observed (Fig. 4.3 c-d). Samples prepared from the dichloromethane fraction also show a granular morphology with somewhat enhanced grain sizes (Fig. 4.4 a-b). After annealing the size of the grains further increases (Fig. 4.4 c-d). This trend is continued in the films prepared from the chloroform fraction (Fig. 4.5 a-b) to form a "blob like" structure. Here, the morphology is only slightly changed after annealing (Figure 4.5 c-d). In general the findings on as-prepared layers are in agreement with the results of SFM studies published by Kline et al. [120].

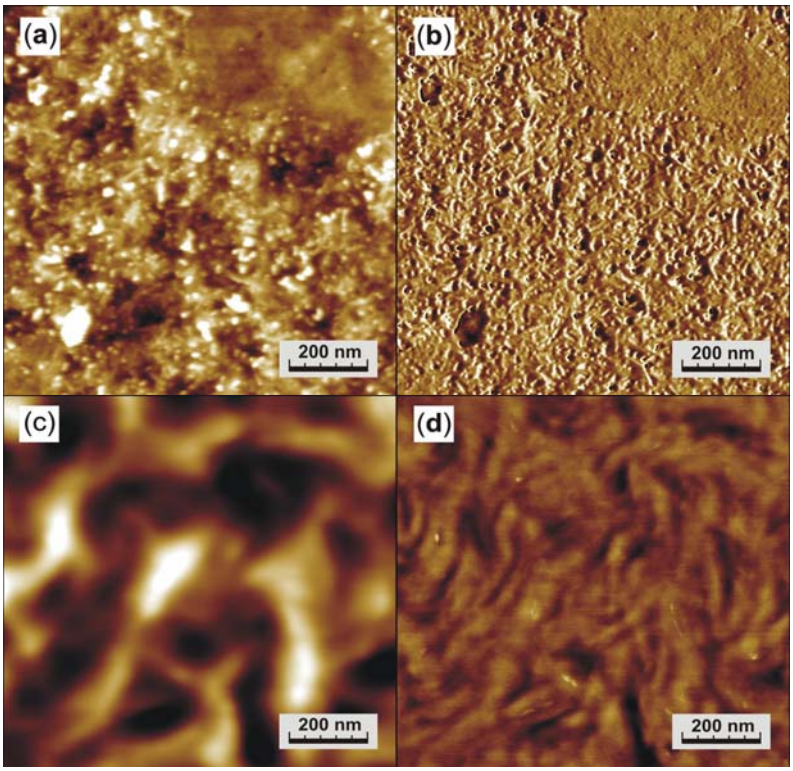

Figure 4.3: SFM height and phase images of as-prepared (a-b) and annealed films (c-d) of the hexane fraction.

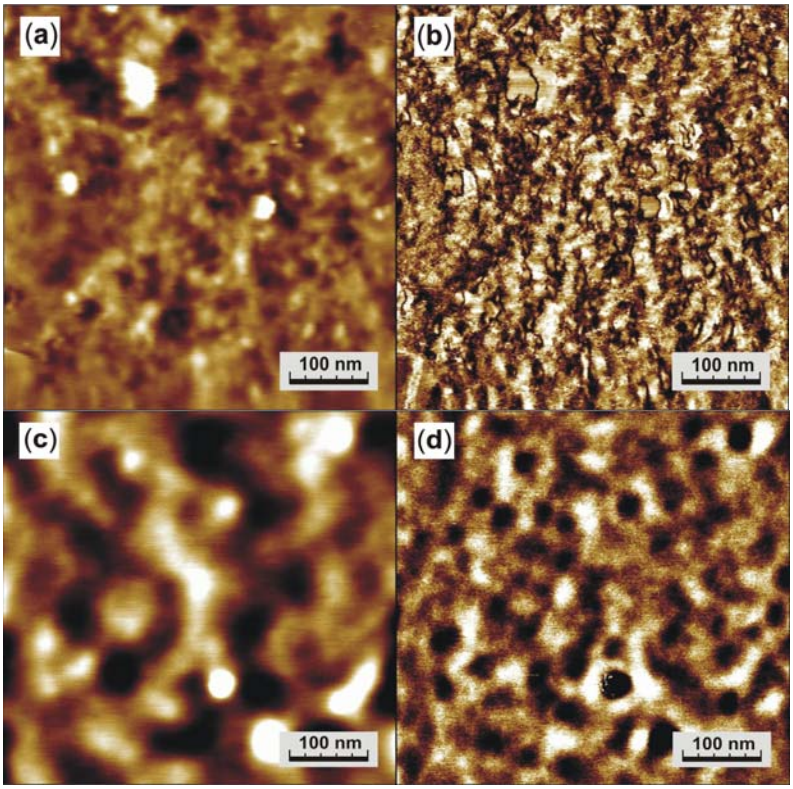

Figure 4.4: SFM height and phase images of as-prepared (a-b) and annealed films (c-d) of the dichloromethane fraction.

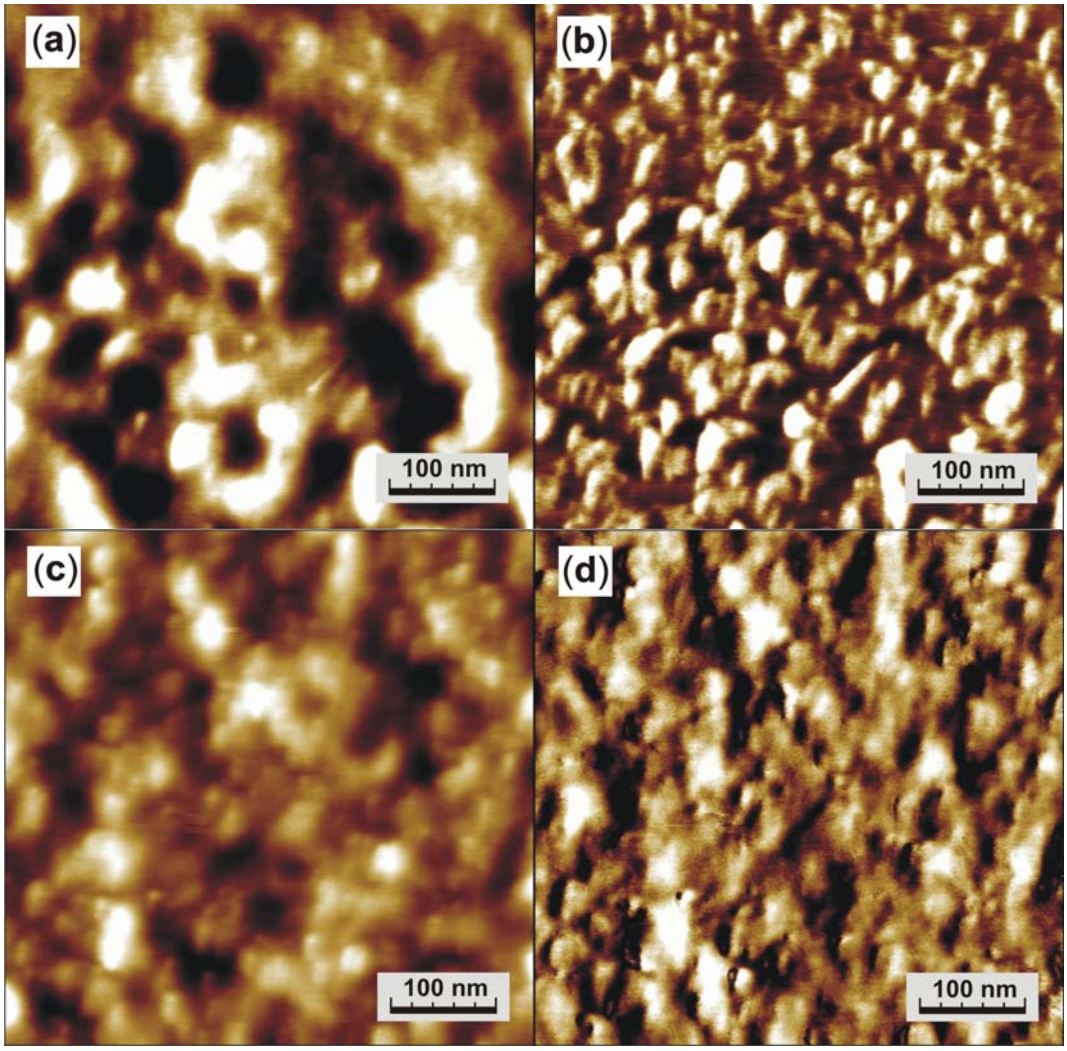

Figure 4.5: SFM height and phase images of as-prepared (a-b) and annealed films (c-d) of the chloroform fraction [7].

4.1.2 Charge mobility in OFETs

OFETs were prepared with P3HT thin films from all different molecular weight fractions. Details of the preparation are described in ref. [7]. All devices exhibited typical transistor properties. The most important OFET characteristic is the field effect mobility μ_{sat}, which is usually extracted from a plot of the square root of the drain current in the saturation regime $I_{D,sat}$ versus gate voltage V_{GS} according to eq. 4.1 [121]:

$$I_{D,sat} = \frac{WC_i}{2L}\mu_{sat}\left(V_{GS} - V_t\right)^2 \qquad \text{Eq. 4.1}$$

Here, W and L are the channel width and length, respectively, C_i is the capacitance of the gate insulator, μ_{sat} is the field-effect mobility in the saturation region and V_t is the so called threshold voltage, at which the transistor turns on. The so-obtained values of μ_{sat} are listed in Table 4.2. The samples were also annealed to 150°C for 5 minutes prior to the deposition of source and drain electrodes, followed by quenching to room temperature. Annealing improved the device performance, except for dichloromethane fraction, where the mobility was somewhat reduced. Based on the incomplete recovery of the solid state adsorption spectrum, this is attributed to a slightly lower degree of interchain order after annealing. Noteworthy, the annealing temperature of 150°C is acceptable for the fabrication of all-plastics OFETs.

Table 4.2: Field-effect mobilities calculated from the square-root plots of the drain current in the saturation region as a function of gate bias and on/off ratios of transistors with as-prepared and annealed (150°C, 5 min) active layers.

Poly(3-hexylthiophene) fractions	μ_{sat} : Mobility [$cm^2V^{-1}s^{-1}$]
Fractionated with Chloroform – *As prepared*	2.6×10^{-3}
Fractionated with Chloroform – *Annealed*	4.2×10^{-3}
Fractionated with Dichloromethane – *As prepared*	1.3×10^{-3}
Fractionated with Dichloromethane – *Annealed*	4.7×10^{-4}
Fractionated with Hexane – *As prepared*	1.6×10^{-5}
Fractionated with Hexane – *Annealed*	4.3×10^{-5}
Fractionated with Ethyl acetate – *As prepared*	5.5×10^{-7}
Fractionated with Ethyl acetate – *Annealed*	2.5×10^{-6}

Interestingly, for these transistors with as-prepared and annealed samples, the charge mobilities increase drastically with increasing molecular weight, namely from μ_{sat} below 10^{-7} $cm^2V^{-1}s^{-1}$ to more than 10^{-3} $cm^2V^{-1}s^{-1}$. In the other word, varying the molecular weight of P3HT by one order of magnitude results in a four orders of magnitude change in the field-effect charge carrier mobility in OFETs. The effect of molecular weight on the performance of OFETs based on P3HT was also investigated by Kline *et al.* [17,120]. The charge mobility data presented here are well comparable to their data. They have proposed a model in that the charge carrier mobility is mainly limited by grain boundaries. Figure 4.6 shows the grain boundary model for low- and high-MW of P3HT. Low-MW P3HT is expected to behave like rigid rods, forming ribbon like crystals in which the chains lay perpendicular to the long axis of the crystal [12]. As can be seen in the SFM image in Fig. 4.6 a, the orientational order of the nanocrystals is quite random and they are poorly interconnected. It was then proposed that the low mobility of low-M_n P3HT is due to grain

boundaries within these multicrystalline layers. On the other hand, high-M_n films consist of long polymer chains with interconnected pathways, thus intergrain transport is more efficient (Fig. 4.6 b).

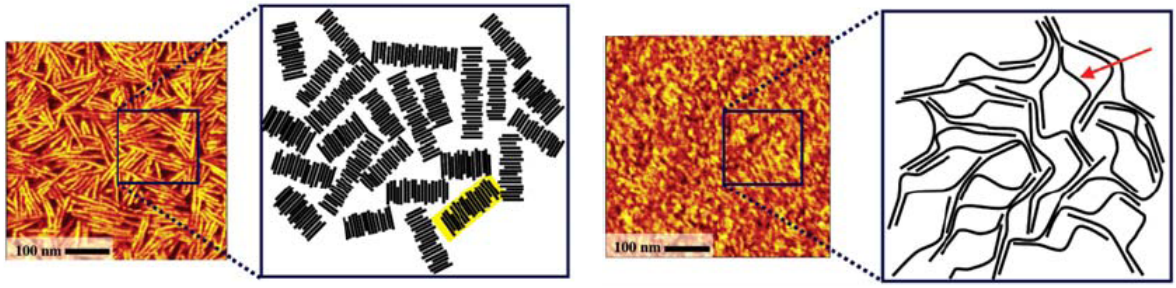

Figure 4.6: Grain boundaries model in P3HT for: (a) low-M_n, where charge carriers are trapped on nanoribbons (highlighted by yellow) (b) High-M_n, where long chains are connecting the ordered regions and soften the boundaries (e.g. like in a place marked with an arrow) [17].

However, the grain boundary model just focuses the charge carrier mobility effect on the very top surface of the total 20-40 nm thickness thin film. The model itself could not provide the structure of the whole thin film including deep layers, which is important for understanding the electric behaviour of a thin film device rather than a monolayer film.

4.1.3 Molecular weight effect on self-assembled conjugated polymer films

Sirringhaus *et al.* have reported that OFETs using highly regioregular P3HT (regioregularity more than 91% head-tail linkages) exhibit field-effect mobilities of 5×10^{-2} to 10^{-1} cm^2/Vs [116]. This was in part attributed to the structural order in the layers prepared from the regioregular polymer. Further, X-ray studies showed that layers spin-coated from highly regioregular P3HT exhibit an orientation of the lamellae parallel to the substrate with the π-π stacking direction in the plane of the substrate (see Figure 4.7). In contrast, spin-coated films of P3HT with low regioregularity (81% HT linkages) consist of lamellae having a face-on orientation (π-π stacking direction perpendicular to the substrate) and a mobility of 2×10^{-4} cm^2/Vs. This indicates that the π-π stacking direction relative to the substrate, which depends on the polymer regioregularity, greatly affects the charge carrier mobility.

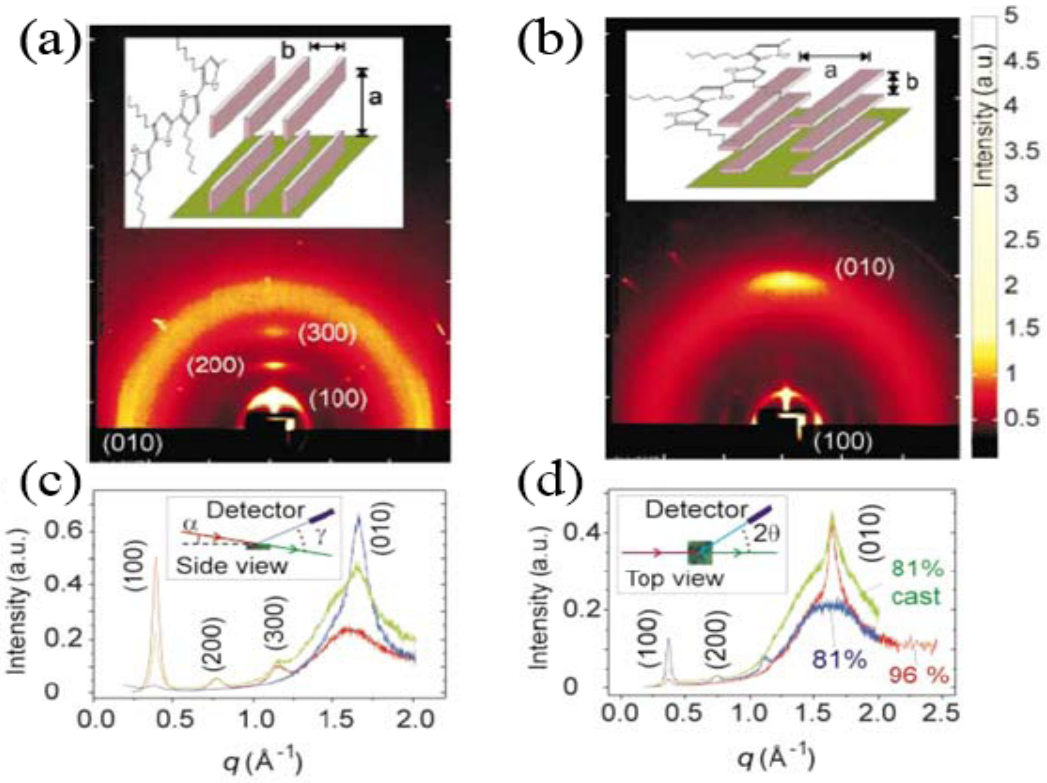

Figure 4.7: Two different orientations of ordered P3HT domains with respect to the substrate, (a) the π-π stacking direction and the side chains are oriented perpendicular to the substrate, (b) the π-π stacking direction and the side chains are oriented parallel to the substrate. (c and d) The change of orientation is confirmed by high resolution synchrotron x-ray diffraction measurements. [116]

Therefore it is clear that in the lowest MW sample the conjugated backbone and the side chains are oriented perpendicular to the substrate (i.e. standing on substrate). X-ray diffraction of this sample has shown the same [7,8]. However, the average length of the lowest MW fraction P3HT (DP = 13) amounts to approx. 5.5 nm, which is just half of the average width of the ribbon observed in Fig. 4.2 (a) and (b). It has been known that the conjugated polymers can form π-π stacking nanoribbons with fully extended single backbones perpendicular to the long axis of the ribbons [12,122,123], whereas it has not been reported that two conjugated chains without specific interaction between each other could pack in one line in a nanoribbon. The lowest MW sample extracted from ethyl acetate solvent is obviously not a highly monodisperse fraction (polydispersity: 1.43). Therefore, the nanoribbons are mainly attributed to P3HTs with lengths of 20-30 repeat units (r.u.), which amounts to about 20% chains of the sample with average r.u. of 13 according to the GPC trace shown in Fig. 4.1 (b). Therefore, apparently the other 80% chains that are not incorporated in the nanoribbon should form some other nanostructures on the substrate. As observed in Fig. 4.2 (a), the space between those nanoribbons is not just the flat substrate.

Despite no regular characteristics, the space area shows different heights indicating a thick amorphous layer beneath the nanoribbons. It is worth noting that the 2 nm average height of the nanoribbons fits well to the width of RR P3HT with the alkyl chains extended as shown in Fig. 4.7 (a).

Therefore a nanostructure model for the lowest MW P3HT thin film is proposed as shown in Figure 4.8, in which a nanoribbon layer is embedded in a thick amorphous matrix. The model is furthermore supported by TEM and X-Ray diffraction (XRD) analysis of the thin films, in which an amorphous background is also found surrounding highly ordered crystalline regions [8]. In addition, since contact mode SFM can provide high resolution images of highly ordered crystalline domains composed of, e.g., pentacene [124] or sixithiophene [125], contact mode SFM measurements were also performed on the lowest MW P3HT. Only smeared images were obtained, indicating that besides highly ordered nanoribbons there is still much rather soft material on the surface.

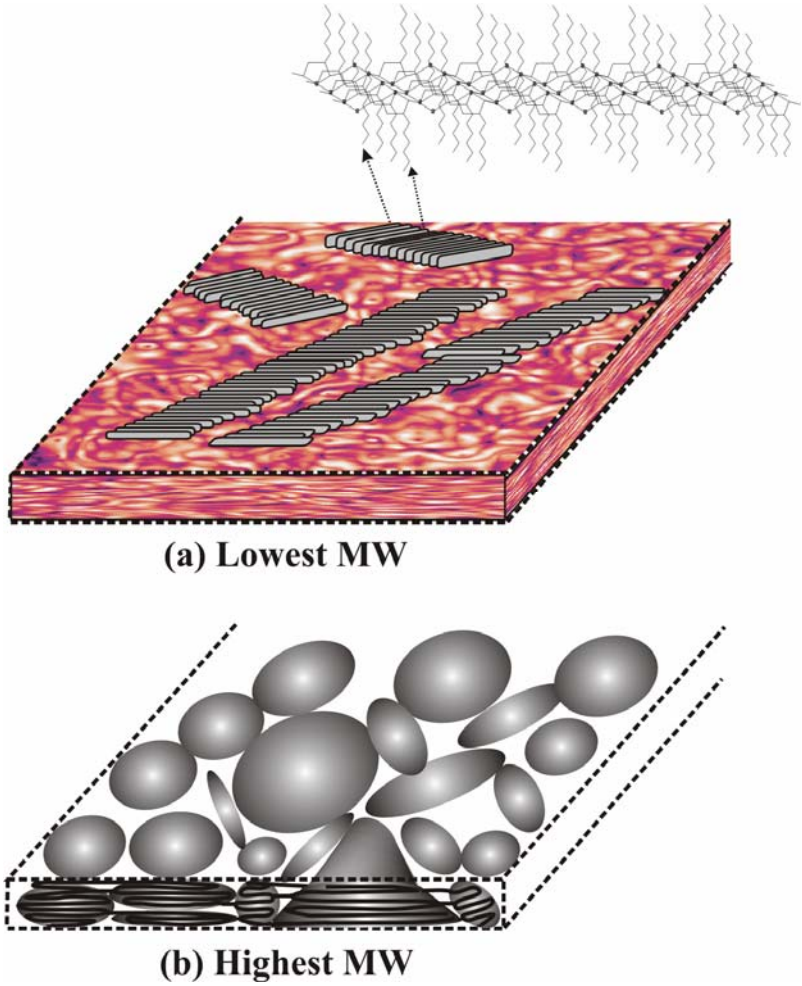

Figure 4.8: (a) Schematic model of the morphologies of the lowest MW P3HT (ethyl acetate fraction) thin film. In the simplified model, the main chain layers in the ordered regions are assumed to be oriented parallel to the substrate plane, with the side chains extending perpendicular to the substrate plane. The crystalline nanoribbons extend to the top layer and consist of fully extended chains. These nanoribbons are embedded in a disordered matrix (shown as red background); (b) Schematic model of the morphologies of highest MW P3HT (chloroform fraction) thin film. The crystalline domains (blobs) consist of partially ordered chains and extend throughout the whole thin film. The long chains must fold back in the crystallite or extend into the disordered phase to interconnect neighbouring domains.

In contrast to the lowest MW P3HT, the highest MW sample displays many blobs with 20-40 nm height and width on the surface as shown in Fig. 4.4 (a) and (b). The rather large melting enthalpy measured by DSC as well as the large intensity of powder X-ray diffraction peaks indicate that a large fraction of the chains is within crystalline domains. However, the rather large width of the diffraction peaks and the almost complete absence of higher order diffraction signals indicate that the order of the chains in these domains is not very good [8]. Therefore we attribute these large blobs to partially ordered crystallites with uniform backbone conformation as sketched in Figure 4.8 (b). Consequently the degree of overall crystallinity in the film is much higher while amorphous regions become small.

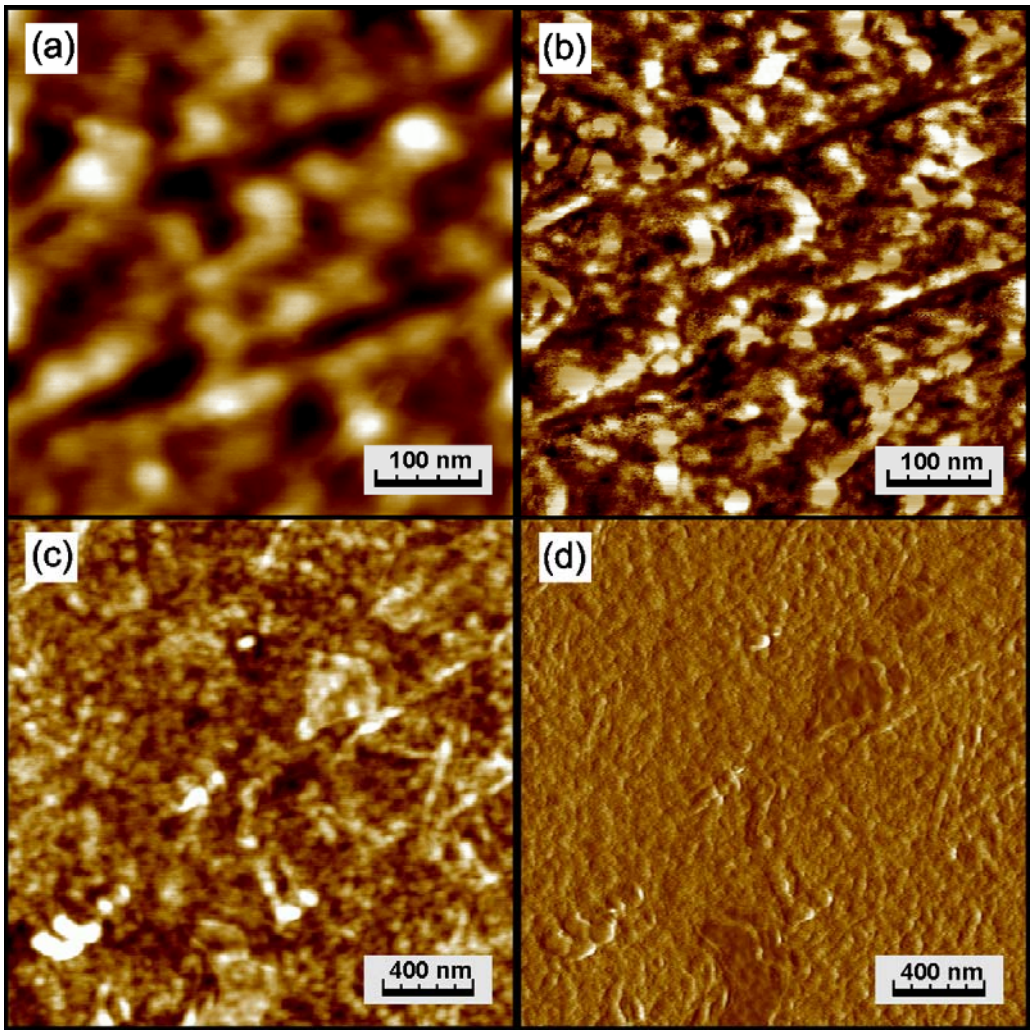

Figure 4.9: SFM height (z range: 10 nm) and phase images of a thin film of P3HT with a MW of 30,000 g/mol (a-b) and thin film of P3HTOT with a MW of 36,000 g/mol (c-d).

In order to prove such a tendency of molecular weight dependant nanostructure, further the morphology of a P3HT sample with MW 30,000 g/mol was measured. The corresponding SFM height and phase images are displayed in Figure 4.9 (a) and (b), which reveal more dense blobs on the surface. On the other hand, the charge mobility of P3HT with 30,000 g/mol MW amounts to 8.6 x 10^{-3} cm^2/Vs, which is much larger than the mobility of the P3TH chloroform fraction with 19,000 g/mol MW. However, the tendency of increasing charge carrier mobility with increasing MW just fits to the homopolymer case, whereas a statistic copolymer of poly[(3-hexylthiophene)-co-(3-octylthiophene)] (P3HTOT) thin film with an even larger MW of 36,000 g/mol exhibited a smaller charge carrier mobility of 7.6 × 10^{-3} cm^2/Vs. The morphology of P3HTOT is displayed in Figure 4.9 (c) and (d), showing a less crystalline surface, which indicates that incorporation of different alkyl chains will

induce an inhomogeneity and thus reduce the uniformity of the polymer backbone conformation, in spite of the highest MW.

The phenomenon that only P3HT with 20-30 repeat units can self-assemble into highly ordered nanoribbons is interesting and worth to discuss here. It is well known that in dilute solutions of polydisperse polymers, the long chains are found preferentially adsorbing on the surface because they loose less translational entropy (per unit mass) in the solution, while they gain approximately the same (total) adsorption energy [126]. Although in some cases short chains may adsorb first due to fast diffusion, they will be finally replaced by longer chains according to the interplay of entropy and enthalpy [21,127].

Thus in the high MW P3HT cases, the adsorption picture is rather simple, if all the polymer chains are already well dissolved in the chosen solvents. Although the polydispersity in different fractions is not so high, it is still reasonable to assume that there are longer chains preferentially adsorbed on the surface. Due to the intramolecular π–π interaction, long chain polymers are in favour to hairpin-like folds on the surface rather than fully stretching. STM studies of P3HT monolayer on an HOPG have shown that polythiophenes are well packed with hairpin-like conformation [128], despite their polydispersity. Although polythiophene is considered as a stiff rod-like molecule, modelling studies indicate that seven or eight consecutive thiophenes in an all-*syn* conformation can make a perfect 180° turn, similar to the β-turn of proteins. Because the enthalpic penalty of 3–5 kcal/mol for the formation of the less-favorable *syn* conformation is acceptable in the system, the regioregular polythiophene constituted the hairpin turn to make a dense packing on surface. On the other hand, due to the high concentration in the solution, surface coverage is easily filled up, therefore longer chains have to densely pack in 3 dimensions. Consequently large crystallites including partially ordered P3HT chains are forming. At the end, smaller chains are filling the empty space between crystallites. This adsorption model can fit to all fractions of P3HT except the lowest MW fraction (ethyl acetate), since it was found that the higher MW fraction, the larger crystallites are observed in surface morphologies (see Fig. 4.3 (a), 4.4 (a), 4.5 (a)).

The exception of the lowest MW fraction is attributed to the formation of nanoribbons during the adsorption. This phenomenon is due to a self-organization process, in which P3HT chains with 20-30 repeat units may self-organize and crystallize to nanoribbons above the amorphous layers. The crystallization into highly ordered nanostructure will cause those chains not only losing lots of translational entropy but also decreasing the enthalpy further;

therefore such a thermodynamical non-equilibrium process may happen only on conjugated chains with certain molecular weight in the system, whereas polymer chains with other lengths only form an amorphous phase that is immiscible with the highly ordered crystalline phase.

In summary self-assembly in many solution-processed, conjugated polymers results in complex nanostructures thin film, in which ordered crystalline domains are embedded in an amorphous matrix. In OFETs the amorphous matrix covers almost the whole interface between conducting layer and gate material. Many publications have suggested that organic semicrystalline provide a better transport than their organic amorphous counterpart [129,130]. This leads to a major weakness for electrical properties of conductive polymers: charge transport is usually limited by the most difficult hopping processes and is therefore dominated by the disordered matrix, resulting in low charge carrier mobilities [115,131]. Based on the results presented here it is agreed that the grain boundary effect is important for charge transport between crystalline domains; however, considering the whole P3HT thin film OFET the uniform conformation of the polymer backbones that reflects the overall crystallinity of the sample is a more critical effect. In order to develop highly conductive polymer OFETs, it is important to understand the semicrystalline nanostructure through a thin film of 20-40 nm thickness, including different domains with different crystallites, which depends on the molecular weight of the polymer.

However, besides molecular weight there are still many variations such as solvents, temperature, speed of spin-coating and surface pressure that may have different consequences for the self-organization process [132]. For example Kline *et al.* have found the width of P3HT nanoribbons from chloroform solution is only around 8 nm, which contains shorter chains than our result from ethyl acetate solution. Therefore controlling different variables in the experiments and understanding the assembling mechanism in much detail will be the key to build well-defined nanostructure of supramolecular polymer films on different scales.

4.2 Self-assembly of single dendronized polymers controlled by dendronization

Self-assembly of molecular nanostructures from macromolecules offers to nanoscience and nanotechnology a powerful tool for both top-down miniaturization and bottom-up nanofabrication approaches [62]. Of particular interest are single polymers whose conformation directly influences the self-assembly of nanostructure [132]. Research on the control over the conformation of single polymeric molecules is inspired by biomacromolecules, which exhibit highly ordered hierarchical structures driven by non-covalent interactions, such as hydrophobic interaction, π-π stacking, or hydrogen bonding [133]. Folding of proteins, e.g., leads to complex tertiary and quaternary structures, which determine their properties and functions [61,134]. Recently ordering phenomena on different length scales controlled by hydrogen bonds have been studied for different single synthetic polymers exhibiting helical secondary structures [68,135,136,137,138]

Dendronized polymers (“denpols”) are a class of comb polymers in which regularly branched units (dendrons) with a specific number of branching layers (generation numbers) are attached to a linear backbone at every repeat unit [18,139,140]. In this way a flexible polymer can be converted into a rigid rod just by proper dendronization [18]. The higher the generation numbers are, the higher is the dendrons' space demand and, thus, the higher interaction between the tightly spaced (typically: 2.5 Å) consecutive dendrons. This increased dendron/dendron interaction leads to an increased shape-persistence which is a key difference of such macromolecules compared to those with the same backbone but without dendritic layer. The dendritic layer however not only impacts the shape-persistence but also has the advantage that its thickness can be systematically varied by taking synthetic measures. Together with the ability of many dendronized polymers to be surface engineered [139,141,142,143], these polymers exhibit interesting application options which include to (a) pattern solid surfaces [144,145], (b) move individualized macromolecules on solid substrates by SFM [13], (c) do first steps towards a bottom-up approach to ordered functional arrays [15,146,147], (d) apply a shielding concept to those representatives with fluorescent or electrically conducting backbones [148], (e) let representatives substituted with mesogenic dendrons self-assemble into ordered bulk material [149,150] and (f) let positively charged representatives self-assemble into huge ordered molecular aggregates [69,151]. Specifically the latter aspect, in which some future potentials is seen for the construction of hierarchically structured molecular objects of unprecedented dimensions, trigger the organic chemists to develop dendronized polymers with

such peripheral functional groups that can be turned into negatively charged ones. In this way the already existing polyelectrolytes on the basis of dendronized polymers with hundreds or even thousands of positive peripheral charges per macromolecule would have interesting counterparts to explore their individual and joint aggregation behavior.

In this chapter, an SFM investigation is presented of individualized second and third generation denpols (Scheme 4.1) both with neutral (**PG2a, PG3a**) and negatively charged peripheral groups (**PG2b, PG3b**), respectively. The branching superstructure of neutral denpols and the self-folding nanostructure of negatively charged denpols will be presented as well.

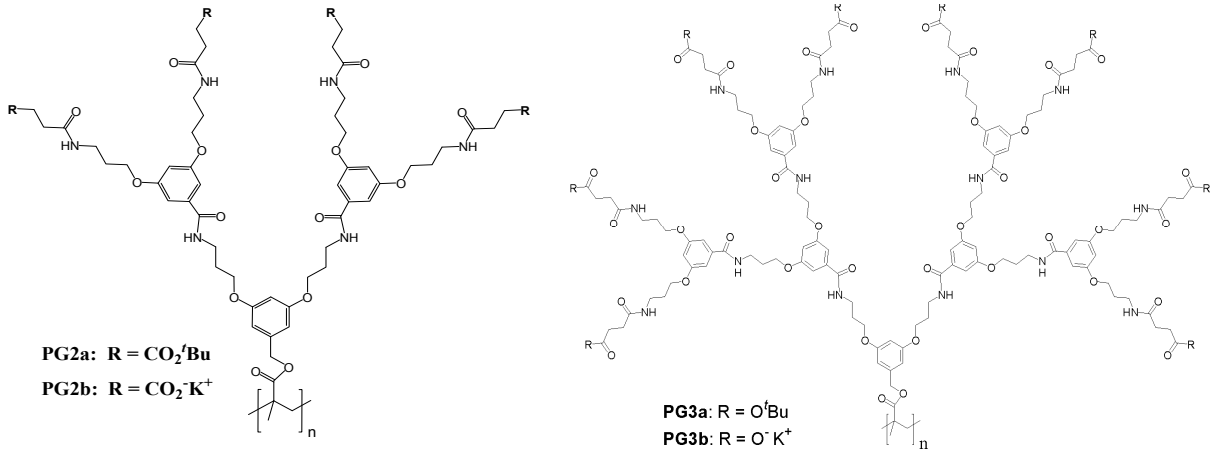

Scheme 4.1: Chemical structure of non-charged and charged second and third generation dendronized polymers PG2a, PG2b, PG3a and PG3b, respectively.

4.2.1 Contour length of denpols investigated by SFM

The synthesis of neutral denpol molecules of second and third generation (**PG2a** and **PG3a**) was described briefly in *Chapter 3.12*. Individualized **PG2a** and **PG3a** were spin-coated from dilute chloroform solutions onto freshly cleaved mica and visualized via tapping-mode SFM. The surface density of adsorbed molecules was varied from closed films to isolated molecules by varying the concentration of the spin coated solution between 5 and 50 mg/L. SFM images of individualized dendronized polymers reveal linear objects with a distribution of lengths. Figure 4.10 shows that with a few exceptions the lengths of **PG2a** and **PG3a** can be determined quantitatively. The sketch lines were carefully drawn along the chosen contours, and then the lengths of these sketch lines were calculated by a home-developed program [110]. Details of the contour length determination from SFM images were described in *Chapter 3.33*.

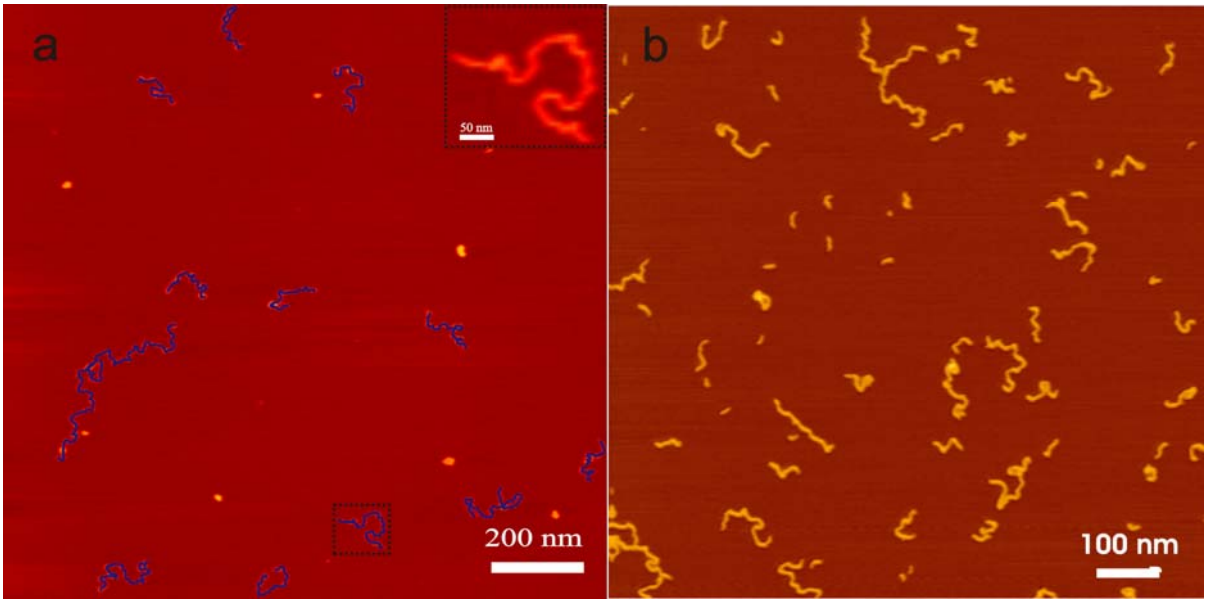

Figure 4.10: (a) SFM image of PG2**a on mica as used for contour lengths determinations. The overlays mark those molecules, for which the lengths have been determined. (b) SFM image of** PG3a **on mica without overlays yet.**

From their contour length distributions the number and weight averaged molecular weights, M_n and M_w, were calculated assuming a length of the repeat unit of 0.25 nm and a molar mass of the repeat unit of 1447 g/mol for **PG2** and 3074 g/mol for **PG3**, respectively. (See Table 4.3).

Table 4.3: Number and weight averaged lengths L_n and L_w and molecular weights M_n and M_w, and the resulting polydispersity Index PDI from SFM data. Noted that PG2a has two samples from different reaction entries (P9 and P10), in which 1.0 mol% and 0.7 mol% AIBN were added, respectively [106].

Sample	Entry	L_n (nm)	M_n (g/mol)	L_w (nm)	M_w (g/mol)	PDI = L_w/L_n
PG2a	P9	197±9	1.1 x 10^6	544±43	3.1 x 10^6	2.76±0.34
PG2a	P10	253±11	1.5 x 10^6	626±57	3.6 x 10^6	2.47±0.33
PG3a	P8	92±4	1.1 x 10^6	179±21	2.2 x 10^6	1.94±0.31

Table 4.4: Conditions for and results of radical polymerization of P9 and P10 (polymerization time: 16 h).

Entry	Product [gram]	DMF [μL]	AIBN [mol %]	Yield [%]	M_n[(a)] [x 10^6]	M_w[(a)] [x 10^6]	M_w[(b)] [x 10^6]	M_n[(c)] [x 10^6]	M_w[152] [x 10^6]
P9	1.00	450	1.0	87	2.6	7.8	5.8	1.1	3.1
P10	2.22	1000	0.7	90	2.9	9.3	7.6	1.5	3.6

(a) GPC results calculated by light scattering signals only

(b) MALLS in DMF without LiBr

(c) SFM contour length analysis

The molecular weights M_n and M_w of **PG2a** determined by SFM were compared to molecular weights determined by GPC and static and dynamic light scattering (MALLS). The absolute numbers of both M_n and M_w for the samples of entries P9 and P10 of Table 4.3 are generally lower than those obtained by GPC and light scattering. There are different possible reasons, one being that the backbone may not be in its all-*trans* conformation, which reduces the average length of the repeat unit to a value below 0.25 nm. Moreover, molecules were not counted for the contour analysis, if they did not exhibit two clearly recognizable ends [139], e.g., if they aggregated intra- or intermolecularly. Although the fraction of objects, which could not be included in the statistical analysis, is below approximately 10 %, it is the very long molecules that are particularly prone to aggregate, thereby lowering the determined average molecular weight. The lowering effect seems irrelevant between different solvents used in light scattering and in SFM measurements, e.g. when the same entry P10 sample dissolved in HFIP for light scattering measurements was spin-coated onto mica and measured by SFM: the resulting M_w was 3.4 x 10^6 g/mol, which is still lower than the value obtained from light scattering. On the other hand, for linear brush polymers consisting of a long main chain with densely grafted linear side chains several studies exist which compare the absolute molecular weight as determined by scattering methods and the length of the polymers as determined by SFM [153,154,155]. The interpretation in terms of apparent length per main chain repeat unit, l_m, on the surface gave strongly varying results, i.e. 0.07 nm < l_m < 0.23 nm depending on side chain length and grafting density which are not always precisely known. The corresponding values for the dendronized polymers of entries P9 and P10 (Table 4.4) are l_m = 0.13 and l_m = 0.12, respectively. It seems that brush and low generation dendronized polymers show a similar contraction behavior upon adsorption to solid substrates. This dense contraction can be

attributed to an interplay between attractive (e.g., van der Waals forces and capillary forces upon drying) and repulsive forces (entropy loss of dendrons due to volume exclusion) [156].

The deprotection of neutral denpols yielding negatively charged denpols has been briefly described in *Chapter 3.12*. **PG2b** and **PG3b** were the deprotected samples originally from entry P10 of **PG2a** and entry P8 of **PG3a**, respectively. They were dissolved in distilled water with a concentration of 5-10 mg/L plus 2% Methanol. To prepare **PG2b** and **PG3b** on mica, poly(L-ornithine) (molar mass 30.000-70.000 g/mol, Sigma, St. Louis, MO) was spin-coated onto mica, and then a drop (10 µl) of denpol aqueous solution was deposited onto poly(L-ornithine) coated mica (PLO mica) for 10 seconds; finally the remaining extra liquid was spun away. Individualized polymers were visualized via tapping-mode SFM. Figure 4.11 shows **PG2b** and **PG3b** on PLO mica respectively. At the same time, **PG2b** was also prepared on HOPG surfaces. For this, first a chloroform solution of octadecylamine ($C_{18}H_{37}NH_2$) (100 mg/L) was spin-coated (50 rps) onto freshly cleaved HOPG to form a monolayer; then a drop (10 µl) of denpol aqueous solution (5-10 mg/L) was deposited onto $C_{18}H_{37}NH_2$ coated HOPG for 10 seconds; afterwards the remaining extra liquid was spun off. M_n and M_w from contour length determinations (Table 4.5) yield the polydispersity of **PG2b** and **PG3b** on PLO mica and **PG2b** on $C_{18}H_{37}NH_2$ coated HOPG, respectively.

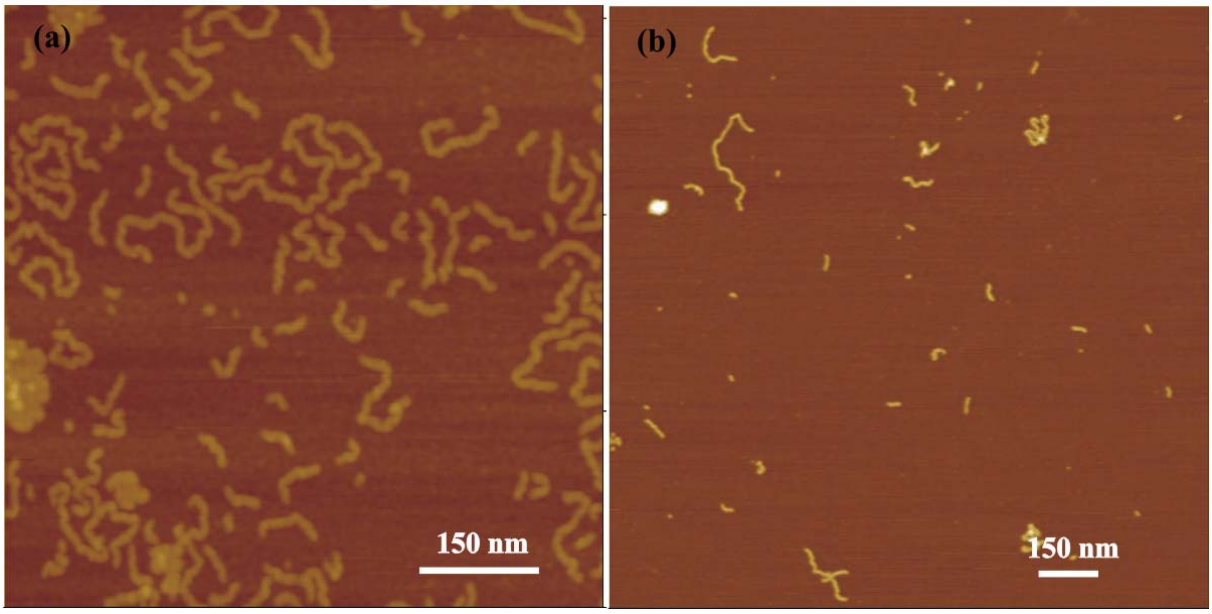

Figure 4.11: (a) SFM image of PG2b **on PLO mica as used for contour lengths determinations. (b) SFM image of** PG3b **on PLO mica.**

Table 4.5: Number and weight averaged lengths L_n and L_w and molecular weights M_n and M_w, and the resulting polydispersity Index PD of PG2b **and** PG3b **from SFM data. The data of** PG2a **and** PG3a **are listed for comparison.**

Sample	entry	L_n (nm)	M_n (g/mol)	L_w (nm)	M_w (g/mol)	PDI = L_w/L_n
PG2b on PLO mica	P10s	128±5	0.74 x 10^6	272±27	1.6 x 10^6	2.13±0.30
PG2b on precoated HOPG	P10s	135±8	0.78 x 10^6	278±38	1.6 x 10^6	2.06±0.41
PG3b on PLO mica	P8s	53±4	0.6 x 10^6	126±24	1.5 x 10^6	2.39±0.62
PG2a on mica	P10	253±11	1.5 x 10^6	626±57	3.6 x 10^6	2.47±0.33
PG3a on mica	P8	92±4	1.1 x 10^6	179±21	2.2 x 10^6	1.94±0.31

The data show that within the statistical error the lengths of **PG2b** are identical on both employed substrates (PLO mica and pre-coated HOPG), indicating that the substrate plays a minor role for this determination. Most surprisingly, it was found that the average lengths of all of the non-charged polymers (**PG2a** and **PG3a**) are about twice as long as for the corresponding charged samples (**PG2b** and **PG3b)**.

In order to verify this half length effect, the contour length distribution of **PG2a** and **PG2b** was plotted. 700 chains of each **PG2a** and **PG2b** were chosen to calculate the contour length, and 291 chains of each **PG3a** and **PG3b** were chosen in case of third generation denpols. The length distribution histogram data as shown in Figure 4.12 and the histograms were fitted to a Schulz-Flory (S-F) distribution shown as solid lines, which is suitable for a radical polymerization terminated by a chain transfer reaction [157]:

$$\Psi(L) = p^{L-1}(1-p) \qquad \text{Eq. 4.2}$$

where p is a real number less than 1, indicating the probability that monomers continue to contribute to the growth of a chain with length of L, or as the probability that A reacts with B;

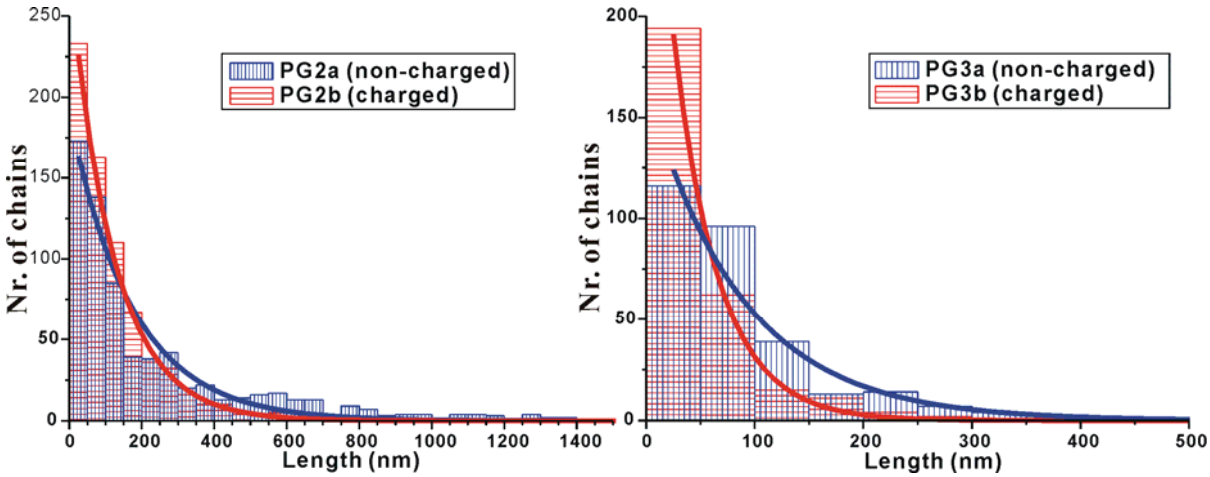

Figure 4.12: Length distributions for linear objects of PG2a **and** PG3a **on mica, and** PG2b **and** PG3b **on pre-coated mica. The total numbers of objects were 700 for** PG2a,b **and 291 for** PG3a,b**. The length histograms with bin size of 50 nm were all fitted to a Schulz –Flory distribution, which is typical for a high degree of radical polymerization.**

The histograms show that the charged samples are dominant in the short length region, while non-charged samples are distributed over a broader range. However, since the length histogram depends on the bin size, i.e. the width of each column, consequently the fitted distribution curve also depends on the bin size. Therefore the bin size has been varied for different samples' distributions. Interestingly, as shown in Figure 4.13, when the bin size for the non-charged samples (**PG2a** and **PG3a**) was chosen twice of the bin size of their charged analogues (**PG2b** and **PG3b**), both distributions in the same generation display a very similar shape but with different bin sizes by factor of two, i.e. the number of chains in the column between 0-50 nm in **PG2a** (Fig. 4.13 a) corresponds roughly to the number of chains in the column between 0-100 nm in **PG2b** (Fig. 4.13 b), or the number of chains in the column between 30-60 nm in **PG3a** (Fig. 4.13 c) corresponds roughly to the number of chains in the column between 60-120 nm for **PG3b** (Fig. 4.13 d).

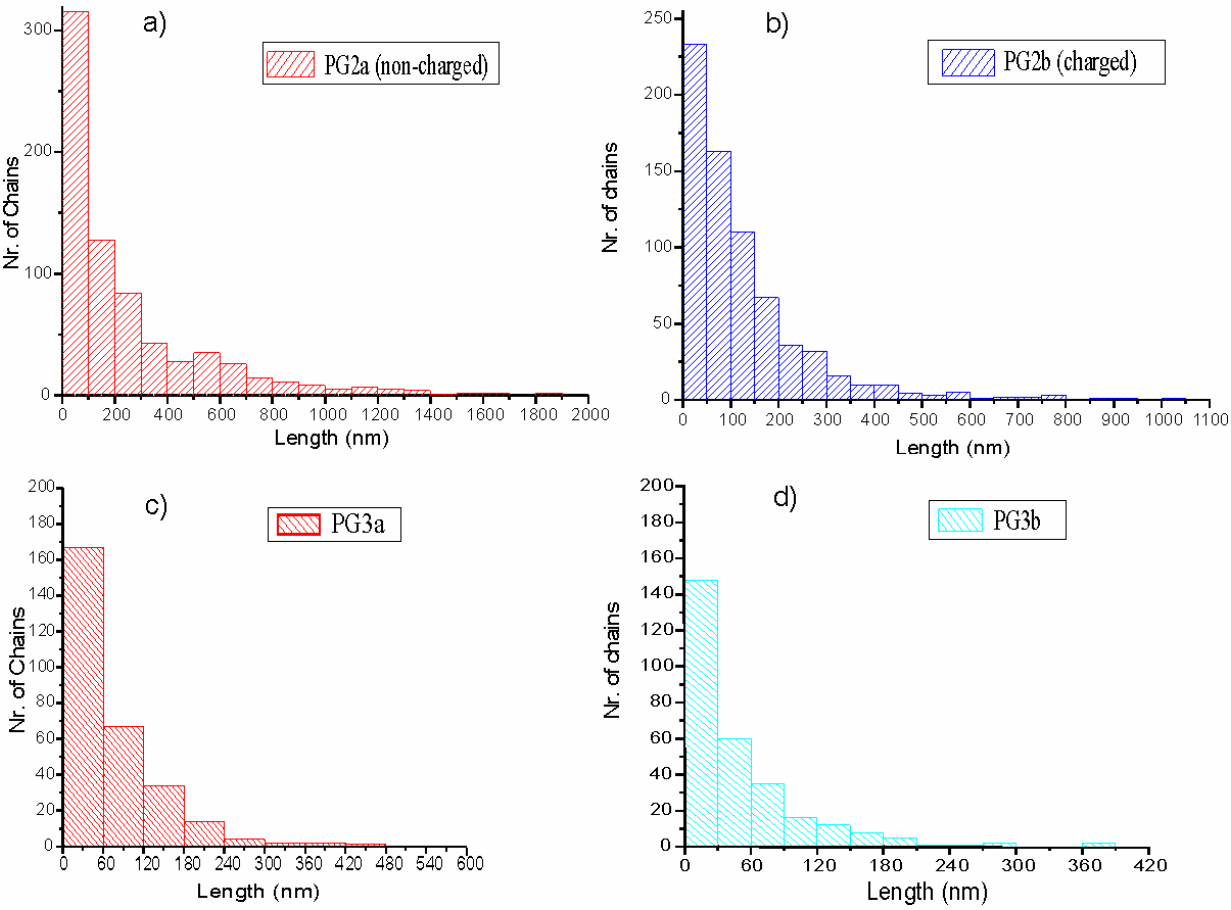

Figure 4.13: Length distributions of (a) PG2a **on mica with bin size 100 nm, (b)** PG2b **on PLO-coated mica with bin size 50 nm, (c)** PG3a **on mica with bin size 60 nm, and (d)** PG3b **on PLO-coated mica with bin size 30 nm**

Such a "half length" effect prompted a study of these contour length data more statistically. All the distribution histograms were fitted to Schulz-Flory distributions. The S-F distribution is deduced from the kinetics of the chemical reaction which led to the polymer chains. In the case of **PG3a** prepared from free radical polymerization, the probability that monomers continue to contribute to the growth of a chain with length L is denoted as p, which is assumed to be independent of the chain length L. If the chain growth is terminated by chain transfer to solvent molecules, the probability to find a chain with length L is $\Psi(L) = p^{L-1}(1-p)$. The total number of chains (with different lengths) is $N = n_m(1-p)$, where n_m is the total number of monomers. Hence the normalized distribution function reads

$$P(L) = Ap^{L-1}(1-p)^2 \qquad \text{Eq. 4.3}$$

with A being a normalization factor.

On the other hand, if the chain growing is terminated by dimerization, the distribution is:

$$P(L) = A(L-1)p^{L-2}(1-p)^3/2 \qquad \text{Eq. 4.4}$$

For long chains of denpols we approximate L-1 and L-2 as L, thus Eq. 4.3 and 4.4 can simplify as:

chain transfer termination $$P(L) = Ap^{L}(1-p)^2 \qquad \text{Eq. 4.5}$$

dimerization termination $$P(L) = ALp^{L}(1-p)^3/2 \qquad \text{Eq. 4.6}$$

The **PG3b** chains are not directly prepared by free radical polymerization, but rather converted from **PG3a.** Therefore it is not appropriate to fit a contour length distribution for **PG3b** directly to S-F functions. It is assumed that the contour lengths *L* of **PG3a** changes systematically to $L_b = f(L_a)$, when **PG3a** is converted to **PG3b**. The function $f(L_a)$ is called transformation function. If the original distribution function of L_a is $P_0(L_a)$, after the transformation, the new distribution becomes:

To chain transfer termination $$P\_(L_b) = \frac{P_0(f^{-1}(L_b))}{f'(L_b)} = A\_\, p^{\frac{L_b}{\alpha}}(1-p)^2/\alpha \qquad \text{Eq. 4.7}$$

where for simplicity we assume $f(L_a)$ to be linear, i.e. $L_b = f(L_a) = \alpha L_a$, $L_a = f^{-1}(L_b) = \frac{L_b}{\alpha}$

and to dimerization termination $$P\_(L_b) = A\_(L_b/\alpha)p^{\frac{L_b}{\alpha}}(1-p)^3/2\alpha \qquad \text{Eq. 4.8}$$

First the contour length distribution of **PG3a** is fitted to a distribution function $P_0(L_a)$ (Eq. 4.5 or 4.6) to obtain *p*. Note that *p* is a parameter characterizing the property of the polymerization process. If both **PG3a** and **PG3b** are chemically prepared from the same batch of polymerization, they should be characterized by the same *p*. Upon using the same *p* and L_b, and by fitting a suitable α we can fit the experimental length data of **PG3b** with the distribution function $P\_(L_b)$ (Eq. 4.7 and 4.8) as shown in Figure 4.14. The transformation parameter α = 0.55 by assuming chain transfer terminating and α = 0.52 by assuming dimerization terminating. The results suggest a linear relationship, $L_b = 0.52\sim0.55L_a$, which again strongly

points to charged denpols shrunk to half the length of the corresponding non-charged analogues.

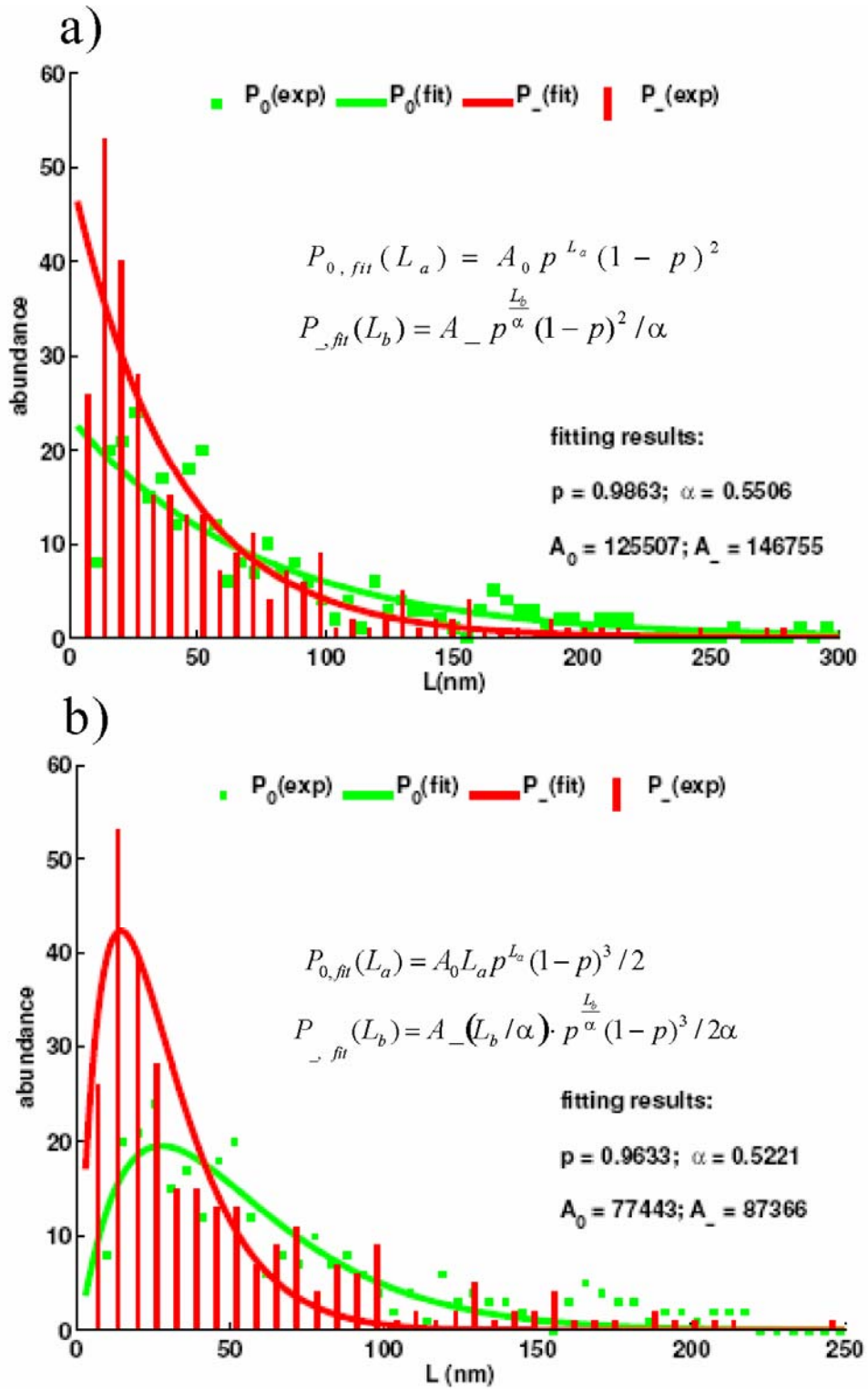

Figure 4.14: Distributions of experimental contour length of PG3a **and** PG3b **with bin sizes of 7 nm and fits for both of them to S-F distribution a) by assuming chain transfer termination or b) by assuming dimerization termination, revealing that the contour length of non-charged denpols L is mapped to L/2 via charging.**

4.2.2 Self-assembled duplex structures and their decomplexation

The statistic analysis of the lengths of the observed worm-like objects allows to map the distribution of the contour length L of the non-charged denpols to the charged analogues: $L_b \rightarrow f(L_a) = L_a/2$ to high precision. This finding can potentially be understood either by (i) a backfolding of the charged polymer to a duplex or (ii) a halfway scission of non-charged polymers to charged analogues, (iii) crumpling, or (iv) scission and subsequent association. While complete backfolding or halfway scission is compatible with a modification of the initial distribution of lengths *P(L)* by a transformation of *L* to *L/2*, which is as observed, cases (iii) and also (iv) would basically tend to result in a much broadened length distribution. The simulation results to be presented below will support the backfolding scenario (i). Moreover mobility issues in the adsorption process have been discussed in detail earlier [110] suggesting that the backfolding events are not initiated during the adsorption process but should have taken place in the solvent prior to adsorption. So in order to rule out (ii) halfway scission, not only the heights but also the widths of single polymers have been measured.

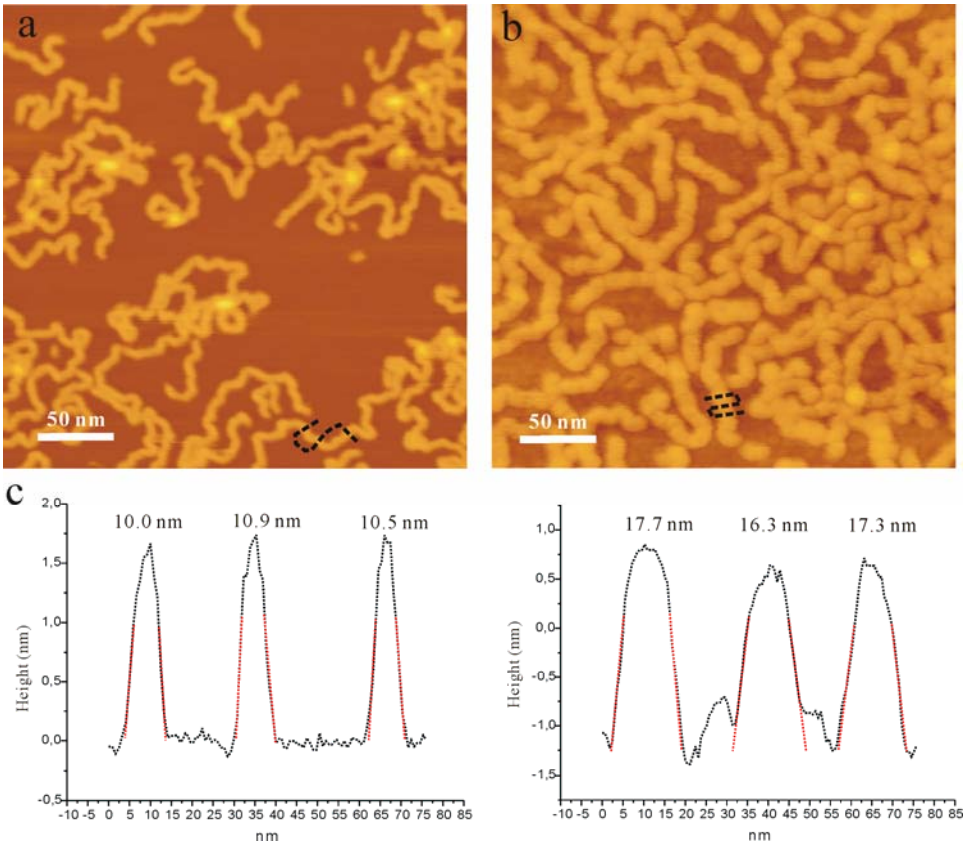

Figure 4.15: SFM tapping mode height images of a) non-charged PG2a on mica; b) charged PG2b on PLO mica; c) cross sections through two different chains along the black dashed lines shown in the upper images. The apparent bottom widths are measured by the widths of extended peak sides (red dotted lines) at average baseline.

Determination of the width of spherical cylinders: Heights and widths of the polymers exhibit a narrow distribution (Figure 4.15), irrespective of whether they are charged or non-charged. Since the exact numbers depend to some extent on the particular SFM-tip, images of both samples **PG2a** and **PG2b** shown in Fig. 4.15 were collected with a particularly sharp tip. It was checked that the tip did not suffer any significant changes by performing the experiments first for **PG2a** followed by **PG2b** and again for the initially used **PG2a**. The values for the two measurements on **PG2a** remained identical. The apparent widths and heights of the molecules on the surface can be determined from cross sections. Several hundred height and width values were taken and averaged. The apparent height increased from (1.67 ± 0.14) nm for **PG2a** to (1.81 ± 0.15) nm for **PG2b**. However, since the absolute values depend on many unknown effects including the sample-surface interaction, tip-surface interaction and the measurement environment [11], no further quantitative interpretation was done.

Table 4.6: Statistical width results of PG2a **and** PG2b **by SFM single molecule measurements**

Denpol	**PG2a**	**PG2b**
measured bottom width *W* in nm	11.1 ± 0.6	16.6 ± 0.8
assumed tip terminal radius *R* in nm	7.5 ± 2.5	7.5 ± 2.5
corrected molecule cylinder diameter *D* in nm	2.1 ± 0.9	4.6 ± 2.0

Table 4.6 shows the corrected widths of **PG2a** and **PG2b** after the obligatory correction process (see details of the commonly applied width correction for a cylinder in *Chapter 3.3*2). The resulting width values reveal that the charged **PG2b** is two times larger than the non-charged **PG2a**. However, since the commonly applied process requires an estimated tip terminal size, large errors may be induced by the correction. Therefore an advanced process of SFM width measurement [158] was applied in this work. First of all, spherical gold colloid particles with 15 nm diameter were applied onto PLO mica surface as a standard sample; then the gold particles were scanned by an SFM tip in tapping-mode (Fig. 4.16). The maximum height of each particle is measured in order to reconstruct the tip as shown in Fig. 4.16 (b). Since the gold particles are incompressible, the maximum height values represent the particles' diameters. Thus the real shape of the isolated gold particles can be reconstructed as shown in Fig. 4.16 (b) (red circles). With the reconstructed gold particle shape, a 3D shape of the SFM tip terminal can be sufficiently reconstructed. Here only its cross section in the fast scanning direction (x axis) is considered as shown in Fig. 4.16 (c), since the following width measurements were performed only along the fast scanning direction.

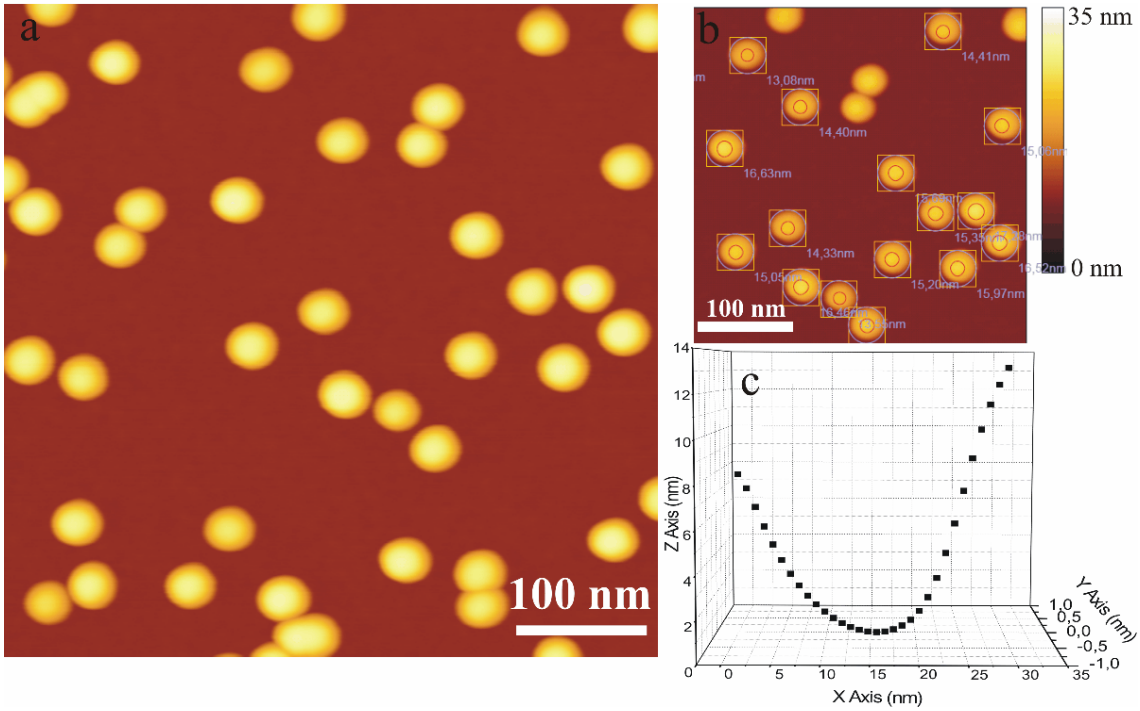

Figure 4.16: (a) SFM image of gold particles for tip calibration; (b) example of a processed image to calibrate an SFM tip by showing the height of each spherical particle and the corresponding "real" sphere as red circle; (c) cross section view of a reconstructed tip along x axis (fast scanning direction).

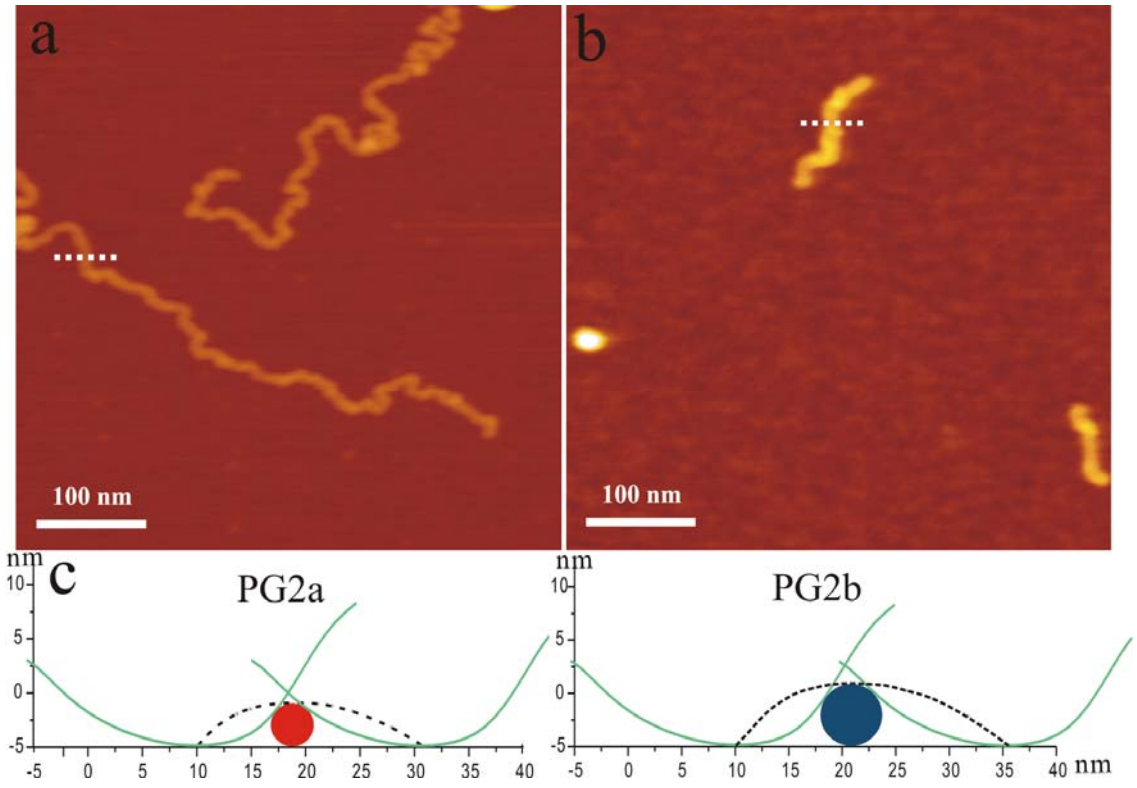

Figure 4.17: SFM height images of a) non-charged PG2a **on mica; b) charged** PG2b **on PLO coated mica; the white dotted lines are example cross section lines; c) shows how to reconstruct molecular cylinders (full circle) by a calibrated tip; the dotted black line is the moving trace of the SFM tip, when the tip interacts with the molecular cylinder [159].**

The calibrated tip was used to measure the non-charged **PG2a** on mica and then the charged **PG2b** on PLO mica. The cross sections were drawn perpendicularly through contours of molecules, which should be along the fast scanning direction (x axis) as shown in Figure 4.17 (a) and (b). Hundreds of cross section measurements were performed on each sample, thus the measured width of non-charged **PG2a** is 20.5 ± 2.1 and that of charged **PG2b** is 25.8 ± 2.1 nm. With these values it was possible to graphically reconstruct a dendronized polymer cylinder in a cross sectional view as shown in Fig. 4.17 (c). The reconstructed **PG2a** and **PG2b** cylinders have diameters of (3.9 ± 0.7) nm and (5.7 ± 0.9) nm, respectively. The resulting width values reveal that the charged **PG2b** is almost 47% thicker than the non-charged **PG2a.** Therefore if the denpol molecule is consider a spherical cylinder due to a high density of surrounding dendrons, the cross sectional area of **PG2a** is almost two times that of the area of the **PG2b** cylinder.

***Self-assembly*:** From the combined contour length and width data the scission process is excluded and instead backfolded duplices of charged denpols are suggested, as shown in Figure 4.18. It has been reported that the cationically charged denpol has become an amphiphilic polyelectrolyte by positively charging the peripheral functional groups which exhibit patterns of hydrophobic and hydrophilic regions on the nanometer scale. With cryo-transmission electron microscopy (Cryo-TEM) double-helices of cationically charged polymers of this sort were discovered [151]. Sheiko *et al.* [3] have also observed plectoneme supercoiled conformations for single polystyrene molecules jacketed by alkylated monodendrons, which have a similar chemical structure as denpols. In addition Tsukruk *et al.* have reported that amphiphilic dendrimers can self-assemble into supramolecular nanofibers at hydrophilic surfaces through dense stacking and packing of the polar cores along the surface and of hydrophobic shells in the topmost layer away from the surface [160]. The hydrophobic interaction is essentially the driving force for the formation of such semicylindrical micelles. Similarly, the individual charged denpols presented here, which are nothing else but a linear array of thousands of dendrons with polar shell and nonpolar core held at tight distance by the polymer backbone, have to reorganize their conformations when exposed to a polar environment. It is difficult for the dendron's polar shells to protect the non-polar core against the surrounding water in all the directions, as suggested by previous simulation studies [161]. Consequently, the self-folded duplex of individual charged denpols is a natural choice to reduce the non-polar surface area in a diluted aqueous solution. The energy price for this is accepted, which is the bending energy associated with the one or two hairpin foldings which are the result of this molecular reorganization process [162]. It should be noted that the duplex structure are

obviously stable when deposited onto the hydrophilic PLO mica surface, without transforming to face-on adsorption as the above mentioned self-assembled dendritic macromolecules do [163].

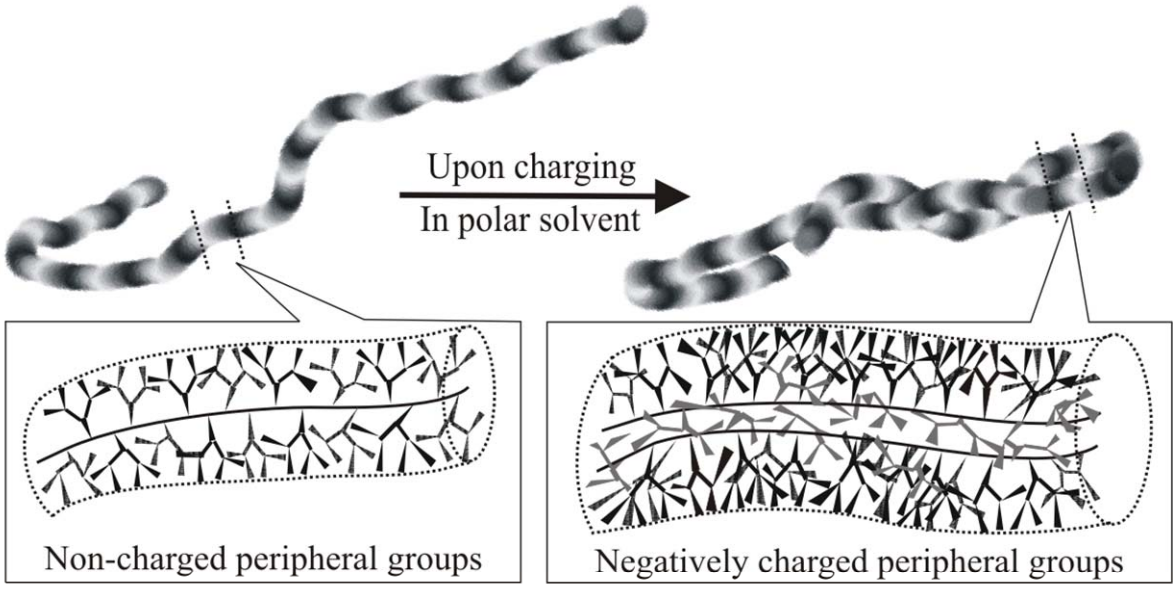

Figure 4.18: Schematic models of a relaxed single non-charged denpol chain (PG2a**) and a self-folding charged denpol chain (**PG2b**), on which the polar peripheral groups densely crowd the non-polar polymer backbone, such that the non-polar surface is significantly reduced in a polar solvent.**

Decomplexation: In order to further investigate the stability and superstructure of the self-folded duplex, the charged denpols **PG2b** were applied to a $C_{18}H_{37}NH_2$ coated HOPG surface. At first, a drop of a diluted aqueous solution of **PG2b** is spin-coated onto a $C_{18}H_{37}NH_2$ submonolayer pre-coated HOPG surface. By spin coating (ca. 50 rps) a thin film layer containing isolated charged denpols is formed on the HOPG surface under ambient conditions. Surprisingly some **PG2b** molecules exhibit an inhomogeneity on the HOPG surface. As shown in Figure 4.19 (a), chain 1 in a zoomed image shows a clear break in the middle, which is also observed for positively charged denpols on fatty acid pre-coated HOPG. An SFM tip manipulation experiment that moves the chain on the surface has verified the chain at the break position is still connected, that is possibly the terminal ends of two backfolding backbones as shown in Fig. 4.18 (b). Moreover, the open hairpin shape of chain 2 and the undulation of chain 3 in Fig. 4.19 (b) strongly suggest that the backfolding duplex can be decomplexed in certain controlled environments.

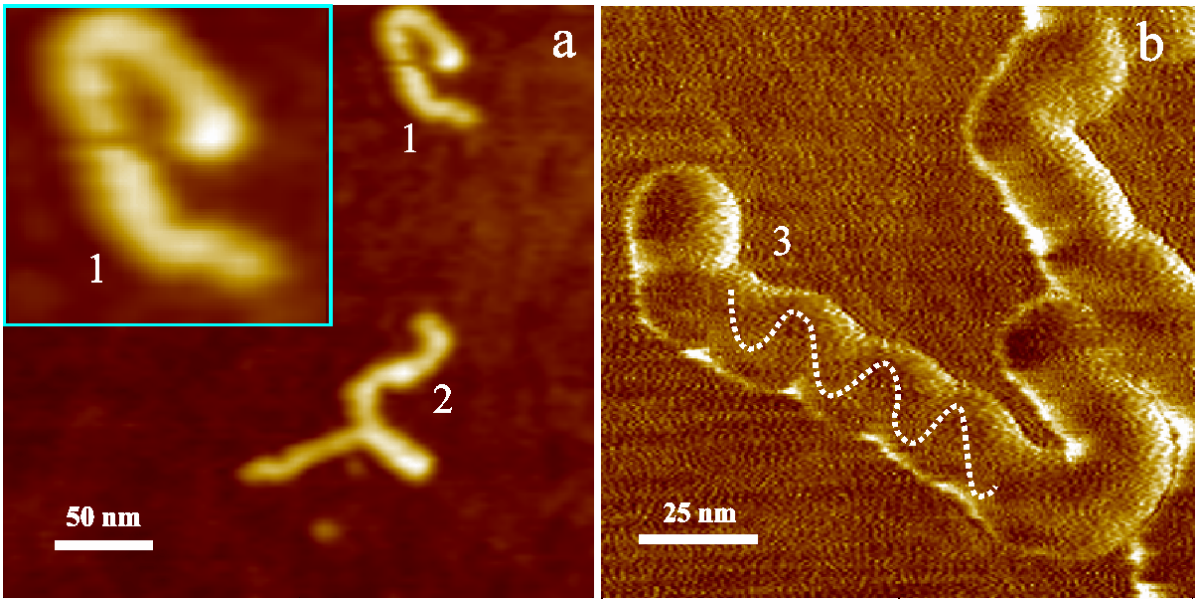

Figure 4.19: PG2b **on $C_{18}H_{37}NH_2$ submonolayer pre-coated HOPG. a) SFM height image with chain 1 exhibiting a discontinuity in the middle and chain 2 having a hairpin shape; b) SFM phase image of a chain showing undulation with a period of 18 nm.**

Therefore it was tried to put a charged denpol under more extreme conditions to possibly cause decomplexation into single-stranded structures. A drop of a diluted aqueous solution of **PG2b** was spin-coated onto the $C_{18}H_{37}NH_2$ monolayer pre-coated HOPG surface. By spin coating (ca. 50 rps), a thin water layer containing isolated charged denpols is formed on the $C_{18}H_{37}NH_2$ monolayer under ambient conditions. The $C_{18}H_{37}NH_2$ molecules in the monolayer are protonated to $C_{18}H_{37}NH_3^+$ under the water layer and then electrostatically adsorb the anionic **PG2b**. This sample was then immediately annealed at 100°C under vacuum (8 mbar) for 30 min and then investigated by SFM. As shown in Figure 4.20 most single **PG2b** molecules appear highly inhomogeneous not only as to their heights and widths but also to their chain contour. Isolated single chains often contain topological branches along the contour. Structural details were analyzed by two marked cross sections (Fig. 4.20 a). The corresponding height profiles are displayed in Fig. 4.20 (b). At the same time, height profiles following lines 3 and 4 along two chains were plotted (Fig. 4.20 c). Cross section 1 results in a peak with 3.15 nm height and 32.8 nm bottom width, and cross section 2 in a peak with 2.25 nm height and 26.5 nm width. Considering broadening effects by a spherical SFM tip with terminal radius R and the apparent measured bottom width $2W$, the corrected spherical cylinder diameter D can be estimated by $D = W^2/2R$, when $R > D/2$. (See details in *Chapter 3.3.2*). Since one and the same tip was used for the image, and the tip-sample interaction (setpoint) was kept constant during scanning, the resulting ratio is independent of the actual SFM tip terminal radius R. Thus, the ratio between the spherical cylinder diameter at cross section 1 and the one at cross section 2 is

about 1.53. The height profile along chain 3 reveals rather inhomogeneous chain heights. There are two significant plateaus at 3.1 ± 0.2 nm and 2.2 ± 0.1 nm, resulting in a ratio between them of about 1.41. Both width and height measurements on chain 3 therefore indicate that there are thicker and thinner regions along the same chain, whereby the cross sectional area in the former is almost two times that of the latter. The analysis of chain 4 shows similar results. If one regards the thin region as caused by a part of a single chain, the thick region obviously reflects the duplex.

The coexistence of single and double-stranded features in the same object manifests that during the drying and annealing process the conformation of the isolated charged denpol changed considerably. This could result from either a diffusion process in which isolated single chains diffuse together to form (imperfect) aggregates on the surface, or a decomplexation event in which isolated duplices break open under the forcing conditions. Negatively charged denpols can be immobilized on positively charged surface due to strong electrostatic interaction [146]. If the surface consists of a protonated $C_{18}H_{37}NH_3^+$ monolayer, a strong surface ripple would prevent adsorbed polyelectrolyte molecules from lateral diffusion [81]. However, the question arises whether the annealing temperature which is well above the melting point of $C_{18}H_{37}NH_2$ on a monolayer (which is 52°C as in the bulk) could induce the polymer molecules to diffuse and form aggregates. The answer to this question is clear: No. If such an effect would be operative not only duplexes but also higher aggregates should be formed which was never observed. In addition some other single polyelectrolyte molecules such as ds-DNA and polystyrene sulphonate, which have also been adsorbed to $C_{18}H_{37}NH_2$ monolayers, did not aggregate after annealing. The ripple of a $C_{18}H_{37}NH_2$ monolayer is obviously pronounced enough to prevent isolated polyelectrolytes from freely moving across the surface.

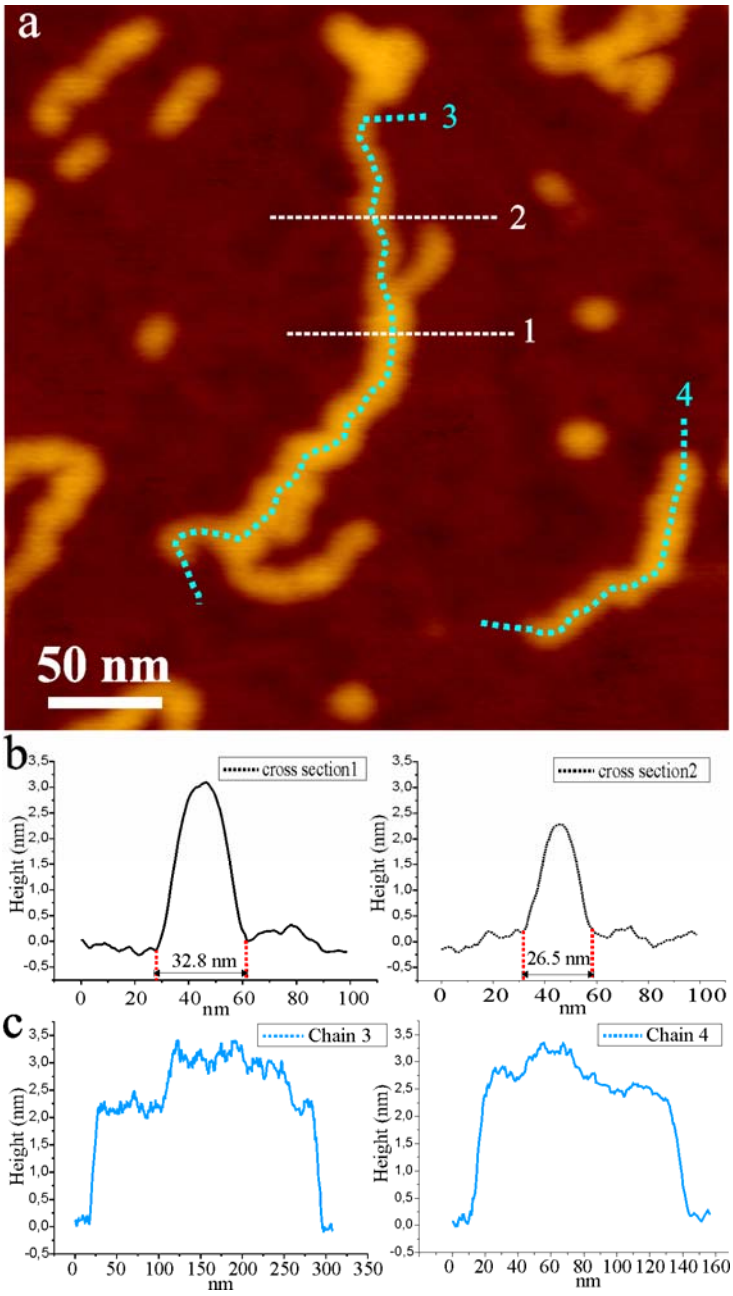

Figure 4.20: (a) High resolution SFM image of split charged PG2b **molecules on octadecylamine monolayer pre-coated HOPG after drying and annealing; (b) Height profiles of cross sections 1 and 2; (c) height profiles of contours 3 and 4 [159].**

Thus, a decomplexation of the duplex is proposed as the process responsible for the results observed by SFM, which can be rationalized as follows. Linear alkyl chains have a strong affinity to the HOPG surface due to van der Waals interactions ([21] see also references therein). Polyelectrolytes electrostatically linked to alkyl chains can suffer stretching [81] and for example ds-DNA can be denaturated during adsorption to alkyl amine covered HOPG surface [22]. Furthermore, a polymer backbone covalently linked to long alkyl chains on every repeat unit can even be ruptured during adsorption [164]. In the experiment reported here, the polar environment (aqueous solution), which is the initial condition for the formation of

charged denpol duplex, was removed in vacuum during the annealing at 100°C. Consequently the two denpol backbones twisted together in solution lose the affinity to each other due to intermolecular repulsion. On the other hand, when the surface temperature is increased to 100°C, the mobility of octadecylamine chains on the surface has slightly increased. Hence the denpol molecules electrostatically adsorbed by mobile alkyl amine chains can locally relax themselves to some extent. When the surface temperature decreases to room temperature after annealing, all the alkyl amine chains in the monolayer and the denpol molecules adsorbed by alkyl amine chains will crystallize on the HOPG surface. Finally what is observed under SFM is possibly the combined result of decomplexation, relaxation and crystallization.

***Manipulation*:** Besides the spontaneous decomplexation of duplex there are many possibilities to manipulate a duplex further. Isolated polymer chains can be manipulated on suitable surfaces using the SFM tip in contact mode [13,15,22]. The spontaneous decomplexation of the duplex initiated attempts to separate the decomplexed individual chains even further with the help of the SFM tip, knowing, of course, that the conditions for this after drying would be challenging. At room temperature alkyl amines such as dodecylamine or octadecylamine are crystalline and any rotation of the remaining duplex backbone during splitting should be severely hampered by large friction forces and the strong interaction between the alkyl chains and HOPG. As shown in Fig. 4.21 (b), stretching the upper arm has effectively separated two backbones in the duplex. However the separation reached the limit soon as shown in Fig. 4.21 (c), the possible reason being a knot, which typically appears in double helical polymers. Further tightening the knot would only cause large resistance that may stem from steric hindrances between the dendrons. Fig. 4.21 (d) sketches the possible knot appearing in a single duplex polymer, though such a well defined double helical conformation may not really exist in the denpol sample.

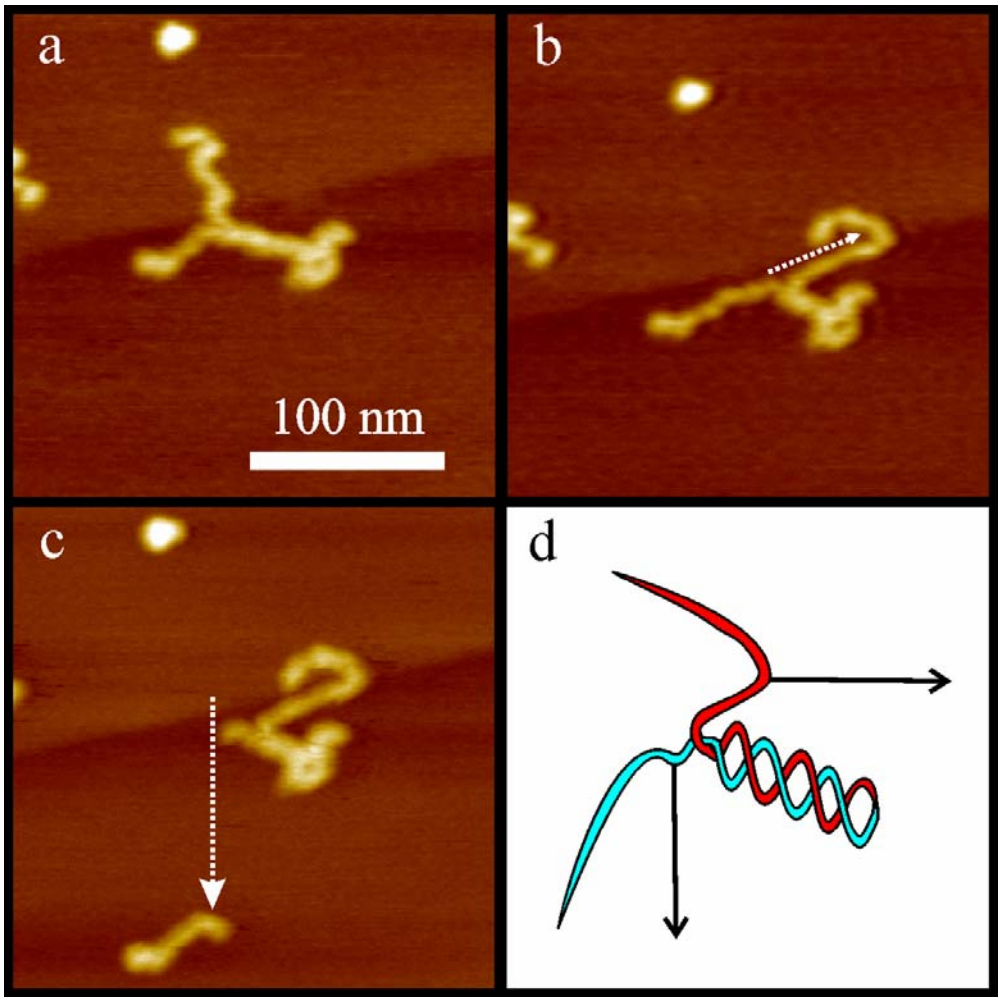

Figure 4.21: (a) SFM image of a PG2b **duplex with spontaneously denatured hairpin shape on the dodecylamine monolayer pre-coated HOPG surface; (b-c) a sequence of SFM tip manipulations in order to split the duplex further; the white arrows show the moving traces of the SFM tip in contact mode; (d) a schematic drawing indicating the knot, which may prevent a further split.**

It was therefore decided to rather try a further separation of a decomplexed strand where no chain rotation is required (see Figure 4.22). At the terminus of a decomplexed duplex, the polymer backbone folded back as shown in Fig. 4.22 (a). The SFM tip was inserted into the topological complex and moved as shown in Fig. 4.22 (b)-(c). Although some dendrons seem to have been scratched off the backbone, the folded duplex backbone was clearly split into two separate backbones, which apparently remain continuous. This result further supports the model in that the duplexes are mainly formed by two single rather than several self-folded denpol molecules.

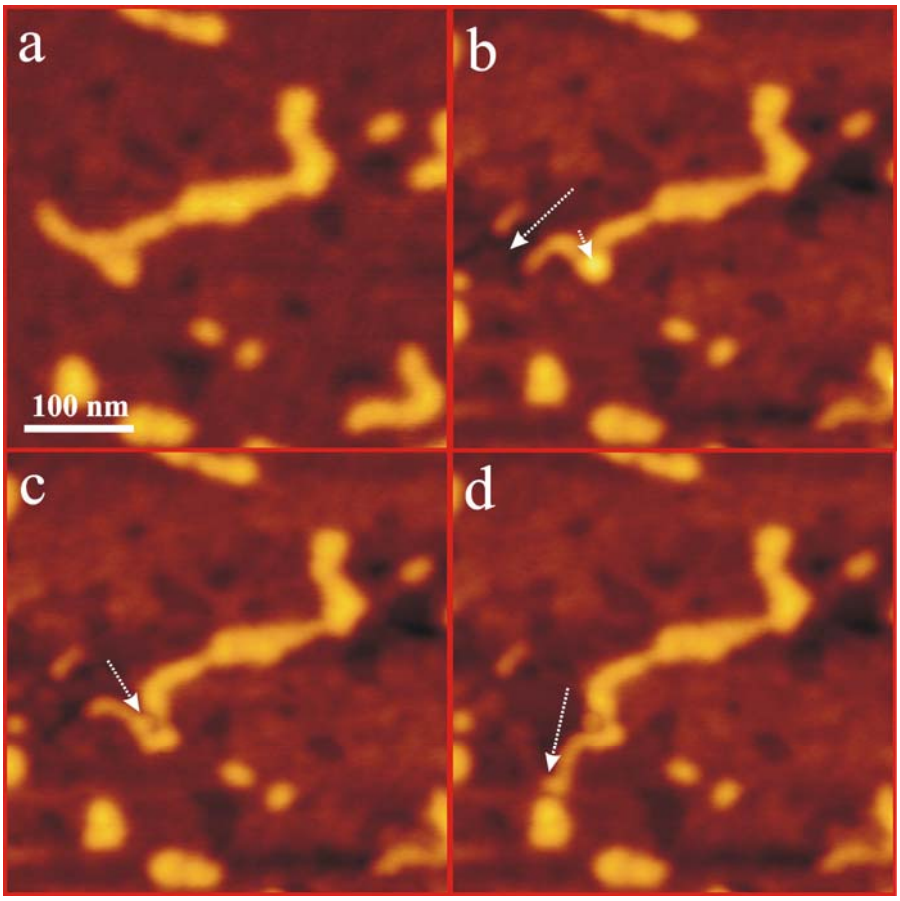

Figure 4.22: (a) Tapping mode SFM image of a charged PG2b on a octadecylamine monolayer coated HOPG after drying and annealing; (b-d) a sequence of SFM tip manipulations in order to decomplex a terminal of the duplex; the white arrows show the moving traces of the SFM tip in contact mode [159].

Simulation: In order to better understand the mechanism of the duplex formation, a computer simulation of single charged denpol was performed in the group of Prof. Martin Kröger (ETH Zurich). The so called Janus chain (JC) model [161] had recently been established and allows to investigate the structure and dynamics of denpols. The model is ultimately based on an *ab-initio* approach and eliminates most of the degrees of freedom of a denpol. It therefore enables the study of the association mechanism, conformation, dynamics, superstructure, and phase diagram of these polymers numerically. The JC is a coarse-grained representation of a denpol which captures essential physical mechanisms of peripherally charged polymers. It replaces each single denpol by a string of Janus beads which are linearly connected by finitely extendable nonlinear elastic springs, while semi-flexibility of such chains (whose strength is determined independently from the molecular architecture) is realized by a bending potential [165]. In addition to multibead chain models frequently used to study conventional, uncharged, and less internally structured polymers [166], each Janus bead carries its own (Janus) vector that allows to reflect the state of the internal structure at its position within the denpol. The orientations of Janus vectors represent the asymmetry of charge distribution on the interface

between the polymers interior and solvent. The vectors point to the direction where the charge density is low and the interface hydrophobic. Hydrophobic interactions in aqueous solvents are the main source of affinity between the model denpols. Hence the Janus vector can also be considered as an indicator of a non-bonded assembly due to hydrophobic attraction. The dynamics of the JC directly follows from the interaction potentials assigned to Janus beads and vectors, while these interaction potentials have been motivated from *ab-initio* studies. A detailed interpretation of the JC model and its few geometrical and mechanical parameters is available [167]. In particular, JCs form double helically interwound fibers due to amphiphilic interactions, and within proper solvent. If the concentration is as low as for the case realized experimentally in this work (concerning denpol chemistry, solvent condition), at low concentrations, these particular JCs tend to interwind with themselves, i.e., backfold. A representative time series is shown in Figure 4.23. The simulation results obviously support the self-folding argument, and the electrostatic interactions seem strong enough (i.e., large compared with thermal energies) to mostly achieve complete backfolding, with a kink at the center of the chain. A type of crumpling occurs within the JC model if the effective solvent quality would be worse in case of charged systems, but globular aggregates rather than well-defined linear structures are observed. Scission is currently not accounted for in the JC model, such that the model cannot disapprove the half-way-scission mechanism, or scission-and-recombination mechanism, directly. However, from independent studies in organic chemistry [86] it is known that the scission energies are large compared to characteristic bending energies for the given dendronized polymers (the energy needed to break a sp3 C-C bond is 80 kcal).

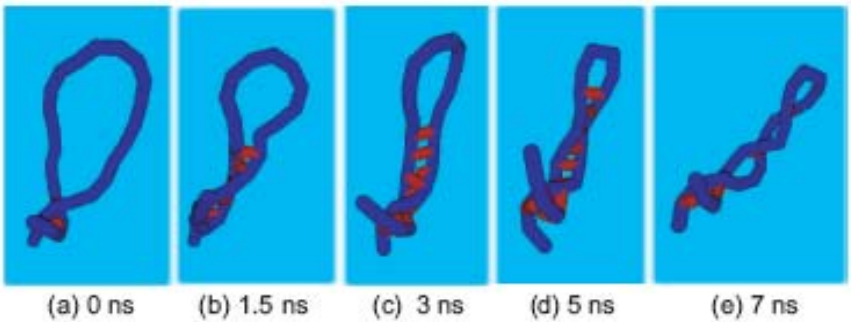

Figure 4.23: Back-folding process. Snap shots taken during the simulation of a PG3b **Janus chain (a single denpol) in aqueous solution. The backbone of the Janus chain with contour length 92 nm is shown in blue. The red bars represent Janus vectors indicating the existence of effectively attractive, non-bonded interactions, which ultimately trigger the assembling process and compete with the penalty for bending. The time evolution is labelled as (a) to (e). Helical inter-winding is a self-stimulating process. A random contact point (a) propagates until the whole chain folds back to itself (e). The particular formation process (a)-(e) required about 7 ns (at room temperature) [159].**

4.2.3 Branching of dendronized polymers investigated by SFM

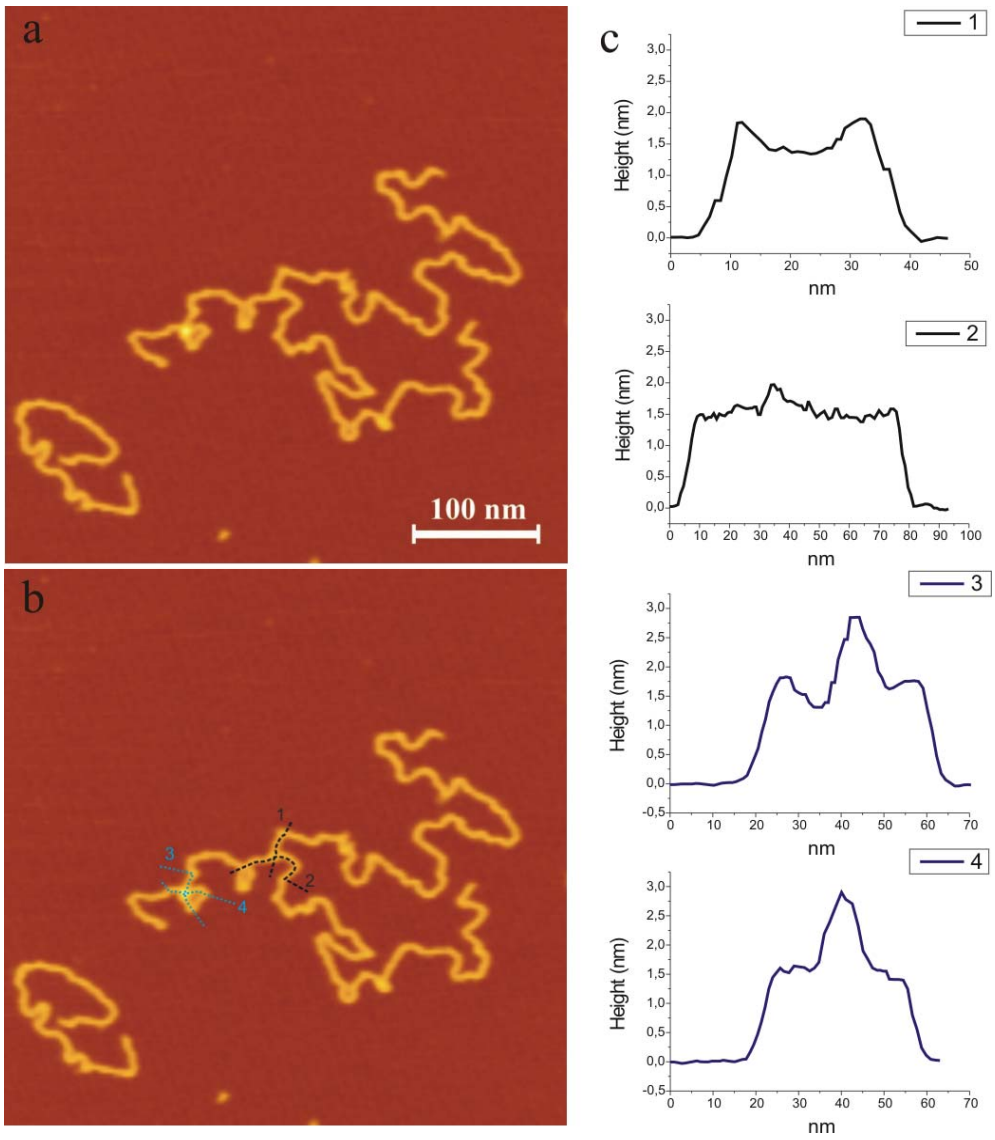

Figure 4.24: (a) Tapping-mode SFM images of individualized protected, non-charged PG2a **from entry P5 on mica, exhibiting branching; the height traces along the contours in (b) indicate chain crossing at the left and branching at the right junction; (c) height profiles of traces in (b).**

In free radical polymerization, branching occurs spontaneously by the replacement of a substituent, e.g, a hydrogen atom, on a monomer subunit, by another covalently bonded chain of that polymer. If it is a rare event, to date it is impossible to determine the low degree of branching through conventional polymer analytical methods such as viscometry, light scattering, GPC. Hence in the following I will present SFM investigations of non-charged denpols, which revealed that by far the most polymer chains are linear, and no self-assembled duplex structures were found. However, occasionally, i.e. on the order of 1% of all cases, main chain branching on **PG2a** samples was observed. Fig. 4.24 displays one example. Different from the topological branches at spontaneously decomplexed duplex **PG2b** (Fig. 4.21), whose

three arms exhibit very imhomogenous heights, at the main chain branches of **PG2a** the height of the three arms does not vary significantly more than along the contours (Fig. 4.24 (c) 1-2). At crossing points of chains, on the other hand, the thickness almost doubles (Fig. 4.24 (c) 3-4).

Due to high friction on mica surfaces, the accidental formation of T-like structures due to the adsorption of two different molecules meeting at one point is extremely unlikely. Provided there is no particular attractive interaction between a chain end and the main chain, this cannot explain the occurrence of about 1% of branched configurations in the diluted sub-monolayers investigated here.

It was also considered to distinguish between covalently and non-covalently connected branches by exerting a force on the junction in order to estimate its strength [15]. However, while one can drag long denpols across a graphite surface using an SFM-tip, the same is not possible on mica, since the friction during manipulation on this substrate is so large that even short molecules break immediately. Figure 4.25 displays SFM images before and after manipulation, indicating that also in this case the interaction with the substrate is too strong to drag a long chain across the surface without breaking it immediately.

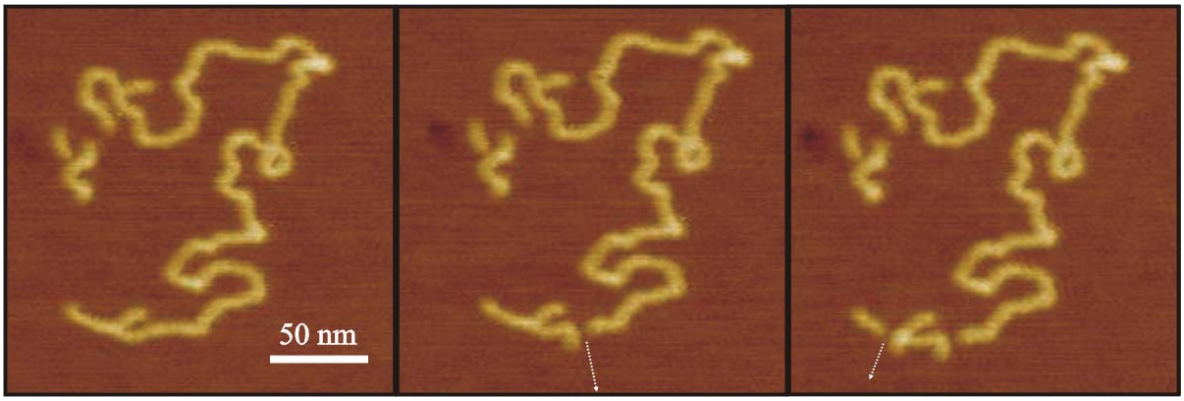

Figure 4.25: Tapping-mode SFM images of individualized non-charged polymers PG2a **(entry P5) on mica before and after tip manipulation in contact mode. Two of three arms of a supposedly branched molecule were broken by SFM tip; the white arrows indicate the direction the SFM-tip followed during the manipulation attempts.**

On the other hand, in order to clarify whether the main chain branching occasionally happened in one synthetic batch or not, samples from different batches of **PG2a** (entry P9 and P10) were thoroughly investigated. The results show branches appearing in both, entry P9 and P10 samples. The lengths of the observed branches (the shortest arm among three) range from 10 to 140 nm, which show no dependence on the synthesis entries or the total length of the main chain. In addition, the position of the branches on the main chain is quite random, i.e. the other

two arms can be tens of nanometers up to several micrometers. All of this indicates that the branching is caused by a quite random process, which can be attributed to a chain transfer reaction during the polymerization.

Chain transfer is one of the ways through which branch formation can occur during polymerization [168]. An active (radical) chain end abstracts, e.g., a hydrogen atom from its own or another independent chain with formation of an inactive chain end and a new radical center. Note that the chain transfer to solvent or monomer is not considered here. If this is active enough to carry on polymerization, it leads to main chain branching and the radical's position marks the branching point. Supposed branching through chain transfer plays a role in the synthesis of denpol **PG2a** and given the steric crowding around its backbone, hydrogen abstraction is considered more likely to take place at the dendritic shell rather than at the backbone. Preferred positions for the abstraction would be the CH bonds α to the ether oxygen atoms, the tert-butyl ester groups or the benzyl groups. These bonds have lower dissociation energies than normal methylenes. A polymerization model study including MMA monomer and G3 dendrons supports the estimate based on SFM measurements that branching takes place in the sub-1% range [106]. It should also be noted that the branches do not seem to only form by a gel effect at high conversion. A recent model study using a G3 macromonomer showed that branches also occur (in the sub-% range) at low conversions (e.g. 13 %) [169].

One may ask the question, if the **PG2b** sample is simply deprotected from **PG2a**, does **PG2b** also have branches though it exhibits the duplex conformation? The answer is YES. Actually, more branches were observed in **PG2b** by SFM, both on PLO mica and pre-coated HOPG. Figure 4.26 shows a branch like structure before and after tip manipulation. However, since the polymer chains are broken due to high friction between denpols and PLO mica, it is hard to prove the stability of the possible branching point. Therefore a manipulation proof on a smooth surface is needed.

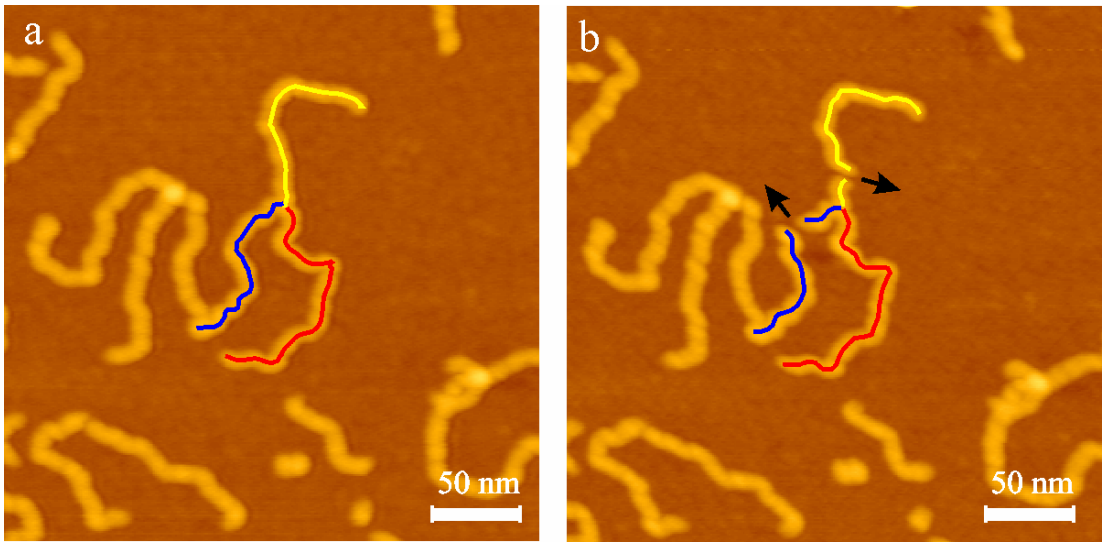

Figure 4.26: Tapping-mode SFM images of individualized negatively charged polymers PG2b **on PLO coated mica before (a) and after (b) manipulation in contact mode. The three arms of a supposedly branched molecule are colored, and black arrows indicate the path the SFM-tip followed during the manipulation attempts.**

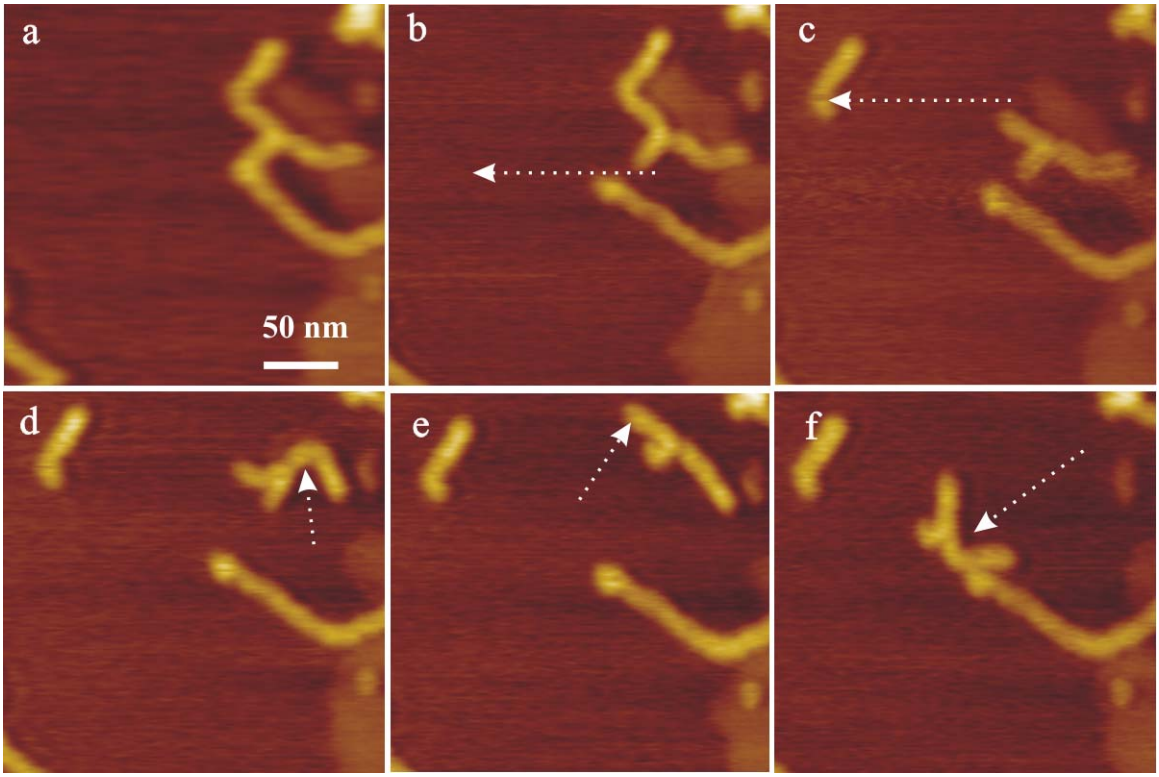

Figure 4.27: Tapping-mode SFM images of individualized negatively charged polymers PG2b **on dodecylamine pre-coated HOPG before (a) and after a sequence of tip manipulation in contact mode (b) – (f). The white arrows indicate the path the SFM-tip followed during the manipulation attempts.**

Figure 4.27 shows a successful tip manipulation of **PG2b** on dodecylamine pre-coated HOPG. Three arms and the branch point could be freely moved on the surface, indicating the stability of the branch structure. However, if considering the complex superstructure induced by the backfolded duplex, the branch structure in charged denpols is not easy to be unravelled. The

argument between chemical main chain branching and topological branching as sketched in Figure 4.28, which needs to be clarified in future work including a more precise manipulation on a surface or in solution.

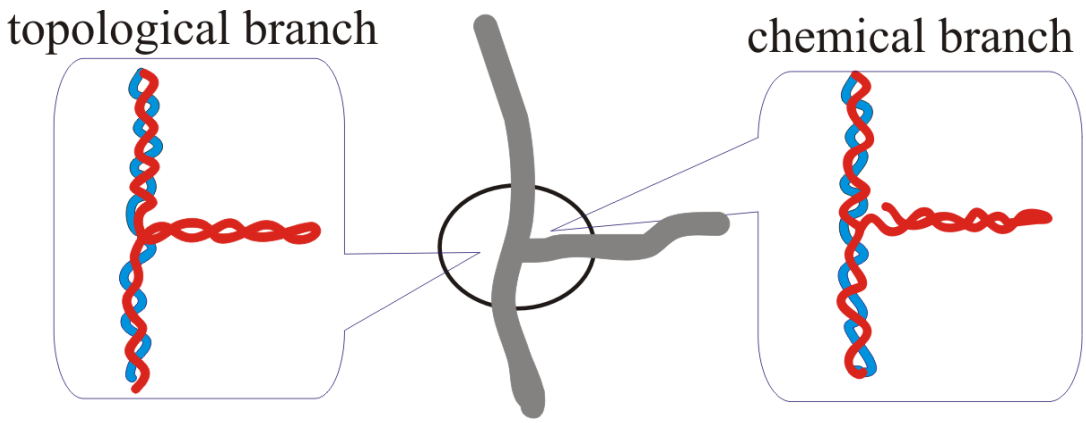

Figure 4.28: Schematic drawing of a chemical branch and a topological branch of a charged denpol, in that the blue contour may be a backfolded contour from the same polymer chain.

***Conclusions on the denpols*:** Due to the dendronization, high molecular weight linear polymers can be easily visualized by SFM. The molecular weight and molecular weight distribution of different denpol samples have been determined by contour length measurements based on SFM imaging. In addition SFM has been used to observe branching of polymer chains which occurs in the present systems at approximately 1% of the chains only. Presently there is no other method available with this kind of sensitivity. Also there is no method exhibiting the potential for positional identification of both the branching site and the lengths of the branches. Individual linear objects formed by the charged denpols **PG2b** and **PG3b** exhibit a contour length, which is only about half that of their non-charged analgoues, and a width, which is about 50% larger. This is attributed to the formation of self-folded supramolecular duplex structures of the charged dendronized polymers, presumably driven by preferred interaction of the dendritic side chains with the polar solvent. Though this duplex formation is naturally less specific than that of DNA, it indicates a concrete and rather robust level of structural hierarchy, which forms on different surfaces and constitutes an important step on the way to create more complex and yet still ordered supramolecular structures. This study is considered an important step towards, first an understanding of the underlying principles that control the generation of 3D matter from individual nano-sized molecular objects, and second these polymers' rational use for the construction of predetermined hierarchical architectures, as it was impressively shown, e.g., by Seeman with DNA [170].

4.3 Conformation of single ds-DNA molecules controlled by polyelectrolyte-amphiphile complexation (PAC)

The ability to manipulate and control molecules and materials on the nanometer scale is a key issue in nanotechnology. Due to its minuscule size and unique biological properties DNA has been widely investigated and applied in nanotechnology [94,170]. For instance there are several techniques, such as magnetic tweezers [94], optical tweezers [28,88] or an SFM probe [24,38], to stretch and overstretch a single ds-DNA molecule in solution, in order to understand the mechanical properties of ds-DNA. Characteristic for these techniques is the fact that they are applied to one molecule at a time. Other experimental methods such as the use of hydrodynamic flow [171], nanochannels [172] or molecular combing [26] can stretch several DNA molecules at a time on a surface. However, none of the aforementioned techniques and methods allows to overstretch ds-DNA in a control manner and then preserve the ds-DNA in the overstretched state on the surface. This, however, would be of interest for the development of a single molecule genomic analysis chip.

On the other hand, interactions between polyeletrolytes and oppositely charged amphiphiles have attracted a lot of interest due to their importance both in fundamental polymer physics and biophysics and for biological and industrial applications [72,73,76]. The interactions between polyelectrolytes and oppositely charged amphiphiles are quite strong and can induce complex formation resulting in highly ordered structures. For instance DNA-cationic amphiphile complexes are under intense investigation due to their highly ordered structures [173] and their potential for DNA transfection in gene therapy. Although polyelectrolyte-amphiphile complexes (PACs) in solution [73] and in the solid state [76] have been well studied, the nature of PACs at solid surfaces, especially the single polyelectrolyte-amphiphile interaction on solid substrates involved in complex formations is not well understood. In recent work it has been demonstrated that a highly oriented pyrolytic graphite (HOPG) surface coated by a self-assembled alkylamine monolayer can serve as a single molecule chip to adsorb polyelectrolytes such as poly(styrene sulfonate) (PSS) [81] or ds-DNA [22], and that single ds-DNA molecules can be manipulated on this surface by an SFM probe [22]. Moreover, amphiphiles bearing long aliphatic chains and polar head groups have been used to direct the growth of almost perfectly straight supramolecular polyelectrolyte complexes on HOPG [82]. This amphiphile templated self-organization turned out to be a very general approach that can be applied to a variety of synthetic and biological polyelectrolytes.

In this chapter, first the preparation of a submonolayer of cationic amphiphiles (alkylamines) coated HOPG surface will be presented, on which the conformation of single anionic polyelectrolyte molecules (ds-DNA) can be controlled. By varying the surface coverage of the amphiphiles on the surface, single plasmid ds-DNA molecules exhibit different conformations ranging from supercoils over open circles finally to overstretched double helices with contour lengths up to 1.4 times that of B-form lengths, due to the formation of almost fully screened DNA-amphiphile complexes on the surface. The significant changes of the plasmid DNA conformations on the solid substrates were visualized by SFM. Furthermore, upon adsorption on the alkylamine coated HOPG surface the double strands of plasmid ds-DNA could be partially split due to local denaturation. The mechanism and control of the splitting size will be discussed. Finally, SFM tip manipulation was applied to ds-DNA with the purpose of constructing functionalized structures and patterns.

4.3.1 Controlled ds-DNA conformation on amphiphile coated HOPG surfaces

A fine tuning of interfacial as well as intermolecular and intramolecular interactions permits to grow ordered mono- and multi-component quasi-1D structures at surfaces. Taking advantage of the known tendency of simple alkanes to physisorb on the HOPG surface, alkanes and their derivatives can crystallize on HOPG in oriented monolayers with their long axes preferably along the crystallographic axes [21,127]. The alkylamines used in this chapter are long chain alkylamines, i.e. octadecylamine ($C_{18}H_{37}NH_2$) or dodecylamine ($C_{12}H_{25}NH_2$).

Submonolayers of long chain alkylamines were prepared by spin-coating of a drop of pre-heated (40°C) alkylamine solution, e.g. octadecylamine (OA) in chloroform at a concentration of 1 ~ 100 mg/L onto the basal plane of HOPG at 40 rounds per second. Depending on the preparation conditions, HOPG substrates may contain different types of surface defects including dislocations, grain boundaries, folds, and terraces [174]. In order to prepare homogeneously pre-coated surfaces, grade ZYB HOPG (Advanced Ceramics Corporation) was chosen, which exhibits a low number of defects per unit surface area. The samples were dried afterwards for 45 minutes in ambient air. A droplet (10-15 µL) of plasmid DNA (MoBiTec GmbH, pUC19, 2686 bp) aqueous solution (10^{-2} g/L) was deposited onto the OA pre-coated HOPG for 10 seconds and removed by spinning it off subsequently. OA has a pK_a of 10.6 [175], and according to the weak acid dissociation equation the pH amounts to $pH = pK_a - \log_{10}\frac{[\sim NH_3^+]}{[\sim NH_2]}$, where $[\sim NH_3^+]$ and $[\sim NH_2]$ are the concentrations of protonated

and deprotonated OA, respectively. The pH of the aqueous DNA solution, which fully covers the OA sub-monolayer, was measured to be 8.7. Thus $\frac{[\sim NH_3^+]}{[\sim NH_2]} = 10^{10.6-8.7} = 79.4$, which means more than 98.7% of the OA molecules under the dilute aqueous DNA solution are protonated at the solid-liquid interface. Thus, negatively charged single DNA molecules were adsorbed onto a protonated OA submonolayer to form PACs due to the strong electrostatic interaction. Although the extra water droplet will be finally removed from the surface by high speed spin-off, it is known that a thin water layer condenses on the hydrophilic surface in ambient conditions [176]. Thereby the formed PACs will be quite stable under the thin water layer.

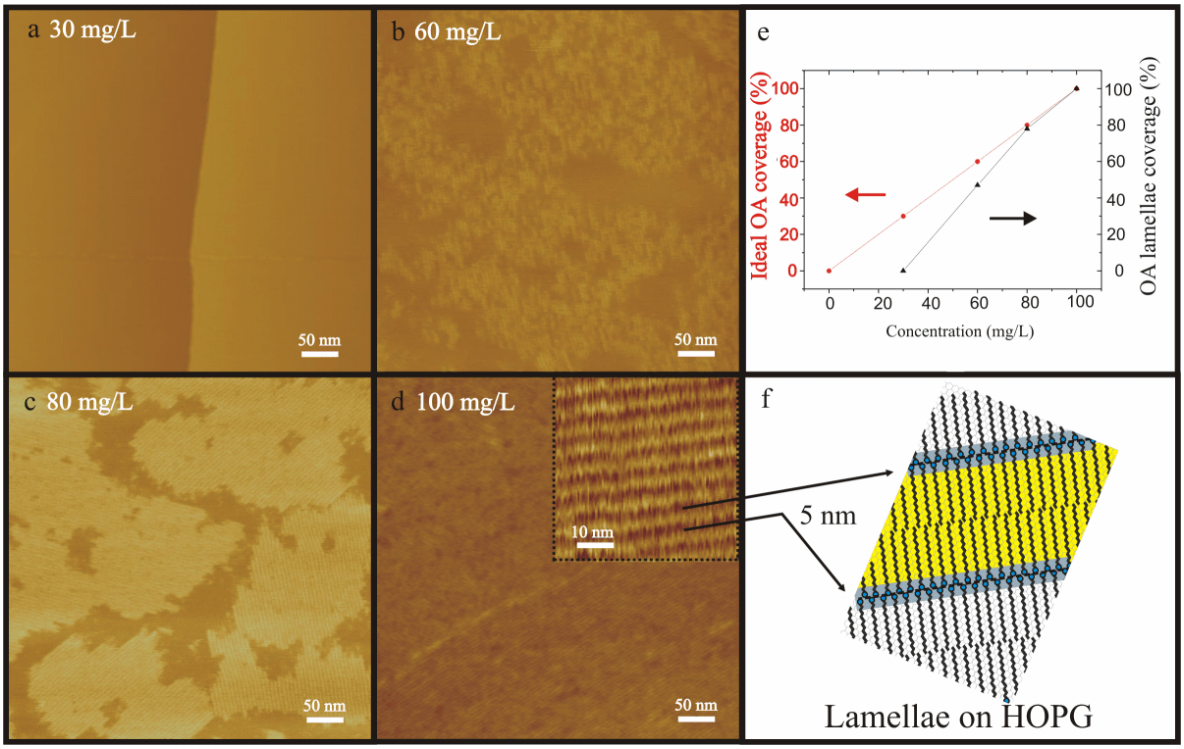

Figure 4.29: (a-c) SFM height image of HOPG surface spin-coated with 30mg/L, 60mg/L and 80mg/L OA solution, respectively; (d) HOPG surface covered by an OA monolayer spin coated with 100mg/L OA solution; insert shows zoomed lamellar rails which fit to lamellar packing mode (f); (e) the dependence between the OA solution concentration and an ideal OA surface coverage (red line) or a real OA lamellar coverage observed by SFM (black line).

Since the melting point of OA is 52°C, at room temperature it can crystallize to lamellar structures on the HOPG surface with a head to head, tail to tail packing model as shown in Fig. 4.29 (f). The coverage of OA on the HOPG surface has been controlled by observing lamellar structures of OA by tapping mode SFM. As shown in Fig. 4.29 (d), when a 100 mg/L OA chloroform solution was used to spin-coat the HOPG surface, a perfect monolayer was formed. Note that a bright line in (d) shows the grain boundary between two lamellar domains. When the same preparation procedure was used to spin-coat HOPG from a 80 mg/L OA

solution, almost 80% area of the HOPG was covered by lamellae. However this ideal was not observed upon using lower concentration OA solutions. As shown in Fig. 4.29 (a) and (b), 60 mg/L OA solution resulted in 50% lamellar coverage and for a 30 mg/L OA solution no lamellae were observed. Therefore, as displayed in Fig. 4.29 (e) the dependence between OA solution concentration and surface coverage of OA submonolayer on HOPG may be described in two ways: first, the "ideal" situation in which the OA coverage on HOPG follows the red line; secondly, the lamellae coverage is lower than the ideal coverage, which indicates that there is a certain amount of OA molecules in an amorphous, disordered state on the HOPG surface. It implies that the lower the concentration of OA, the higher is the ratio of amorphous to crystalline phase. Therefore, three types of an OA submonolayer on HOPG shall be considered: 1) a low coverage submonolayer prepared from 1-30 mg/L OA solution, for which no lamellae are formed; 2) an intermediate coverage submonolayer prepared from 30-80 mg/L OA solution, for which lamellae and disordered molecules coexist on the surface; 3) a high coverage submonolayer prepared from 80-100 mg/L OA solution, on which only a lamellar phase is formed on the surface.

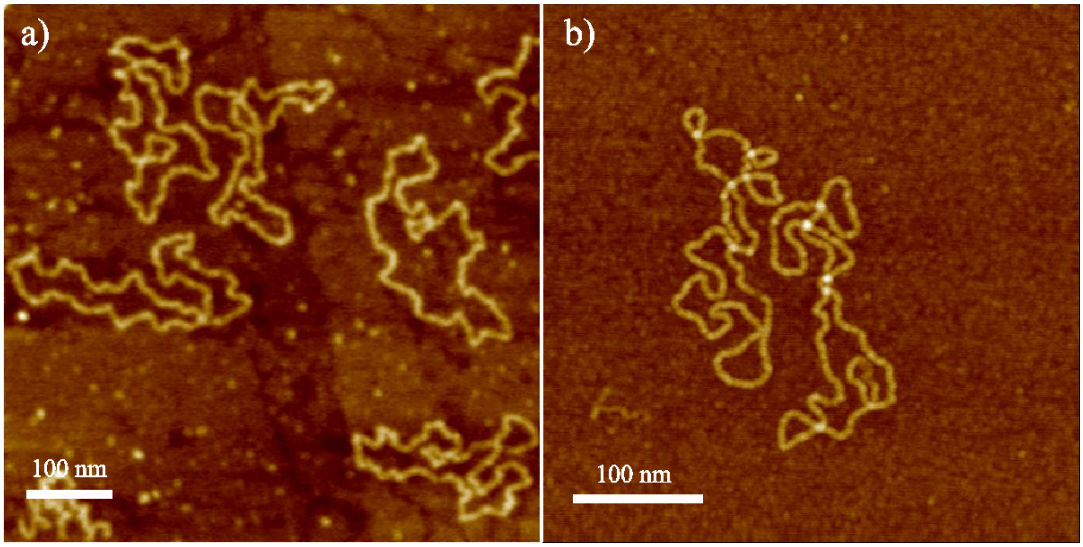

Figure 4.30: SFM height images of plasmid ds-DNA (pUC 19) on high coverage OA submonolayer coated HOPG (a) and on PLO coated mica (b).

Fig. 4.30 (a) displays plasmid ds-DNA on HOPG coated with high coverage OA submonolayer prepared from 90 mg/L OA chloroform solution. Fig. 4.30 (b) shows the ds-DNA molecules on PLO mica prepared from the same DNA aqueous solution. The preparation of PLO mica refers to *Chapter 3.1.1*. It has been reported that the adsorbed structure of plasmid DNA can be described as a projection from the 3D conformation in solution onto the flat cationic polymer coated surface [177], indicating that no other deformation occurs upon adsorption to a flat

polylysine coated mica surface [178]. Since the roughness of the PLO mica was as low as 0.11 nm (RMS), and the measured average contour length of plasmid DNA (pUC 19 with 2686 bp) amounted to 914 ± 7 nm, it is concluded that plasmid DNA on PLO mica is simply immobilized from solution without conformation deformation, and its B-form secondary structure has also been well reserved. The average contour length of plasmid DNA on high coverage OA submonolayer was measured as 915 ± 12 nm. As shown in Fig. 4.30 no significant topology difference was found between DNA on a high coverage OA (sub)monolayer and DNA on PLO mica, indicating that a high coverage (sub)monolayer of OA is a suitable surface to immobilize DNA from solution, reflecting the DNA conformation in solution.

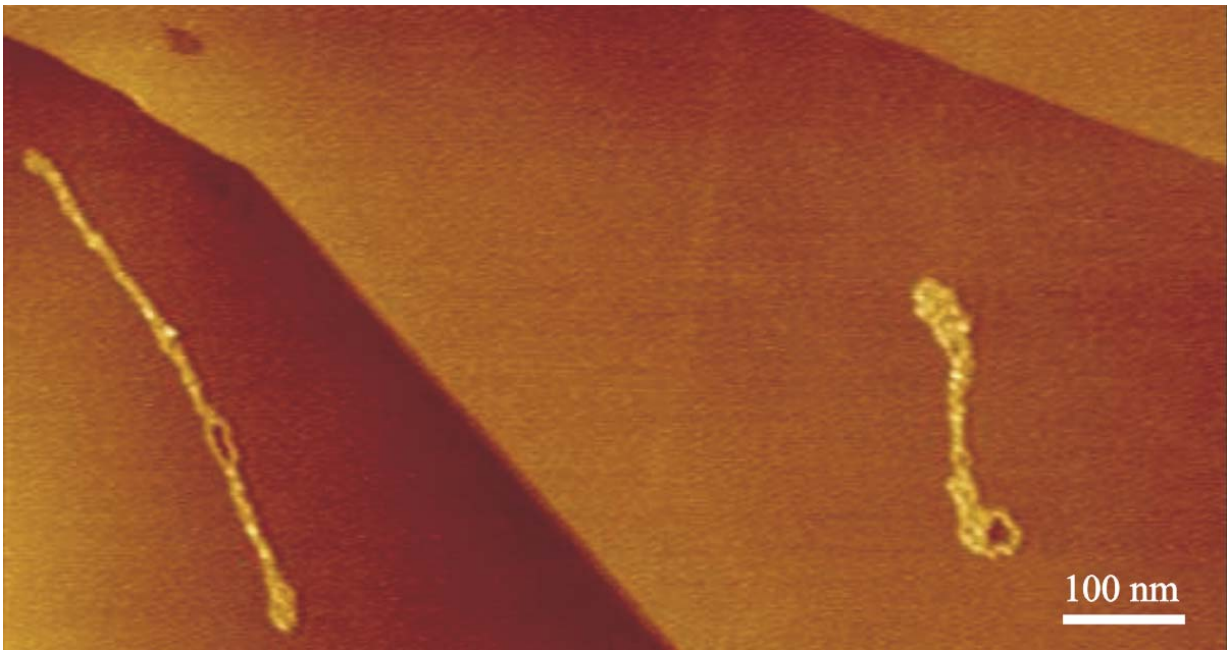

Figure 4.31: SFM height images of plasmid ds-DNA (pUC 19) on extremely low coverage OA submonolayer coated HOPG (spin-coating of 1 mg/L OA solution).

When the same plasmid DNA solution was applied to a very low coverage OA submonolayer, significant conformation changes were observed. Fig. 4.31 displays circular plasmid ds-DNA on a HOPG surface spin-coated with a 1 mg/L OA solution. The DNA molecules exhibit supercoiled conformations. Upon careful examination of high resolution SFM images, it is found that the chirality of the supercoiling is right handed negative supercoiling, consistent with what has been observed before [179].

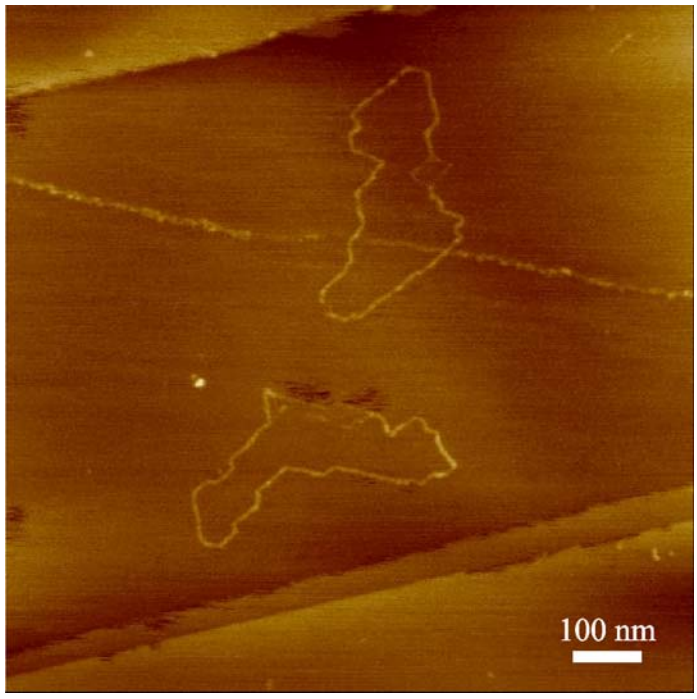

Figure 4.32: SFM height image of plasmid ds-DNA (pUC 19) on low coverage OA submonolayer coated HOPG (spin-coating of 20 mg/L OA solution).

Plasmid ds-DNA molecules deposited on low coverage OA submonolayer coated HOPG (spin coated from 20 mg/L OA solution) do not exhibit supercoiling. However there is always one part of the double-stranded DNA split into two single-stranded chains as shown in Fig. 4.32. This means the circular DNA exhibits an open circle topology without supercoiling but with partial splitting.

When the concentration of the OA solution is increased further to 30 mg/L, the lamellar structure starts to appear on the surface. Moreover, as shown in Fig. 4.33 (a), upon adsorption plasmid ds-DNA is spontaneously stretches on the surface. The lengths and the angles of the straight contours indicate, surprisingly, that the ds-DNA molecules have been overstretched with respect to the B-form DNA in solution rather than simply stretched, and, moreover, are oriented with respect to the lamellae. As shown in Fig 4.33 (b), based on the data of more than 30 ds-DNA molecules recorded on the sample partially shown in Fig 4.33 (a), the distribution of angles of the straight segments exhibits six peaks with angle differences between each other of approximately 60°, which is consistent with the 3-fold symmetry of long chain alkyl amine lamellae on the HOPG (0001) surface. On the other hand, the average contour length of the pUC 19 ds-DNA amounts to 1054 ± 34 nm, indicates that the ds-DNA molecules have been overstretched 1.15 times with respect to the B-form length. Figs. 4.33 (c) and (d) display

ds-DNA molecules that were overstretched on high coverage OA submonolayers, which were prepared from spin coating of 60 mg/L and 70 mg/L OA solution, respectively.

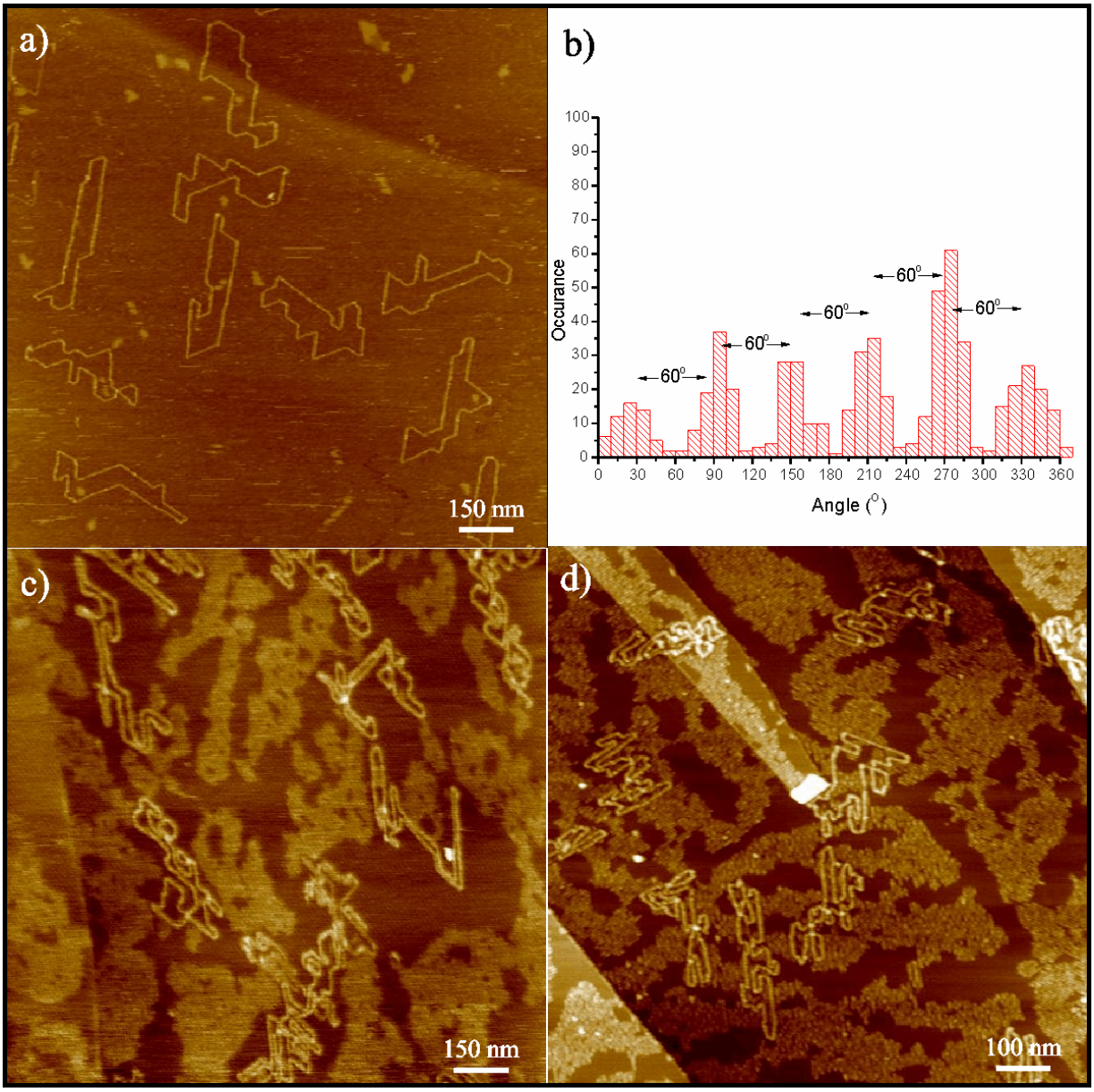

Figure 4.33: (a) SFM height image of orientated plasmid ds-DNA (pUC 19) on intermediate coverage OA submonolayer coated HOPG (spin-coating of 30 mg/L OA solution); (b) angle distribution of stretched contours in (a) relative to the horizontal axis od SFM image; (c, d) SFM height images of orientated plasmid ds-DNA on middle coverage OA submonolayer coated HOPG, which corresponds to approximately 50% and 60% lamellar coverage, respectively.

So far three types of conformations were described: supercoiling, open circle with split and oriented overstretching, all observed on certain OA submonolyer coated HOPG. If the experimental procedure for preparing the OA submonolayer is kept constant, the plasmid DNA conformation can be controlled by the coverage of the OA submonolayer on HOPG as described in Fig. 4.34. Of course the boundary concentrations 10 mg/L, 30 mg/L and 80 mg/L

include some error, e.g., because the preparation of the OA submonolayers may be influenced by ambient temperature and humidity.

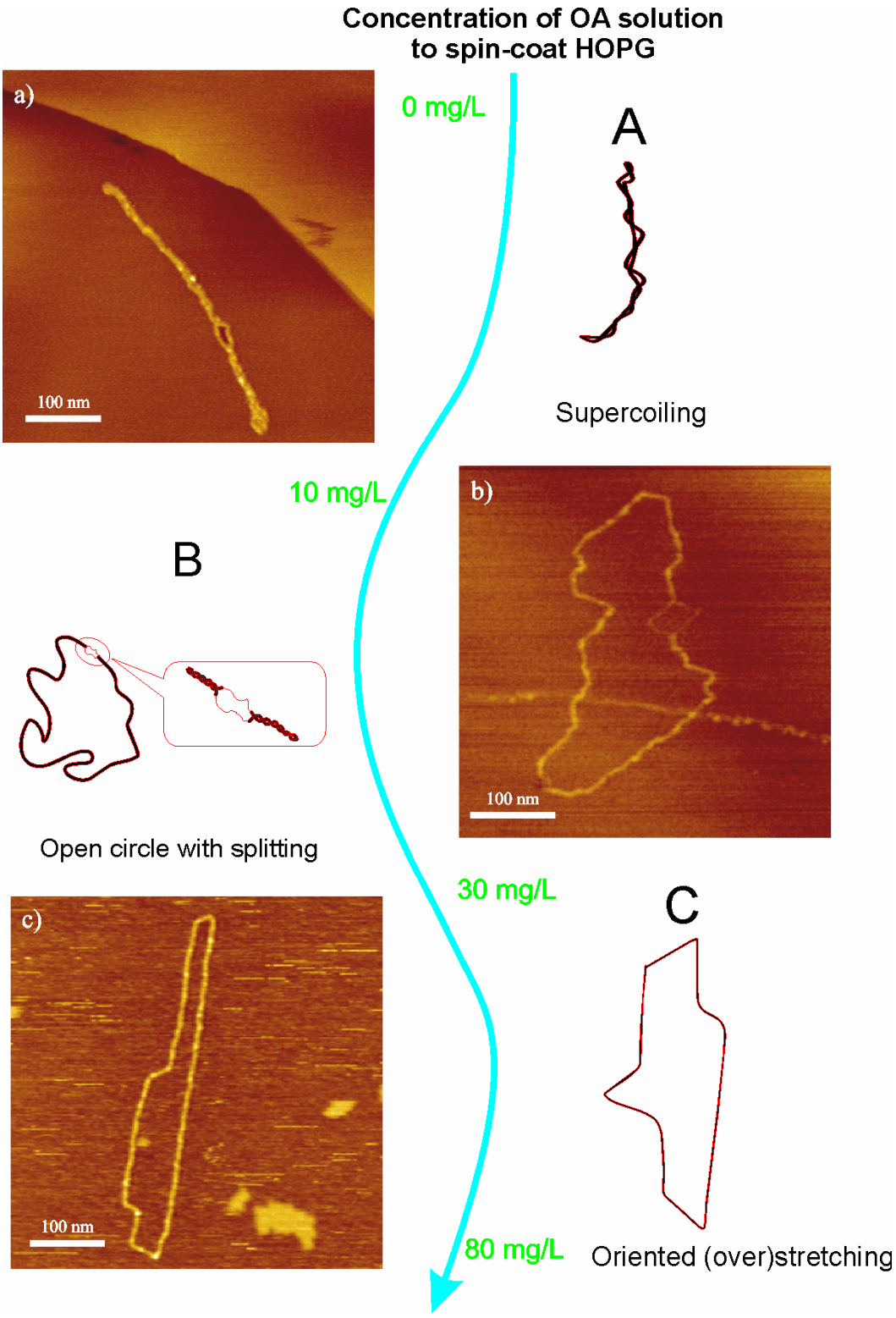

Figure 4.34: The dependence between plasmid ds-DNA conformations on OA submonolayer and the concentrations of OA solution to prepare the OA submonolayer.

Of course the question may be raised: "Why and how can the conformations of plasmid ds-DNA be controlled by the different coverages of the OA submonolayers?" Thus in the following a mechanism will be discussed to form different ds-DNA conformations. Further applications will be presented thereafter.

4.3.2 Spontaneously overstretching ds-DNA by PAC formation

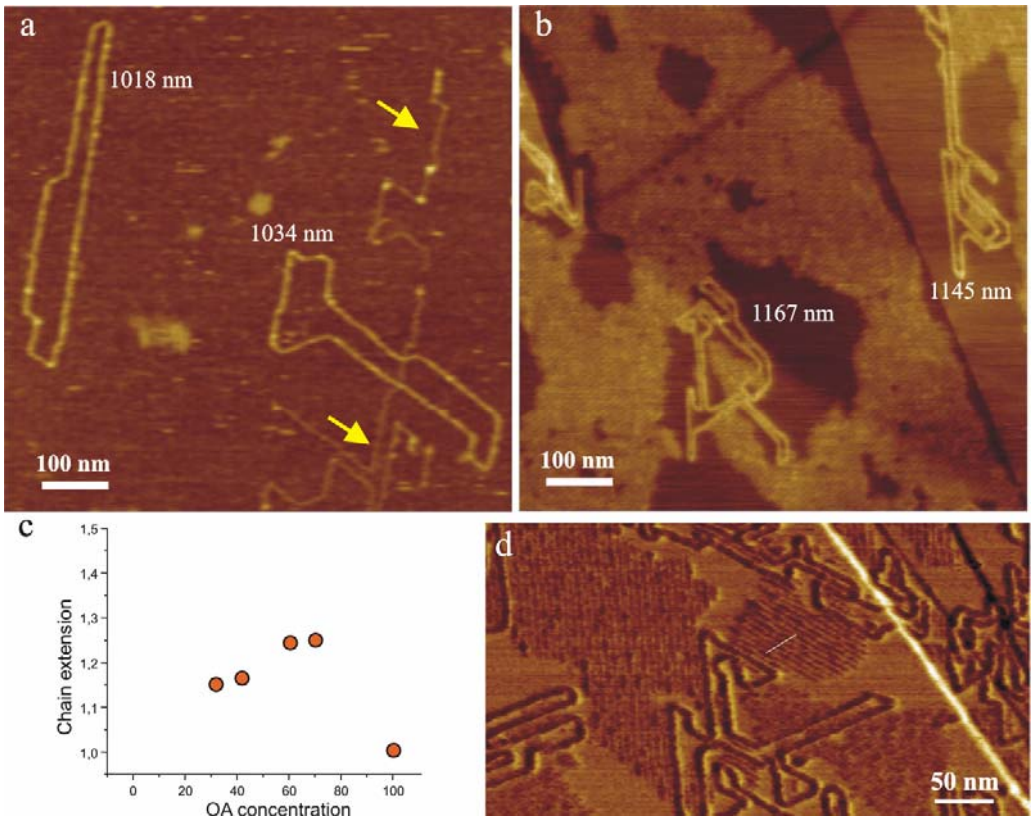

Figure 4.35: Overstretching plasmid ds-DNA (pUC 19) and ss-DNA (marked by yellow arrows) on OA submonolayer on HOPG coated by 30 mg/L OA solution (a) and by 60 mg/L OA solution (b); (c) the relative length extension of overstretched plasmid ds-DNA over its B-form length on submonolayers of different concentrations of OA solution; (d) SFM phase image of oriented overstretched ds-DNA and lamellae of OA submonolayer.

Figs. 4.35 (a) and (b) show that ds-DNA molecules are overstretched on HOPG spin-coated with solutions of 30 mg/L and 60 mg/L OA in chloroform. The precise contour length of the ds-DNA molecules on the SFM images has been determined with a home developed program [110]. The dependence of the relative chain extension over its B-form length (913 nm) on the concentration of the OA solutions used for spin-coating HOPG is shown in Fig. 4.25 (c). For each OA submonolayer with coverages up to the the full OA monolayer the contour lengths of more than 20 plasmid ds-DNA molecules (pUC 19) have been averaged. Obviously the relative

extension is 1 on the OA monolayer, which was spin-coated from a 100 mg/L OA solution. On the OA submonolayers, two regions were found: on low coverage submonolayers, plasmid ds-DNA molecules were spontaneously overstretched to around 1.15 times their B-form length; on intermediate coverage submonolayers plasmid ds-DNA molecules were spontaneously overstretched to around 1.25 times their B-form length.

The question arises, why ds-DNA can be overstretched on the intermediate coverage OA submonolayer? The answer is PAC**s**. It is known that polyelectrolyte chains form PACs with oppositely charged amphiphile molecules in solution [180]. Polyelectrolytes such as poly(sodium 4-styrensulfonate) (PSS) can form PACs with trimethylhexadecylammonium bromide in solution and be stretched upon adsorption on the HOPG surface [81]. The mechanism of such stretching is illustrated in Fig. 4.36 (a). The fully compensated (stoichimetric 1:1) PACs are stretched on graphite due to self-assembly of the alkyl chains along a lattice axis. The projected length of two repeat units of PSS in the preferred *all-trans* conformation (0.50 nm) is comparable to a minimum distance (0.51 nm) between amphiphile molecules in a crystalline monolayer on graphite for OA for example, as can be estimated from reference [181].

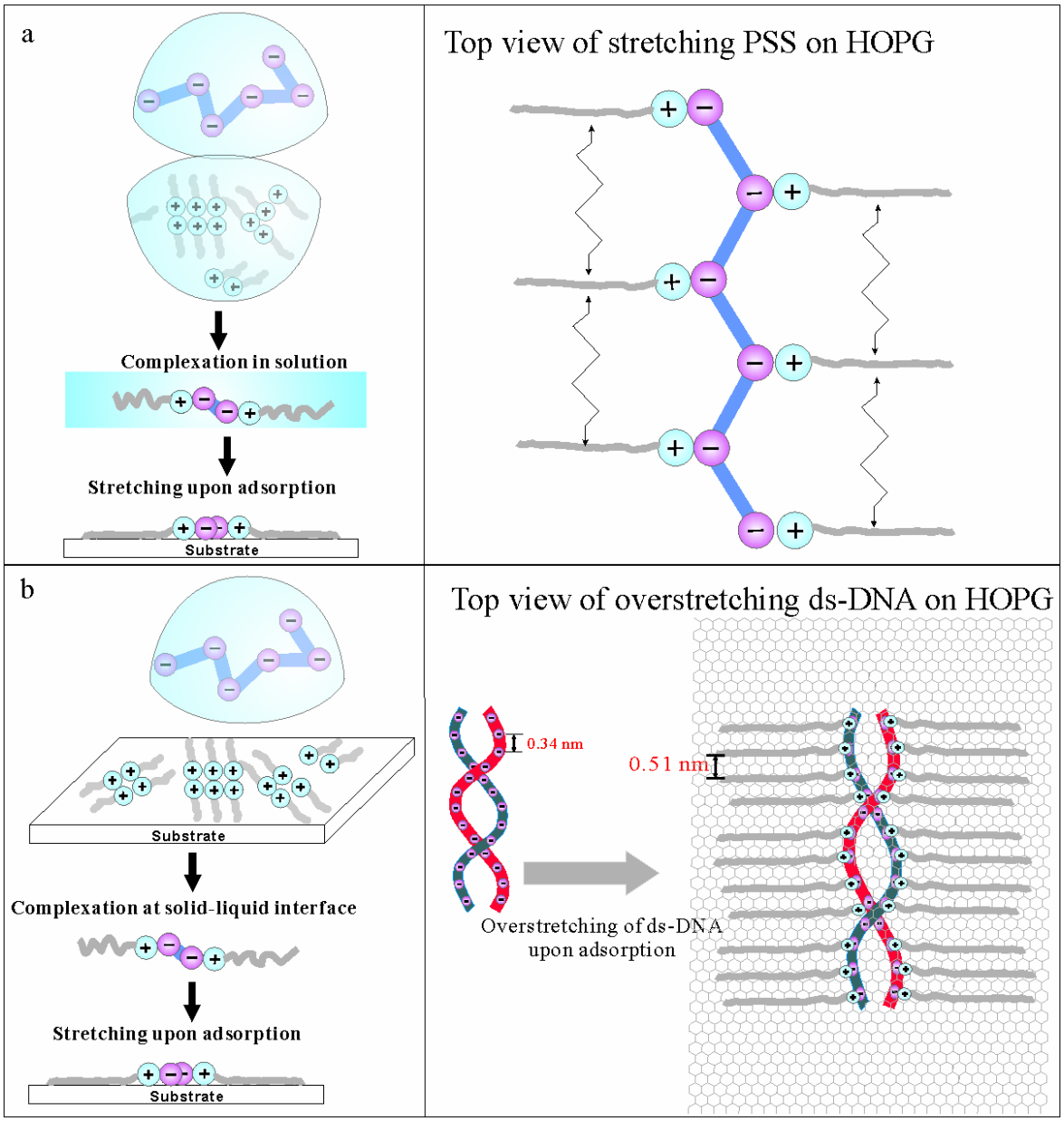

Figure 4.36: (a) Illustration of the experimental procedure of the "solution method" and mechanism of stretching of polyelectrolytes such as PSS; (b) Illustration of the experimental procedure of the "interface method" and mechanism of overstretching of ds-DNA.

Different from the experiments in which PAC was formed in solution (solution method), the DNA-OA complex in the present experiment is directly formed at the solid-liquid interface and then overstretched on the solid substrate as illustrated in Fig. 4.36 (b). At first OA molecules replace small counter ion molecules to electrostatically bind to the negatively charged phosphate groups on ds-DNA, while the system entropy is increased. Thanks to the double helix structure of B-form ds-DNA, the distance between neighboring phosphate groups is 0.34 nm. When OA molecules that are electrostatically bound to the phosphate groups start to rearrange on HOPG surface, the repulsion force between neighboring long alkyl chains keep the OA chains on HOPG at the minimum distance of 0.51 nm. The ds-DNA, thus, can be

elongated up to a maximum of 1.5 times (0.51 nm / 0.34 nm) of its B-form length if it is a fully compensated (stoichimetric 1:1 ratio) PAC. (It is known that ds-DNA can be extended up to 2 times of its B-form length [39].) However, as can be observed in Fig. 4.35 (c) and is illustrated in Fig 4.36 (b), in fact fully overstretched ds-DNA was not observed. The maximum overstretch of 1.25 indicates that the PACs at the solid-liquid interface are not fully compensated due to the interaction with the monolayer. Instead, at least 50% i.e. (1.5-1.25)/(1.5-1) of the phosphate groups remain bound to low molar mass counterions or amphiphiles not incorporated in an adsorbed monolayer. The high resolution SFM phase images such as Fig. 4.35 (d) show that PACs are typically adsorbed to areas between lamellar domains or at their edges, indicating that the PACs are mainly formed by DNA molecules bound to alkylamine molecules that are not in the lamellar but in the more disordered phase. However, also the disordered alkylamine molecules cannot be arbitrarily deformed on the graphite surface. The effect described here may be also used to explain why PACs at low lamellar coverage are less overstretched than PACs at intermediate lamellar coverage submonolayers as observed in Fig. 4.35 (c). In the latter case more alkylamine molecules exist in the small amorphous phases between the lamellar domains, allowing more highly compensated PACs to be formed.

Compared to the solution method the solid-liquid interface method has some obvious advantages: It allows 1) to prepare isolated high molecular weight polyeletrolyte molecules on a solid substrate with stretched or overstretched conformations, 2) to avoid possible aggregation of PACs in solution when the amphiphile is over-dosed, 3) to simplify the experiment since there is no need to wash and extract PACs from solution, 4) to spontaneously overstretch both double-stranded and also single-stranded DNA (ss-DNA) on a surface (marked by yellow arrows in Fig. 4.35 (a)) without chemical modification or external mechanical deformation of the DNA molecule.

There are many reasons for wanting to (over)stretch both double and single-stranded DNA. Stretched or overstretched DNA could one day be sequenced using scanning probe techniques, such as SNOM or STM. DNA chip makers may benefit from such an approach in order to optimize the accessibility of the attached sequences, and hence their density. Optical microscopy now has a breadth of resolution-increasing techniques that could possibly take advantage of fluorescently labeled stretched DNA, allowing for parallel detection of sequences [182]. Another possible use of a stretched ss-DNA template could be enzyme activity studies. In particular, it would be interesting to study the interaction of DNA binding proteins with such an elongated ss-DNA, possibly shedding light on whether the phosphate backbone or the base

pairs are involved in the binding process. Moreover, the ability to encode information in DNA sequences may also be used for patterning materials and nanocrystals, and stretched strands of ss-DNA may be most useful for this [183].

In order to achieve maximum spontaneous overstretching of ds-DNA, another experiment was performed. The key seems to be using the more flexible disordered OA molecules in order to better compensate the charge of ds-DNA by the OA. Since chloroform and water are immiscible, the OA in chloroform was spin-coated on HOPG without drying. Onto the OA submonolayer covered by a thin layer of chloroform the aqueous DNA solution was directly applied. Thereby a water-chloroform interface was formed as shown in Fig. 4.37 (a). Despite their affinity to HOPG, compared to the limited amount of DNA molecules there was still a huge amount of OA molecules "swimming" in chloroform. Therefore ds-DNA and OA molecules can freely bind to each other at the liquid-liquid interface, and form fully compensated PAC in 3D without chain elongation. Afterwards the surface was annealed at 60°C for 20 minutes to remove all the liquids. With the fully compensated PAC adsorbed to HOPG eventually the maximum spontaneously overstretched ds-DNA was obtained. Fig. 4.37 (b) displays a plasmid ds-DNA overstretched to 1.46 times of its B-form length. The maximum overstretching of 1.5 times extension was also observed by an improved experimental procedure [184]. Compared to other DNA extension experiments relying on a liquid flow, a receding meniscus, or for instance electrophoresis, the method presented here can elongate ds-DNA in a controlled manner to a defined extension and preserve the overstretched samples for long time.

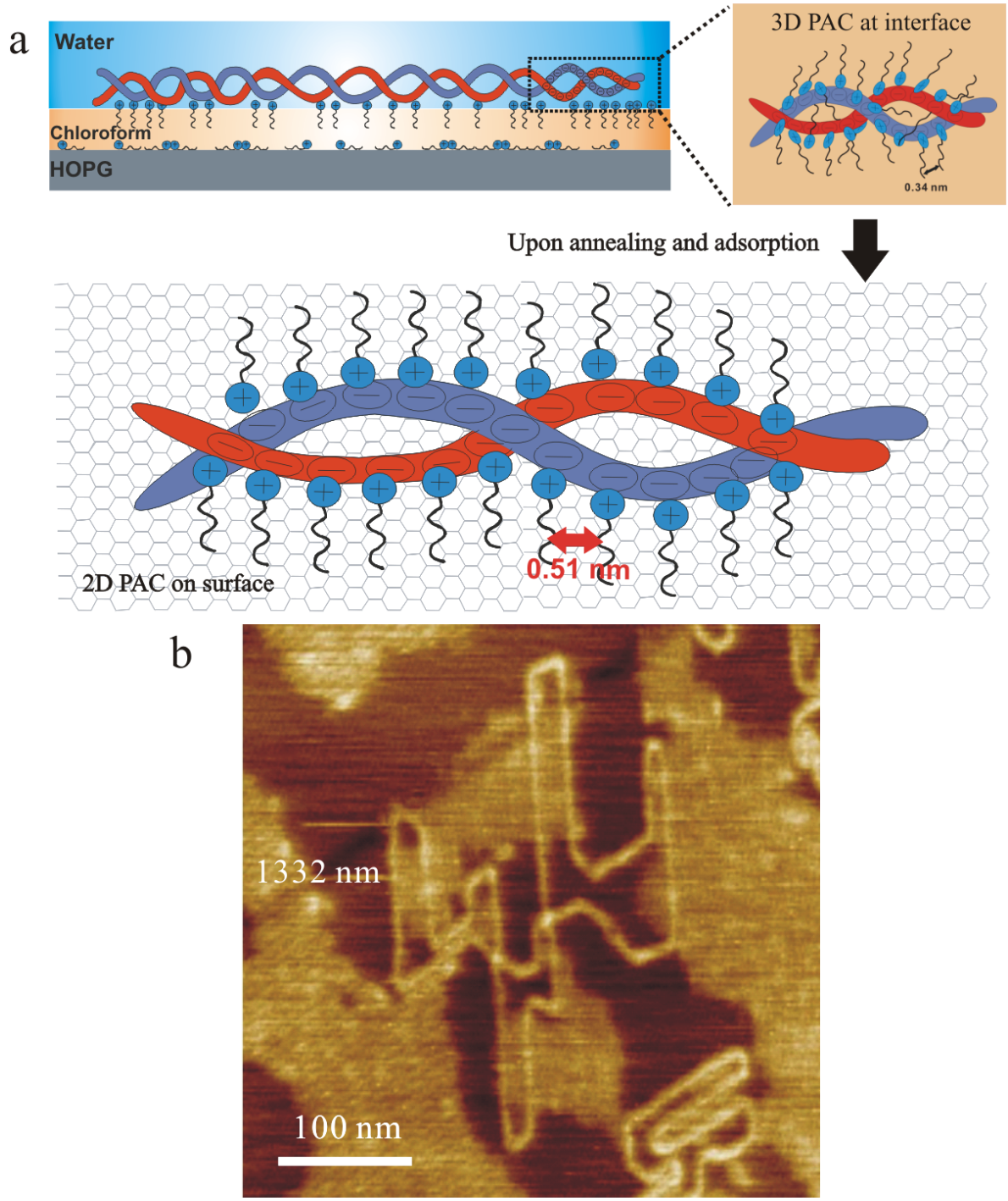

Figure 4.37: (a) Illustration of improved experimental procedure of "liquid-liquid interface method" and mechanism of overstretching of ds-DNA; (b) an example of 1.46 times overstretched ds-DNA after "liquid-liquid interface method".

4.3.3 Supercoiling and splitting of ds-DNA on alkylamine coated HOPG

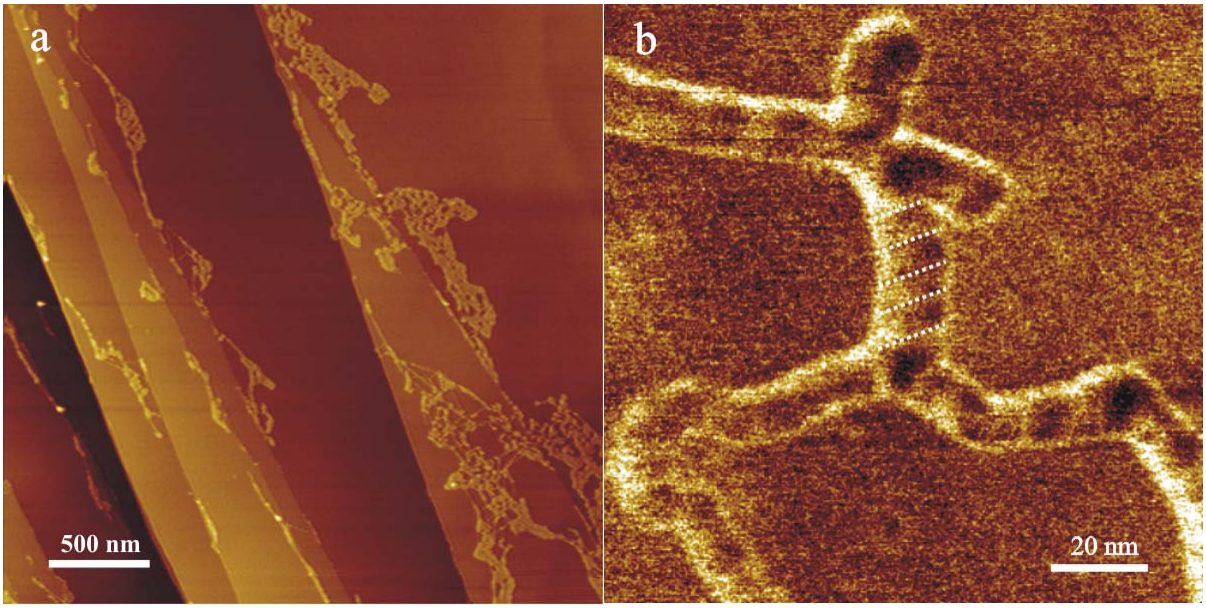

Figure 4.38: (a) plasmid ds-DNA molecules aggregate onto bare HOPG after spin-coating; (b) SFM phase image indicates a right-handed supercoiled conformation, with white lines guiding the eye to recognize the pitch.

On very low coverage OA submonolayers (prepared by OA solution < 10 mg/L), plasmid ds-DNA formed supercoils on the HOPG surface. In order to understand the observation first DNA molecules are considered as highly charged polyelectrolytes. If applied onto a bare HOPG surface as shown in Fig. 4.38 (a), they interact only weakly with the hydrophobic HOPG surface and therefore aggregate. This implies that polyelectrolytes tend to form compact conformations on a hydrophobic surface, since within a compact aggregate they minimize hydrophobic-hydrophilic interfaces. It implies also that the molecules are rather mobile on the surface and aggregate before the solvent is evaporated. However, at very low OA surface coverage DNA molecules are immobilized before they could aggregate. The isolated plasmid ds-DNA molecules also tend to form compact conformations, such as the largely right-handed supercoiled conformation shown in Fig. 4.38 (b). On the other hand, it is known that plasmid DNA can exhibit right-handed supercoiling in aqueous solutions with high salt concentrations due to torsional stress [185], which can be directly observed by TEM [46] and SFM [179]. The plasmid ds-DNA supercoiling is described by the linking number $L_k = T_w + W_r$ = constant (T_w: twist number, the number of helical turns along the molecule and Wr: writhe number, a measure of the coiling of the DNA axis about itself) [186]. When DNA molecules from an aqueous solution are adsorbed to the surface with a few OA molecules, the twist number (T_w), can vary (increasing) due to the change of the local DNA environment compared to the solution and the

minimization of hydrophobic-hydrophilic interfaces. In order to keep the linking number constant, the writhe number (W_r) has to change to smaller. This implies negative supercoiling ($\Delta W_r < 0$), which appears as right-handed writhing of the DNA backbone across itself, i.e. right-handed supercoiling. Therefore the supercoiling is probably not only due to the thermodynamics governing the polyelectrolyte absorption, but also the effect of induced torsional stress plays a role, which occurs upon changing the ionic strength of the solution at the interface.

As the OA surface coverage increases (prepared by OA solutions between 10 mg/L and 30 mg/L), more amphiphiles can bind to the DNA chain, which immobilize the DNA molecule more tightly on the surface. Accordingly, either diffusion limited aggregation or across axis rotation (writhing) is difficult on the surface. Surprisingly plasmid ds-DNA molecules were observed to split on the surface, i.e. some of the hydrogen bonds between two DNA strands break, resulting in a local splitting of the double strands as shown in Fig. 4.32. The splitting increases the twist number per unit length and thus releases the torsional stress induced by the increasing ionic strength. Although the breaking of the hydrogen bonds is not energetically favored if supercoiling is allowed, the energy price to break a hydrogen bond of 2-5 Kcal/mol is much smaller than the energy needed to dissolve a C_{18} n-alkane chain from HOPG into liquid. It is known that the desorption energy of C_{18} n-alkane chain from HOPG amounts to about 150 KJ/mol (~36 Kcal/mol) [187].

The splitting occurs upon the adsorption of plasmid ds-DNA onto the low OA surface coverage submonolayer, where supercoiling is forbidden but oriented overstretching is not yet occuring either. The required concentration range of the applied OA solution is quite narrow. In order to investigate this phenomenon in detail, it was decided to apply plasmid ds-DNA onto dodecylamine ($C_{12}H_{25}NH_2$) pre-coated HOPG surfaces. Since dodecylamine (DA) has a bulk melting point of 27°C, at room temperature it is always in a disordered phase even on the HOPG surface; therefore, a lamellar structure of DA was never observed by SFM at room temperature. On the other hand, the desorption energy of C_{12} n-alkane on HOPG of about 115 KJ/mol is relatively small, therefore even by applying a concentration that is 10 times higher than the OA monolayer concentration, DA still forms a disordered layer on HOPG under ambient conditions. Accordingly a large concentration range of DA solutions can be used to prepare a disordered layer, on which plasmid ds-DNA molecules neither supercoil nor overstretch, but split.

Figs. 4.39 (a) and (b) show a phase and a height image of pUC 19 plasmids on a DA disordered layer spin-coated by a 500 mg/L DA chloroform solution. By both phase and height contrast one and only one split of double strands can be recognized on every plasmid. Interestingly, after keeping the same pUC 19 aqueous solution used in (b) at ambient conditions for one week instead of storing it at 4°C in the dark, the same experiment resulted in images like the one shown in Fig. 4.39 (c), which does not exhibit any split on any plasmid ds-DNA. Repeated experiments indicated that this DNA cannot be split any more, probably because one of the two strands of the plasmid has been cleaved induced by light or thermal degradation [188], or possibly an enzymatic damaging process. This nicked ds-DNA does not need supercoiling or split to release local torsional stress [186].

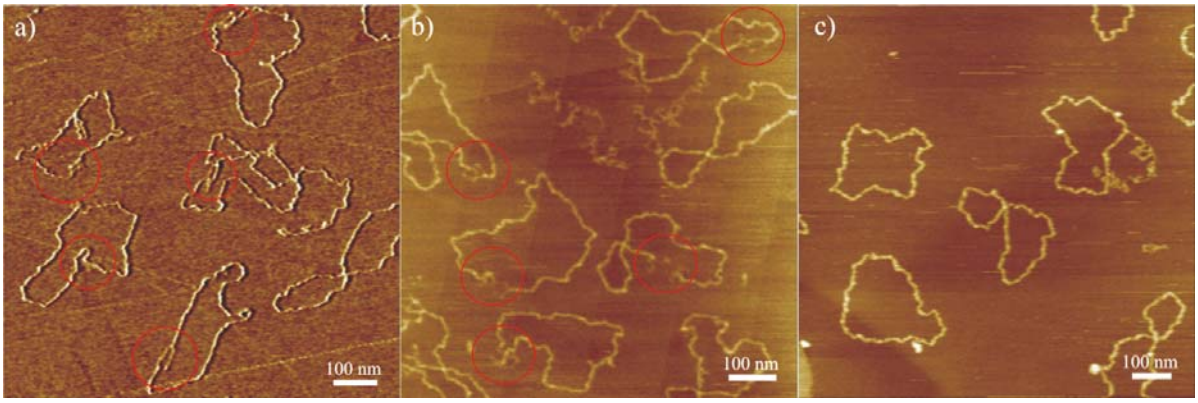

Figure 4.39: SFM phase (a) and height image (b) of plasmid ds-DNA splits, prepared on a 500 mg/L DA solution spin-coated disordered layer on HOPG; one split (red circle) is found for every fully shown plasmid; (b) SFM height image of nicked plasmid ds-DNA molecules without split on the same DA disordered layer on HOPG.

The other important characteristic of the split is that the size of the split can be roughly controlled. Since DA molecules are in a disordered amorphous state at room temperature, they can only form a relatively homogenous layer on HOPG, even though the surface coverage cannot be exactly measured. Therefore, in order to prepare DA layer the same experimental procedure was used as employed for OA submonolayers. The concentration of the DA solution was used to control the surface coverage. As Fig. 4.40 displays, plasmid ds-DNA pBR 322 with 4361 bps and 1483 nm B-form contour length was applied onto 700 mg/L (a) and 1000 mg/L (b) DA solution spin-coated layer on HOPG, respectively. The sizes of the splits on the same surface are similar due to the homogeneity of the surface coverage. By applying DNA onto different DA surface coverages, the average split size has been roughly estimated at different concentrations, in order to achieve the maximum split. Note that the size of the split was measured by the contour length of the exposed single strand; if two single strands at one split have different lengths, the longer one is taken, since there may be hairpins or coil structures

occurring on the short one. However, if a mixture of pUC 19 and pBR 322 plasmids is applied onto the same surface, these two kinds of plasmids exhibit very different split sizes as shown in Fig. 4.41 (a). Fig. 4.42 (b) provides the dependence of the split size on the DA solution concentration applied. It clearly shows that longer plasmid DNA provides in larger splits, which is attributed to the fact that the longer DNA bears a larger torsional stress.

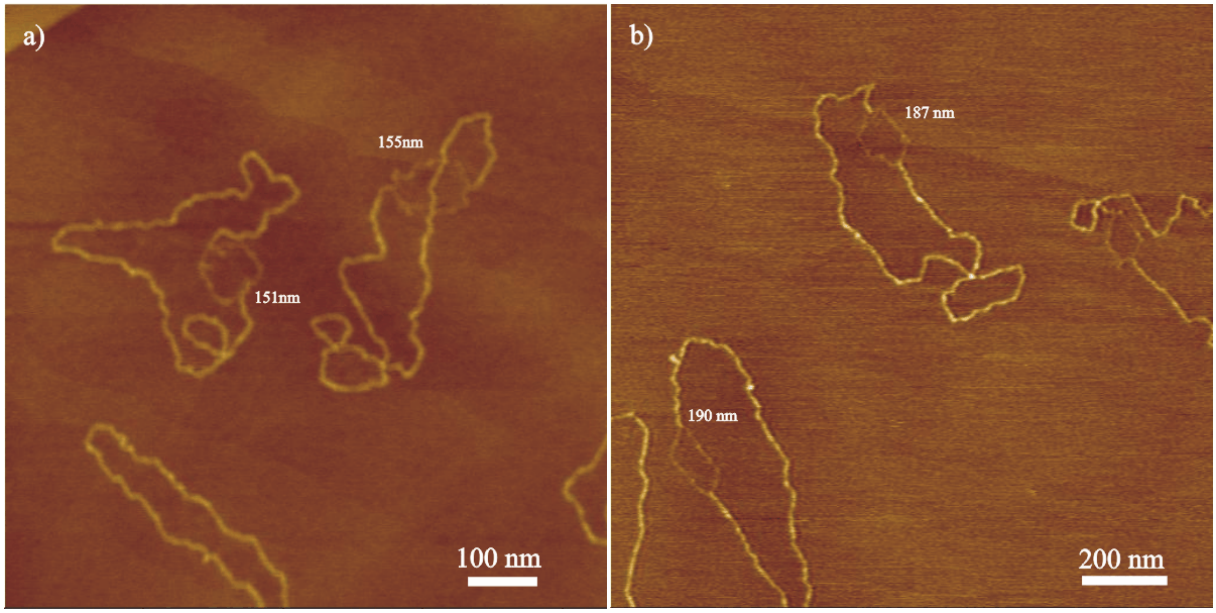

Figure 4.40: SFM height image of plasmid ds-DNA molecules (pBR 322) split on 700 mg/L (a) and 1000 mg/L (b) DA solution spin-coated disordered layer on HOPG, the lengths of the split single strands are indicated.

On the other hand, from Fig. 4.41 (b) one can figure out an optimal concentration of around 1000 mg/L for the largest average split size. The more amorphous DA molecules on the surface may induce not only a larger torsional stress, but also the higher horizontal surface friction, which hinders the double strands to split further on the surface. However, it should be made clear that the estimate of a 1000 mg/L DA solution as optimal concentration is quite rough, since the average split size at each concentration has a standard deviation around 10%; for instance pUC 19 at 1000 mg/L exhibits 95 ±10 nm splits and pBR 322 at 1000 mg/L splits of 184 ±15 nm. Nevertheless, the dependence shown here implies the following facts: 1) longer plasmid DNA produce larger splits, irrespective of the DA layer concentration; 2) there should be an optimal surface coverage existing, on which plasmid DNA can compress more helical pitches with less surface friction. Moreover, with large splits on ds-DNA it opens more opportunities for manually separating two split single strands further by means of SFM manipulation, which will discussed in the next chapter.

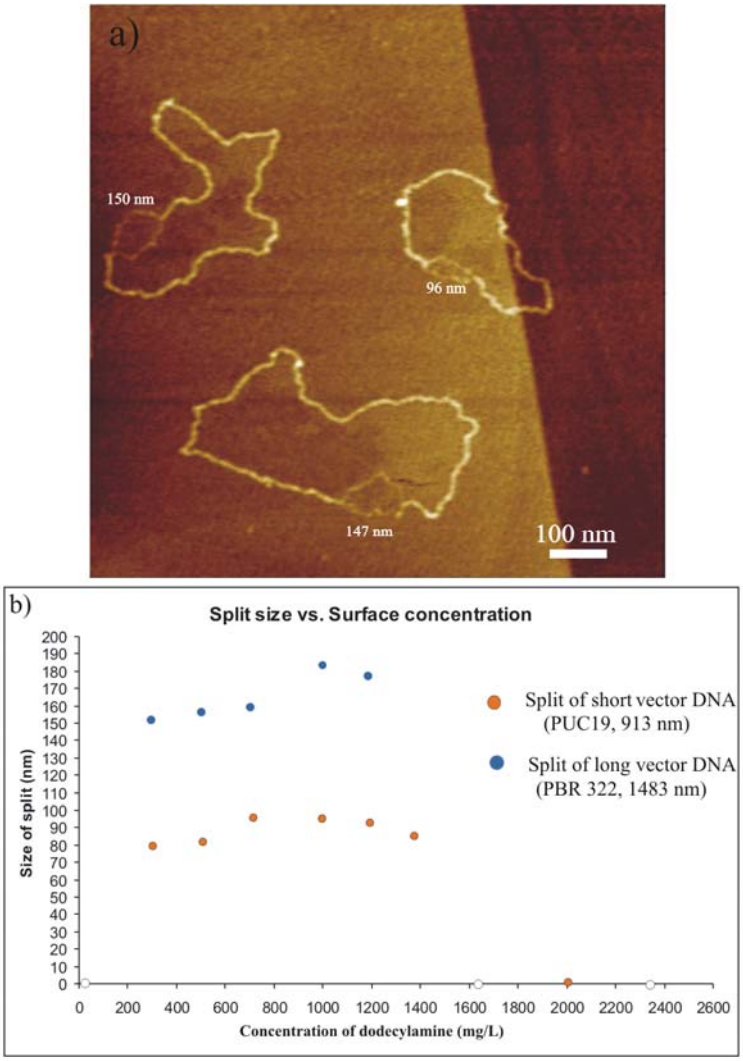

Figure 4.41: (a) SFM height image of mixed plasmid ds-DNA molecules (pUC 19 and pBR 322) split on 700 mg/L DA solution spin-coated layer on HOPG; the lengths of the split single strand is indicated; (b) Spin-coated DA concentration dependent split sizes of pUC 19 plasmid (orange) and pBR 322 (blue).

***Conclusion of the conformation control of ds-DNA based on PAC*:** It has been demonstrated that single ds-DNA can form PACs with octadecylamine (OA) molecules on OA submonolayer coated HOPG. By controlling the OA surface coverage the plasmid ds-DNA conformations can be spontaneously controlled, ranging from supercoiling, open circle with split, to spontaneously overstretching up to 1.5 times of its B-form length. On the other hand single ds-DNA can form PACs with dodecylamine (DA) molecules on DA coated HOPG. By controlling the surface coverage of DA, the splitting size of the plasmid can be controlled. Thus, long chain alkylamine coated HOPG provide a powerful single molecule workbench, on which it is possible to fabricate different 2-D molecular architectures from single macromolecules. Moreover, the work on splitting ss-DNA from ds-DNA and overstretching ss-DNA on surface will shed light on the new opportunities for direct encoding of DNA sequences on surfaces combined with ultrahigh-resolution methods such as STM and Tip Enhanced Raman Spectroscopy.

4.4 Stretching and splitting of single polymer duplexes by SFM manipulation

Nanofabrication aims at building structures with nanoscale features, which can be used as components, devices, or systems in large quantities and at potentially low costs. These nanostructures should allow their integration into complex hierarchical products. Generally, nanoscale features refer to any characteristic that is between 0.1 and 100 nm in size. Most current technologies used in industry for nanofabrication have evolved from conventional lithographic processes, which have been developed for the semiconductor industry for making microelectronic circuits and components. However, there are many challenges to conventional lithographic techniques as they are approaching their fundamental size limits. Fabrication strategies are therefore required to secure cost-effective and technically feasible options. Currently, a scanning probe microscopy (SPM) -based technology has become increasingly popular in the fabrication of nanoscale structures due to its moderate cost and great technical potential.

After its inception in 1981, SPM has been used to gain knowledge of surface structures and molecular organization in the fields of physics, chemistry, and biology and has enjoyed widespread acceptance in many areas of science and technology. Concurrently, SPM has emerged as an essential tool in the fabrication of nanoscale structures, especially for directly inducing selective modifications on a surface with a precise localization of the defined pattern. An STM tip was used to move single atoms [189] and small molecules [190] [191] across solid substrates at very low temperatures. Macromolecules [13], single atoms [192], carbon nanotubes [193] and nanoparticles [194] [195] have been manipulated on solid substrates using the SFM tip under ambient conditions. For manipulation of a macromolecule a most critical issue is its interaction with the substrate, which is usually either too weak, causing the molecule to diffuse rapidly across the surface, or it is too strong, causing a long molecule to break during manipulation. The interaction with the substrate can be tuned by a layer of amphiphile molecules, so that macromolecules can be readily imaged in tapping mode and manipulated in contact mode SFM at ambient conditions [22].

On the other hand, during the past ten years, a series of single macromolecule experiments provided detailed insight into inter- and intramolecular forces, providing relevant information on molecular mechanisms [39]. Among them the mechanical properties of DNA attracted the interest of both physicists and biologists, because of their importance to numerous biological processes, such as DNA transcription, gene expression and regulation, and DNA replication

[38]. Early mechanical experiments with single DNA molecules were mainly performed in bulk liquids, where DNA has been stretched by pulling on one end of the macromolecule with an optical tweezer [94] or an SFM-tip [98], while the other end is fixed either by another optical tweezer or a solid substrate. As high forces were applied to the molecule, a highly cooperative conformational transition was discovered, where the natural B-form DNA is converted into a new overstretched conformation called S-DNA [28]. The related theoretical models have cast light on the molecular details of the overstretching transition [41]. However, the mechanical properties of single molecules on a solid surface, especially concerning on the overstretching transition or even on the breakage transition at higher forces, still remain open to explore. Therefore a new method that is able to manipulate molecules on a solid surface and then to probe the high-resolution structure of manipulated molecules is eventually needed [196].

4.4.1 Manipulation of DNA on Dodecylamine coated HOPG

It has been demonstrated before that a dodecylamine (DA) coated HOPG surface can function as a workbench to adsorb single anionic polyelectrolytes such as ds-DNA and manipulate them with a SFM tip [22]. Some nice examples are displayed in Fig. 4.42 displaying a vector ds-DNA that was cut and moved to a horse shape even on a surface covered with a DA multilayer (left) and a long linear ds-DNA that was cut and the parts moved by the SFM tip to shape a Christmas tree (right). The experimental details can be found in Chapter 3.4.

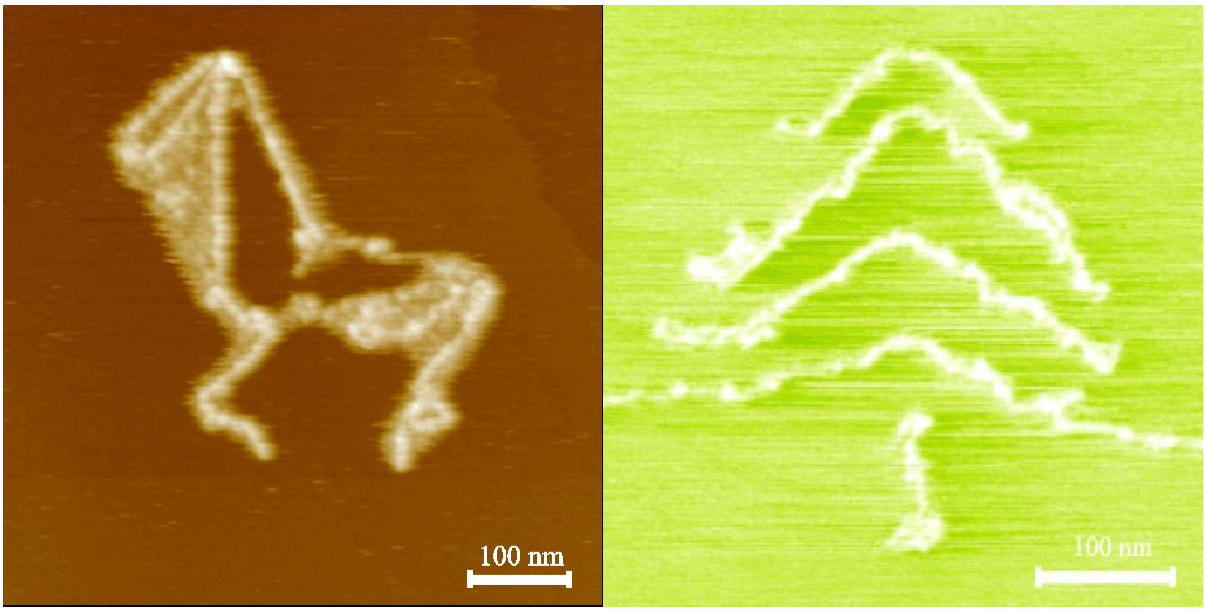

Figure 4.42: Left: SFM height image of a plasmid ds-DNA on HOPG with more than a monolayer of DA molecules shaped into a horse (conducted by Veeco Litho Program); Right: SFM height image of a linear ds-DNA, which was cut and moved to shape a tree (conducted by home developed SFM manipulator).

On the other hand, DA coated HOPG has been proven to be a good surface to immobilize polyelectrolyte molecules at room temperature, because DNA molecules bind to DA molecules to form stable DNA-DA complex, as DNA on a OA submonolayer does. By applying a strong point force exerted by an SFM tip in contact mode, the complex moves, following the point force; then after the external force is removed, the complex is stable and immobile on the surface at room temperature due to the interaction between DA and HOPG. In order to test the stability of the DNA-DA complex on HOPG, the surface temperature of HOPG was increased from 25°C in 10°C intervals up to 85°C, and SFM tip manipulation was conducted *in-situ*. As can be seen in Fig. 4.43, until heating up to 75 °C the complex became slightly mobile after manipulation. No such relaxation was observed before heating up to 75°C indicating that at room temperature the DNA-DA complex is immobile enough even if the DA surface coverage is low.

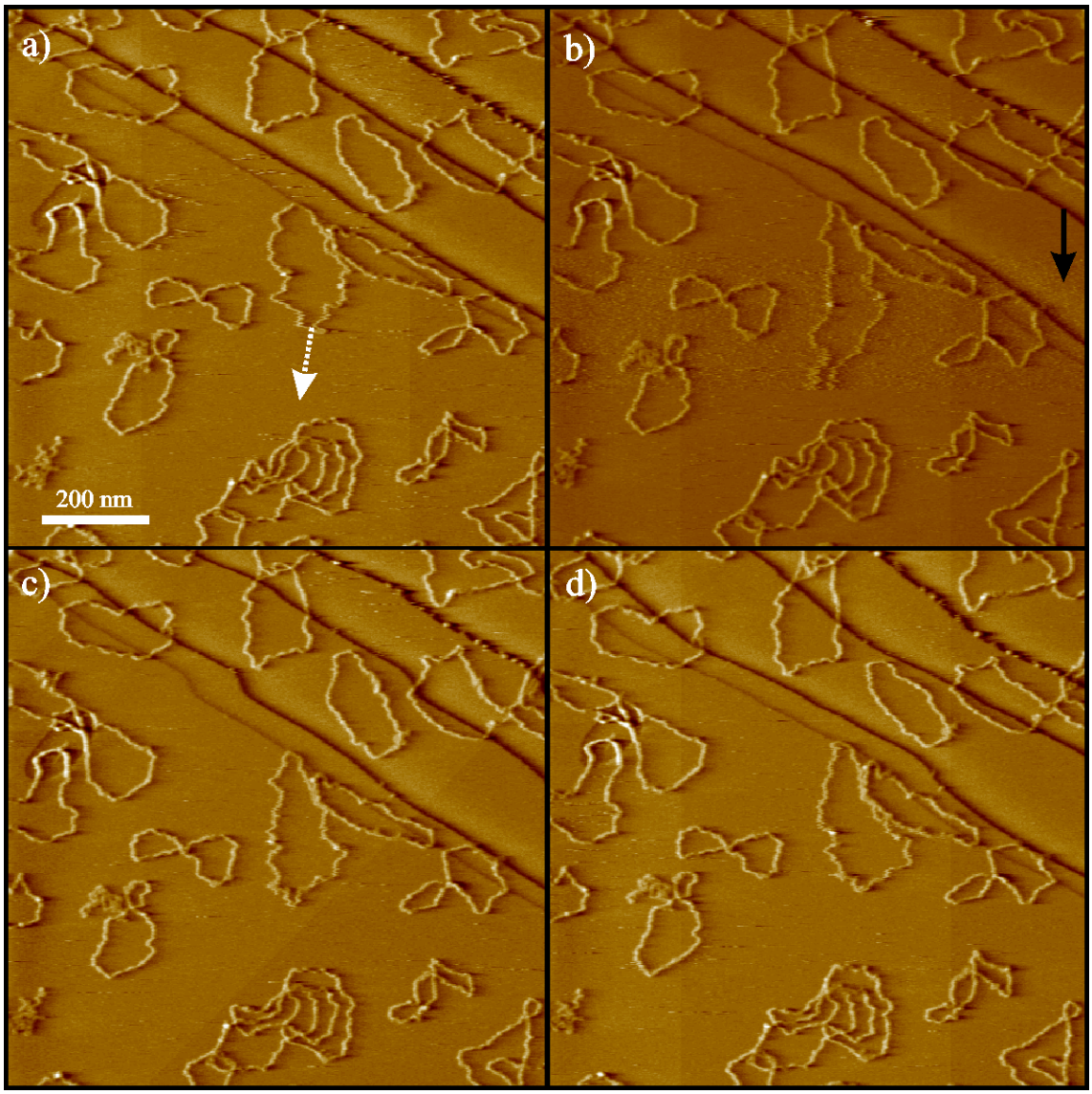

Figure 4.43: SFM height images of plasmid ds-DNA molecules on a DA submonolayer on HOPG spin-coated from a 200 mg/L DA solution, the surface is being annealed at 70°C. (a) Before SFM tip manipulation, white arrow indicates the manipulation tip moving trace; (b) 2 minutes after tip manipulation, the stretched chain slowly relaxed back; black arrow indicates the slow scan direction; DNA molecule continued to relax slightly in (c) until finally they are immobilized in (d), which was already 6 minutes after manipulation.

Plasmid ds-DNA on DA coated HOPG exhibits unique properties, in particular splitting upon adsorption and the fact that they can be manipulated by an SFM. This triggered the idea to attempt splitting the open double strands further on the surface, with the aim to have two complete separate single-strand DNA chains. The motivation to have single-stranded DNA and elongate them has been introduced in Chapter 4.32. A successful manipulation experiment on a surface can promote the workbench of DA coated HOPG to be a powerful DNA chip.

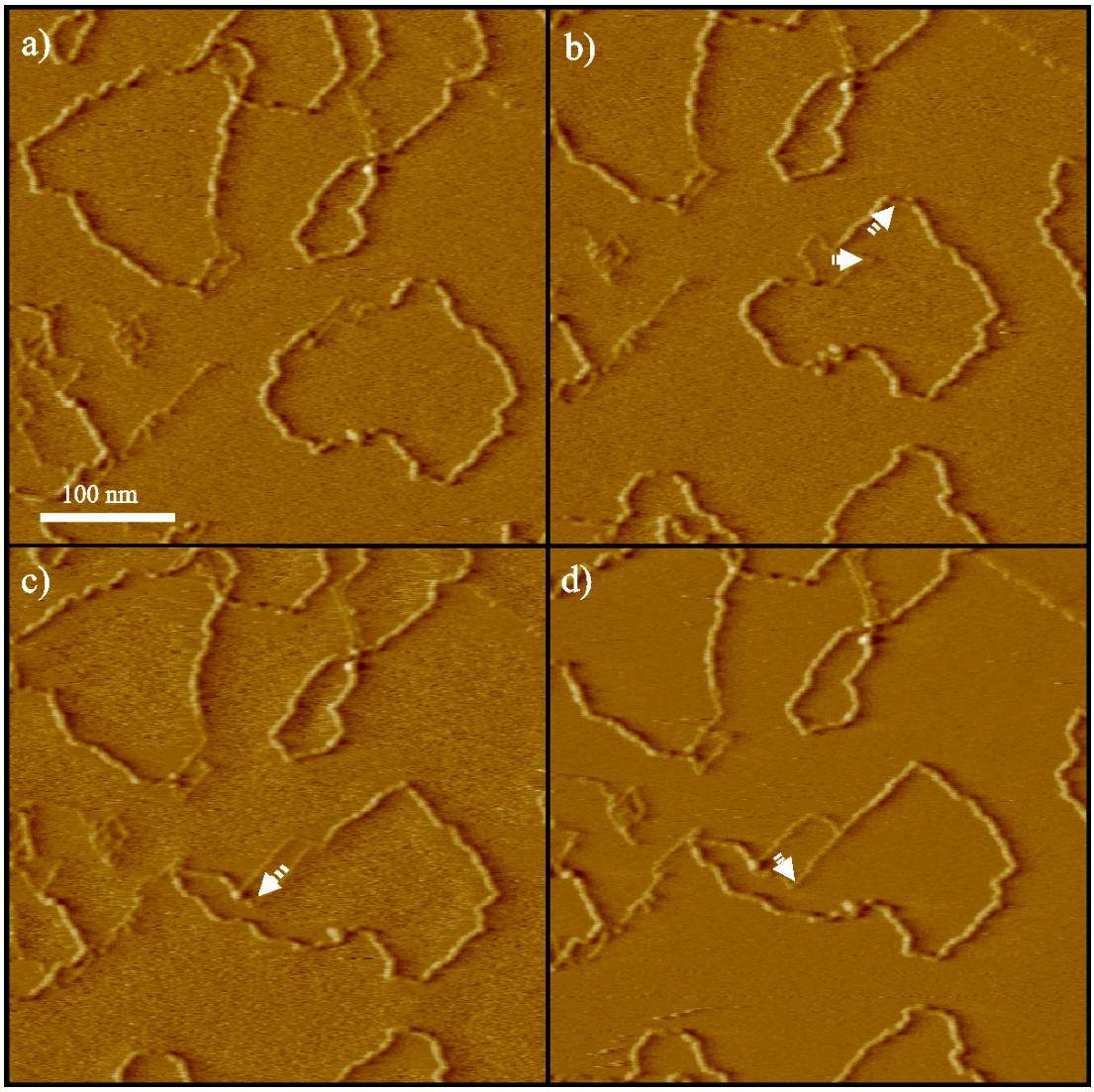

Figure 4.44: (a) SFM phase image of a split plasmid ds-DNA on DA coated HOPG surface; (b-d) a sequence of SFM tip manipulations in order to separate the split further; the white arrows show the moving traces of the SFM tip in contact mode.

As expected the SFM tip manipulation could be well applied to split single strands. Fig. 4.44 shows coiled single strands in (a) which after a series of SFM tip manipulation steps were stretched as shown in (d). However, when the length of the enlarged split was measured before and after tip manipulation, an interesting observation was made. As shown in Fig. 4.45 (a), as one marks two reference points on the ds-DNA, the lengths of the double strands from the two respective reference points to the split points amount to 104 nm and 134 nm. One may expect that they become shorter upon enlarging the 82 nm split single strand parts, since a further split may further compress the pitch of the double strands and shorten their lengths. But after a series of tip manipulation steps a different result was obtained as shown in Fig. 4.45 (e): The length of the single strands increased to 145 nm, but the two double stranded chain part also increased (105 nm and 157 nm), which means that the length increase of the single strands is largely from

(over)stretching of a coiled conformation rather than from further splitting double strands. Therefore the same problem as discussed in Chapter 4.22 occurs again: to separate the single strands in a helical duplex needs to rotate the duplex on the surface in order to allow for a tight knot to be unwound as Fig. 4.45 (f) shows. However, so far the anionic polyelectrolyte linked to long chain alkylamine molecules (OA and DA) is impossible to rotate on the surface by SFM tip manipulation. Obviously a new manipulation method based on a new surface preparation is needed to overcome this limit.

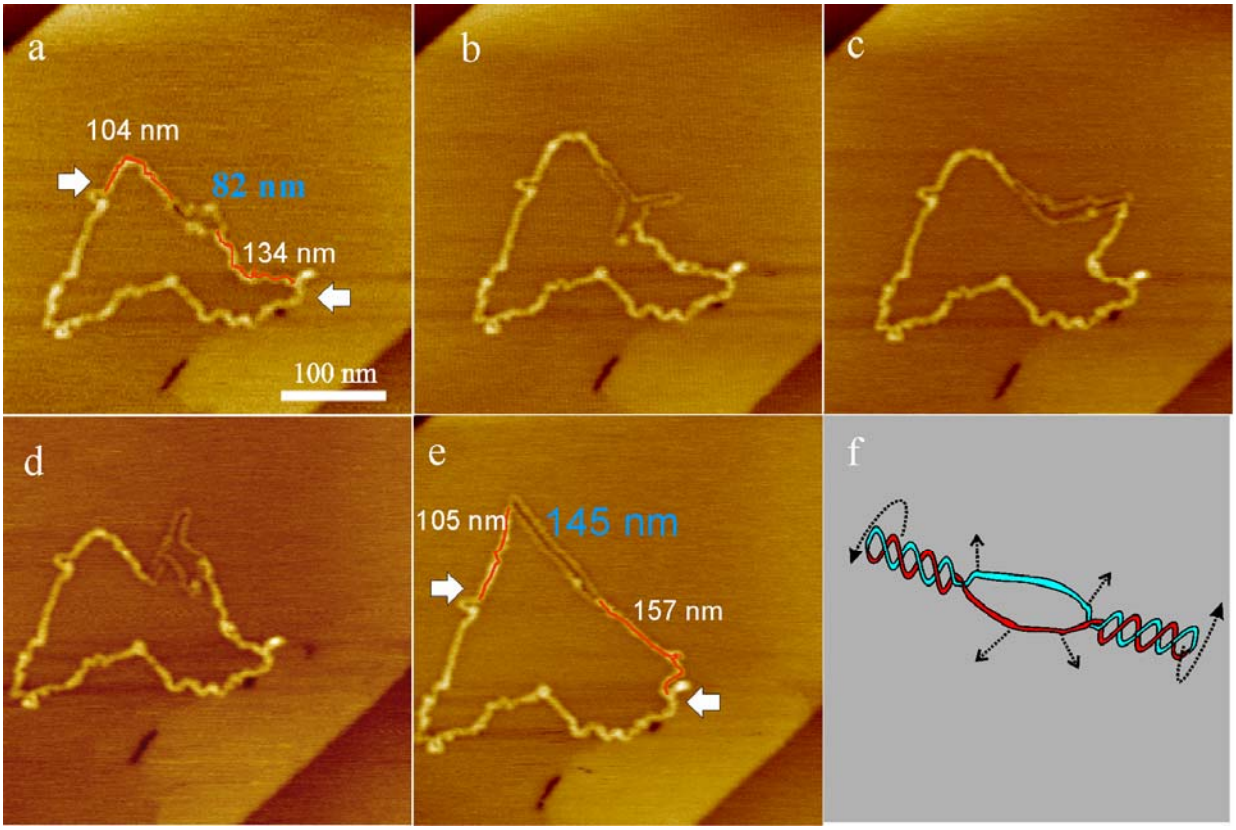

Figure 4.45: (a) SFM height image of a split plasmid ds-DNA on a DA coated HOPG surface; (b-e) a sequence of SFM tip manipulations in order to separate the split further; (f) a schematic drawing indicating the knots of double strands, which prevent the further split.

4.4.2 The "blowing effect" – a new manipulation method on a surface

In sub-chapter 4.4.1 a combination of two "working tools" has been introduced, an SFM-tip and a specific surface layer, which allow free shaping of single macromolecules on surfaces. However, with this manipulation method only a point force can be exerted on the polymer. In the present sub-chapter the new so called "blowing effect" will be described, which provides a way to exert a homogenous force to shape a whole polymer molecule at once, and to approach perfectly circular shapes of single polymer molecules. The key is an ultrathin liquid film.

Dynamical processes in ultrathin liquid films are crucial for phenomena such as lubrication, wetting and spreading. A powerful instrument for investigations of ultrathin liquid films is the surface force apparatus (SFA) [197]. In the SFA an ultrathin liquid layer is confined between two atomically smooth mica surfaces and forces required to displace the surfaces are measured. The measurements with the SFA demonstrate that the properties of liquids confined in ultrathin layers are qualitatively different from the bulk [197,198]. The SFA, however is not capable of measurements of dynamics in ultrathin liquid films on free surfaces. Therefore it is necessary to find a kind of sensor which can sensitively detect the dynamics in ultrathin liquid films on surfaces. On the other hand, in some of our unpredicted experiments we surprisingly observed that single polymer chains, such as ds-DNA, poly(styrene sulfonate) (PSS) or dendronized polymer could blow to circular shape in ultrathin liquid films on a free surface during scanning by SFM. In particular plasmid vector ds-DNA molecules are appropriate for such experiments because of their unique properties: they can be substantially and reversibly elongated [28,29,99] under applied stress, and they are monodispersed polymer rings. Hence, the story of "blowing effect" starts: on one side plasmid ds-DNA molecules serve as nano-sensors for the examination of pressures in ultrathin liquid films on a surface, on the other side the pressures in ultrathin liquid films are applied to manipulate plasmid ds-DNA conformations on surfaces.

There are two ways to prepare ultrathin liquid films on a surface. In the two-steps preparation as sketched in Fig. 4.46 (a), ultrathin liquid films are prepared directly by spin-coating of liquid amphiphiles: $C_4H_9NH_2$ or $C_6H_{13}NH_2$ onto HOPG. For spin coating, a droplet (~5 mL) of liquid is applied on the graphite surface rotating at 40 rps. A sub-monolayer of anionic polyelectrolytes, such as plasmid DNA molecules (pUC19, 2686 bps) is applied from a dilute aqueous solution (2 mg/L) by putting a drop on the freshly precoated substrate for 5 seconds and spinning it off subsequently. Liquid amphiphiles on the one hand provide an affinity of

DNA molecules to the graphite surface, and on the other hand form an ultrathin liquid film at room temperature.

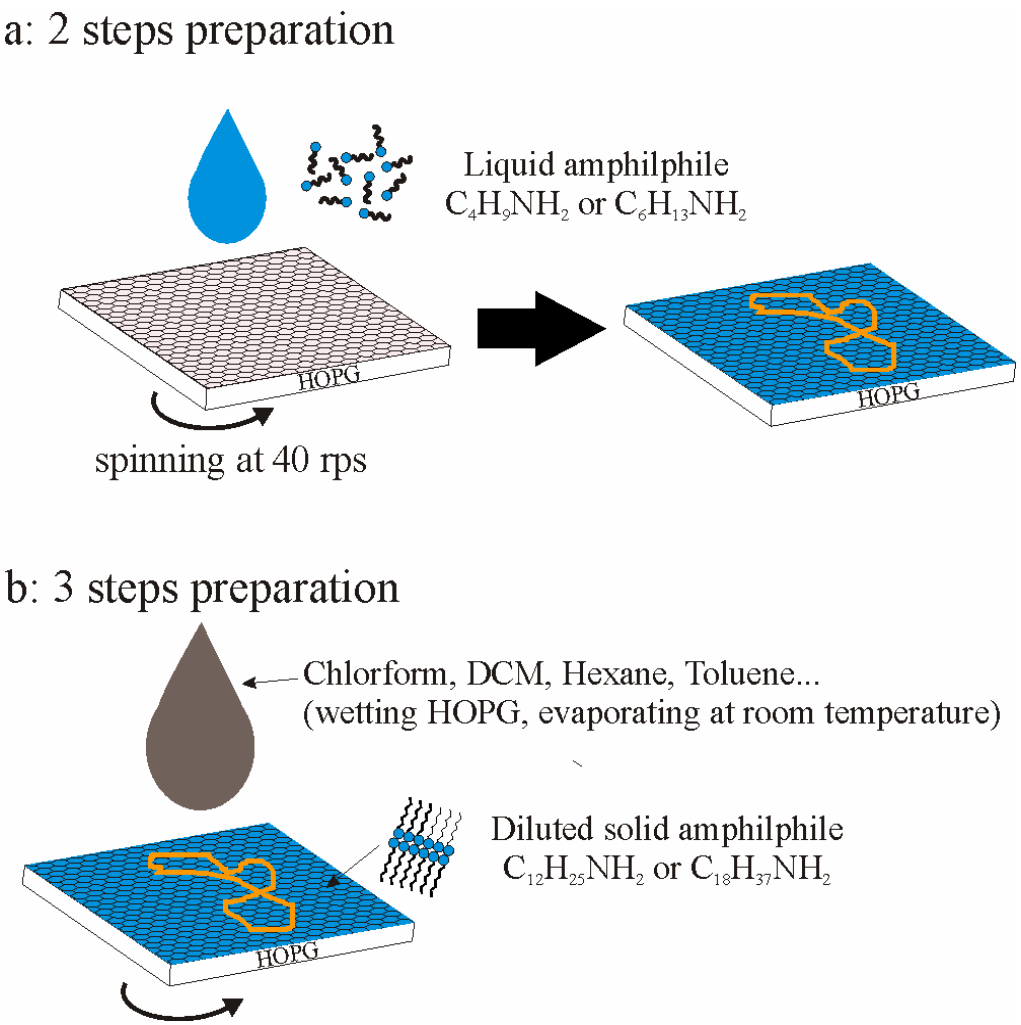

Figure 4.46: Procedure to prepare samples for the blowing effect on plasmid DNA on alkylamine coated HOPG.

In the three-steps preparation as sketched in Fig. 4.46 (b), a droplet of a chloroform solution of long chain amphiphile molecules such as dodecylamine ($C_{12}H_{25}NH_2$) (0.1-0.5 g/L) or octadecylamine ($C_{18}H_{37}NH_2$) (0.01-0.05 g/L), is spin-coated on HOPG at 40 rps. The long chain solid amphiphiles immobilize DNA sufficiently for imaging with tapping mode SFM. On the other hand long chain amphiphiles allow SFM tip manipulation of the DNA molecules across the surface. After applying a sub-monolayer of anionic polyelectrolytes, such as plasmid DNA molecules on it, the surface is dried at 40°C for half an hour to remove all the chloroform. After drying of chloroform, the ultrathin liquid film can be restored by spin-coating (40 rps) a new drop of different wetting liquids, such as dichloromethane, chloroform, hexane, benzene, acetone, or toluene, which will be explained subsequently with further details.

4.4.2.1 Experimental observations of the blowing effect

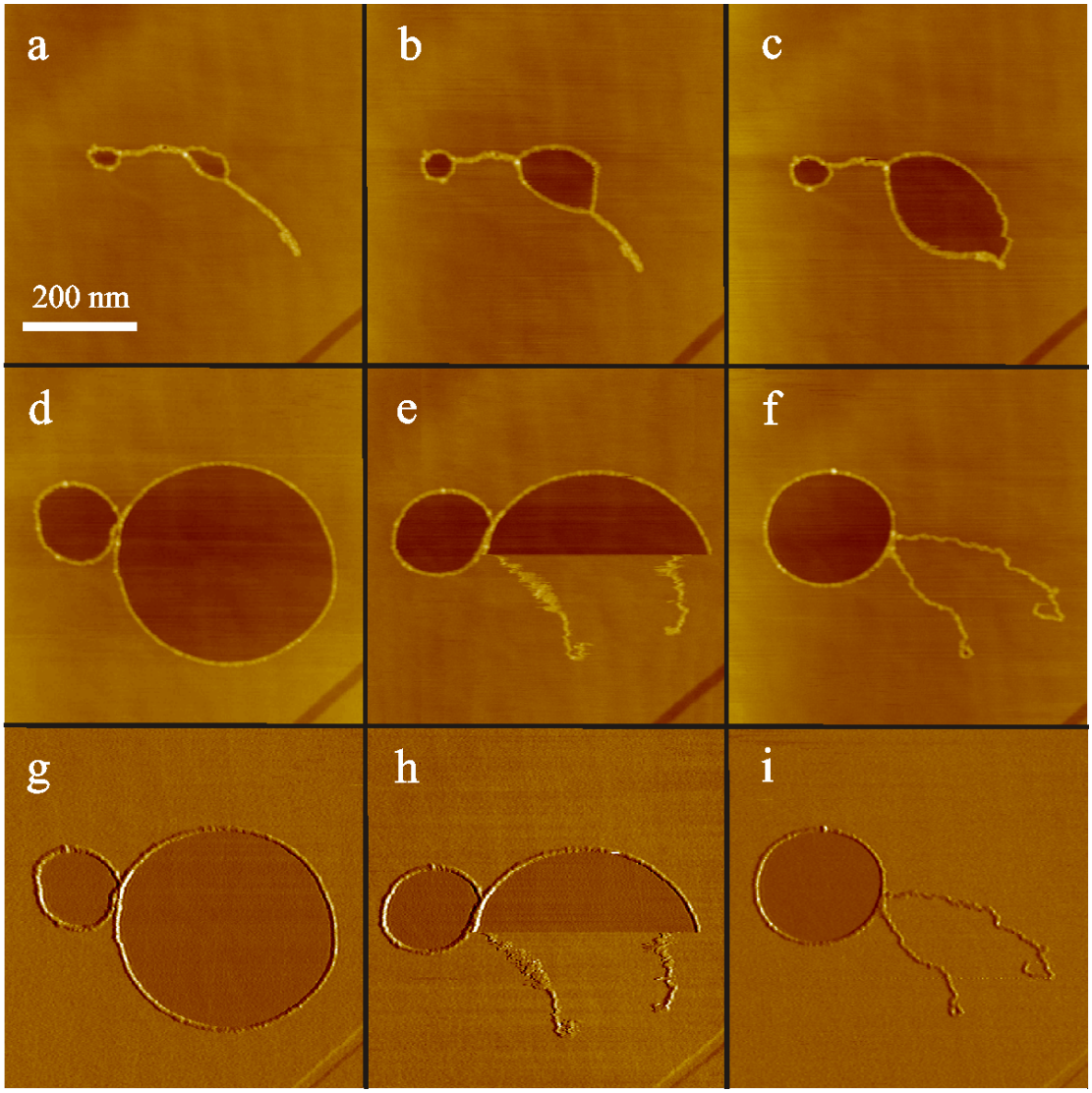

Figure 4.47: : a) - d) SFM tapping mode height images, revealing the unravelling of an initially supercoiled vector ds-DNA on $C_4H_9NH_2$ upon repeated SFM-scanning of the same surface area. e) During one of the scans the largest loop breaks; the slow scan direction is indicated with the arrow. f) After a few scans the smaller loop stabilizes its size and does not grow under continues scanning. g) - i) SFM tapping mode phase images taken simultaneously with the height images d) – f) respectively.

Fig. 4.47 (a) displays tapping-mode SFM images of an initially supercoiled vector ds-DNA deposited onto graphite covered with $C_4H_9NH_2$ (butylamine) at ambient conditions. A few repeated scans of the whole image caused the two initial loops of the DNA to grow until finally two almost circular "bubbles" appear. DNA molecules outside the scan area remain in disordered conformations, which is demonstrated by increasing the scan area after a few scans. In all cases, SFM height and phase images reveal a difference between inside and outside of the blowing loops. The difference between the SFM height and phase data inside and outside of the loops is identical for all loops in one scan area and does not change during growth of the

bubbles (Fig. 4.47 a-d). Linear polymer molecules which do not form loops are not affected by the scanning.

The blowing effect was also observed with polymer molecules deposited on graphite surface coated with an ultrathin liquid film only, i.e. without amphiphiles. Vector DNA molecules (pUC19) were applied to a graphite surface by drying a droplet of dilute DNA solution in milli-Q water (10^{-3} g/l). SFM imaging of the dry surface revealed aggregates of DNA molecules with occasional small molecular loops protruding out of the aggregates, which has been shown in Fig. 4.38 (a). SFM imaging shortly after spin coating of hexane reveals that the loops formed by the DNA molecules blow, which one can see by the characteristic contrast between inside and outside of the loops and by the blown shape of the loops (Fig. 4.48 a-b). The contrast between inside and outside of the loop disappears, after breakage of one of the DNA loops by the SFM tip manipulation (Fig 4.48 b-c).

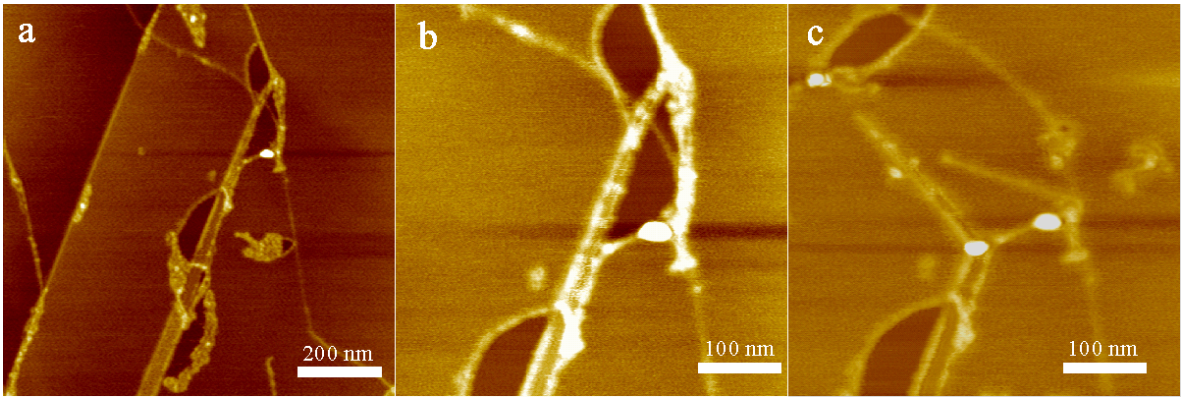

Figure 4.48: a) Blowing of DNA loops on uncoated HOPG after application of hexane. b) Zoom-in from a). c) The contrast between inside and outside of the loop disappears after breaking one of the DNA molecules with the SFM tip manipulation.

Upon the blowing, the circumference of the vector ds-DNA circles can become as long as 2.0 times the contour length of B-form ds-DNA, indicating that the DNA is overstretched in this state (Fig. 4.49 a-b). The area enclosed by the DNA loops can increase considerably during blowing; for example the larger loop in Fig. 4.47 (d) increases 30 times. Large DNA circles can break and quickly the height and phase for the area inside level up with the area outside (Fig. 4.47 e, h and 4.49 c). When the molecular loop is broken, the force stretching it disappears and the DNA relaxes into a less stretched conformation, yet longer than B-form ds-DNA (Fig. 4.49 d). After a few scans the size of the remaining bubbles stabilizes and it does not grow anymore under continuous scanning (Fig. 4.47 f). The DNA loops also grow and can break during repeated tapping in the center of the loops, which is demonstrated by zooming into the center of

a DNA loop after the first scan. This experiment implies that the DNA loops can blow in the absence of the direct interaction between the SFM tip and the DNA strand.

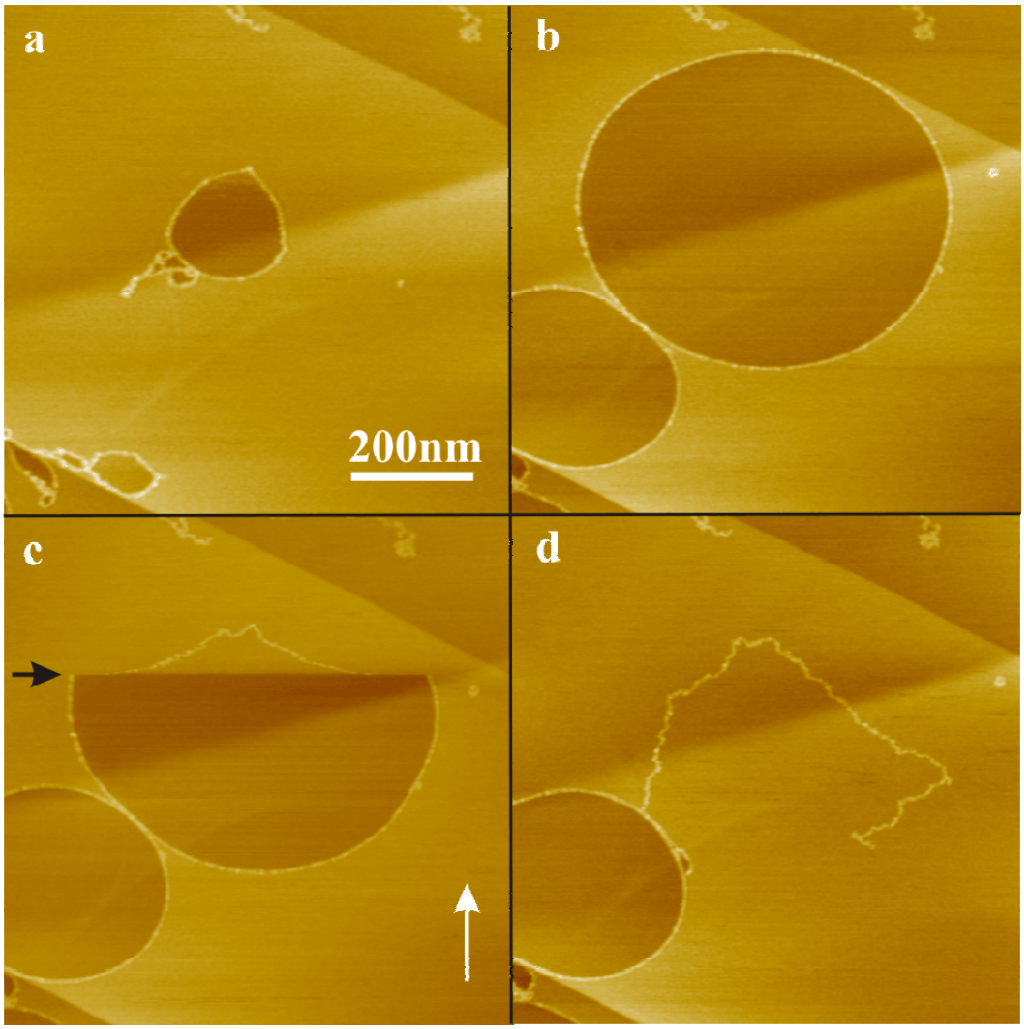

Figure 4.49: SFM tapping-mode height images, revealing the "blowing" of vector DNA molecules on a film of $C_4H_9NH_2$: a) initially coiled molecules start to blow during the first scan; b) after a few scans the vector DNA molecules are fully blown into circles; the length of the molecule in the center is 1840 nm, which corresponds to 2.0 times overstretching of its B-form length (915 nm); c) during the next scan the largest molecule breaks and quickly the contrast between inside and outside disappears and the DNA molecule relaxes into less stretched conformation (the slow scan direction and scanned line where molecule broke are indicated by white and black arrows, respectively); d) on the next image made during the next scan, the molecule has relaxed into a less stretched form, which is still 1340 nm long. The conformation of the broken molecule does not change noticeably with further scanning.

The effect of expansion of polymer loops into circles can only be observed for a limited time, which depends on the nature of the coating liquid and on its temperature. For example, while for neat $C_4H_9NH_2$ with a boiling point (b.p.) of 76°C blowing upon SFM scanning stops after roughly 50 minutes at room temperature (~20°C), for $C_6H_{13}NH_2$ (b.p.: 131°C) blowing can be still observed 24 hours after sample preparation. The time during which the blowing effect can be observed will be referred to as "active" time. The vanishing of the blowing effect is not

abrupt, rather it is found that the DNA loops blow and break more readily at the beginning of the active period. The difference in phase and height between inside and outside of the blown loops disappears when the sample becomes inactive. For the investigated systems the active time decreases with increasing temperature (e.g. there is no blowing for neat $C_4H_9NH_2$ after annealing at 40°C for 20 minutes). The dependence of the active time on both temperature and boiling point of the liquids indicates that vanishing of the blowing effect is due to the evaporation of the liquid coating. All samples can be repeatedly re-activated upon spin-coating organic solvents such as dichloromethane, chloroform, hexane, benzene, acetone, or toluene onto the sample.

For the liquids with high boiling points, i.e. toluene (b.p. 111°C) and $C_6H_{13}NH_2$ (hexylamine, b.p.: 131°C), the active time starts not immediately after spin-coating the liquid but after some induction time, which can be as long as two hours for $C_6H_{13}NH_2$ at room temperature or ten to twenty minutes for toluene, indicating that some amount of liquid has to evaporate before the system becomes active. This observation indicates that the blowing effect is present only when the liquid film is very thin. Since the polymer molecule visually acts as a boundary separating the films inside and outside of the loop, the thickness of the liquid film during the active time should be comparable or less than the diameter of the molecules, i.e. less than e.g. the diameter of ds-DNA molecule, which is about 2 nm in B-form [34].

Blown DNA circles relax slowly upon cease of the scanning into a less stretched state. If the scanning is restarted within the active time, the loops reshape back into circles. When the sample becomes inactive, i.e. no new loops can be blown, already blown loops relax slowly into a less stretched state both during and in the absence of scanning (Fig. 4.50). On graphite coated with short chain amphiphiles the relaxed conformation tends to become less regular (Fig. 4.50 a-c), while on long chain amphiphiles ($C_{18}H_{37}NH_2$) it exhibits hexagons (Fig. 4.50 d). The relaxation of circles into hexagons manifests the hexagonal symmetry of the substrate consisting of the graphite and the long chain alkylamines, which, like alkanes and many of their derivatives, adsorb on the basal plane of graphite with their long axes preferably along the crystallographic axes [21].

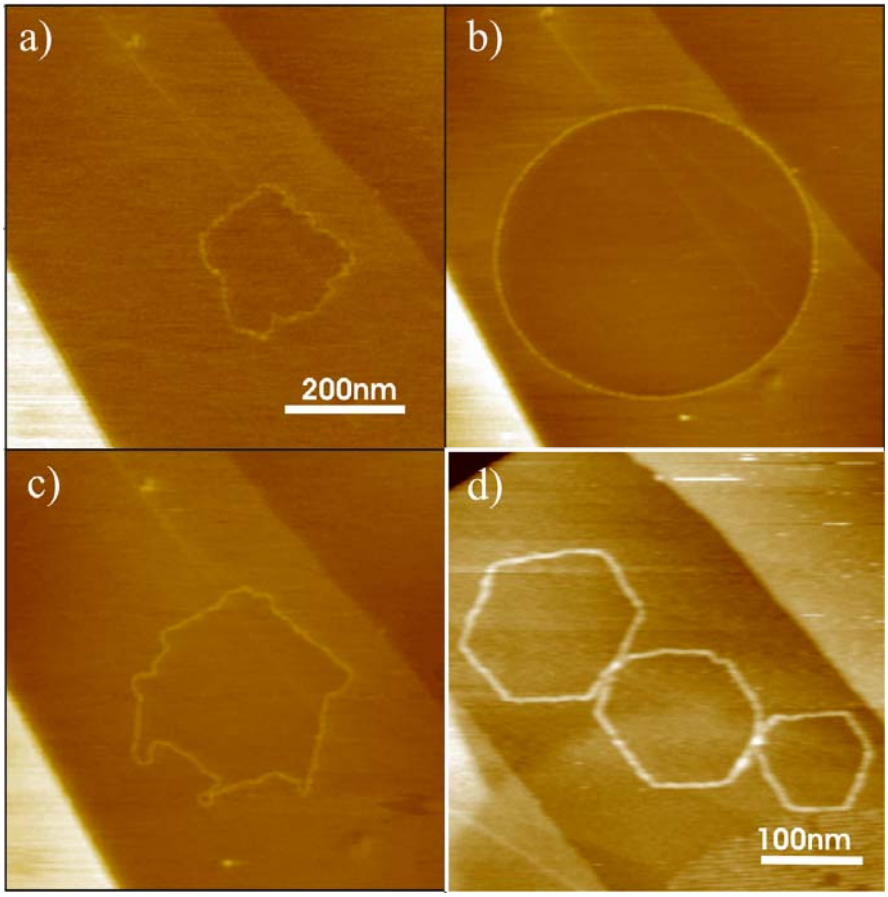

Figure 4.50: SFM height images show a vector DNA on graphite coated with $C_{12}H_{25}NH_2$ and refreshed with hexane; a) first scan; the length of the DNA molecule is 915 nm, which corresponds to the B-form; b) after a few scans, the loop blows to circle and stabilizes its shape at 1590 nm length. Next the tip is retracted for two hours and image c) is recorded thereafter; no difference between inside and outside of the DNA loop can be detected and the DNA loop does not change its shape during scanning, which indicates the inactive state; the length of the DNA molecule is 1380 nm, which is still significantly longer than the B-form length; d) Relaxation into hexagons of DNA blown on graphite coated with $C_{18}H_{37}NH_2$ chloroform solution.

On the longer chain amines $C_{12}H_{25}NH_2$ and $C_{18}H_{37}NH_2$, typically more supercoiled twists remain on the surface after blowing, resulting in several touching circles of different diameters (Fig. 4.50 d and Fig. 4.51 a). Defects on the surface like monoatomic step edges on graphite confine the motion during blowing (Fig. 4.51 a). Analogously, loops have been formed randomly by crossings of linear DNA on the same substrates. Also these loops could be blown into bubbles as shown in Fig. 4.51 b. An intriguing observation is that the blowing effect is also found on a hydrophilic mica surface, if a hydrophilic solvent such as hexafluoroisopropanol is spin-coated on the surface. Fig. 4.51 c shows that the height contrast is different between inside and outside of topological loops formed by non-charged G2 dendronized polymers even though the dendronized polymers are immobilized on the mica surface, indicating the formation of ultrathin liquid layer inside the polymer loops.

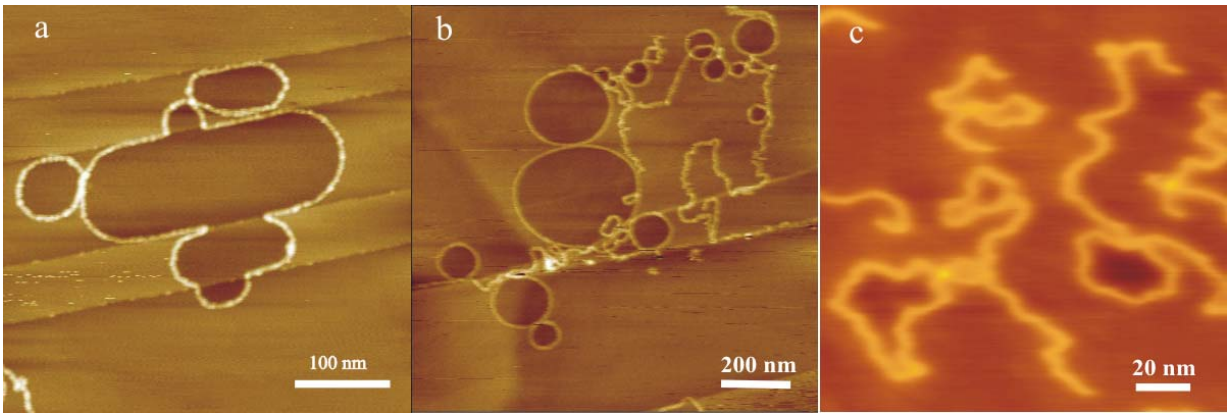

Figure 4.51: a) Several topologically formed loops of one ds-DNA on $C_{12}H_{25}NH_2$ can blow independently from each other and defects on the surface like monoatomic step edges on graphite confine the motion of the polymer during blowing; b) Topological loops formed by linear DNA molecules can be blown to bubbles on $C_{12}H_{25}NH_2$; c) Dendronized polymers on the mica surface coated by an ultrathin hexafluoroisopropanol film.

Regarding the difference in the phase images between inside and outside of the blowing loops, we recall that the phase lag between oscillations of the external force and of the position of the tip depends on the viscoelastic properties of the liquid film the tip interacts with [199]. The phase lag mapped on the phase images reflects therefore the difference between surfaces covered with different liquid films. However it is difficult to quantify the phase and height difference exactly, due to their dependence on tip and tapping conditions. In order to characterize the phases inside and outside the loop further the amplitude of the oscillating tip was recorded as a function of the tip-sample distance for a bare graphite surface, a graphite surface freshly coated with $C_4H_9NH_2$, and both inside and outside of DNA loops blown on a film of $C_4H_9NH_2$ during active time of blowing (Fig. 4.52). For these measurements first an SFM image was taken, then the tip was moved to the desired location, the feedback was switched off and the tip oscillating at a frequency close to its resonance frequency was extended towards the surface. While the amplitude-distance dependence measured on graphite is linear over a range determined by the amplitude of the tip oscillation for both approach and retraction (which is consistent with a solid substrate and hard cantilevers [200]), it exhibits hysteresis, similarly for both graphite with freshly spin-coated $C_4H_9NH_2$, and outside of DNA loops blown on graphite surface coated with $C_4H_9NH_2$ during active time.

The hysteresis can be explained by the formation of a meniscus connecting the tip and the fluid film [201,202]. Quite noise-free images indicate that during imaging the tip vibration prevents meniscus formation. However, when the tapping amplitude is sufficiently reduced due to the interaction with the surface, a meniscus can form and the tip jumps into contact [201]. Upon retraction, the existing meniscus damps the tip oscillations resulting in hysteresis between

approach and retraction. The amplitude-distance dependence measured inside the blown loop does not exhibit hysteresis, indicating that the meniscus does not form; however, it exhibits a glitch. After the DNA breakage the amplitude-distance dependence measured inside the loop starts to exhibit hysteresis indistinguishable from outside of the DNA loop, indicating that the liquid film outside the loop flows into the now open area inside the loop. The hysteresis measured outside of the blown loops disappears when the samples become inactive, and the glitch appears typical for the amplitude-distance dependence measured inside a blown DNA loop (Fig. 4.52 b). Amplitude-distance dependences measured one day after the application of $C_4H_9NH_2$ are linear, which is typical for bare graphite (Fig. 4.52 a).

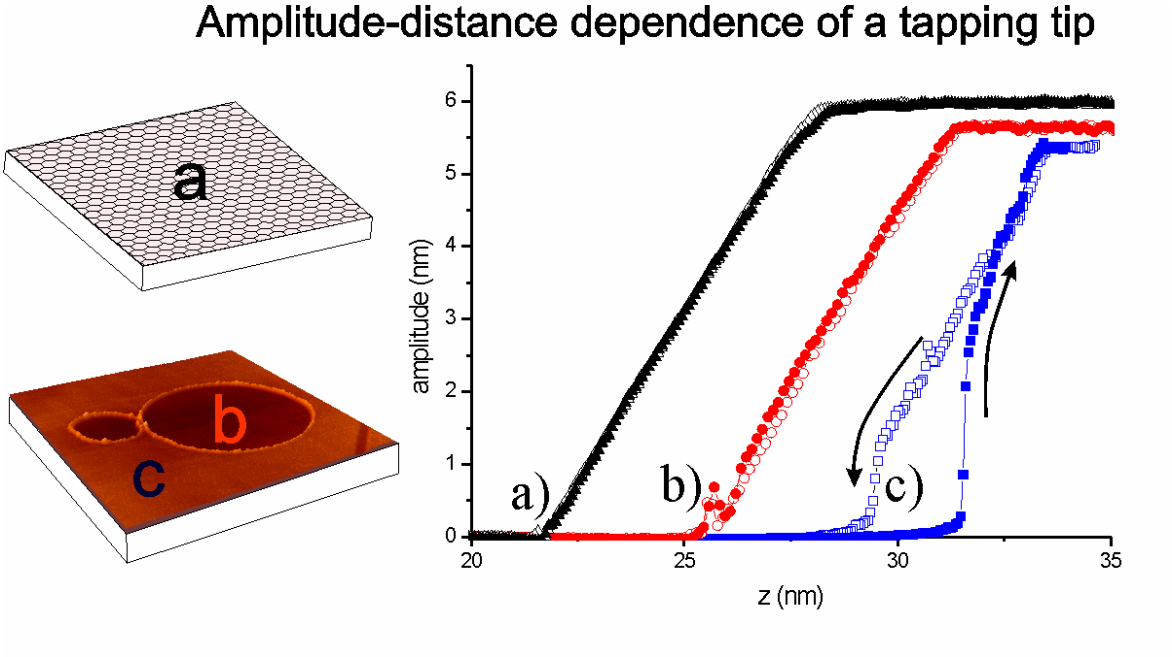

Figure 4.52: Typical amplitude-distance dependences of a tapping tip a) on freshly cleaved graphite, b) inside of a DNA-loop blown on graphite coated with $C_4H_9NH_2$ during active blowing time, and c) same as b) but outside of the blown DNA-loop; a hysteresis between approach and retraction similar to c) is observed for graphite freshly coated with $C_4H_9NH_2$ without DNA applied. All amplitude-distance dependences are corrected with respect to piezo creep and shifted along x-axis for clarity. Open and closed symbols are for approach and retraction, respectively.

4.4.2.2 The mechanism of the blowing effect

The circular shape and the difference between inside and outside of the blown loops suggest that the process of the loop expansion is determined by a difference in the surface pressure, $\Delta\sigma$, and consequently a tangential force along the polymer, F_t, which is proportional to the length of the loop and amounts to $F_t = \Delta\sigma \cdot L/2\pi$ for perfectly circular loops. This is in agreement with the observed breaking of large loops only. The experimental results indicate that the

interaction of two crossed DNA strands can be sufficiently high to prevent sliding of the strands upon blowing and breaking of DNA loops (Fig 4.47 d-f). Thus it is reasonable to suggest that loops of a multiply twisted DNA molecule blow incoherently. Therefore, the force stretching each loop must be proportional to the length of the loop. Hence the total length of a blown vector DNA with multiple loops should be significantly shorter than the length of a single vector DNA loop, which is again in good agreement with the experiment. While the blowing effect can be explained by the surface pressure difference, the origin of this difference must be clarified, which will be done in the following.

Liquids at the interface with a solid differ from their bulk state since they order in molecular layers parallel to the substrate surface. With a surface forces apparatus, the layers can be squeezed out one by one at increasing normal forces, indicating solid-like behavior in the direction normal to the substrate. Similar layered behavior is observed for free liquid thin films on a surface [203]. Computer simulations [204], measurements of shear forces [205] and tracer dye diffusion [14,206], however, indicate liquid-like behavior parallel to the substrate. Therefore, we regard an ultrathin layer of a liquid on a solid substrate as a quasi 2D-liquid. Notably, such a layer may be used to transmit forces isotropically across a surface.

Even though liquids may evaporate macroscopically rather fast, it is known that an ultrathin liquid film can stay for a long time on a surface being captured by the van-der-Waals interactions with the surface [203]. In our case SFM force spectroscopy measurements have indicated a film of liquid on the basal plane of graphite during the active time of blowing (Fig. 4.52). Therefore, it is concluded that an ultrathin film of liquid is present at the surface during this time, and that the system passes to an inactive state upon evaporation of the liquid. The faster the evaporation, the shorter is the active time. Since the blowing effect is observed only when the surface is covered with the liquid film, it is associated with the presence of the liquid film.

In some cases, the formation of circular structures on surfaces upon drying of a liquid film was observed and attributed to a dewetting process [207]. However, the blowing observed in the present case cannot be explained by such an instability, since after breakage of the loop no dewetting is observed; instead the liquid film outside the loop flows into the now open area inside the loop (Fig. 4.49 c, d), which indicates stability of the homogenous surface coverage.

The experimental findings discussed above show that the interaction of the tapping SFM tip with the ultrathin fluid layer creates a new, metastable state of the film inside the loop,

characterised by a smaller thickness than the outside film and by a surface pressure σ, which is higher than the one in the outside layer. This excess pressure causes blowing of the loop into a bubble. Upon ceasing of scanning, the metastable state of the film relaxes to a stable one, equilibrating its pressure and thickness with that of the outside liquid. Creation of a metastable state is not possible without pumping energy into a system; this energy is provided by the SFM's tip oscillations. Blowing of the loops upon tapping in the center of the loops indicates that it must be the liquid film, which isotropically pushes the polymer loop outwards under the action of repeated tapping by the SFM tip. The closed topology of the loop is of primary importance for the effect observed. While the tapping inside the bounded area creates an increased pressure sufficient for blowing, the local increase of pressure in the outside area would only result in liquid flow in an unbounded region, which does not have to move large objects like molecular loops against friction forces. Moreover, the existence of a molecular loop serving as an impenetrable wall between the inside and outside fluid prevents the metastable fluid state inside the loop from the immediate contact with the regions outside the scanning area being close to thermodynamical equilibrium. Such contact accelerates the decay of the metastable state and leads to a fast equilibration in the outside layer. Thermodynamical considerations support this picture of a metastable state.

The overall surface pressure exerted on the loop is the sum of the partial surface pressures σ_i in each molecular layer. In equilibrium, the chemical potentials of all molecular layers in contact have to be the same. The chemical potential in equilibrium is a monotonously growing function of the pressure, because $(\partial\mu_i / \partial\sigma_i)_T = 1/x_i > 0$ with $x_i = N_i / A$ being the number of molecules in a layer per unit surface, a consequence of the Gibbs-Duhem relation $SdT + Nd\mu + Ad\sigma = 0$ under isothermal conditions. Considering the upper layer as being in thermodynamic equilibrium, one has to assume that the pressure is a nondecaying function of x_i. Being intensive, the pressure at a given temperature T can depend on the extensive variables N_i and A only through the intensive combination $x_i = N_i / A$. On the other hand, according to the condition of thermodynamic stability $(\partial\sigma_i / A)_T \le 0$, which implies $(\partial x_i / \partial\sigma_i)_T \ge 0$. Thus, the overall pressure is a nondecaying function of the coverage in the upper layer, and therefore the state with a thinner film and higher surface pressure inside the loop and a thicker film from the outside violates the conditions of thermodynamic stability and is metastable. The metastability can be observed also experimentally as relaxation of the liquid

film thickness inside DNA loop upon breakage of the loop (Fig. 4.49 c, d) and the relaxation of the blown loop into a less stretched state upon cease of scanning (Fig. 4.50 a-d).

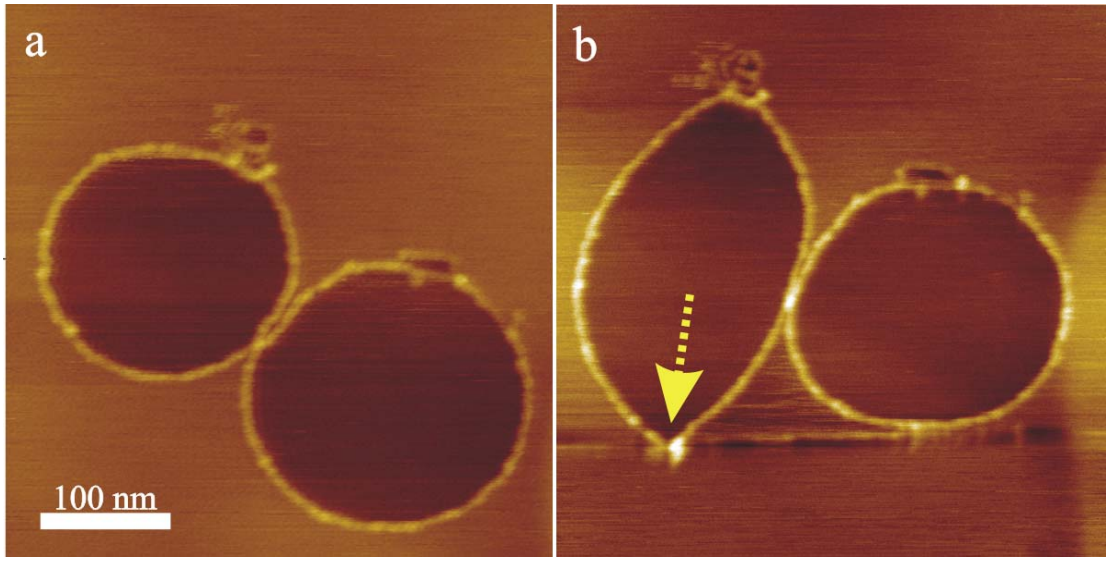

Figure 4.53: Tapping mode SFM images of a blown DNA loop on $C_4H_9NH_2$ coated HOPG before (a) and after (b) SFM tip manipulation.

The fast relaxation of the blown DNA loops upon their breakage is attributed to the metastability of the blown loops. The question remains, however, but what prevents relaxation of the metastable blown loops for long times in the absence of scanning and keeps the circular shape of the blown DNA loops? Only partial relaxation is observed of an overstretched DNA molecule upon its breakage and in the absence of tapping (Fig. 4.49 and 4.50 b, c). Similar partial relaxation can be observed in the absence of liquid film, after stretching DNA directly with an SFM tip in contact mode [22]. Therefore, partial relaxation is attributed to molecule-surface interactions and one may also attribute the metastability of the blown loops to molecule-surface friction. However, since relaxation of the DNA length upon breakage of the loop (Fig 4.49 c, d) happens much faster than the relaxation in the absence of the scanning, molecule-surface interactions cannot explain the long lifetime of the blown DNA loops. Relaxation of the blown DNA loops into a less stretched conformation upon drying of the ultrathin liquid film indicates that the liquid film is responsible for the shape stability of the blown loops. The shape stability must be provided by the liquid film inside the loop, since the stabilization of the overstretched DNA by the film outside of the loop would indicate its tendency to dewet the surface, which is not the case as discussed above. The shape stability of the film inside the loop implies it has less liquid like properties, which is corroborated with the absence of a meniscus formation (Fig 4.52 b). The disappearance of the hysteresis outside of the blown loops and the appearance of the glitch, during drying of the film, indicates that the liquid

film inside the DNA loop is thinner than outside during active time and that the sample becomes inactive when the film outside of the DNA loops becomes identical to the film inside. On the other hand, the existing of such a thinner 2-D liquid layer has been also supported by SFM tip manipulation. Fig. 4.53 indicates that after stretching the blown DNA loop by SFM tip in contact mode, the ultrathin liquid layer inside the loop on the one hand moves across the surface indicating liquid like property, and on the other hand maintains the loop area indicating solid like properties.

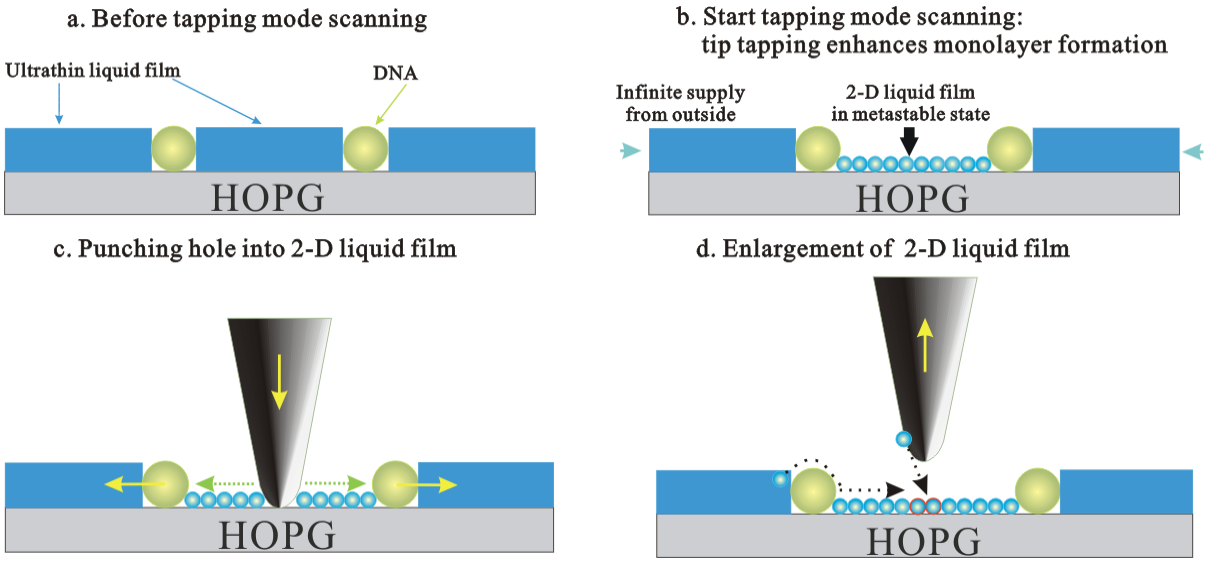

Figure 4.54: Schematic drawing of the model of blowing effect mechanism.

A qualitative model is illustrated in Fig. 4.54 explaining a microscopic mechanism behind the blowing effect. At first the evaporation of the liquid at room temperature leads to an ultrathin liquid film formed on the surface. For the sake of simplicity, it is assumed that the thicker liquid film outside consists of two molecular layers, and the liquid film inside of the loop corresponds to a monolayer. The initial formation of the monolayer inside the loop may be attributed to "hammering" molecules from the second into the first layer, as well as to punching holes in the layer which are then filled by the molecules from the second layer and from the tip. (The scan area outside loop does not form the monolayer due to infinite liquid supply outside scan area, which recovers the outside thicker layer immediately after scanning induced monolayer.) Both mechanisms increase the layer surface and create additional pressure. The latter mechanism also persists when the monolayer is formed. The fact that faster scanning speeds and smaller scan areas both lead to a stronger blowing effect supports the mechanism. The given explanation for the metastability of the monolayer is based on the assumption of a very high binding energy of the molecules to the graphite surface and a somewhat lower binding energy to

the tip material, which, however, allows for wetting of the tip by the molecules of the fluid; the latter is corroborated with the observed meniscus formation. Therefore the tip can gather molecules from the second layer of the film outside the loop [14] and bring them to the interior of the circle. The growth of the area inside of the loop up to 10 times the initial area cannot be explained without assuming such a mechanism of molecular transport. On the other hand, the molecules from the monolayer inside the loop are not transported back, an assumption which is corroborated by the absence of effects connected with meniscus formation when tapping inside the loop.

The question arises, why does the ultrathin layer inside the loop sustain the pressure exerted by both the outside fluid and the stretched loop for such long times? The metastable state can be attributed to a slow nucleation and subsequent growth of an additional layer by molecules changing from a highly populated first layer into a sparsely populated second one. The adsorption energies of molecules of organic solvents on graphite are fairly high. For example, at room temperature the adsorption energy of $C_4H_9NH_2$ is ~ 14 k_BT [208,209], and ~ 19 k_BT for benzene [210]. A relatively high energy barrier for nucleation makes the overall process slow. The change of the configuration of the DNA in the course of time (Fig. 4.49 b, c) can be explained by such a nucleation, possibly accelerated by molecules of the liquid crawling over the DNA from the outside, or by molecules exchanging through the gas phase. A layer of liquid confined at the solid surface due to the energy barrier for formation of a new molecular layer behaves as a quasi 2-D liquid, which transfers pressure homogeneously across the surface, as long as the pressures developed in the layer are sufficiently smaller than $\Delta E / a$, where a is a projected area of a molecule. Taking a=0.44 nm^2 for benzene, the adsorption energy density for a monolayer of benzene is ~175 mN/m. The minimal contour length of DNA loops which is observed to break during blowing was about 1 μm. Apparently there are not any direct measurements of ds-DNA molecules breaking strength. Breaking strengths of synthetic polymer molecules are 2-5 nN [211]; a surface pressure of ~30 mN/m would be sufficient to break a 1 μm long synthetic polymer molecule. The information available on the properties of the adsorbate is not sufficient to obtain quantitative estimates of the lifetimes of such metastable states, but it is consistent with the qualitative picture given above.

4.4.2.3 Unravelling supercoiling and splitting ds-DNA

As introduced in Chapter 4.3, plasmid ds-DNA can form supercoils on alkylamine coated HOPG upon adsorption. In nature topoisomerase helps supercoiled DNA to unravel the supercoiling topology [208], but on a solid surface unravelling supercoiling through non-biological means has never been performed. Fig. 4.47 provides strong indication that supercoiling DNA can be unravelled by the blowing effect, even though the process is too fast to be directly followed, and the chain is finally broken. Therefore experiment was improved in two steps: At first $C_6H_{13}NH_2$ was applied instead of the highly volatile $C_4H_9NH_2$ or the long chain alkylamine as amphiphile to precoat HOPG. Low concentration of $C_6H_{13}NH_2$ (100 mg/L) chloroform solution was spin-coated on HOPG to form a submonolayer of $C_6H_{13}NH_2$. Supercoiled DNA electrostatically complexed to $C_6H_{13}NH_2$ molecules thus has a rather large mobility to rotate on the surface. Secondly, toluene was applied as solvent to generate the blowing effect. With this a long active time and a mild blowing effect was obtained. Fig. 4.55 displays a plasmid DNA with a long supercoiled part that was gradually unravelled. In a manipulation process within 30 min one can clearly follow how a circle with a diameter of around 100 nm was expanded to a circle with a diameter of about 400 nm and an enclosed area increased by more than ten times.

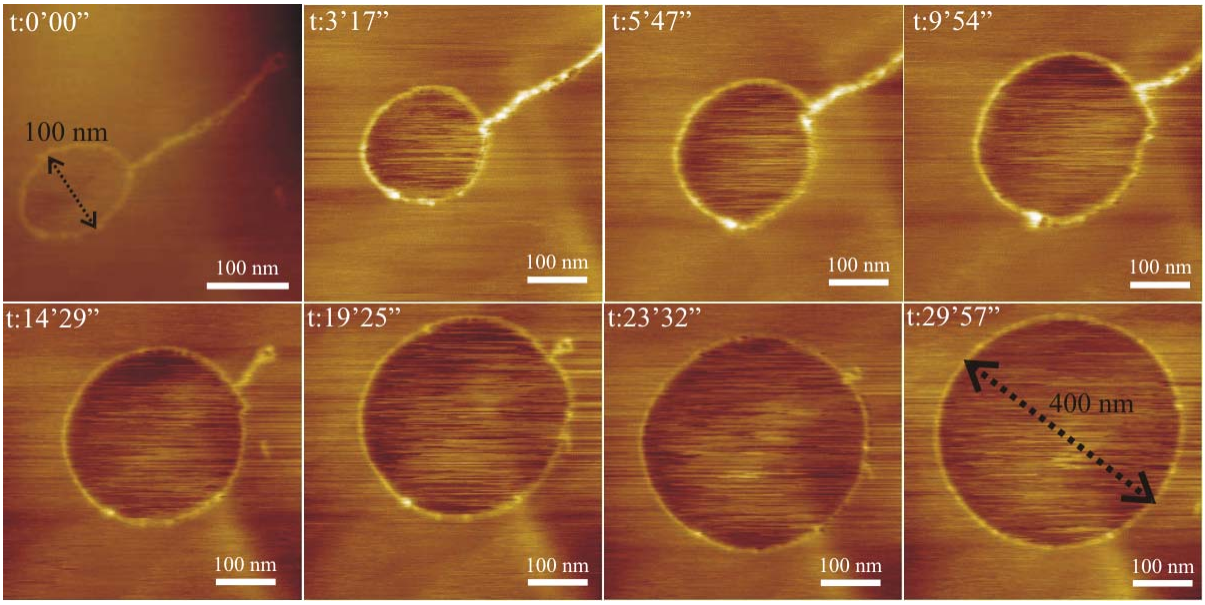

Figure 4.55: Supercoiled plasmid DNA gradually unravelled on $C_6H_{13}NH_2$ coated HOPG by the blowing effect.

Based on the success of unravelling supercoiling another challenging problem was tackled: splitting the double helix of DNA. Fig. 4.45 has illustrated the difficulty of SFM tip manipulation to split further the open duplex. While the homogenous 2-D surface pressure can

unfold the supercoils as sketched in Fig 4.56, the same strategy may be imagined to be applied to split ds-DNA. It was noticed that a free end seems important for the rotation of supercoiling. Fig. 4.56 step (A) indicates that cutting ds-DNA may be necessary to rotate the helical double strands.

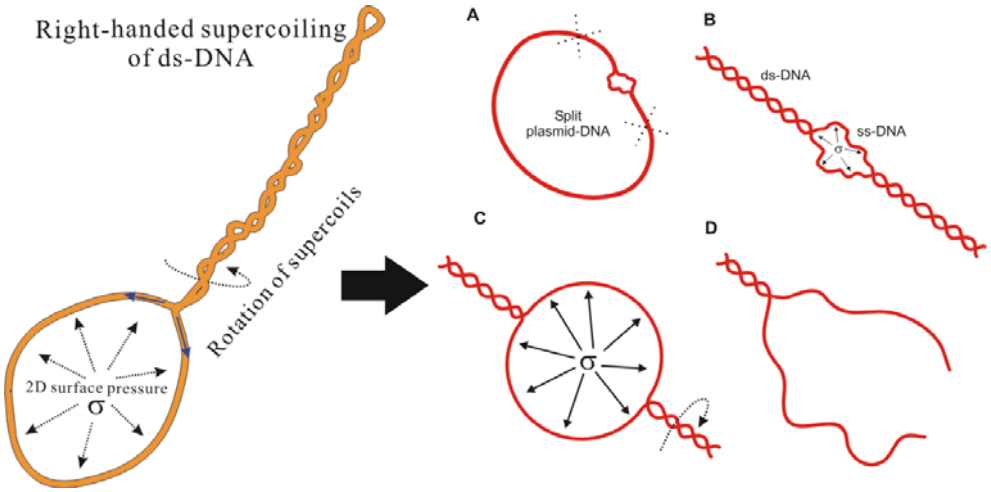

Figure 4.56: Schematic drawings of unravelling supercoiled DNA and a proposed strategy used to split double helices of DNA

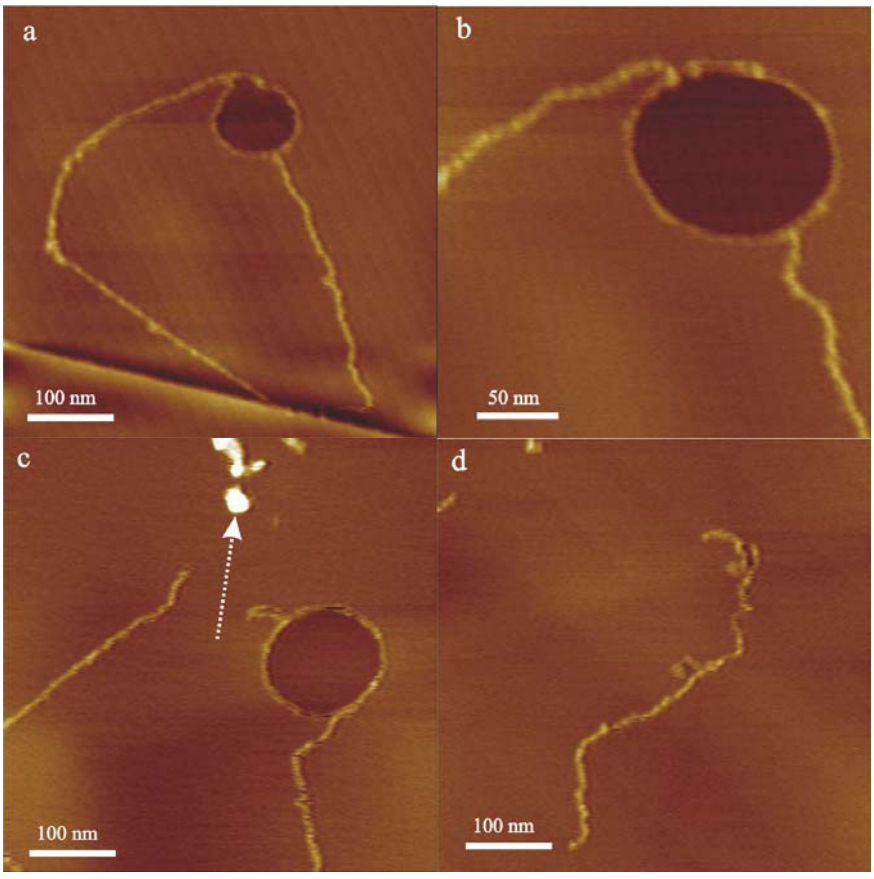

Figure 4.57: SFM tapping mode images of a split ds-DNA manipulated by blowing effect and SFM tip (white arrow shows the trace). The single strand of DNA finally ruptured due to too large surface pressure

Fig. 4.57 shows an attempt to apply the strategy to open a double helix. When a ds-DNA molecule was split on a $C_6H_{13}NH_2$ submonolayer (1000 mg/L) coated HOPG, a drop of n-hexane as blowing solvent was spin-coated onto the surface. Using SFM tip manipulation one end of a blown loop was cut as shown in (c). However, too large surface pressure produced by the blowing effect finally broke the single strand of DNA, which resists much smaller rupture forces than ds-DNA [196]. In future work, upon varying the blowing solvent and the scan parameters it may be possible to generate a moderate blowing effect, which does not impair the single strand of DNA at all. I is believed that the strategy combining the blowing effect with SFM tip manipulation will allow to unfold complex duplex superstructures on surfaces.

4.4.2.4 Stretching coiled block copolymers

Block copolymers are attractive materials due to their variable and predictable morphologies and broad range of applications in the field of nanostructured materials [212]. Compared to homopolymers, however, it is difficult to investigate the morphology of single block polymers on surfaces. Namely it is hard to distinguish different blocks in the copolymer on the surface due to different chemical structures; therefore, the properties of different blocks such as molecular weight and the interaction with the surface become less predictable. In order to distinguish different blocks in a single block copolymer chain [3,213] or in a copolymer thin film [213,214], the key is to control the conformations of the different blocks on the surface.

Recently a novel class of linear block copolymers containing DNA as a biological segment has recently been introduced [215]. These DNA–polymer hybrid materials formally represent polyelectrolyte block copolymers, the organic segment of which was chosen either to be hydrophobic or hydrophilic. When polyethylene glycol (PEG) is chosen as the organic component, PEG can function as an enhancer in a polymerase chain reaction (PCR), thereby triblock copolymers dsDNA-*b*-PEG-*b*-dsDNA or even pentablock PEG-dsDNA-*b*-PEG-*b*-dsDNA-PEG copolymers exhibiting nucleic acid units with lengths of 167, 225 and 500 base pairs (bps) can be synthesized [216] as illustrated in Fig. 4.58. Due to very different chemical structures between ds-DNA and PEG, it was attempted to determine some physical properties of these block copolymers, e.g. nanomechanical properties or the molecular weight of the PEG block, on the surface with the help of SFM manipulation.

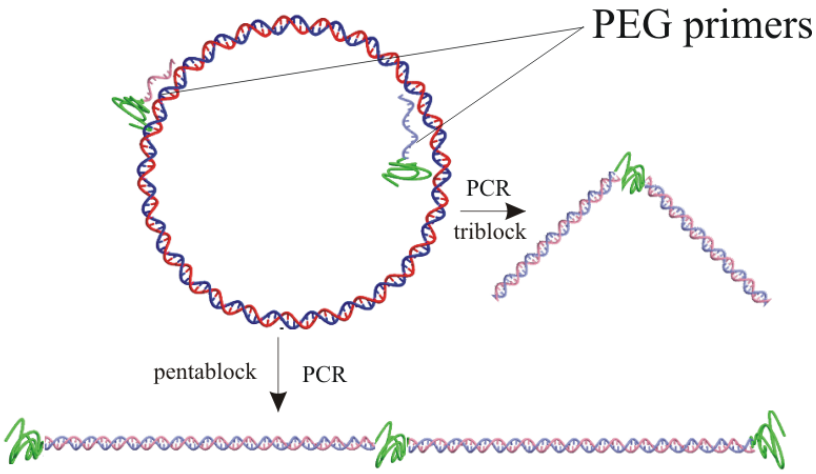

Figure 4.58: Schematic representation of the build-up of DNA triblock- and DNA pentablock copolymers upon using PCR.

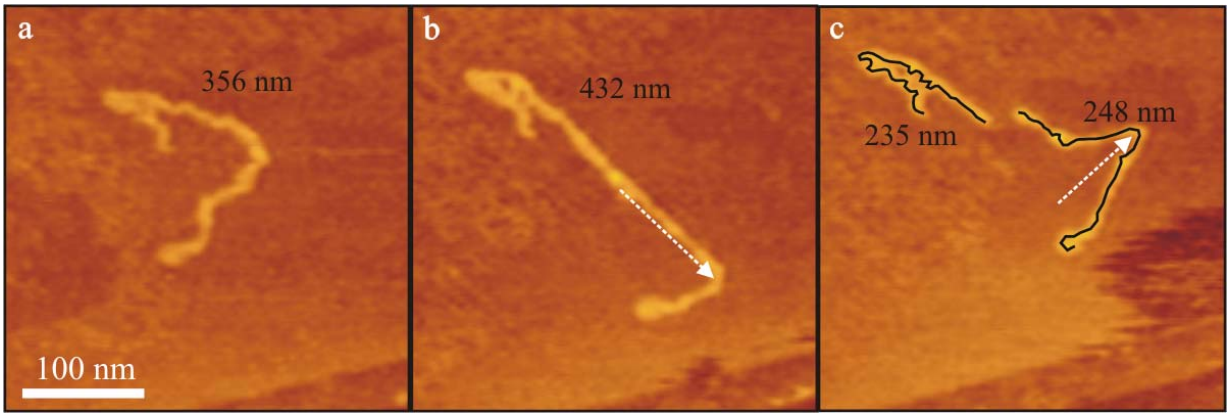

Figure 4.59: Tapping mode SFM topographical images of a DNA (500 bp)-*b*-PEG-*b*-DNA (500 bp) triblock copolymer on $C_{12}H_{25}NH_2$ pre-coated HOPG before (a) and after (b and c) manipulation. White dotted arrows in (b) and (c) indicate the moving traces of SFM tip during manipulation in contact mode. The black solid lines in (c) following the triblock contours were used to calculate the contour lengths.

In order to investigate their nanomechanical properties single block copolymers were manipulated by the SFM tip. Fig. 4.59 (a) displays a tapping mode SFM image of a triblock copolymer with two nucleic acid blocks of 500 bps connected by the PEG unit (~2000 g/mol). It has a measured contour length of 356 nm, in which 2 x 500 bps B-form ds-DNA contribute 340 nm length and 2000 g/mol PEG contributes about 16 nm length. The sample was deposited on an HOPG surface pre-coated with a sub-monolayer of dodecylamine ($C_{12}H_{25}NH_2$, from 300 mg/L chloroform solution), and SFM tip manipulation was carried out. As shown in Fig. 4.59 (b), the triblock copolymer was elongated to 432 nm after dragging by the SFM tip along the moving trace marked with a dotted arrow. Fig. 4.59 (c) shows the resulting structures after dragging the triblock copolymer in the direction perpendicular to its stretching axis. As a consequence the hybrid was broken due to a pulling force larger than ~1500 pN, as estimated

from the frictional force of ds-DNA on HOPG [217]. From several of these experiments and careful contour length measurements it became apparent that the breaking point was located at the center of the triblock rather than at the tip-molecule contact point. The total length of two broken pieces amounts to 483 nm, which means that compared to the original length of 356 nm the triblock copolymer was 1.4 times elongated upon dragging across the surface, if the small contribution in length of PEG was neglected.

The elongation of the single triblock molecule reveals the unique mechanical properties of ds-DNA, i.e. B-form ds-DNA can be overstretched to the S-form by a factor of 1.7 in solution [28] or 2 times on a surface [26]. In the tip manipulation experiment it is noticed that both ends of the triblock was almost immobilized on the surface. The final elongation of the triblock chain of 1.4 times is therefore the average elongation of different pieces along the whole chain. On the other hand, the manipulation of ds-DNA by the SFM tip has shown that the maximum force acting on the molecule is at the position where the SFM tip contacts the molecular chain [217]. Interestingly, the scission of the triblock does not occur at the position loaded by the maximum force but almost at the center region of the triblock. It is consistent with the fact that ss-DNA has a much smaller Young's modulus than ds-DNA under the same force loading conditions [28]. SFM cantilever pulling experiments have also proven that the covalent bond in polysaccharides can be ruptured at about 1000 pN [211] while ds-DNA remains unbroken at the same force. Similarly, in the horizontal manipulation of triblock molecules the single PEG backbone breaks at a lower force (about 1500 pN at 100 nm/s horizontal pulling velocity) than ds-DNA, which is consistent with a much stronger break force of the latter.

However, as displayed in Fig. 4.59 (a-c), the PEG polymer incorporated in the middle of the triblock cannot be distinguished from ds-DNA. This can be attributed to the fact that the polymer may relax into a densely packed globule after manipulation and before imaging, due to restoring forces on the one hand and low surface friction on the other. For the case of the short and flexible PEG block without specific interactions with the dodecylamine coated HOPG surface, assuming a bulk density of PEG of 1.2 g/cm^3, the 2000 g/mol PEG block (average MW of commercial product) may condense into a cylinder with 2 nm diameter (same as ds DNA) and only 1 nm length, which is so small that it cannot be distinguished from the ds-DNA in the SFM images.

In order to distinguish different blocks in a single copolymer chain, the key is to control the conformations of the different blocks on the surface, which in the present case for single

molecule imaging is limited by the compact PEG globule. However, this limit has been overcome by SFM imaging after the blowing manipulation, in which the PEG moiety could be distinguished from ds-DNA by SFM (Fig. 4.60 a). In this experiment a thin film of chloroform was spin-coated on the same surface, in order to generate a surface pressure inside a topological crossover triblock loop by a tapping SFM tip, which can stretch and overstretch the triblock chain, and even stabilize the overstretched chain. Fig. 4.60 (a) displays a blown triblock hybrid loop, where a thin polymer chain with about 18 nm length bridges two thick chains aside. The length of the thin part corresponds to the stretched contour length of the PEG exhibiting about 48 repeat units (3.77 Å per PEG repeat unit) and about 2110 g/mol molecular weight. Fig. 4.60 (b) shows a raw height profile of the down part of the blown chain, indicating a clear height dip in the middle. According to a height profile along the whole contour after correction for the background height, the thin chain part has an average apparent height of 0.46 ± 0.08 nm, while the two thick chain parts exhibit an average height of 0.80 ± 0.17 nm. Therefore the thin chain in the middle is attributed to the PEG block, and the thick chains aside to ds-DNA.

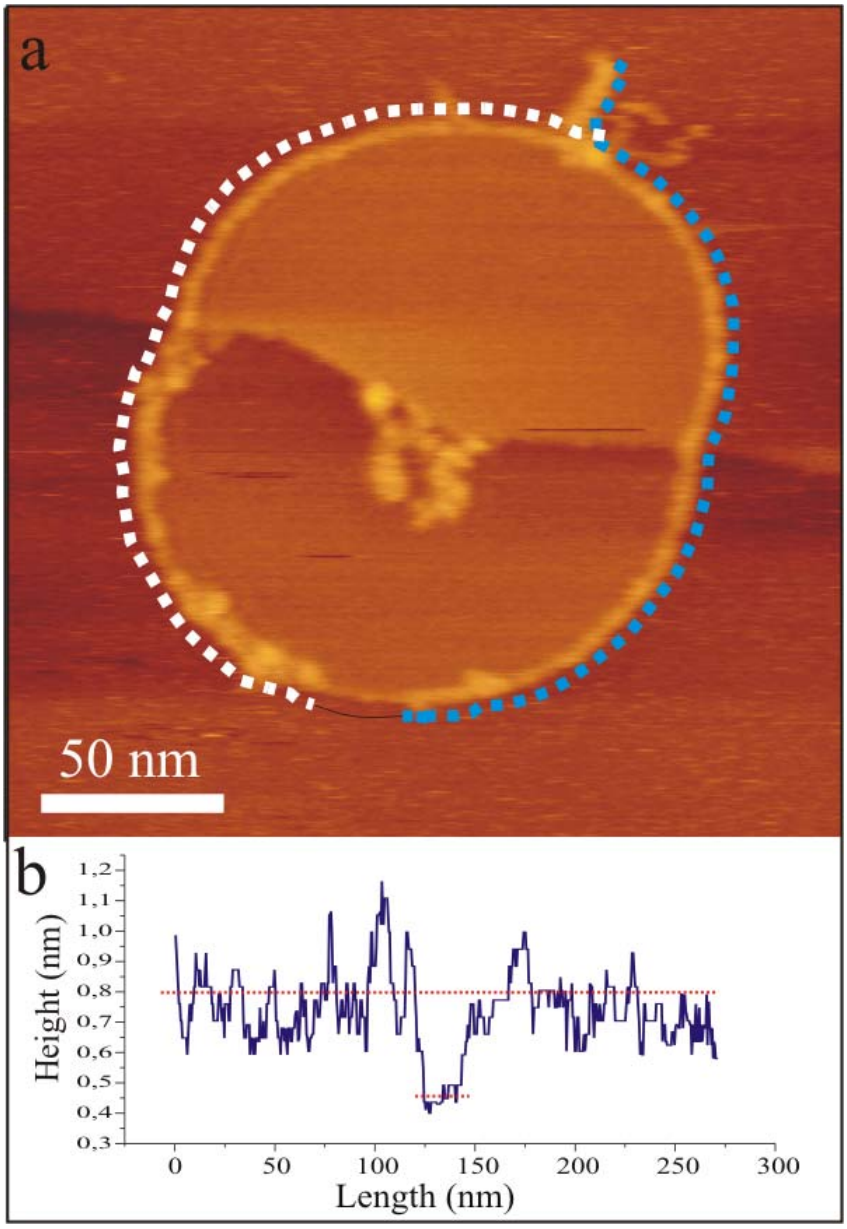

Figure 4.60: (a) Tapping mode SFM image of a DNA (500 bps)-*b*-PEG-*b*-DNA (500 bps) triblock molecule, which formed a topological crossover loop across a step edge of the HOPG surface covered by an ultrathin chloroform layer, and which had been blown by the tapping SFM tip. The white and blue dotted lines sketch the contours of the two ds DNA blocks while the black solid line sketches the PEG contour. The unidentified material inside the loop is attributed to impurities deposited from the solution. (b) A raw height profile of a contour covering the down part of the blown loop from the dotted white arrow to the solid white arrow indicated in (a). The contour recording was programmed to trace the largest height points along the chain in order to avoid manual drawing mistakes. The dotted and solid red lines in the height profile indicate the averaged heights of the whole thick ds-DNA contour and the thin PEG contour, respectively, after background height correction [218].

In summary, the SFM tip manipulation allows to investigate the nanomechanical properties of the triblock hybrids, which so far has only been demonstrated for neat DNA and dendronized polymers. The dragging-breaking experiments revealed that the single PEG backbone breaks at a force at which the ds-DNA backbones keep unbroken, thereby identifying the mechanical weak point of the DNA-polymer hybrids. The blowing effect was applied to blow circular

topologies, so that the ds-DNA and the organic polymer chain have been extended and the contours of the three blocks could thereby be imaged separately on the surface. To the best of our knowledge, this experiment afforded for the first time to visualize the three blocks of a single linear triblock copolymer chain with recognizable contours by SFM. In future work these two manipulation methods together may be employed to investigate circular polymers closed by various bonds, including multivalent coordination bonds.

4.4.2.5 Calculations of rupture force of ds-DNA

To understand the rupture process of ds-DNA under applied force is of fundamental importance in biology and single molecular mechanics [38]. However the single molecule manipulation techniques, which can stretch and break single polymer chains, such as pulling with an SFM cantilever, microneedles, or optical tweezers have failed to measure the rupture force of ds-DNA. The reason is the fact that the attachment between ds-DNA and micro force transducers have been broken prior to the rupture of ds-DNA chain.

By applying the blowing effect to plasmid ds-DNA, manipulation and imaging can be performed simultaneously; the different conformations of ds-DNA under tension such as stretched, overstretched and eventually ruptured chains can be imaged. However the main problem of the blowing effect is that one cannot directly measure the force applied to the DNA chain.

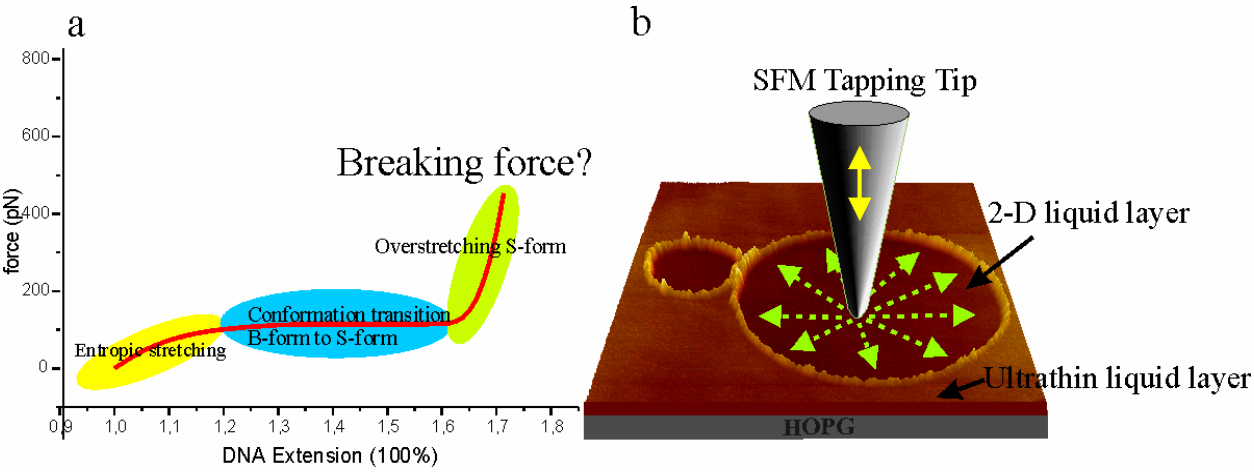

Figure 4.61: (a) A typical stress-strain dependence of ds-DNA measured in solution [29]; (b) 3-D SFM image and illustration of a blown circular ds-DNA with rings due to self-crossing ds-DNA. An SFM tip tapping on a quasi 2-D liquid layer pushes the liquid molecules along the surface and creates a pressure difference, which causes a radial force to stretch the circle.

How to solve this problem? The answer is the unique mechanical properties of ds-DNA under tension (Fig. 4.61 a). It is well known that by a pulling force around 110 pN, unnicked ds-DNA will undergo a structural transition i.e. a transition from B-form to S-form DNA [29]. Such a characteristic structural transition can be monitored by SFM imaging, i.e. the contour length of blown circles can be measured. When monodisperse plasmid DNA molecules are deposited on $C_{12}H_{25}NH_2$ submonolayer precoated HOPG, they often form self-crossing loops with different sizes on the surface, as shown for example in Fig. 4.61 (b). When these loops are blown to circles, they should be either in B-from (left side of the force plateau) or in S-form (right side of the force plateau). If the ds-DNA on the surface is assumed to have the same stress-strain dependence as in solution, it is possible to calculate the rupture force of ds-DNA from the blowing experiment.

In the blowing effect, the thinner layer with high pressure inside the loop and the thicker layer with lower pressure outside the loop result in a surface pressure difference, $\Delta\sigma$, which causes a radial force and consequently a tangential force along the polymer, which amounts to F_t. If the frictional force associated with the motion across the surface is not too large, then $\Delta\sigma$ is constant during blowing; the tangential force acting on each loop thus can be calculated from $\Delta\sigma$, i.e. $F_t = \Delta\sigma * L / 2\pi$, where L is contour length of a blown loop. The force exerted on a loop is therefore proportional to its contour length, which can be measured in SFM images. Assuming that the stress-strain dependence $\Psi(F)$ for the ds-DNA molecule on the surface is the same as that in solution, one may estimate $\Delta\sigma$. For example, the multiply twisted ds-DNA molecules on the surface (Fig. 4.62) with a known total length $L_b = 913$ nm in the B-form, under certain tangential force will be overstretched according to the stress-strain dependence, i.e. $\Psi(F_t) = L_i / L_{ib}$, (L_i is the length of the blown loop i in a molecule, L_{ib} is the length of the loop i in B-form). Since each topologically formed loop in a DNA molecule is blown independently, it is just needed to estimate one $\Delta\sigma$ for the whole surface, and then calculate each F_t for each blown loop. With known F_t one may can look up the stress-strain dependence $\Psi(F)$ to find the relative extension L_i/L_{ib}; thus L_{ib} can be obtained. Finally if $\Sigma L_{ib} = L_b$ is 913 ± 90 nm, one may accept the estimated $\Delta\sigma$. Fig. 4.62 displays one example of the several multiply twisted and broken ds-DNA molecules on the surface after the blowing. By estimating $\Delta\sigma = 2\pi/2.4$, one may calculate L_{ib} for each circle in B-form as shown in Tab. 4.7. Therefore the loop in chain 4 was broken under a force around 700 pN. The highest $\Delta\sigma$ which we was detected so far due to the strong blowing effect was 6 mN/m. 2686 base pairs ds-DNA single molecular circles were observed to overstretch up to 2 times of their B-form length, before they break at a value

of $\Delta\sigma$ around 1.7 mN/m. The minimum force to rupture ds-DNA is thus estimated as 500 ± 100 pN [219].

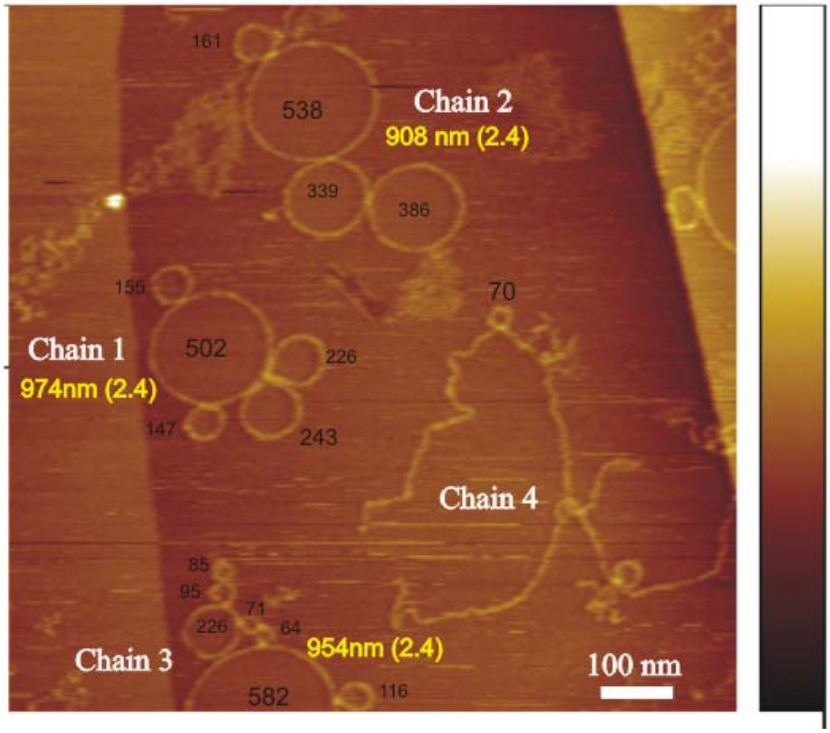

Figure 4.62: SFM image of several blown multiply twisted and broken ds-DNA molecules on the surface after blowing. The contour length of each circle (black) and the calculated L_b (yellow) are indicated.

Table 4.7: Calculation of L_{bi} according to length data acquired from Fig. 4.62 after estimating Δσ.

Chain 1	***L_i (nm)***	***F_t(pN)***	***Relative Extension***	***L_{bi} (nm)***
$2\pi/\Delta\sigma = 2.4$	155	65	1,085	143
	147	61	1,079	136
	243	101	1,207	201
	226	94,	1,164	194
	502	209	1,672	300
				L_b
				974
Chain 2	***L_i (nm)***	***F_t(pN)***	***Relative Extension***	***L_{bi} (nm)***
$2\pi/\Delta\sigma = 2.4$	161	67	1,089	148
	339	141	1,645	206
	386	161	1,655	233,2
	538	224	1,675	321
				L_b
				908
Chain 3	***L_i (nm)***	***F_t(pN)***	***Relative Extension***	***L_{bi} (nm)***
$2\pi/\Delta\sigma = 2.4$	476	198	1,669	285
	235	98	1,184	199
	221	92	1,155	191
	146	61	1,077	137
	147	61	1,079	136
				L_b
				947
Chain 4	***L_i (nm)***	***F_t(pN)***	***Relative Extension***	***L_{bi} (nm)***
$2\pi/\Delta\sigma = 2.4$	70	21	1,024	68
				845

The rupture force which was estimated here is much smaller than the value measured by SFM cantilever pulling or optical trap experiments [24,38], but it is close to the strength predicted by molecular combing [26]. It is known that the chemical bond strength varies when the force loading rate is changed [39]. Therefore the rupture event at a finite temperature thus is a function of force and force loading time. In future work by controlling the blowing speed one may apply a dynamic force load and a static force load together to study the time-dependent mechanical properties of ds-DNA.

4.4.3 Conclusions of stretching and splitting single polymer chains by SFM manipulation

It has been demonstrated that single polymer molecules on an appropriate surface can be manipulated with an SFM tip in contact mode. The force exerted by the motion of the SFM tip is a point force, i.e. it is heterogeneous. On the other hand it has been shown how to create ultrathin liquid films on surfaces. A pressure created by an SFM tip in an ultrathin liquid film allows to exert a homogeneous force on a single macromolecular ring. This so called “blowing effect” provides a new tool for fabricating macromolecular nanostructures, unravelling polymer superstructures, and allowing further investigations of the mechanical properties of ds-DNA and other synthetic and biologically relevant macromolecules and their complexes. For ds-DNA overstretching to 2.0 times of its B-form length has been observed, followed by the rupture of the molecules. Since the surfaces can be activated by many different organic liquids, the blowing effect is a quite general phenomenon.

5 Conclusions and Perspectives

In this thesis polymeric nanostructures from highly attractive, functional synthetic and biological macromolecules have been investigated at interfaces, employing SFM techniques that on the one hand allow their visualization, and on the other hand provide means for *in-situ* manipulation. In order to effectively control the nanostructures at surfaces, interfaces, and in thin films, different self-assembly strategies have been applied for different polymer molecules. From high resolution SFM images, molecular level nanostructures of P3HT thin films, and highly charged single dendronized polymers and DNA-amphiphile complexes could be derived. With SFM manipulations including a newly developed SFM blowing technique, the nanostructure and the mechanical properties of single plasmid ds-DNA as well as of DNA-PEG copolymers were determined.

First, the effect of molecular weight was investigated on nanostructures within self-assembled thin films of P3HT. Self-assembly of solution-processed, conjugated polymers results typically in complex nanostructured thin films, in which ordered crystalline domains are embedded in an amorphous matrix. Fractionation of polydispersed P3HT was used to control the thin film morphology. In the thin films from the lowest molecular weight fraction only polymers with lengths of 20-30 repeat units could self-assemble into highly ordered nanoribbons. They were embedded in an amorphous matrix that causes the lowest charge carrier mobilities in these materials. On the other side, in the thin films from the highest molecular weight fraction, long polymer chains form large domains with partially ordered crystallites throughout the whole film. Therefore the overall degree of crystalline domains in the film is much higher, and consequently the charge mobilities in thin film OFETs exhibit also the highest numbers among all the samples. It is concluded that the charge carrier mobility is strongly depending on the uniform conformation of the polymer backbones rather than a grain boundary effect. In the future, varying parameters during the self-assembly of the thin films, like the solvent and the temperature may allow to produce highly ordered crystalline thin films with higher conjugated backbone lengths, thus leading to even higher charge carrier mobilities of thin film OFETs.

Second, nanostructures of single dendronized polymers were investigated. SFM allowed to determine for the first time branching within these polymer chains. It occurs in the present systems at a concentration of approximately 1% only. Presently there is no other method

available with this kind of sensitivity and the potential for positional identification of both the branching site and the lengths of the branches. Another particularly interestingly discovery was made upon varying the electrical charge of dendronized polymers. Individual linear objects formed by polymers with charged second and third generation dendritic side chains exhibit self-folding into duplexes, i.e. supramolecular nanostructures, presumably driven by the preferred interaction of the dendritic side chains with the polar solvent. Though this duplex formation is naturally less specific than that of, e.g., DNA, it indicates a concrete and rather robust level of structural hierarchy which constitutes an important step on the way to create more complex and yet still ordered supramolecular structures. Further experiments such as on the self-assembly of an anionic dendronized polymer with cationic polyelectrolytes at the single molecular level should help not only to further investigate the underlying principles that control the generation of 3D matter from individual nano-sized molecular objects, but also extend the polymers' use for the construction of predetermined hierarchical architectures.

Besides the synthetic chemical dendronization a physico-chemical approach was applied to control the formation of single polymeric nanostructures at a surface. It was demonstrated that the conformation of plasmid ds-DNA can be controlled by the adsorption to a molecularly modified graphite surface from supercoiling, through open circles with duplex splits, to spontaneously overstretching up to 1.5 times of the B-form length. The control is achieved through the submonolayer density of octadecylamine on HOPG, which allows for the formation of DNA-octadecylamine complexes. Upon using a shorter chain analogue it is possible to control the length of splits of plasmid ds-DNA. Thus, long chain alkylamine coated HOPG provides a powerful "workbench" for single macromolecules, which allows to exert well defined forces covering a large range from pico- to nano-newtons, thereby allowing to fabricate highly interesting molecular architectures from single macromolecules, and moreover to probe their mechanical properties. In the future, splitting ss-DNA from ds-DNA and stretching ss-DNA on this workbench may be employed for direct decoding of DNA sequences if ultrahigh-resolution methods such as STM or Tip Enhanced Raman Spectroscopy can be combined with the workbench.

Finally a physical approach: SFM manipulation was directly applied to control single molecule nanostructures at surfaces. It was demonstrated that single polymer molecules on the appropriate surface can be manipulated by the SFM tip in contact mode. The force

exerted by the motion of the SFM tip can provide a strong heterogeneous point force. On the other hand, a new SFM manipulation method, the so called “SFM blowing” technique was developed. It was demonstrated that an ultrathin liquid film on a graphite surface allows to create a substantial surface pressure with a tapping SFM tip. This has been used to exert a homogeneous force on a single macromolecular ring. The blowing effect provides a new tool for fabricating macromolecular nanostructures, or for unravelling polymeric superstructures. For instance, the experiment afforded for the first time to visualize the three blocks of a single linear triblock copolymer chain with recognizable contours. Further investigations allowed to determine mechanical properties of ds-DNA and other synthetic and biologically relevant macromolecules and their complexes. It was the first time that overstretching of 2.0 times of ds-DNA B-form length followed by the rupture of the molecules could be visualized *in-situ* by SFM. The minimum force to rupture ds-DNA was thus estimated as 500 ± 100 pN. Since the surfaces can be activated by many different organic liquids, the blowing effect revealed a general physical phenomenon. In the future, SFM tip manipulation and the SFM blowing technique may be employed to investigate the mechanical properties of other chemical bonds, for example coordination bonds which close polymer circles. Moreover, the complete split of ds-DNA appears viable.

Bibliography

[1] Binnig, G.; Rohrer, H.; Gerber, C. und Weibel, E. (1982): Surface Studies by Scanning Tunneling Microscopy, Physical Review Letters 49 [1], pp. 57-61.

[2] Binnig, G.; Quate, C. und Gerber, C. (1986): Atomic Force Microscope, Physical Review Letters 56, pp. 930.

[3] Sheiko, S. S. und Möller, M. (2001): Visualization of macromolecules - A first step to manipulation and controlled response, Chemical Reviews 101 [12], pp. 4099-4123.

[4] Bustamante, C.; Marko, J. F.; Seggia, E. D. und Smith, S. B. (1994): Entropic elasticity of lambda-phage DNA, Science 265, pp. 1599.

[5] Bustamante, C. und Keller, D. (1995): Scanning Force Microscopy in Biology, Physics Today 48 [12], pp. 32-38.

[6] Hansma, H. G.; Vesenka, J.; Siegerist, C.; Kelderman, G.; Morrett, H.; Sinsheimer, R. L.; Elings, V.; Bustamante, C. und Hansma, P. K. (1992): Reproducible Imaging and Dissection of Plasmid Dna Under Liquid with the Atomic Force Microscope, Science 256 [5060], pp. 1180-1184.

[7] Zen, A.; Pflaum, J.; Hirschmann, S.; Zhuang, W.; Jaiser, F.; Asawapirom, U.; Rabe, J. P.; Scherf, U. und Neher, D. (2004): Effect of molecular weight and annealing of poly (3-hexylthiophene)s on the performance of organic field-effect transistors, Advanced Functional Materials 14 [8], pp. 757-764.

[8] Zen, A.; Saphiannikova, M.; Neher, D.; Grenzer, J.; Grigorian, S.; Pietsch, U.; Asawapirom, U.; Janietz, S.; Scherf, U.; Lieberwirth, I. und Wegner, G. (2006): Effect of molecular weight on the structure and crystallinity of poly(3-hexylthiophene), Macromolecules 39 [6], pp. 2162-2171.

[9] Samori, B.; Nigro, C.; Armentano, V.; Cimieri, S.; Zuccheri, G. und Quagliariello, C. (1993): Dna Supercoiling Imaged in 3 Dimensions by Scanning Force Microscopy, Angewandte Chemie-International Edition in English 32 [10], pp. 1461-1463.

[10] Samori, P.; Ecker, C.; Gössl, I.; de Witte, P. A. J.; Cornelissen, J. J. L. M.; Metselaar, G. A.; Otten, M. B. J.; Rowan, A. E.; Nolte, R. J. M. und Rabe, J. P. (2002): High shape persistence in single polymer chains rigidified with lateral hydrogen bonded networks, Macromolecules 35 [13], pp. 5290-5294.

[11] Zhuang, W.; Ecker, C.; Metselaar, G. A.; Rowan, A. E.; Nolte, R. J. M.; Samori, P. und Rabe, J. P. (2005): SFM characterization of poly(isocyanodipeptide) single polymer chains in controlled environments: Effect of tip adhesion and chain swelling., Macromolecules 38 [2], pp. 473-480.

[12] Samori, P.; Francke, V.; Müllen, K. und Rabe, J. P. (1999): Self-assembly of a conjugated polymer: from molecular rods to a nanoribbon architecture with molecular dimensions, Chemistry-A European Journal 5 [8], pp. 2312-2317.

[13] Shu, L. J.; Schlüter, A. D.; Ecker, C.; Severin, N. und Rabe, J. P. (2001): Extremely long dendronized polymers: Synthesis, quantification of structure perfection, individualization, and SFM manipulation, Angewandte Chemie-International Edition 40 [24], pp. 4666-+.

[14] Piner, R. D.; Zhu, J.; Xu, F.; Hong, S. H. und Mirkin, C. A. (1999): "Dip-pen" nanolithography, Science 283 [5402], pp. 661-663.

[15] Barner, J.; Mallwitz, F.; Shu, L. J.; Schlüter, A. D. und Rabe, J. P. (2003): Covalent connection of two individual polymer chains on a surface: An elementary step towards molecular nanoconstructions, Angewandte Chemie-International Edition 42 [17], pp. 1932-1935.

[16] Heeger, A. J. (2001): Semiconducting and metallic polymers: The fourth generation of polymeric materials (Nobel lecture), Angewandte Chemie-International Edition 40 [14], pp. 2591-2611.

[17] Kline, R. J.; McGehee, M. D.; Kadnikova, E. N.; Liu, J. S.; Frechet, J. M. J. und Toney, M. F. (2005): Dependence of regioregular poly(3-hexylthiophene) film morphology and field-effect mobility on molecular weight, Macromolecules 38 [8], pp. 3312-3319.

[18] Schlüter, A. D. und Rabe, J. P. (2000): Dendronized polymers: Synthesis, characterization, assembly at interfaces, and manipulation, Angewandte Chemie-International Edition 39 [5], pp. 864-883.

[19] Böttcher, C.; Schade, B.; Ecker, C.; Rabe, J. P.; Shu, L. J. und Schlüter, A. D. (2005): Double-helical ultrastructure of polycationic dendronized polymers determined by single-particle cryo-TEM, Chemistry-A European Journal 11 [10], pp. 2923-2928.

[20] Rabe, J. P.; Rabolt, J. F.; Brown, C. A. und Swalen, J. D. (1985): Polymerization of 2 Unsaturated Fatty-Acid Esters in Langmuir-Blodgett-Films As Studied by Ir Spectroscopy, Thin Solid Films 133 [1-4], pp. 153-159.

[21] Rabe, J. P. und Buchholz, S. (1991): Commensurability and Mobility in 2-Dimensional Molecular-Patterns on Graphite, Science 253 [5018], pp. 424-427.

[22] Severin, N.; Barner, J.; Kalachev, A. A. und Rabe, J. P. (2004): Manipulation and overstretching of genes on solid substrates, Nano Letters 4 [4], pp. 577-579.

[23] Bustamante, C.; Macosko, J. C. und Wuite, G. J. L. (2000): Grabbing the cat by the tail: Manipulating molecules one by one, Nature Reviews Molecular Cell Biology 1 [2], pp. 130-136.

[24] Clausen-Schaumann, H.; Seitz, M.; Krautbauer, R. und Gaub, H. E. (2000): Force spectroscopy with single bio-molecules, Current Opinion in Chemical Biology 4 [5], pp. 524-530.

[25] Bensimon, A.; Simon, A.; Chiffaudel, A.; Croquette, V.; Heslot, F. und Bensimon, D. (1994): Alignment and Sensitive Detection of Dna by A Moving Interface, Science 265 [5181], pp. 2096-2098.

[26] Bensimon, D.; Simon, A. J.; Croquette, V. und Bensimon, A. (1995): Stretching Dna with A Receding Meniscus - Experiments and Models, Physical Review Letters 74 [23], pp. 4754-4757.

[27] Smith, D. P. E.; Bryant, A.; Quate, C. F.; Rabe, J. P.; Gerber, C. und Swalen, J. D. (1987): Images of A Lipid Bilayer at Molecular Resolution by Scanning Tunneling Microscopy, Proceedings of the National Academy of Sciences of the United States of America 84 [4], pp. 969-972.

[28] Smith, S. B.; Cui, Y. J. und Bustamante, C. (1996): Overstretching B-DNA: The elastic response of individual double-stranded and single-stranded DNA molecules, Science 271 [5250], pp. 795-799.

[29] Leger, J. F.; Romano, G.; Sarkar, A.; Robert, J.; Bourdieu, L.; Chatenay, D. und Marko, J. F. (1999): Structural transitions of a twisted and stretched DNA molecule, Physical Review Letters 83 [5], pp. 1066-1069.

[30] Strick, T. R.; Allemand, J. F.; Bensimon, D.; Bensimon, A. und Croquette, V. (1996): The elasticity of a single supercoiled DNA molecule, Science 271 [5257], pp. 1835-1837.

[31] Avery, OT; MacLeod, CM und McCarty, M. (1944): Studies on the chemical nature of the substance including transformation of pneumococcal types, J.Exp.Med. 79, pp. 137.

[32] Watson, J. D. und Crick, F. H. C. (1953): A structure of deoxyribose nucleic acid, Nature 171, pp. 737-738.

[33] Bloomfield, V. A. (1996): DNA condensation, Current Opinion in Structural Biology 6, pp. 334.

[34] Saenger, W. (1984): *Principles of nucleic acid structure*., Springer Verlag, New York.

[35] de Gennes, P-G (1979): Scaling Concepts in Polymer Physics, Cornell University Press, Ithaca, New York.

[36] Rivetti, C.; Guthold, M. und Bustamante, C. (1996): Scanning force microscopy of DNA deposited onto mica: Equilibration versus kinetic trapping studied by statistical polymer chain analysis, Journal of Molecular Biology 264 [5], pp. 919-932.

[37] Tylor, W. H. und Hagerman, P. J. (1990): Application of the method of phage T4 DNA ligase-catalyzed ring-closure to the study of DNA structure. II. NaCldependence of DNA flexibility and helical repeat, Journal of Molecular Biology 212, pp. 363.

[38] Bustamante, C.; Smith, S. B.; Liphardt, J. und Smith, D. (2000): Single-molecule studies of DNA mechanics, Current Opinion in Structural Biology 10 [3], pp. 279-285.

[39] Strick, T. R.; Dessinges, M. N.; Charvin, G.; Dekker, N. H.; Allemand, J. F.; Bensimon, D. und Croquette, V. (2003): Stretching of macromolecules and proteins, Reports on Progress in Physics 66 [1], pp. 1-45.

[40] Wang, M. D.; Yin, H.; Landick, R.; Gelles, J. und Block, S. (1997): Stretching DNA with optical tweezers, Biophysical Journal 72, pp. 1335.

[41] Marko, J. F. (1998): DNA under high tension: Overstretching, undertwisting, and relaxation dynamics, Physical Review e 57 [2], pp. 2134-2149.

[42] Cluzel, P.; Lebrun, R.; Heller, C.; Lavery, R.; Viovy, J.-L.; Chatenay, D. und Caron, F. (1996): DNA: an extensible molecule, Science 271, pp. 792.

[43] Lebrun, R. und Lavery, R. (1996): Modelling extreme deformations of DNA, Nucleic Acids Research 24, pp. 2260.

[44] Allemand, J. F.; Bensimon, D.; Lavery, R. und Croquette, V. (1998): Stretched and overwound DNA form a Pauling-like structure with exposed bases, Proceedings of the National Academy of Sciences of the United States of America 95, pp. 14152.

[45] Luger, K und Mäder, A. W (1997): Crystal structure of the nucleosome core particle at 2.8Å resolution, Nature *389*, pp. 252.

[46] Boles, T. C.; White, J. H. und Cozzarelli, N. R. (1990): Structure of Plectonemically Supercoiled Dna, Journal of Molecular Biology 213 [4], pp. 931-951.

[47] White, J. (1969): Self linking and the Gauss integral in higher dimensions, Am.J.Math. 91, pp. 693.

[48] Weil, R. und Vinograd, J. (1963): The cyclic coil helix and cyclic forms of polyoma viral DNA , Proceedings of the National Academy of Sciences of the United States of America 50, pp. 730.

[49] Kornberg, A. und Baker, T. (1992): DNA Replication, Freeman, San Francisco.

[50] Jenkins, A. D.; Kratochvil, P; Stepto, R. F. T. und Suter, U. W. (1996): Glossary of basic terms in polymer science, Pure and Applied Chemistry 68, pp. 2287.

[51] Frechet, J. M. J. und Tomalia, D. A. (2002): Dendrimers and other dendritic polymers, Wiley, New York.

[52] Frechet, J. M. J. (2003): Dendrimers and other dendritic macromolecules: from building blocks to functional assemblies in nanoscience and nanotechnology., J Polym Sci Part A: PolymChem 41, pp. 3713.

[53] Schlüter, A. D. (1998): Dendrimers with polymeric core: towards nanocylinders, Topics Curr.Chem. 197, pp. 165.

[54] Frauenrath, H. (2005): Dendronized polymers - building a new bridge from molecules to nanoscopic objects, Progress in Polymer Science 30, pp. 325.

[55] Zhang, A. F.; Shu, L. J.; Bo, Z. S. und Schlüter, A. D. (2003): Dendronized polymers: Recent progress in synthesis, Macromolecular Chemistry and Physics 204 [2], pp. 328-339.

[56] Percec, V.; Ahn, C. H.; Bera, T. K.; Ungar, G. und Yeardley, D. J. P. (1999): Coassembly of a hexagonal columnar liquid crystalline superlattice form polymer(s) coated with a three-cylinderical bundle supramolcular dendrimer, Chemistry-A European Journal 5, pp. 1070.

[57] Bo, Z. S.; Rabe, J. P. und Schlüter, A. D. (1999): A poly(para-phenylene) with hydrophobic and hydrophilic dendrons: Prototype of an amphiphilic cylinder with the potential to segregate lengthwise, Angewandte Chemie-International Edition 38 [16], pp. 2370-2372.

[58] Suijkerbuijk, B. M. J. M.; Shu, L. J.; Gebbink, R. J. M. K.; Schlüter, A. D. und van Koten, G. (2003): Single-site catalysts on cylinderical dendronized polymer support beyond nanosize, Organometallics 22, pp. 4175.

[59] Albrecht, M. und van Koten, G. (2001): Platinum group organometallics based on "pincer" complexes: Sensors, switches, and catalysts., Angewandte Chemie-International Edition 40, pp. 3750.

[60] Lehn, J. M. (1988): Supramolecular Chemistry - Scope and Perspectives Molecules, Supermolecules, and Molecular Devices, Angewandte Chemie-International Edition in English 27 [1], pp. 89-112.

[61] Gianni, S.; Guydosh, N. R.; Khan, F.; Caldas, T. D.; Mayor, U.; White, G. W. N.; DeMarco, M. L.; Daggett, V. und Fersht, A. R. (2003): Unifying features in protein-folding mechanisms, Proceedings of the National Academy of Sciences of the United States of America 100 [23], pp. 13286-13291.

[62] Lehn, J. M. (1995): Supramolecular Chemistry: Concepts and Perspectives, VCH, Weinheim, Germany.

[63] Lehn, J. M. (1990): Perspectives in Supramolecular Chemistry - from Molecular Recognition Towards Molecular Information-Processing and Self-Organization, Angewandte Chemie-International Edition in English 29 [11], pp. 1304-1319.

[64] Nakano, T. und Okamoto, Y. (2001): Synthetic helical polymers: Conformation and Function, Chemical Reviews 101 [12], pp. 4013.

[65] Chen, J. T.; Thomas, E. L.; Ober, C. K. und Mao, G. P. (1996): Self-Assembled Smectic Phases in Rod-Coil Block Copolymers, Science 273, pp. 343.

[66] Leclere, P.; Hennebicq, E.; Calderone, A.; Brocorens, P.; Grimsdale, A. C.; Müllen, K.; redas, J. L. und azzaroni, R. (2003): Supramolecular organization in block copolymers containing a conjugated segment: a joint AFM/molecular modeling study, Progress in Polymer Science 28, pp. 55.

[67] Surin, M.; Marsitzky, A.; Grimsdale, A. C.; Müllen, K.; Lazzaroni, R. und Leclere, P. (2004): Microscopic Morphology of Polyfluorene-Poly(ethylene oxide) Block Copolymers: Influence of the Block Ratio, Advanced Functional Materials 14, pp. 708.

[68] Cornelissen, J. J. L. M.; Rowan, A. E.; Nolte, R. J. M. und Sommerdijk, Najm (2001): Chiral architectures from macromolecular building blocks, Chemical Reviews 101 [12], pp. 4039-4070.

[69] Gössl, I.; Shu, L. J.; Schlüter, A. D. und Rabe, J. P. (2002): Molecular structure of single DNA complexes with positively charged dendronized polymers, Journal of the American Chemical Society 124 [24], pp. 6860-6865.

[70] Ikkala, O. und ten Brinke, G. (2002): Functional materials based on self-assembly of polymeric supramolecules, Science 295 [5564], pp. 2407-2409.

[71] Ikkala, O. und ten Brinke, G. (2004): Hierarchical self-assembly in polymeric complexes: Towards functional materials, Chemical Communications [19], pp. 2131-2137.

[72] Faul, C. F. J. und Antonietti, M. (2003): Ionic self-assembly: Facile synthesis of supramolecular materials, Advanced Materials 15 [9], pp. 673-683.

[73] Zhou, S. Q. und Chu, B. (2000): Assembled materials: Polyelectrolyte-surfactant complexes, Advanced Materials 12 [8], pp. 545-556.

[74] Antonietti, M.; Conrad, J. und Thünemann, A. (1994): Polyelectrolyte-Surfactant Complexes - A New-Type of Solid, Mesomorphous Material, Macromolecules 27 [21], pp. 6007-6011.

[75] Antonietti, M. und Thünemann, A. (1996): Polyelectrolyte-lipid complexes as membrane mimetic systems, Current Opinion in Colloid & Interface Science 1 [5], pp. 667-671.

[76] Ober, C. K. und Wegner, G. (1997): Polyelectrolyte-surfactant complexes in the solid state: Facile building blocks for self-organizing materials, Advanced Materials 9 [1], pp. 17-&.

[77] Lindman, B. und Thalberg, K. (1993): Interactions of Surfactants with Polymers adn Proteins, CRC Press, Boca Raton, FL.

[78] Wegner, G. und Rühe, J. (1989): The Structural Background of Charge-Carrier Motion in Conducting Polymers, Faraday Discussions 88, pp. 333-+.

[79] Radler, J. O.; Koltover, I.; Salditt, T. und Safinya, C. R. (1997): Structure of DNA-cationic liposome complexes: DNA intercalation in multilamellar membranes in distinct interhelical packing regimes, Science 275 [5301], pp. 810-814.

[80] Koltover, I.; Salditt, T.; Rädler, J. O. und Safinya, C. R. (1998): An inverted hexagonal phase of cationic liposome-DNA complexes related to DNA release and delivery, Science 281 [5373], pp. 78-81.

[81] Severin, N.; Rabe, J. P. und Kurth, D. G. (2004): Fully extended polyelectrolyte-amphiphile complexes adsorbed on graphite, Journal of the American Chemical Society 126 [12], pp. 3696-3697.

[82] Severin, N.; Sokolov, I. M.; Miyashita, N.; Kurth, D. G. und Rabe, J. P. (2007): Self-sorting of polyelectrolyte-amphiphile complexes on a graphite surface, Macromolecules 40 [14], pp. 5182-5186.

[83] Tseng, A. A. und Notargiacomo, A. (2005): Nanoscale fabrication by nonconventional approaches, Journal of Nanoscience and Nanotechnology 5 [5], pp. 683-702.

[84] Israelchvili, J. (1992): Intermolecular and Surface Forces, Academic Press, San Diego.

[85] Elings, V. und Gurley, J. (1993): U. S. Patent 5,266,801.

[86] Atkins, P. und de Paula, J. (2002): Physical Chemistry, Oxford University Press, New York.

[87] Strick, T.; Allemand, J. F.; Croquette, V. und Bensimon, D. (2000): Twisting and stretching single DNA molecules, Progress in Biophysics & Molecular Biology 74 [1-2], pp. 115-140.

[88] Chu, S. (1991): Laser Manipulation of Atoms and Particles, Science 253 [5022], pp. 861-866.

[89] Kishino, A. und Yanagida, T (1988): Force measurements by micromanipulation of a single actin filament by glassneedles., Nature 334 [6117], pp. 74-76.

[90] Rief, M.; Gautel, M.; Oesterhelt, F.; Fernandez, J. M. und Gaub, H. E. (1997): Reversible unfolding of individual titin immunoglobulin domains by AFM, Science 276 [5315], pp. 1109-1112.

[91] Rief, M.; Oesterhelt, F.; Heymann, B. und Gaub, H. E. (1997): Single molecule force spectroscopy on polysaccharides by atomic force microscopy, Science 275 [5304], pp. 1295-1297.

[92] Wuite, G. J. L.; Smith, S. B.; Young, M.; Keller, D. und Bustamante, C. (2000): Single-molecule studies of the effect of template tension on T7 DNA polymerase activity, Nature 404 [6773], pp. 103-106.

[93] Kitamura, K.; Tokunaga, M.; Iwane, A. H. und Yanagida, T. (1999): A single myosin head moves along an actin filament with regular steps of 5.3 nanometres, Nature 397 [6715], pp. 129-134.

[94] Smith, S. B.; Finzi, L. und Bustamante, C. (1992): Direct Mechanical Measurements of the Elasticity of Single Dna-Molecules by Using Magnetic Beads, Science 258 [5085], pp. 1122-1126.

[95] Strick, T.; Allemand, J. F.; Bensimon, D.; Lavery, R. und Croquette, V. (1999): Phase coexistence in a single DNA molecule, Physica A 263 [1-4], pp. 392-404.

[96] Strick, T. R.; Bensimon, D. und Croquette, V. (1999): Micro-mechanical measurement of the torsional modulus of DNA, Genetica 106 [1-2], pp. 57-62.

[97] Pauling, L. und Corey, R. B. (1953): A Proposed Structure for the Nucleic Acids, Proceedings of the National Academy of Sciences of the United States of America 39 [2], pp. 84-97.

[98] Rief, M.; Clausen-Schaumann, H. und Gaub, H. E. (1999): Sequence-dependent mechanics of single DNA molecules, Nature Structural Biology 6 [4], pp. 346-349.

[99] Clausen-Schaumann, H.; Rief, M.; Tolksdorf, C. und Gaub, H. E. (2000): Mechanical stability of single DNA molecules, Biophysical Journal 78 [4], pp. 1997-2007.

[100] EssevazRoulet, B.; Bockelmann, U. und Heslot, F. (1997): Mechanical separation of the complementary strands of DNA, Proceedings of the National Academy of Sciences of the United States of America 94 [22], pp. 11935-11940.

[101] Strunz, T.; Oroszlan, K.; Schäfer, R. und Güntherodt, H. J. (1999): Dynamic force spectroscopy of single DNA molecules, Proceedings of the National Academy of Sciences of the United States of America 96, pp. 11277.

[102] Maslova, M. V.; Gerasimova, L. G. und Forsling, W. (2004): Surface properties of cleaved mica, Colloid Journal 66 [3], pp. 322-328.

[103] Hooks, D. E.; Fritz, T. und Ward, M. D. (2001): Epitaxy and molecular organization on solid substrates, Advanced Materials 13 [4], pp. 227-+.

[104] Loewe, R. S.; Khersonsky, S. M. und McCullough, R. D. (1999): A simple method to prepare head-to-tail coupled, regioregular poly(3-alkylthiophenes) using grignard metathesis, Advanced Materials 11 [3], pp. 250-+.

[105] Trznadel, M.; Pron, A. und Zagorska, M. (1998): Effect of molecular weight on spectroscopic and spectroelectrochemical properties of regioregular poly(3-hexylthiophene), Macromolecules 31 [15], pp. 5051-5058.

[106] Kasemi, E.; Zhuang, W.; Rabe, J. P.; Fischer, K.; Schmidt, M.; Colussi, M.; Keul, H.; Yi, D.; Colfen, H. und Schlüter, A. D. (2006): Synthesis of an anionically chargeable, high-molar-mass, second-generation dendronized polymer and the observation of branching by scanning force microscopy, Journal of the American Chemical Society 128 [15], pp. 5091-5099.

[107] Seebeck, F. P.; Woycechowsky, K. J.; Zhuang, W.; Rabe, J. P. und Hilvert, D. (2006): A simple tagging system for protein encapsulation, Journal of the American Chemical Society 128 [14], pp. 4516-4517.

[108] Butt, H. J.; Guckenberger, R. und Rabe, J. P. (1992): Quantitative Scanning Tunneling Microscopy and Scanning Force Microscopy of Organic Materials, Ultramicroscopy 46 [1-4], pp. 375-393.

[109] Gensler, M. (2008): Diplomaarbeit: Untersuchung von Aß42 Peptiden mit Rasterkraftmikroskopie, Humboldt University Berlin.

[110] Ecker, C. (2005): Conformations of single polymer chains on surfaces - non-equilibrium, equilibrium and manipulation, Humboldt University Berlin.

[111] Shu, L. J.; Schlüter, A. D.; Barner, J. und Rabe, J. P. (2001): Synthesis of a fourth generation dendronized polystyrene and SFM manipulation of cylindrical nanoobjects on surfaces, Abstracts of Papers of the American Chemical Society 221, pp. U419-U419.

[112] Friend, R. H.; Gymer, R. W.; Holmes, A. B.; Burroughes, J. H.; Marks, R. N.; Taliani, C.; Bradley, D. D. C.; Dos Santos, D. A.; Bredas, J. L.; Logdlund, M. und Salaneck, W. R. (1999): Electroluminescence in conjugated polymers, Nature 397 [6715], pp. 121-128.

[113] Brabec, C. J.; Sariciftci, N. S. und Hummelen, J. C. (2001): Plastic solar cells, Advanced Functional Materials 11 [1], pp. 15-26.

[114] Dimitrakopoulos, C. D. und Malenfant, P. R. L. (2002): Organic thin film transistors for large area electronics, Advanced Materials 14 [2], pp. 99-+.

[115] Hoeben, F. J. M.; Jonkheijm, P.; Meijer, E. W. und Schenning, A. P. H. J. (2005): About supramolecular assemblies of pi-conjugated systems, Chemical Reviews 105 [4], pp. 1491-1546.

[116] Sirringhaus, H.; Brown, P. J.; Friend, R. H.; Nielsen, M. M.; Bechgaard, K.; Langeveld-Voss, B. M. W.; Spiering, A. J. H.; Janssen, R. A. J.; Meijer, E. W.; Herwig, P. und de Leeuw, D. M. (1999): Two-dimensional charge transport in self-organized, high-mobility conjugated polymers, Nature 401 [6754], pp. 685-688.

[117] Bao, Z.; Dodabalapur, A. und Lovinger, A. J. (1996): Soluble and processable regioregular poly(3-hexylthiophene) for thin film field-effect transistor applications with high mobility, Applied Physics Letters 69 [26], pp. 4108-4110.

[118] Thomas, E. L. (1993): "Structure and Properties of Polymers", in Materials Science and Technology - A Comprehensive Treatment (Eds: R. W. Cahn, P. Haasen, E. J. Kramer), Wiley-VCH, Weinheim.

[119] Samori, P.; Francke, V.; Mangel, T.; Müllen, K. und Rabe, J. P. (1998): Poly-para-phenylene-ethynylene assemblies for a potential molecular-nanowire: an SFM study, Optical Materials 9 [1-4], pp. 390-393.

[120] Kline, R. J.; McGehee, M. D.; Kadnikova, E. N.; Liu, J. S. und Frechet, J. M. J. (2003): Controlling the field-effect mobility of regioregular polythiophene by changing the molecular weight, Advanced Materials 15 [18], pp. 1519-+.

[121] Horowitz, G. (1998): Organic field-effect transistors, Advanced Materials 10 [5], pp. 365-377.

[122] Samori, P.; Francke, V.; Müllen, K. und Rabe, J. P. (1998): Growth of solution cast macromolecular pi-conjugated nanoribbons on mica, Thin Solid Films 336 [1-2], pp. 13-15.

[123] Samori, P.; Sikharulidze, I.; Francke, V.; Müllen, K. und Rabe, J. P. (1999): Nanoribbons from conjugated macromolecules on amorphous substrates observed by SFM and TEM, Nanotechnology 10 [1], pp. 77-80.

[124] Puntambekar, K.; Dong, J. P.; Haugstad, G. und Frisbie, C. D. (2006): Structural and electrostatic complexity at a pentacene/insulator interface, Advanced Functional Materials 16 [7], pp. 879-884.

[125] Loiacono, M. J.; Granstrom, E. L. und Frisbie, C. D. (1998): Investigation of charge transport in thin, doped sexithiophene crystals by conducting probe atomic force microscopy, Journal of Physical Chemistry B 102 [10], pp. 1679-1688.

[126] Fleer, G. J.; Cohen Stuart, M. A.; Scheutjens, J. M. H. M.; Cosgrove, T. und Vincent, B. (1993): Polymers at interfaces, Chapman & Hall, London, UK.

[127] Samori, P.; Severin, N.; Müllen, K. und Rabe, J. P. (2000): Macromolecular fractionation of rod-like polymers at atomically flat solid-liquid interfaces., Advanced Materials 12 [8], pp. 579-582.

[128] Mena-Osteritz, E. (2002): Superstructures of self-organizing thiophenes, Advanced Materials 14 [8], pp. 609-616.

[129] Babel, A. und Jenekhe, S. A. (2003): High electron mobility in ladder polymer field-effect transistors, Journal of the American Chemical Society 125 [45], pp. 13656-13657.

[130] Zen, A. (2007): Charge Transport in Poly(3-hexylthiophene) and in Highly Soluble Oligothiophene Field-Effect Transistors, University of Potsdam, Germany.

[131] Kim, J. (2002): Assemblies of conjugated polymers. Intermolecular and intramolecular effects on the photophysical properties of conjugated polymers, Pure and Applied Chemistry 74 [11], pp. 2031-2044.

[132] Tsukruk, V. V. (1997): Assembly of supramolecular polymers in ultrathin films, Progress in Polymer Science 22 [2], pp. 247-311.

[133] Whitesides, G. M. und Grzybowski, B. (2002): Self-assembly at all scales, Science 295 [5564], pp. 2418-2421.

[134] Tanford, C. (1978): HYDROPHOBIC EFFECT AND ORGANIZATION OF LIVING MATTER, Science 200 [4345], pp. 1012-1018.

[135] Brunsveld, L.; Folmer, B. J. B.; Meijer, E. W. und Sijbesma, R. P. (2001): Supramolecular polymers, Chemical Reviews 101 [12], pp. 4071-4097.

[136] Cornelissen, Jjlm; Donners, Jjjm; de Gelder, R.; Graswinckel, W. S.; Metselaar, G. A.; Rowan, A. E.; Sommerdijk, Najm und Nolte, R. J. M. (2001): beta-helical polymers from isocyanopeptides, Science 293 [5530], pp. 676-680.

[137] Jahnke, E.; Lieberwirth, I.; Severin, N.; Rabe, J. P. und Frauenrath, H. (2006): Topochemical polymerization in supramolecular polymers of oligopeptide-functionalized diacetylenes, Angewandte Chemie-International Edition 45 [32], pp. 5383-5386.

[138] Schlaad, H.; Krasia, T. und Antonietti, M. (2004): Superhelices of poly[2-(acetoacetoxy)ethyl methacrylate], Journal of the American Chemical Society 126 [36], pp. 11307-11310.

[139] Shu, L. J.; Gössl, I.; Rabe, J. P. und Schlüter, A. D. (2002): Quantitative aspects of the dendronization of dendronized linear polystyrenes, Macromolecular Chemistry and Physics 203 [18], pp. 2540-2550.

[140] Zhang, A.; Wei, L. H. und Schlüter, A. D. (2004): Narrowly distributed dendronized polymethacrylates by reversible addition-fragmentation chain transfer (RAFT) polymerization, Macromolecular Rapid Communications 25 [7], pp. 799-803.

[141] Grayson, S. M. und Frechet, J. M. J. (2001): Divergent synthesis of dendronized poly(p-hydroxystyrene), Macromolecules 34 [19], pp. 6542-6544.

[142] Ouali, N.; Mery, S.; Skoulios, A. und Noirez, L. (2000): Backbone stretching of wormlike carbosilane dendrimers, Macromolecules 33 [16], pp. 6185-6193.

[143] Zhang, A. F.; Barner, J.; Goessl, I.; Rabe, J. P. und Schlüter, A. D. (2004): A covalent-chemistry approach to giant macromolecules and their wetting behavior on solid substrates, Angew.Chem.-Int.Edit. 43 [39], pp. 5185-5188.

[144] Percec, V.; Ahn, C. H.; Cho, W. D.; Jamieson, A. M.; Kim, J.; Leman, T.; Schmidt, M.; Gerle, M.; Moller, M.; Prokhorova, S. A.; Sheiko, S. S.; Cheng, S. Z. D.; Zhang, A.; Ungar, G. und Yeardley, D. J. P. (1998): Visualizable cylindrical macromolecules with controlled stiffness from backbones containing libraries of self-assembling dendritic side groups, J.Am.Chem.Soc. 120 [34], pp. 8619-8631.

[145] Stocker, W.; Schurmann, B. L.; Rabe, J. P.; Forster, S.; Lindner, P.; Neubert, I. und Schlüter, A. D. (1998): A dendritic nanocylinder: Shape control through implementation of steric strain, Advanced Materials 10 [10], pp. 793-797.

[146] Al Hellani, R.; Barner, J.; Rabe, J. P. und Schlüter, A. D. (2006): Covalent connection of individualized, neutral, dendronized polymers on a solid substrate using a scanning force microscope, Chemistry-A European Journal 12 [25], pp. 6542-6551.

[147] Barner, J.; Al Hellani, R.; Schlüter, A. D. und Rabe, J. P. (2009): Synthesis with single macromolecules: Covalent connection between a neutral dendronized polymer and polyelectrolyte chains as well as graphene edges., Macromolecular Rapid Communications in press.

[148] Pogantsch, A.; Wenzl, F. P.; List, E. J. W.; Leising, G.; Grimsdale, A. C. und Müllen, K. (2002): Polyfluorenes with dendron side chains as the active materials for polymer light-emitting devices, Advanced Materials 14 [15], pp. 1061-+.

[149] Kwon, Y. K.; Chvalun, S. N.; Blackwell, J.; Percec, V. und Heck, J. A. (1995): Effect of Temperature on the Supramolecular Tubular Structure in Oriented Fibers of A Poly(Methacrylate) with Tapered Side-Groups, Macromolecules 28 [5], pp. 1552-1558.

[150] Rapp, A.; Schnell, I.; Sebastiani, D.; Brown, S. P.; Percec, V. und Spiess, H. W. (2003): Supramolecular assembly of dendritic polymers elucidated by H-1 and C-13 solid-state MAS NMR spectroscopy, Journal of the American Chemical Society 125 [43], pp. 13284-13297.

[151] Bottcher, C.; Schade, B.; Ecker, C.; Rabe, J. P.; Shu, L. J. und Schlüter, A. D. (2005): Double-helical ultrastructure of polycationic dendronized polymers determined by single-particle cryo-TEM, Chemistry-A European Journal 11 [10], pp. 2923-2928.

[152] Cacialli, F.; Wilson, J. S.; Michels, J. J.; Daniel, C.; Silva, C.; Friend, R. H.; Severin, N.; Samori, P.; Rabe, J. P.; O'Connell, M. J.; Taylor, P. N. und Anderson, H. L. (2002): Cyclodextrin-threaded conjugated polyrotaxanes as insulated molecular wires with reduced interstrand interactions, Nature Materials 1 [3], pp. 160-164.

[153] Borner, H. G.; Beers, K.; Matyjaszewski, K.; Sheiko, S. S. und Moller, M. (2001): Synthesis of molecular brushes with block copolymer side chains using atom transfer radical polymerization, Macromolecules 34 [13], pp. 4375-4383.

[154] Gerle, M.; Fischer, K.; Roos, S.; Müller, A. H. E.; chmidt, M.; heiko, S. S.; rokhorova, S. und öller, M. (1999): Main chain conformation and anomalous elution behavior of cylindrical brushes as revealed by GPC/MALLS, light scattering, and SFM, Macromolecules 32 [8], pp. 2629-2637.

[155] Li, C. M.; Gunari, N.; Fischer, K.; Janshoff, A. und Schmidt, M. (2004): New perspectives for the design of molecular actuators: Thermally induced collapse of single macromolecules from cylindrical brushes to spheres, Angewandte Chemie-International Edition 43 [9], pp. 1101-1104.

[156] Ecker, C.; Severin, N.; Shu, L. J.; Schlüter, A. D. und Rabe, J. P. (2004): Glassy state of single dendronized polymer chains, Macromolecules 37 [7], pp. 2484-2489.

[157] Flory, P. J. (1953): Principles of Polymer Chemistry, Cornell University Press, Ithaca, New York.

[158] Vesenka, J.; Miller, R. und Henderson, E. (1994): 3-Dimensional Probe Reconstruction for Atomic-Force Microscopy, Review of Scientific Instruments 65 [7], pp. 2249-2251.

[159] Zhuang, W.; Kasemi, E.; Ding, Y.; Kroger, M.; Schlüter, A. D. und Rabe, J. P. (2008): Self-folding of charged single dendronized polymers, Advanced Materials 20 [17], pp. 3204.

[160] Ornatska, M.; Peleshanko, S.; Genson, K. L.; Rybak, B.; Bergman, K. N. und Tsukruk, V. V. (2004): Assembling of amphiphilic highly branched molecules in supramolecular nanofibers, Journal of the American Chemical Society 126 [31], pp. 9675-9684.

[161] Ding, Y.; Ottinger, H. C.; Schlüter, A. D. und Kröger, M. (2007): From atomistic simulation to the dynamics, structure and helical network formation of dendronized polymers: The Janus chain model, Journal of Chemical Physics 127 [9].

[162] Chandler, D. (2005): Interfaces and the driving force of hydrophobic assembly, Nature 437 [7059], pp. 640-647.

[163] Tsukruk, V. V. (1998): Dendritic macromolecules at interfaces, Advanced Materials 10 [3], pp. 253-+.

[164] Sheiko, S. S.; Sun, F. C.; Randall, A.; Shirvanyants, D.; Rubinstein, M.; Lee, H. und Matyjaszewski, K. (2006): Adsorption-induced scission of carbon-carbon bonds, Nature 440 [7081], pp. 191-194.

[165] Kroger, M. (2004): Simple models for complex nonequilibrium fluids, Physics Reports-Review Section of Physics Letters 390 [6], pp. 453-551.

[166] Kroger, M.; Ilg, P. und Hess, S. (2003): Magnetoviscous model fluids, Journal of Physics-Condensed Matter 15 [15], pp. S1403-S1423.

[167] Kroger, M.; Peleg, O.; Ding, Y. und Rabin, Y. (2008): Formation of double helical and filamentous structures in models of physical and chemical gels, Soft Matter 4 [1], pp. 18-28.

[168] Odian, G. (1991): Principles of Polymerization, Wiley, New York.

[169] Kasemi, E. und Schlüter, A. D. (2007): An easy accessible homologous set of first to fifth generation dendritic methacrylic macromonomers and their polymerizations, New Journal of Chemistry 31 [7], pp. 1313-1320.

[170] Seeman, N. C. (2003): DNA in a material world, Nature 421 [6921], pp. 427-431.

[171] Perkins, T. T.; Smith, D. E. und Chu, S. (1997): Single polymer dynamics in an elongational flow, Science 276 [5321], pp. 2016-2021.

[172] Tegenfeldt, J. O.; Prinz, C.; Cao, H.; Chou, S.; Reisner, W. W.; Riehn, R.; Wang, Y. M.; Cox, E. C.; Sturm, J. C.; Silberzan, P. und Austin, R. H. (2004): The dynamics of genomic-length DNA molecules in 100-nm channels, Proceedings of the National Academy of Sciences of the United States of America 101 [30], pp. 10979-10983.

[173] Raedler, J. O.; Koltover, I.; Jamieson, A.; Salditt, T. und Safinya, C. R. (1998): Structure and interfacial aspects of self-assembled cationic lipid-DNA gene carrier complexes, Langmuir 14 [15], pp. 4272-4283.

[174] Ohler, M.; Baruchel, J. und Galez, P. (1995): An X-Ray-Diffraction Topographic Study of Highly Oriented Pyrolytic-Graphite, Journal of Physics D-Applied Physics 28 [4A], pp. A78-A83.

[175] Lide, D. R. (1998): Handbook of Chemistry and Physics, CRC Press, London UK.

[176] Hu, J.; Xiao, X. D.; Ogletree, D. F. und Salmeron, M. (1995): Imaging the Condensation and Evaporation of Molecularly Thin-Films of Water with Nanometer Resolution, Science 268 [5208], pp. 267-269.

[177] Tanigawa, M. und Okada, T. (1998): Atomic force microscopy of supercoiled DNA structure on mica, Analytica Chimica Acta 365 [1-3], pp. 19-25.

[178] Bussiek, M.; Mucke, N. und Langowski, J. (2003): Polylysine-coated mica can be used to observe systematic changes in the supercoiled DNA conformation by scanning force microscopy in solution, Nucleic Acids Research 31 [22].

[179] Samori, B.; Siligardi, G.; Quagliariello, C.; Weisenhorn, A. L.; Vesenka, J. und Bustamante, C. J. (1993): Chirality of Dna Supercoiling Assigned by Scanning Force Microscopy, Proceedings of the National Academy of Sciences of the United States of America 90 [8], pp. 3598-3601.

[180] Antonietti, M.; Burger, C. und Thünemann, A. (1997): Polyelectrolye-surfactant complexes: A new class of highly ordered polymer materials, Trends in Polymer Science 5 [8], pp. 262-267.

[181] Cyr, D. M.; Venkataraman, B.; Flynn, G. W.; Black, A. und Whiteside, G. M. (1996): Functional group identification in scanning tunneling microscopy of molecular adsorbates, Journal of Physical Chemistry B 100 [32], pp. 13747-13759.

[182] Michalet, X.; Ekong, R.; Fougerousse, F.; Rousseaux, S.; Schurra, C.; Hornigold, N.; vanSlegtenhorst, M.; Wolfe, J.; Povey, S.; Beckmann, J. S. und Bensimon, A. (1997): Dynamic molecular combing: Stretching the whole human genome for high-resolution studies, Science 277 [5331], pp. 1518-1523.

[183] Alivisatos, A. P.; Johnsson, K. P.; Peng, X. G.; Wilson, T. E.; Loweth, C. J.; Bruchez, M. P. und Schultz, P. G. (1996): Organization of 'nanocrystal molecules' using DNA, Nature 382 [6592], pp. 609-611.

[184] Liang, H (2007): Master Thesis, Humboldt Unversity Berlin.

[185] Peterson, C. A.; Gray, D. M.; Gray, H. B. und Legerski, R. J. (1993): Evidence for A Salt-Induced Conformational Transition in Uv-Irradiated Superhelical Pm2 Dna, Biochimica et Biophysica Acta 1216 [2], pp. 265-272.

[186] Benham, C. J. und Mielke, S. P. (2005): DNA mechanics, Annual Review of Biomedical Engineering 7, pp. 21-53.

[187] Gellman, A. J. und Paserba, K. R. (2002): Kinetics and mechanism of oligomer desorption from surfaces: n-alkanes on graphite, Journal of Physical Chemistry B 106 [51], pp. 13231-13241.

[188] Lindahl, T. (1993): Instability and Decay of the Primary Structure of Dna, Nature 362 [6422], pp. 709-715.

[189] Eigler, D. M. und Schweizer, E. K. (1990): Positioning Single Atoms with A Scanning Tunneling Microscope, Nature 344 [6266], pp. 524-526.

[190] Gimzewski, J. K. und Joachim, C. (1999): Nanoscale science of single molecules using local probes, Science 283 [5408], pp. 1683-1688.

[191] Stroscio, J. A. und Eigler, D. M. (1991): Atomic and Molecular Manipulation with the Scanning Tunneling Microscope, Science 254 [5036], pp. 1319-1326.

[192] Oyabu, N.; Custance, O.; Yi, I. S.; Sugawara, Y. und Morita, S. (2003): Mechanical vertical manipulation of selected single atoms by soft nanoindentation using near contact atomic force microscopy, Physical Review Letters 90 [17].

[193] Kim, D. H.; Koo, J. Y. und Kim, J. J. (2003): Cutting of multiwalled carbon nanotubes by a negative voltage tip of an atomic force microscope: A possible mechanism, Physical Review B 68 [11].

[194] Ramachandran, T. R.; Baur, C.; Bugacov, A.; Madhukar, A.; Koel, B. E.; Requicha, A. und Gazen, C. (1998): Direct and controlled manipulation of nanometer-sized particles using the non-contact atomic force microscope, Nanotechnology 9 [3], pp. 237-245.

[195] Martin, M.; Roschier, L.; Hakonen, P.; Parts, U.; Paalanen, M.; Schleicher, B. und Kauppinen, E. I. (1998): Manipulation of Ag nanoparticles utilizing noncontact atomic force microscopy, Applied Physics Letters 73 [11], pp. 1505-1507.

[196] Bustamante, C.; Bryant, Z. und Smith, S. B. (2003): Ten years of tension: single-molecule DNA mechanics, Nature 421 [6921], pp. 423-427.

[197] Horn, R. G. und Israelachvili, J. N. (1981): Direct Measurement of Structural Forces Between 2 Surfaces in A Non-Polar Liquid, Journal of Chemical Physics 75 [3], pp. 1400-1411.

[198] Zhu, Y. und Granick, S. (2003): Reassessment of solidification in fluids confined between mica sheets, Langmuir 19 [20], pp. 8148-8151.

[199] Garcia, R.; Tamayo, J. und San Paulo, A. (1999): Phase contrast and surface energy hysteresis in tapping mode scanning force microsopy, Surface and Interface Analysis 27 [5-6], pp. 312-316.

[200] Burnham, N. A.; Behrend, O. P.; Oulevey, F.; Gremaud, G.; Gallo, P. J.; Gourdon, D.; Dupas, E.; Kulik, A. J.; Pollock, H. M. und Briggs, G. A. D. (1997): How does a tip tap?, Nanotechnology 8 [2], pp. 67-75.

[201] Bardon, S.; Valignat, M. P.; Cazabat, A. M.; Stocker, W. und Rabe, J. P. (1998): Study of liquid crystal prewetting films by atomic force microscopy in tapping mode, Langmuir 14 [10], pp. 2916-2924.

[202] Herminghaus, S.; Fery, A. und Reim, D. (1997): Imaging of droplets of aqueous solutions by tapping-mode scanning force microscopy, Ultramicroscopy 69 [3], pp. 211-217.

[203] Forcada, M. L. und Mate, C. M. (1993): Molecular Layering During Evaporation of Ultrathin Liquid-Films, Nature 363 [6429], pp. 527-529.

[204] Cui, S. T.; Cummings, P. T. und Cochran, H. D. (1999): Molecular dynamics simulation of the rheological and dynamical properties of a model alkane fluid under confinement, Journal of Chemical Physics 111 [3], pp. 1273-1280.

[205] Raviv, U.; Laurat, P. und Klein, J. (2001): Fluidity of water confined to subnanometre films, Nature 413 [6851], pp. 51-54.

[206] Mukhopadhyay, A.; Zhao, J.; Bae, S. C. und Granick, S. (2002): Contrasting friction and diffusion in molecularly thin confined films, Physical Review Letters 89 [13].

[207] Herminghaus, S.; Jacobs, K.; Mecke, K.; Bischof, J.; Fery, A.; Ibn-Elhaj, M. und Schlagowski, S. (1998): Spinodal dewetting in liquid crystal and liquid metal films, Science 282 [5390], pp. 916-919.

[208] Champoux, J. J. (2001): DNA topoisomerases: Structure, function, and mechanism, Annual Review of Biochemistry 70, pp. 369-413.

[209] Hentschke, R.; Schurmann, B. L. und Rabe, J. P. (1992): Molecular-Dynamics Simulations of Ordered Alkane Chains Physisorbed on Graphite, Journal of Chemical Physics 96 [8], pp. 6213-6221.

[210] Zacharia, R.; Ulbricht, H. und Hertel, T. (2004): Interlayer cohesive energy of graphite from thermal desorption of polyaromatic hydrocarbons, Physical Review B 69 [15].

[211] Grandbois, M.; Beyer, M.; Rief, M.; Clausen-Schaumann, H. und Gaub, H. E. (1999): How strong is a covalent bond?, Science 283 [5408], pp. 1727-1730.

[212] Bates, F. S. und Fredrickson, G. H. (1999): Block copolymers - Designer soft materials, Physics Today 52 [2], pp. 32-38.

[213] Kumaki, J. und Hashimoto, T. (2003): Conformational change in an isolated single synthetic polymer chain on a mica surface observed by atomic force microscopy, Journal of the American Chemical Society 125 [16], pp. 4907-4917.

[214] Stocker, W.; Beckmann, J.; Stadler, R. und Rabe, J. P. (1996): Surface reconstruction of the lamellar morphology in a symmetric poly(styrene-block-butadiene-block-methyl methacrylate) triblock copolymer: A tapping mode scanning force microscope study, Macromolecules 29 [23], pp. 7502-7507.

[215] Alemdaroglu, F. E. und Herrmann, A. (2007): DNA meets synthetic polymers - highly versatile hybrid materials, Organic & Biomolecular Chemistry 5 [9], pp. 1311-1320.

[216] Safak, M.; Alemdaroglu, F. E.; Li, Y.; Ergen, E. und Herrmann, A. (2007): Polymerase chain reaction as an efficient tool for the preparation of block copolymers, Advanced Materials 19 [11], pp. 1499-+.

[217] Barner, J. (2010): PhD Thesis, Humboldt University Berlin.

[218] Alemdaroglu, F. E.; Zhuang, W.; Zöphel, L.; Wang, J.; Berger, R.; Herrmann, A. und Rabe, J. P. (2009): Generation of Multiblock Copolymers by PCR: Synthesis, Visualization and Nanomechanical Properties, Nano Letters 9, pp. 3658-3662.

[219] Zhuang, W.; Severin, N.; Sokolov, I. M. und Rabe, J. P. (2006): Blowing polymer bubbles on surfaces, Polymeric Materials: Science & Engineering 95 [597], pp. 598-599.

Lebenslauf

Wei Zhuang

Der Lebenslauf wir nicht im Internet veröffentlicht.

Publications

Effect of molecular weight and annealing of poly (3-hexylthiophene)s on the performance of organic field-effect transistors.
Zen, A., Pflaum, J., Hirschmann, S., Zhuang, W., Jaiser, F., Asawapirom, U., Rabe, J.P., Scherf, U., Neher, D.,
Advanced Functional Materials **2004,** *14*, 757

SFM characterization of poly(isocyanodipeptide) single polymer chains in controlled environments: Effect of tip adhesion and chain swelling.
Zhuang, W., Ecker, C., Metselaar, G.A, Rowan, A.E., Nolte, R.J.M., Samori, P., Rabe, J.P.,
Macromolecules **2005**, *38,* 473

A simple tagging system for protein encapsulation.
Seebeck, F.P., Woycechowsky, K.J., Zhuang, W., Rabe, J.P., Hilvert, D.,
Journal of the American Chemical Society **2006,** *128*, 4516

Synthesis of an anionically chargeable, high-molar-mass, second-generation dendronized polymer and the observation of branching by scanning force microscopy.
Kasemi, E., Zhuang, W., Rabe, J.P., Fischer, K., Schmidt, M., Colussi, M., Keul, H., Yi, D., Colfen, H., Schlüter, A.D.,
Journal of the American Chemical Society **2006,** *128*, 5091

Blowing polymer bubbles on surfaces.
Zhuang, W., Severin, N., Sokolov, I.M., Rabe, J.P.,
Polymeric Materials: Science & Engineering **2006,** *95*, 598

Blowing DNA Bubbles.
Severin, N., Zhuang, W., Ecker, C., Kalachev, A.A., Sokolov, I.M., and Rabe, J.P.,
Nano Letters **2006**, *6*, 2561

Organic field-effect transistors utilising oligothiophene based swivel cruciforms.
Zen, A., Pingel, P., Jaiser, F., Neher, D., Grenzer, J., Zhuang, W., Rabe, J.P., Bilge, A., Grabrecht, F., Nehls, B., Farrell, T., Scherf, U., Grozema, F.C., and Siebbeles, L.D.,
Chemistry of Materials **2007,** *19*, 1267

Self-folding of charged single dendronized polymers.
Zhuang, W., Kasemi, E., Ding, Y., Kroger, M., Schlüter, A. D., Rabe, J.P.,
Advanced Materials **2008,** *20*, 3204

Optical switching study of an azobenzene rigidly linked to a hexa-*peri*-hexabenzocoronene derivative in solution and at a solid-liquid interface.
Ai, M., Groeper, S., Zhuang, W., Dou, X., Feng, X., Müllen, K., Rabe, J.P.,
Applied Physics A, Material Science and Processing, **2008**, *93*, 277

Generation of Multiblock Copolymers by PCR: Synthesis, Visualization and Nanomechanical Properties.
Alemdaroglu, F.E., Zhuang, W., Zöphel, L., Wang, J., Berger, R., Herrmann, A., Rabe, J.P.,
Nano Letters **2009,** *9,* 3658

Erklärung

Hiermit erkläre ich, die vorliegende Arbeit selbständig und ohne unerlaubte Hilfe angefertigt zu haben und nur die angegebene Literatur und Hilfsmittel verwendet zu haben. Ich habe mich anderwärts nicht um einen Doktorgrad beworben und besitze einen entsprechenden Doktorgrad nicht. Ich erkläre die Kenntnisnahme der dem Verfahren zugrunde liegenden Promotionsordnung der Mathematisch-Naturwissenschaftlichen Fakultät I der Humboldt-Universität zu Berlin.

Wei Zhuang

Berlin, 23. October 2009